THE MULTIDISCIPLINARY DESIGN PROBLEM AS A DYNAMICAL SYSTEM

A Thesis
Presented to
The Academic Faculty

by

Bradley A. Steinfeldt

In Partial Fulfillment
of the Requirements for the Degree
Doctor of Philosophy in the
School of Aerospace Engineering

Georgia Institute of Technology
August 2013

THE MULTIDISCIPLINARY DESIGN PROBLEM AS A DYNAMICAL SYSTEM

Approved by:

Dr. Robert D. Braun, Advisor
School of Aerospace Engineering
Georgia Institute of Technology

Mr. Gregg H. Barton
Mission Design Group
C. S. Draper Laboratory, Inc.

Dr. Ian G. Clark
Entry, Descent, and Landing and
Advanced Techologies Group
Jet Propulsion Laboratory

Dr. Brian J. German
School of Aerospace Engineering
Georgia Institute of Technology

Dr. Panagiotis Tsiotras
School of Aerospace Engineering
Georgia Institute of Technology

Date Approved: June 24, 2013

To my parents, Brian E. and M. Annette Steinfeldt.

To my maternal grandparents, William P. and Jean T. Alexander.

To my paternal grandparents, Wayne F. and Margaret M. Steinfeldt.

I'm on my feet, I'm on the floor, I'm good to go

So come on Davey, sing me something that I know

—Jimmy Eat World

ACKNOWLEDGEMENTS

There are really no words that can adequately acknowledge the support of the numerous people I have received during the course of my graduate career. However, I will try to briefly acknowledge just a few of those who made this research possible.

To begin with, I have been honored to have had the opportunity to learn from my advisor, **Prof. Robert Braun**. You have taught me more than you know and have helped to shape me to be the engineer and person I am today. The patience, support, fervor, perceptiveness, wisdom, savvy, scholarship, clarity, and ingenuity that you have shown me throughout my graduate studies is truly remarkable. Thank you.

The guidance provided by my committee has been invaluable throughout the development of this research. I owe each of you my heartfelt gratitude for your time and dedication to making this work what it is today. **Mr. Gregg Barton**, your support and mentoring throughout the years, while performing this research and at Draper is appreciated more than words can express, thanks. **Dr. Ian Clark**, thank you for your thoughts, advisement, and intellectual curiosity during your time at Georgia Tech and while serving on my committee. **Prof. Brian German**, you provided a plethora of knowledge, resources, and encouragement during this endeavor, thank you. **Prof. Panagiotis Tsiotras**, I truly appreciate the direction and push to stretch myself that you provided both in class and while developing this thesis.

Throughout the majority of my graduate career, I have been supported by the Charles Stark Draper Laboratory, both on-campus and through summer work experiences. They embody their original mission of "pioneer[ing] in science and technology, contribut[ing] to the national interest, and promot[ing] the transfer of technology through education." I would like to acknowledge just a few of the people that have

made my interactions with Draper special—**Amer Fejzic**, **David Woffinden**, **Linda Fuhrman**, **Mark Jackson**, **Matt Fritz**, **Phil Hattis**, **Scott Thompson**, **Seamus Tuohy**, and **Steve Paschall**.

I have been fortunate to be part of the Space System Design Lab (SSDL) during my graduate career, without the support of many its members this work would not have happened. These folks have not just been colleagues, they have provided a fervent sounding board, support network, and social outlet for me while at Georgia Tech. **Mike Grant**, with whom I took all but one class, took qualifying exams, and performed countless hours of research—I do not know what to say, buddy, I would not be who I am or know as much as I do without you. Thanks! **Ashley Korzun**, **Ben Stahl**, **Chris Cordell**, **Chris Tanner**, **Grant Rossman**, **Gregory Lantoine**, **Ian Meginnis**, **Jarret Lafleur**, **Jenny Kelly**, **Jimmy Young**, **Milad Mahzari**, **Nitin Arora**, **Patrick Chai**, **Richard Otero**, **Som Dutta**, **Zach Putnam**, **Zarrin Chua**, and the rest of my labmates throughout the years in the SSDL, thank each of you for being the definition of scholars and for your companionship.

In addition to my companions in the SSDL, many more friends supported me through this journey. **Andrzej Stewart**, **Antja Chambers**, **Ashley Tarpley**, **Brad Maxwell**, **Jeff Story**, **Jerred Chute**, **Nina Patel**, **Shaun Tarpley**, **Suzanne Oliason**, and **Yvonne Stephens** are just a few of these friends. You are all phenomenal for putting up with me, thanks!

Finally, this work would not have been possible without the unconditional love and support of my family. **Mom and Dad**, you instilled a thirst for knowledge early on and have done whatever it takes to enable me to satisfy that thirst. Thank you for all of your sacrifices that have empowered me to follow my dreams. **Grandma and Granddaddy Alexander**, thank you for the flawless guidance and the push to be the best Brad I can be. **Grandpa Steinfeldt** thank you and **Grandma Steinfeldt** for being amongst my strongest advocates and instilling a sense of passion in me.

TABLE OF CONTENTS

LIST OF TABLES

LIST OF FIGURES

NOMENCLATURE

Acronyms

CA	Contributing Analysis
CBAero	Configuration Based Aerodynamics tool
CG	Center of Gravity
CO	Collaborative Optimization
CSSUA	Concurrent Subsystem Uncertainty Analysis
DeMAID	Design Manager's Aid for Intelligent Decomposition
DOE	Design of Experiments
DSM	Design Structure Matrix
EDL	Entry, Descent, and Landing
FPI	Fast Probability Integration
FPKE	Fokker-Plank-Kolmogorov Equation
GN&C	Guidance, Navigation, and Control
LMI	Linear Matrix Inequality
MDA/O	Multidisciplinary Design Analysis/Optimization
MDO	Multidisciplinary Design Optimization
MOPSO	Multi-objective Particle Swarm Optimizer
MSD	Mean Squared Deviation

NASA	National Aeronautics and Space Administration
NLP	Nonlinear Programming
OBD	Optimizer Based Decomposition
PERT	Program Evaluation and Review Technique
RSE	Response Surface Equation
RSM	Response Surface Methodology
SADT	Structured Analysis and Design Technique
SNOPT	Sparse Nonlinear Optimization
SoS	System of Systems
SSA	System Sensitivity Analysis
SUA	System Uncertainty Analysis

Roman Variables

$\dot{q}$	Heat rate
$\mathbf{0}_q$	$q \times 1$ vector of zeros
$\mathbf{1}_q$	$q \times 1$ vector of ones
$\mathbf{A_j}$	Matrix describing the state contribution of the j^{th} contributing analysis, $\mathbf{A_j} \in \mathbb{R}^{l_j \times m}$
$\mathbf{A}_k$	Matrix describing the state components to the dynamical system at iterate k
$\mathbf{B_j}$	Matrix describing the deterministic input contribution of the j^{th} contributing analysis, $\mathbf{B_j} \in \mathbb{R}^{l_j \times d}$

$\mathbf{b}^{(i)}$	Vector that lies in the dual cone $\mathcal{D}(\mathcal{P}^{(i)})$
$\mathbf{B}_k$	Matrix describing the input (control) components to the dynamical system at iterate k
$\mathbf{C_j}$	Matrix describing the probabilistic input contribution of the j^{th} contributing analysis, $\mathbf{C_j} \in \mathbb{R}^{l_j \times p}$
$\mathbf{C}_k$	Matrix describing the state components to the output of the dynamical system at iterate k
$\mathbf{d_j}$	Bias associated with the j^{th} contributing analysis, $\mathbf{d_j} \in \mathbb{R}^{l_j}$
$\mathbf{D}_k$	Matrix describing the input (control) components to the output of the dynamical system at iterate k
$\mathbf{f}(\cdot)$	Concatenation of the contributing analyses input-output relationships
$\mathbf{f}(\cdot)$	General state dynamical system relationship
$\mathbf{F}_i(\cdot)$	Symmetric polynomial matrix used in the sum-of-squares problem
$\mathbf{g}(\cdot)$	General output dynamical system relationship
$\mathbf{g}(\cdot)$	Inequality design constraints
$\mathbf{H}$	Observation model
$\mathbf{h}(\cdot)$	Equality design constraints
$\mathbf{I_{n\times n}}$	The $n \times n$ identity matrix
$\mathbf{K}$	Kalman gain
$\mathbf{M}$	Matrix describing the linear combination of the pertinent contributing analyses outputs to the design's response, $\mathbf{M} \in \mathbb{R}^{1\times q}$

$\mathbf{p}$	Design parameters
$\mathbf{Q}$	Covariance of the random noise associated with the model
$\mathbf{Q}$	Positive semi-definite matrix used in the sum-of-squares problem
$\mathbf{Q}$	Unitary matrix in Schur decomposition
$\mathbf{R}$	Covariance of the random noise associated with the observation of the system
$\mathbf{r}$	Position vector
$\mathbf{r}(\cdot)$	Design response
$\mathbf{S}$	Residual covariance
$\mathbf{S}$	Sample covariance matrix
$\mathbf{s}$	Vector of state constraints
$\mathbf{u_d}$	Deterministic system-level inputs into the design, $\mathbf{u_d} \in \mathbb{R}^d$
$\mathbf{u_p}$	Probabilistic system-level inputs into the design, $\mathbf{u_p} \in \mathbb{R}^p$
$\mathbf{U}$	Upper triangular matrix
$\mathbf{u}$	Control variable in the optimal control problem
$\mathbf{u}$	Design variables
$\mathbf{V}$	Matrix whose columns are the (generalized) eigenvectors
$\mathbf{v}$	Random noise associated with the observation of the system, $\mathbf{v} \sim \mathcal{N}(\mathbf{0}, \mathbf{R})$
$\mathbf{w}$	Random noise associated with the model, $\mathbf{w} \sim \mathcal{N}(\mathbf{0}, \mathbf{Q})$

$\mathbf{w}(\mathbf{y})$	Equality constraints that are a function of the state
$\mathbf{W}_k$	Complex-valued matrix
$\mathbf{y_j}$	Contributing analysis output, $\mathbf{y_j} \in \mathbb{R}^{l_j}$
$\mathbf{y}$	Concatenation of all contributing analyses output, the state variable, $\mathbf{y} \in \mathbb{R}^m$
$\mathbf{z}$	State observation
$\mathbf{z}(\cdot)$	Column vector in the sum-of-squares problem whose entries are monomial in $(\cdot)$
A	Area
a	Ellipsoid semi-major axis
b	Ellipsoid semi-minor axis
C_D	Drag coefficient
c_i	Weighting variable in the sum-of-squares solution
C_L	Lift coefficient
d	Dimensionality of the deterministic inputs, *i.e.*, $d = \dim(\mathbf{u_d})$
d_{miss}	Miss distance
E	Young's modulus
f	Force magnitude
$f(\cdot)$	Arbitrary scalar mapping
$f_{\mathbf{uy}}(\mathbf{u}, \mathbf{p})$	Joint probability distribution function of $\mathbf{u}$ and $\mathbf{p}$

g	Magnitude of the acceleration due to gravity
$g(\cdot)$	Scalar arbitrary function
H	Atmospheric scale height
h	Altitude
$H(\cdot)$	Hamiltonian
I	Mass moment of inertia
k	Iterate index
k_k	Dimensionality of the control equality constraints in the discrete optimal control problem
k_s	Sutton-Graves constant
k_{C_D}	Drag coefficient multiplier
k_{C_L}	Lift coefficient multiplier
l	Length
$L(\cdot)$	Lagrangian
L/D	Lift-to-drag ratio
l/d	Deployable length to vehicle diameter ratio
l_j	Dimensionality of the j^{th} contributing analysis's output, *i.e.*, $l_j = \dim(\mathbf{y_j})$
m	Dimensionality of the concatenated contributing analyses's outputs, $m = \sum_{i=1}^{n} l_j$

m	Mass
n	Number of contributing analyses
p	Deployable internal pressure
p	Dimensionality of the probabilistic inputs, *i.e.*, $p = \dim(\mathbf{u_p})$
p_k	Dimensionality of the state equality constraints in the discrete optimal control problem
Q	Integrated heat load
q	Dimensionality of the pertinent contributing analyses' responses that contribute to the design objective
q	Order of the contributing analyses
q_k	Dimensionality of the control inequality constraints in the discrete optimal control problem
r	Order of the response
r	Radius
r_k	Dimensionality of the state inequality constraints in the discrete optimal control problem
r_n	Stagnation radius
s	Dimensionality of the input space, $s = d + p$
T	Tension
t	Dimensionality of the response
v	Velocity magnitude

$V(\cdot)$	Lyapunov function
$v_i(\cdot)$	Monomial function in $(\cdot)$
W	Weight
w	Constant factor for exponential stability
w	Parameter weights
$w(\cdot)$	Mapping from $\mathbb{R}^n \to \mathbb{R}$ that is continuous at the equilibrium point
z	Ellipsoid altitude

Greek Variables

α	Scaling factor or weight on the mean value
β	Ballistic coefficient, $\beta = \dfrac{m}{C_D A}$
β	Reduction factor for exponential systems
β	Scaling factor or weight on the spread of the distribution
$\boldsymbol{\beta}$	Deterministic input contribution in the fixed-point iteration equation, $\boldsymbol{\beta} \in \mathbb{R}^{m \times d}$
$\boldsymbol{\delta}$	Bias in the fixed-point iteration equation, $\boldsymbol{\delta} \in \mathbb{R}^m$
$\boldsymbol{\gamma}$	Probabilistic input contribution in the fixed-point iteration equation, $\boldsymbol{\gamma} \in \mathbb{R}^{m \times p}$
$\boldsymbol{\Lambda}$	State contribution in the fixed-point iteration equation, $\boldsymbol{\Lambda} \in \mathbb{R}^{m \times m}$
$\boldsymbol{\lambda}$	Lagrange multiplier
$\boldsymbol{\mu}$	Lagrange multiplier

$\boldsymbol{\nu}$	Lagrange multiplier
$\boldsymbol{\omega}(\mathbf{y})$	Inequality constraints that are a function of the state
$\boldsymbol{\Phi}(k, j)$	Discrete state transition matrix from iterate k to iterate j
$\boldsymbol{\Psi}$	Matrix transformation
$\boldsymbol{\Sigma}$	Covariance matrix
$\boldsymbol{\zeta}$	Transformation variable
δ	Deployable material thickness
ϵ	Convergence tolerance
γ	Flight path angle
$\kappa(\cdot)$	Function describing a mapping from $\mathbb{C}^{n\times n} \rightarrow \mathbb{R}$
μ	Mean value ($\mu_{(\cdot)} = \mathbb{E}(\cdot)$)
μ_g	Gravitational parameter
ν	Poisson's ratio
Ω	Set of objective functions
ϕ	Longitude
$\phi(\cdot)$	Continuous function describing a mapping from $\mathbb{R}^n \rightarrow \mathbb{R}$
$\phi(\cdot)$	Terminal state cost
ψ	Heading angle
ρ	Density
ρ_{X_i,X_j}	Product-moment coefficient between X_i and X_j, $\rho_{X_i,X_j} \in [-1, 1]$

Σ	Set of admissible states
σ	Bank angle
σ	Standard deviation ($\sigma_{(\cdot)} = \sqrt{\sigma^2_{(\cdot)}} = \sqrt{\mathbb{E}((\cdot) - \mathbb{E}(\cdot))^2} = \sqrt{\mathbb{E}((\cdot) - \mu_{(\cdot)})^2}$
σ^2	Variance ($\sigma^2_{(\cdot)} = \mathbb{E}((\cdot) - \mathbb{E}(\cdot))^2 = \mathbb{E}((\cdot) - \mu_{(\cdot)})^2$)
σ_t	Material tensile strength
σ_y	Yield strength
θ	Latitude
$\{\lambda_i\}$	Set of eigenvalues

Script Variables

$\mathcal{A}$	Region of attraction
$\mathcal{C}^n[a, b]$	n times continuously differentiable function on the interval $[a, b]$
$\mathcal{D}$	Open neighborhood of the equilibrium point
$\mathcal{J}(\cdot)$	Objective function
$\mathcal{L}(\cdot)$	Optimal control path cost
$\mathcal{N}(\boldsymbol{\mu}, \boldsymbol{\Sigma})$	Normal random variable with mean $\boldsymbol{\mu}$ and covariance $\boldsymbol{\Sigma}$
$\mathcal{N}(\mu, \sigma^2)$	Normal random variable with mean μ and variance σ^2
$\mathcal{O}$	Big-O complexity
$\mathcal{P}^{(i)}$	Convex cone for the discrete optimal control problem
$\mathcal{Q}^{(i)}$	Convex cone for the discrete optimal control problem
$\mathcal{S}$	Set of sigma points used in the unscented transform, $\boldsymbol{\mathcal{S}} = \{\boldsymbol{\sigma}_i\}$

$\mathcal{T}$	Set of times
$\mathcal{U}$	Set of admissible inputs (controls)
$\mathcal{U}(x_{\min}, x_{\max})$	Uniform random variable which varies between $x_{\min}$ and $x_{\max}$
$\mathcal{V}$	Set of Lyapunov function candidates
$\mathcal{X}_s$	Domain of exponential stability
$\mathcal{Y}$	Set of output functions
$\{\boldsymbol{\mathcal{X}}_i\}$	Set of trial points used in the unscented transform
$\{\boldsymbol{\mathcal{Y}}_i\}$	Set of propagated trial points used in the unscented transform

Variable Superscripts and Subscripts

$(\cdot)_e$	Equilibrium of $(\cdot)$
$(\cdot)^*$	Root value or optimum value of $(\cdot)$
$(\cdot)_0$	Initial value of $(\cdot)$
$(\cdot)_f$	Final value of $(\cdot)$
$(\cdot)_k$	Iterate k of $(\cdot)$
$(\cdot)_T$	Target value of $(\cdot)$
$(\cdot)_{accuracy}$	Accuracy of $(\cdot)$
$(\cdot)_{baseline}$	Reference to the baseline of $(\cdot)$
$(\cdot)_{j\|k}$	Estimate at j given observations up to and including k
$(\cdot)_{miss}$	Miss distance of $(\cdot)$
$(\cdot)_{nom}$	Nominal value of $(\cdot)$

$(\cdot)_{vert}$	Vertical component of $(\cdot)$
$\bar{(\cdot)}$	Mean value of $(\cdot)$
$\hat{(\cdot)}$	Estimate of the mean of $(\cdot)$
$\tilde{(\cdot)}$	Nominal value of $(\cdot)$

Functions and Operators

$(\cdot)^H$	Conjugate transpose of $(\cdot)$
$(\cdot)^T$	Transpose of $(\cdot)$
$(\cdot)^{-1}$	Inverse of $(\cdot)$
$\Im(\cdot)$	Imaginary part of $(\cdot)$
$\lambda_{\max}(\cdot)$	Function which returns the maximum eigenvalue of $(\cdot)$
$\mathbb{E}(\cdot)$	Mathematical expectation of $(\cdot)$
$\Re(\cdot)$	Real part of $(\cdot)$
$P\left[(\cdot)\right]$	Function which returns the probability of $(\cdot)$

Spaces

$\mathbb{C}$	Set of complex numbers
$\mathbb{R}$	Set of real numbers
$\mathbb{R}_+$	Set of all positive real numbers (*i.e.*, $\mathbb{R}_+ = \{x : x \in [0, \infty)\}$)
$\mathbb{Z}$	Set of all integers
$\mathbb{Z}_+$	Set of all positive integers (*i.e.*, $\mathbb{Z}_+ = \{0, 1, 2, 3, \ldots\}$)

SUMMARY

The design of complex systems requires of analyses from numerous disciplines. When each of the disciplines use the same information, have a common set of assumptions, and satisfy the constraints imposed on the design, the design is said to be converged. The convergence process for complex, multidisciplinary designs may be lengthy. Finding an optimal design can be computationally burdensome, particularly for design space exploration when uncertainties are considered. Dynamical systems theory has established techniques for their analysis. Exploiting an analog between the multidisciplinary design problem and dynamical systems enables leveraging of these resources in a new domain. Viewing the multidisciplinary design process as a dynamical system broadens the computational tools available, increases the number of analyses that can be performed, and potentially speeds the design-analysis cycle. Casting this problem as a dynamical system is a departure from the developed techniques applied in multidisciplinary design.

Finding a converged multidisciplinary design can be thought of as a multidimensional root-finding problem. The numerical process to identify the roots of the design is typically an iterative one, where subsequent iteration relies on information from prior iterates. This iteration scheme can employ methods from dynamical systems theory, which evolves a state by a fixed rule. In this work, it is shown that use of root-finding techniques allows the multidisciplinary design problem to be recast as a dynamical system enabling rapid solution using established theory.

In this investigation, theoretical foundations are developed for casting the multidisciplinary design problem as a discrete dynamical system, including handling of

constraints within the design. Three particular techniques from the domain of dynamical system theory are developed and utilized to yield a linear rapid robust design methodology.

1. **Stability analysis**: The existence of a converged design (for a given iteration scheme) is shown to be determinable using dynamical system stability analysis, where the conditions for asymptotic stability are shown to be identically equal to those required for convergence.

2. **Optimal control**: Constraints on the design variables and outputs of the contributing analyses are shown to be accommodated in a similar way that state and control constraints are treated in optimal control theory. Adjoining conditions to the objective function allows handling of both of these constraint types at the same level of the optimization hierarchy.

3. **Estimation theory**: A design's robustness characteristics (*i.e.*, the mean and variance) is shown to be analyzable using a Kalman filter (for linear designs), where the mean state and covariance matrix are products of propagating the filter until the design converges. This technique allows for the accounting of uncertainties within the model itself as well as within the parameters of the design.

Each of these dynamical systems techniques is demonstrated independently as well as in an ensemble in the robust design of engineering systems. As an ensemble, a rapid methodology for robust multidisciplinary design is formulated which finds a conservative upper bound of the variance of the design to a scalar objective function. Analytic test problems are solved to illustrate the benefits of this approach. The developed methodology is then applied to the design of a deployable aerodynamic surface for a strategic system in which an increase in range or an improvement in landed accuracy is sought.

CHAPTER I

BACKGROUND AND MOTIVATION

1.1 Multidisciplinary Design

According to the Accreditation Board in Engineering and Technology *engineering design* is defined as[1]:

> **Definition: Engineering Design**
>
> *Engineering design* is the process of devising a system, component, or process to meet desired needs. It is a decision-making process (often iterative), in which the basic sciences, mathematics, and the engineering sciences are applied to convert resources optimally to meet the stated needs.

This definition lists several important characteristics of engineering design: (1) it is usually an iterative process, (2) it is intended to meet a need (or objective), and (3) it is an optimization process. Consider designing the following

1. A bracket to support a given load
2. A circuit to regulate a voltage
3. The trajectory for an existing vehicle
4. A sensor to take in information and output synthesized information

Each of these have the common trait that the performance (or how well the design satisfies the need) can be quantified explicitly for the environment in which it is expected to perform. In turn, this quantification can guide the design process in order to obtain an optimum. Additionally, given appropriate data, each of these problems

can be designed by a single discipline without the need for outside interaction. Often, the system, component, or process being designed is comprised of many components and disciplines that must have interaction with each other in order to obtain a design that fulfills the stated need. Such is the case when designing

1. A wing for an aircraft
2. A bridge across a body of water
3. A robot that autonomously cleans the floors of a house

Ackoff defines a system as[2]

Definition: System

A *system* is a set of two or more interrelated elements of any kind that satisfies the following conditions:

1. The properties or behavior of each element of the set has an effect on the properties or behavior of the set taken as a whole.
2. The properties and behavior of each element, and the way they affect the whole, depend on the properties and behavior of at least one other element in the set. Therefore, no part has an independent effect on the whole and each is affected by at least one other part.
3. Every possible subgroup of elements in the set has the first two properties: each has a nonindependent effect on the whole. Therefore, the whole cannot be decomposed into independent subsets. A system cannot be subdivided into independent subsystems.

The definition of a system can be extended to include complex systems. For complex systems, there are many contributing analyses (CAs) that contribute to the complete design of the system. The CAs in the design represent an analysis, process, or subsystem in the design of the complex system. In addition, there is generally some control of the inputs into each of the CAs that govern the solution process. This leads to the following extension of the engineering design definition for complex systems.

Definition: Complex System Design

Complex system design is an engineering design where the system, component, or process being designed to meet desired needs is made up of a hierarchy of systems, components, or processes.

When each of the CAs is thought of as a system in and of itself, the complex system may also be referred to as a System of Systems (SoS). There are many definitions of a SoS[3, 4, 5, 6, 7, 8, 9, 10]. Each has separate requirements, such as those in Ref. [9] which require that for a complex system to be a SoS each of the CAs must be independent, have some form of communication, and work towards a common mission. Whereas Ref. [3] requires that a SoS have operational and managerial independence, geographic distribution, emergent behavior, and evolutionary development. The common thread for each of these definitions is that the complex system is composed of several CAs that may each be thought of as systems themselves.

It may be the case in complex system design where the CAs span different domains of expertise (*e.g.*, structures, trajectory, and budget) and design decisions made in one discipline significantly affect the performance in another discipline. In this case, the complex system is referred to as a multidisciplinary design.

Definition: Multidisciplinary Design

Multidisciplinary design is the engineering design of a complex system in which at least two of the contributing analyses are from domains of different disciplines and the performance of one discipline is affected by design decisions in another discipline.

Inherently the design of most aerospace systems is multidisciplinary, which is why it is the multidisciplinary design context that this research is built upon.

1.1.1 Multidisciplinary Analysis vs. Design

Multidisciplinary analysis problems and multidisciplinary design problems are fundamentally complementary—design is an extension of analysis. The difference between the analysis problem and the design problem lies in the existence of requirements. These requirements are constraints that the system, component, or process must meet. In addition, the design problem has a sense of optimality associated with it. One solution to the multidisciplinary design problem involves wrapping an optimizer around a multidisciplinary analysis framework for the desired problem. Constraints in the optimization procedure are then obtained by either directly or indirectly translating the requirements on the system. In the research that follows, it is in this sense that the multidisciplinary design problem is approached, one where the design requirements are handled as constraints. That is, in the research that follows *multidisciplinary design* means the process of finding a vector of design variables, $\mathbf{u}$, for a given set of problem parameters, $\mathbf{p}$, that solves the optimization problem

$$\left.\begin{array}{ll} \textbf{Optimize}: & \mathcal{J}(\mathbf{u},\mathbf{p}) \\ \textbf{Subject to}: & g_i(\mathbf{u},\mathbf{p}) \leq 0, \quad \forall i \in \{1,\ldots,n_g\} \\ & h_j(\mathbf{u},\mathbf{p}) = 0, \quad \forall j \in \{1,\ldots,n_h\} \\ \textbf{By varying}: & \mathbf{u} \end{array}\right\} \tag{1}$$

for a complex system in which at at least two CAs are from disparate disciplines. In the multidisciplinary design problem given by Eq. (1), $\mathcal{J}(\mathbf{u},\mathbf{p})$ is the objective function describing how well the design performs, the $g_i(\mathbf{u},\mathbf{p})$ are the inequality constraint(s) (requirements) to be met, and the $h_j(\mathbf{u},\mathbf{p})$ are the equality constraint(s) (requirements) to be met. Furthermore, the computation of the objective function, $\mathcal{J}(\mathbf{u},\mathbf{p})$, is dependent on several CAs which represent models of disparate disciplines. Whereas, *multidisciplinary analysis* is the process of evaluating $\mathcal{J}(\mathbf{u},\mathbf{p})$, $g_i(\mathbf{u},\mathbf{p})$, and $h_i(\mathbf{u},\mathbf{p})$ for a given set of design variables, $\mathbf{u}$, and problem dependent parameters, $\mathbf{p}$.

1.1.2 Multidisciplinary Design Representations

The vast amount of information required to complete a design, particularly in multidisciplinary problems, can be managed by using a graphical representation of the design. The decomposition of a design into appropriate CAs and identification of information flow has been shown to provide perceptive insight into the design process[11, 12, 13, 14]. The flow of information contributes significantly to the difficulty of the problem[11]. Consider the case when a CA relies on information of a subsequent CA, this is known as a coupled design as the first CA must make assumptions on the information provided by the second and the two must iterate until the information used between the two CAs is consistent. This is a more difficult problem than the non-iterative problem posed when the first CA did not rely on any information from a subsequent CA.

Several traditional techniques exist for the graphical representation of multidisciplinary designs. Amongst these techniques are directed graphs, or digraphs, Program Evaluation and Review Technique (PERT) diagrams, Structured Analysis and Design Technique (SADT) diagrams, and Design Structure Matrices (DSMs) .

Directed graphs represent the design as a mapping of interconnected nodes. In this representation, the nodes represent the CAs and the links represent the information transfer from one CA to another CA and the direction of this transfer[15]. However, node locations are arbitrarily decided which can lend itself to a cluttered and seemingly non-informative diagram for complex systems. PERT diagrams use the fundamental concepts of the directed graphs; however PERT diagrams exhibit an element of time. In this representation, nodes represent milestones of the design with the distance between the nodes representing the time. Along each link between the nodes are the CAs that need to be completed between milestones[16]. The benefit of such a representation is the ability to rapidly identify the critical path of the project and project completion. The downside to the traditional PERT diagram, is that they

lose information regarding the sequence of the CAs between milestones and in particular any iteration that may be required between CAs. SADT represents designs as a system of interconnected boxes and arrows. This method splits out the directed graphs into a box diagram representation. Each CA is its own box diagram and then the CAs are integrated together at a high level. The benefit of SADT is that it allows a structured way to show the information contained within a directed graph, including information feedback. However, ultimately the SADT diagrams provide only a glimpse into the design because the actual information flow from a high level between multiple CAs is not immediately evident without looking within multiple box diagrams. DSMs address the primary shortcomings of the previous techniques by imposing a structure to the design representation. A DSM is a square matrix which maps the information flow between CAs. In the static sense, a DSM is referred to as an N^2 diagram, because if the design is composed on N CAs, the matrix's dimension is $N \times N$[17]. Within the DSM, the nodes along the diagonal of the matrix are the representative CAs while the off-diagonal elements represent information flow. In particular, for a matrix $\mathbf{A}$, element $a_{ij},\ i \neq j$ is non-zero (represented by a dot) if node i provides information to node j. Feedback is readily identified using this technique if $a_{ij} \neq 0,\ i > j$.

Figure 1 shows two representative DSMs for the designs of (a) a launch vehicle and (b) an engine in an automobile[18, 19]. These show two common graphical depictions of the DSM. In each of these diagrams the CAs are represented along the diagonal of the matrix, while the dots connecting links in the upper triangular part of the matrix represent feed-forward information flow and dots in the lower triangular part of the matrix represent feedback information flow. In addition, the size of the dot in the engine example provides an additional piece of information—the strength of coupling between the CAs. Due to the relative clarity in illustrating the CA interactions, this research will rely on the DSM representation of multidisciplinary designs.

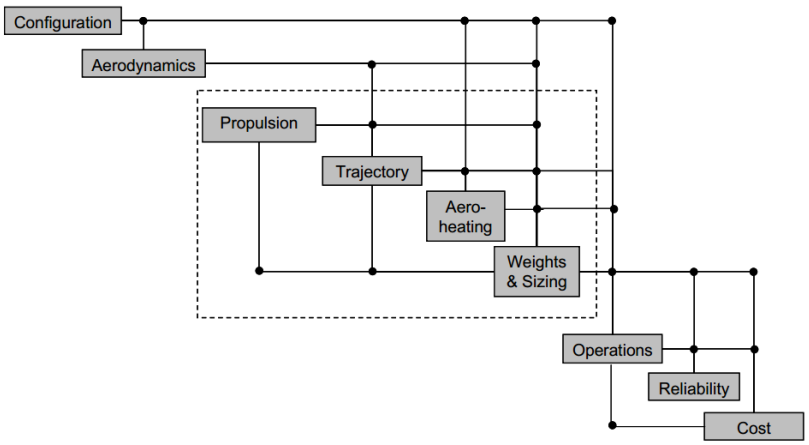

(a)

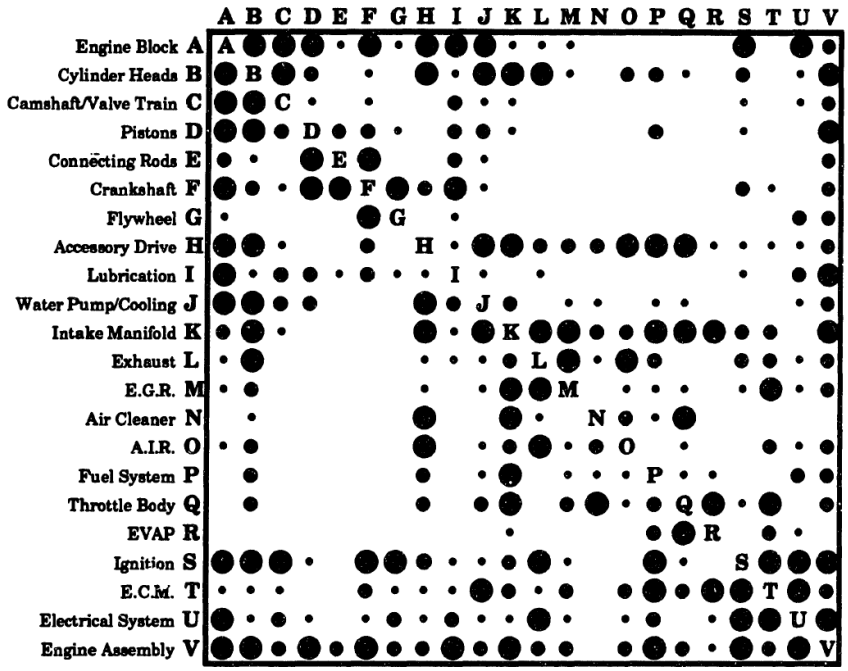

(b)

Figure 1: Sample Design Structure Matrices for the design of (a) a launch vehicle and (b) an automobile engine.

1.1.3 Multidisciplinary Design Optimization

As discussed previously, engineering design implies that there is an optimal solution. The process of identifying this optimum requires implementing a methodology that is more sophisticated than that required by single discipline systems. This is a

consequence of the inherent coupling between CAs in the multidisciplinary problem. Multidisciplinary design optimization (MDO) techniques attempt to overcome the computational burden that is a result of the large number of design variables within the problem, inherent nonlinearities, and multi-objective nature of the problem. The number of design variables in a multidisciplinary design is likely to be significantly larger than that of a single analysis[20, 21]. This computational problem is compounded by the so-called "curse of dimensionality" since the time required to analyze and optimize multidisciplinary problems increase at faster than linear rates[22]. In addition to the computational burden of MDO techniques, there also exist organizational challenges which may cause large coordination efforts to be required in order to transfer the data necessary between CAs[22].

For aerospace applications, monolithic sizing and synthesis codes have been traditionally relied upon. The representation of each discipline within these monolithic codes were principally built upon historical data in order to make the analysis computationally tractable. Advanced conceptual design has pushed the limits of these historical data sets requiring designers to base decisions on either extrapolation of these data or to obtain the disciplinary data using high fidelity analysis. It is in deference to the latter that the majority of the multidisciplinary design analysis/optimization (MDA/O) community has built techniques for coupling sophisticated analysis tools for each CA. Several approaches are surveyed below.

System Sensitivity Analysis: System sensitivity analysis (SSA) is a method for analyzing the system-level total derivatives based on CA-level partial derivatives[23, 24, 25, 26, 27]. The system is described as a set of analyses with vectors of information flowing between the various CAs. The technique then iterates to converge the design more efficiently using the system-level derivative information. In addition, the system-level derivatives can be used with a gradient-based optimizer to find values for certain

system-level design variables that are able to be mathematically removed from the CA level optimizers.

A sample DSM for the use of SSA is shown in Fig. 2 and the resulting global sensitivity equations are shown in Eq. (2)[28].

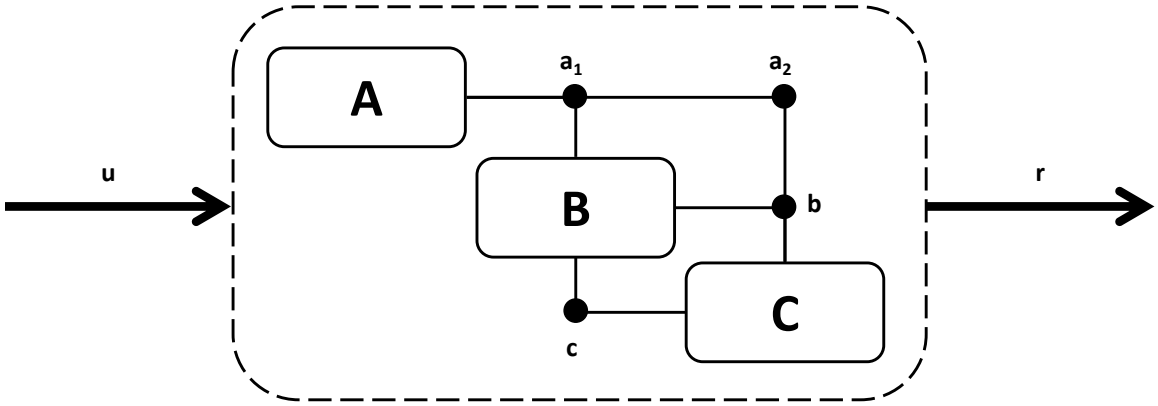

Figure 2: Sample Design Structure Matrix for SSA.

$$\begin{pmatrix} \mathbf{I} & \mathbf{0} & \mathbf{0} & \mathbf{0} & \mathbf{0} \\ \mathbf{0} & \mathbf{I} & \mathbf{0} & \mathbf{0} & \mathbf{0} \\ -\frac{\partial \mathbf{b}}{\partial \mathbf{a}_1} & \mathbf{0} & \mathbf{I} & -\frac{\partial \mathbf{b}}{\partial \mathbf{c}} & \mathbf{0} \\ \mathbf{0} & -\frac{\partial \mathbf{c}}{\partial \mathbf{a}_2} & -\frac{\partial \mathbf{c}}{\partial \mathbf{b}} & \mathbf{I} & \mathbf{0} \\ \mathbf{0} & -\frac{\partial \mathbf{r}}{\partial \mathbf{a}_2} & -\frac{\partial \mathbf{r}}{\partial \mathbf{b}} & \mathbf{0} & \mathbf{I} \end{pmatrix} \begin{pmatrix} \frac{d\mathbf{a}_1}{d\mathbf{u}} \\ \frac{d\mathbf{a}_2}{d\mathbf{u}} \\ \frac{d\mathbf{b}}{d\mathbf{u}} \\ \frac{d\mathbf{c}}{d\mathbf{u}} \\ \frac{d\mathbf{r}}{d\mathbf{u}} \end{pmatrix} = \begin{pmatrix} \frac{\partial \mathbf{a}_1}{\partial \mathbf{u}} \\ \frac{\partial \mathbf{a}_2}{\partial \mathbf{u}} \\ \frac{\partial \mathbf{b}}{\partial \mathbf{u}} \\ \frac{\partial \mathbf{c}}{\partial \mathbf{u}} \\ \frac{\partial \mathbf{r}}{\partial \mathbf{u}} \end{pmatrix} \tag{2}$$

Optimal Decomposition: Instead of changing the methods that each CA employs, optimal decomposition reorganizes the design in order to improve efficiency. This reorganization minimizes the amount of feedback within the design and, when necessary, ensures that coupled CAs are located near each other.

One MDO software implementing optimal decomposition principles is the Design Manager's Aid for Intelligent Decomposition (DeMAID) developed at NASA's Langley Research Center[29]. Given a DSM, relative coupling between CAs, and relative computational expenses, DeMAID will find the optimal order of execution for the multidisciplinary design. This is useful for the case when the DSM organization is not intuitive. More recent methods for the optimal decomposition of a design rely on mutual information to measure the data dependence between CAs or forced-based clustering to discover the sub-graph structure within the design[30].

Optimizer-Based Decomposition: Optimizer-based decomposition (OBD) is a single-level optimization method that eliminates feedforward and feedback loops. The elimination of these loops is done through the use of compatibility constraints which ensure a converged design uses consistent variable values for the coupling variables[31, 32]. Additionally, the potential conflict between the system-level design objectives and CA-level design objectives are eliminated in OBD by allowing all of the design variables to be chosen by the system-level optimizer.

Collaborative Optimization: Collaborative Optimization (CO) is a bi-level decomposition technique where the system level optimizer coordinates the optimization at the lower CA level in order to achieve an overall system objective[33, 34, 31, 35, 36, 37, 38]. The coupling between CAs is handled through compatibility constraints as with OBD; however, these constraints are implemented by assessing the difference in the target value set at the system-level and the actual values used by the CAs. The unique implementation of the compatibility constraints allows distributed optimization of the problem and is therefore more aptly scalable.

1.2 Robust Multidisciplinary Design

1.2.1 Design Uncertainty

Uncertainty is not knowing with certainty a value or an action. More formally, uncertainty is defined as[39]

Definition: Uncertainty

Uncertainty is the quality or state of being indefinite or indeterminate.

The ramifications of uncertainty on design could potentially mean that a design that meets the design requirements and objectives in a deterministic environment may not do so when the design is assessed probabilistically. Uncertainty can be classified in several categories as shown in Table 1.

Table 1: Types of uncertainty in the conceptual design process.

Uncertainty Source	**Description**	**Example**	**Reference**
Physical Modeling	Inaccuracies in the physical modeling of the system	Using an exponential atmosphere to represent the actual atmosphere	[40], [41], [42], [43], [44], [45], [46], [47], [48], [49], [50], [51]
Unknown Operating Conditions	Unknowns in the operating environment of the system	Degraded performance or failure of a satellite in a communications constellation	[52], [53], [54], [55], [56], [28]

Within the design community, an accepted measure of design uncertainty is the spread of the distribution. This can be characterized by the variance, σ^2, or standard deviation, σ, about the mean[57, 58]. Figure 3 shows a normal distribution and it can be seen that the smaller the standard deviation (or variance), the tighter the distribution, while a larger standard deviation (or variance) implies that the spread of the distribution is large.

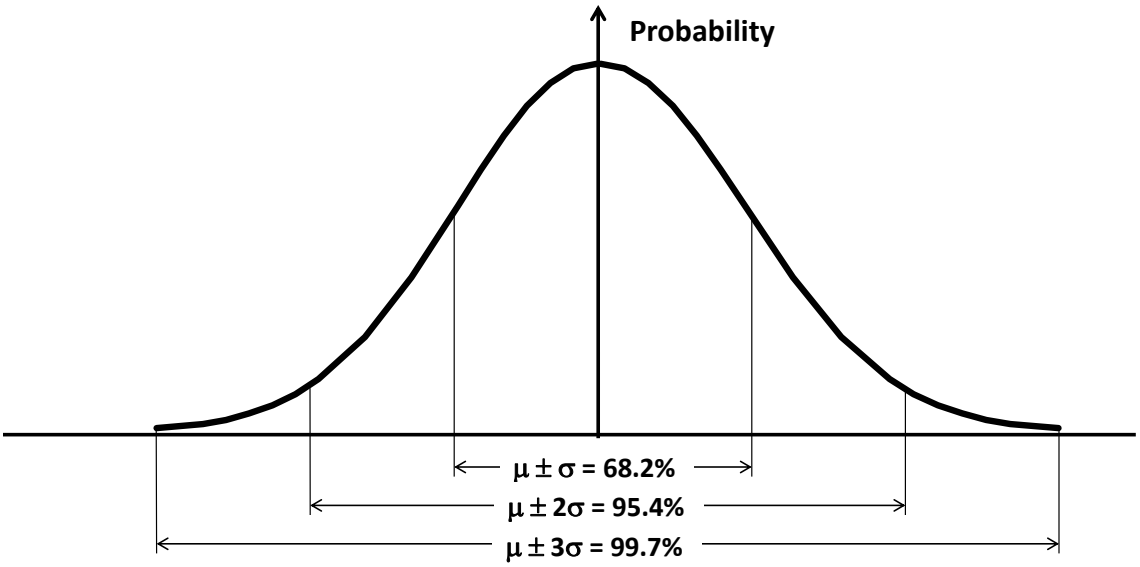

Figure 3: Normal distribution.

1.2.2 Propagating Uncertainty

There are several methods for propagating the uncertainty through a system. The following are current methods that can be used to obtain statistical information for various types of systems:

Analytical Methods: Propagation of the uncertainty through a system can be achieved analytically for a small subset of problems (*e.g.*, linear systems with defined, analytic probability distributions)[59]. For algebraic systems, the exact propagation of the uncertainty is governed by the Liouville equation whereas for dynamical systems uncertainty propagation is governed by the Fokker-Plank-Kolmogorov equation (FPKE)[60, 61, 62]. However, both the Liouville equation and FPKE are partial differential equations whose analytic solution is possible only for stationary distributions and for relatively simplistic systems.

Sampling Methods: Sampling methods, such as Monte Carlo analysis, obtain the

distribution of a given objective function by running successive deterministic simulations with values chosen from random distributions for the stochastic variables associated with the problem[63]. The stochastic variables continue to be sampled and evaluated in the deterministic simulation until a statistically stationary distribution is obtained. The clear advantage of sampling methods are that for a large enough sample size they give the probability distribution being sought and they provide statistical insight into the results. However, the computational runtime can be prohibitive and only in the limit does the resultant probability distribution represent true probability distribution. One way to bypass the computational runtime associated with direct sampling is to use metamodeling techniques to create a curve fit of the system's response. This is called the response surface methodology (RSM) [64, 65, 66, 67, 68]. Commonly, a quadratic equation is used and in this case, the surrogate model is referred to as a second-order response surface equation (RSE) .

Most Probable Point Methods: Most probable point methods obtain an estimate for the cumulative distribution function for probabilistic system design[69, 70, 71, 72, 73, 74, 75, 76, 77, 78, 79, 80, 81]. In particular, these methods take a known input distribution and evaluate it against a constraint function that is a requirement of the design. While there are a wide variety of techniques that can be classified as a most probable point method, these methods generally transform the input distribution into the standard normal space where each of the random variables are assumed to be independent. Using an approximation of the constraint, the first design point is found by minimizing the distance to the mean of the probability density function in standard normal space while satisfying the approximate constraint. The cumulative distribution function is found by allowing the constraint value to vary (*i.e.*, instead of exactly satisfying the constraint function, it satisfies the constraint function plus

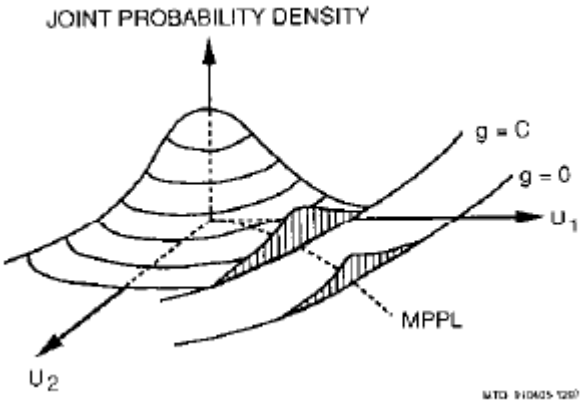

Figure 4: Visualization of the most probable point method with the most probable point locus.

a bias). The probability of exceeding the constraint boundary can then be approximated. This is shown graphically in Fig. 4 where the constraint function is given by g and the locus of the minimum distance to the mean of the probability distance in standard normal space is identified as MPPL[71]. Fast probability integration (FPI) is a well known technique from this class. FPI is an advanced mean value method and was developed at the Southwest Research Institute[78]. The advantage of these methods is the ability to generate accurate results while keeping the number of function evaluations to a computationally tractable value as compared to sampling methods. However, the degree of approximation can greatly alter the accuracy of the results.

Linear Covariance Methods: Linear covariance analysis has its roots in the Kalman filter[82, 83, 84]. Assuming a normal distribution, which is entirely defined by the mean and the variance of the distribution, a covariance matrix describing the initial covariance of the system can be found. The nominal dynamics of the system are then propagated which is assumed to be the mean of the distribution. Next, the dynamics are linearized about the nominal trajectory and the covariance matrix is updated based on optimal estimation theory. The result is a covariance matrix at

each point along the nominal dynamics which can be used to ascertain the joint probability density of the distribution. However, inherently the method does not allow for the analysis of the algebraic systems since there is not a defined dynamical system.

Other Methods: There are several other techniques for propagating the uncertainty through a system. For algebraic systems, these include techniques based on bounding methods, differential analysis, Fourier analysis, polynomial chaos, and reliability analysis[59, 85, 80, 86, 85, 79, 87, 88, 89]. For dynamic systems, these include the use of numerical approximations to the FPKE equation, stochastic averaging, linearization, Gaussian closure, and Gaussian mixture techniques[90, 91, 92, 93, 94, 95, 96, 97, 98]. All of these techniques rely on approximation techniques or are only applicable in situations where the functional form of the system and distribution meet certain requirements (*e.g.*, the system is described by a polynomial).

1.2.3 Robust Design

In design the goal is traditionally to find the best solution to a given objective[99, 100, 101, 102, 103]. However, this optimum could lead to large variations in the objective function around the optimum when the model or operating conditions are uncertain, as is the case in the majority of engineering problems[33, 104]. This motivates the need for robust design where the design is to perform as expected despite these uncertainties.

Definition: Robust Design

Robust design is the process of devising a system, component, or process to meet desired needs and meet a quality standard even in the presence of physical modeling uncertainties and unknown operating conditions.

A graphical depiction of robust design is shown in Fig. 5.

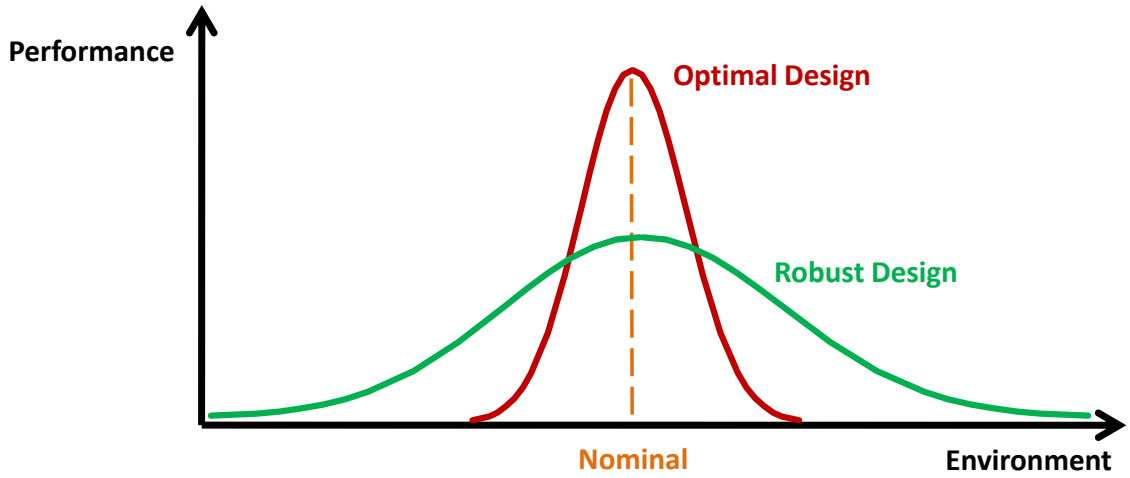

Figure 5: Robust design optimization compared to traditional design optimization.

The objective of robust design is to achieve a trade off between the mean value of the response and the variance[105, 106, 107, 108, 109]. By achieving this compromise between the mean objective value and the variance, the *quality* of the design is improved. The techniques for robust design of systems range from Taguchi methods to more sophisticated methods that are capable of optimizing directly measures of robustness and are briefly surveyed below.

Taguchi Methods: Taguchi robust design is a robust design method that obtains the control (design) variables which yield the least amount of variability to the uncontrollable (noise) factors in the design. This method obtains a robust design by assessing linearized variations in the response to a reduced design space determined through a design of experiments (DOE) in order to enable more rapid design space exploration. The settings for the control variables are then chosen by optimizing the mean squared deviation (MSD), which simultaneously minimizes the variation in the objective function and shifts the mean to the desired target. However, this method shows difficulty when accounting for nonlinear effects, including interactions between control variables, dynamically changing processes, and nonlinear MSD behavior with

control variables. In addition, it only provides a relative measure of robustness rather than an absolute measure and cannot be compared between designs and does not account directly for design constraints[110, 104, 111, 112].

Nonlinear Programming Methods: Other robust design methods use traditional optimization methods in a direct way. In particular, they use nonlinear programming (NLP) methods to formulate the design problem. As opposed to Taguchi methods, these methods are able to directly consider the constraints within the design. Several different objective functions are usually considered. One is an objective function that is a linear combination of the mean response and the spread of the response such as that shown in Eq. (3).

$$\mathcal{J}(\mathbf{u}, \mathbf{p}) = \alpha\mu_r(\mathbf{u}, \mathbf{p}) + \beta\sigma_r(\mathbf{u}, \mathbf{p}) \tag{3}$$

In Eq. (3), α and β are scaling factors or weights, μ_r is the mean response, and σ_r is the standard deviation of the response. Another formulation is in terms of the feasibility. In this case, the objective function is given by

$$\mathcal{J}(\mathbf{u}, \mathbf{p}) = P\left[g_i(\mathbf{u}, \mathbf{p}) \leq 0 \mid h_j(\mathbf{u}, \mathbf{p}) = 0\right] = \int\limits_{\substack{g_i(\mathbf{u},\mathbf{p})\leq 0 \\ h_j(\mathbf{u},\mathbf{p})=0}} f_{\mathbf{up}}(\mathbf{u}, \mathbf{p}) d\mathbf{u} d\mathbf{p} \tag{4}$$

where $f_{\mathbf{up}}(\mathbf{u}, \mathbf{p})$ is the joint probability density function of $\mathbf{u}$ and $\mathbf{p}$.

Practically, obtaining the statistical quantities needed in these objectives (*i.e.*, μ_r, σ_r, or $f_{\mathbf{up}}(\mathbf{u}, \mathbf{p})$) analytically is unlikely. Therefore, the majority of techniques in the literature obtain them by using a sampling method[113, 114, 104, 115]. The downside to this approach is that it can be computationally intractable to optimize on a statistically relevant sample if the function evaluation cost is significant.

One way to reduce the computational cost is by using approximation techniques for the response of the design using a metamodel such as an RSE[116, 117, 118, 119].

However, approximating a complex design space using simplified models can be difficult. Another method for robust design when it is important to identify the feasibility of a design is the extreme condition approach developed by Du and Chen[85]. This approach derives the range of responses by min-max optimizations of the ranges of the input and model uncertainties and then uses the results to find the optimum set of design variables.

Non-statistical Methods: Not all techniques for robust design rely on computing the statistics of the design's response. Some of these include worst case analysis, corner space analysis, and variation patterns. Worst case analysis assumes that all of the system's uncertainties can occur simultaneously in the worst possible combination[120]. The effect on the constraint functions are then estimated based on a Taylor series expansion and this is used to determine the feasibility of the design. Corner space evaluation is a similar concept; however, the variation in design variables and parameters are not used to evaluate the variations in constraints[105]. Instead, a corner space is defined which consists of the vertices of the space defined by the designs close to the target design point when perturbed under uncertainties. Robust designs are then found by ensuring that the corner space touches the original design constraints. Finally, variation patterns exploits the fact that uncertainties may be correlated with each other and is a geometrical technique that identifies robust designs at a given confidence level[121]. The shape of the design variable distribution, or pattern, is determined by their distribution and the size is determined by the confidence level. For regular shapes, this allows rapid searching of robust designs; however, for irregular shapes, the search can be computationally difficult.

1.2.4 Robust Multidisciplinary Design

The concept of robust multidisciplinary design is relatively new and few authors discuss accounting for uncertainties in this context. Work by Gu *et al.* attempt to address this topic by representing model uncertainty as a bias to the system output and applying the concept of worst case analysis combined with sensitivity analysis to obtain a robust design[122, 123, 119]. This method, to date, fails to account for generic uncertain parameter representations and model error estimation. Du and Chen developed two different techniques to perform robustness analysis and design of multidisciplinary systems, system uncertainty analysis (SUA) and concurrent subsystem uncertainty analysis (CSSUA)[124, 125]. These techniques borrow concepts from system sensitivity analysis at both the the local and global level in order to guide the multidisciplinary design process.

System Uncertainty Analysis: SUA uses the mean values of the inputs to determine the mean values of the coupling variables and CA outputs. The mean values are then used to obtain first-order Taylor series approximations for the outputs of each CA which are then used to formulate a linear representation of the entire multidisciplinary design's response. Since the response obtained is linear, uncertainty can be propagated analytically to obtain the mean and variance of the design's response.

Concurrent System Uncertainty Analysis: CSSUA parallelizes the assessment of the variances in SUA. In order to achieve this parallel process, optimization is used to find the mean of each CA output by targeting the mean value of each of the coupling variables. Once these are found, the mean value of the design's response can be found by substituting the mean of the coupling variable with the sub-optimization result. Finally the same technique from SUA is used to obtain the linear representation of the multidisciplinary design's robustness.

1.3 Dynamical Systems

A dynamical system uses a fixed rule to describe the evolution of a state. There are two components of a dynamical system, a state vector which provides the state of the system and a function which is the fixed rule describing how the state will evolve.

Definition: Dynamical System

Dynamical systems are functional relationships where a fixed rule describes how a state evolves. It requires:

1. A state variable (or vector) which characterizes the system
2. A fixed rule describing how the state changes

Consider the ideal pendulum shown in Fig. 6.

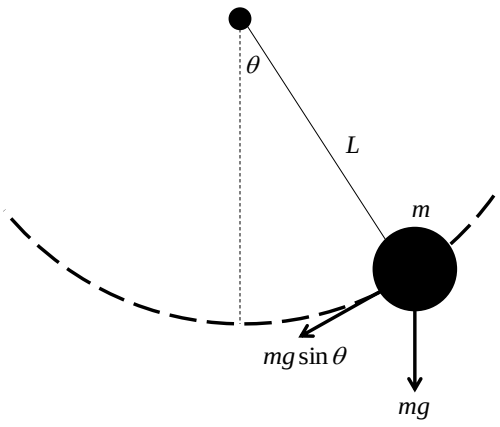

Figure 6: An ideal pendulum.

In this example the bob has a mass m and is attached by a rigid rod of length L to a fixed, frictionless pivot. The state of this dynamical system can be described by two parameters. For this example, consider the angle that the pendulum makes with

the vertical and the rotation rate of the pendulum recognizing there are other states that could be used to describe the bob's motion, such as its horizontal and vertical position. Since gravity pulls the bob down with a force mg, it can be resolved into two components: one which acts parallel to the rod and one which acts perpendicular. Only the second affects the motion of the system. Applying Newton's Second Law for a constant mass, an equation in terms of θ, the angle the pendulum makes with the vertical and the other parameters of the problem is able to be obtained:

$$\ddot{\theta} = -\frac{g}{L}\sin\theta$$

This can be reduced to a first order system by making the substitution, $x_1 = \theta$ and $x_2 = \dot{\theta}$. With a (state) vector denoted as $\mathbf{x} = (x_1\ x_2)^T$, the first-order system is given by

$$\dot{\mathbf{x}} = \begin{pmatrix} \dot{x}_1 \\ \dot{x}_2 \end{pmatrix} = \mathbf{f}(\mathbf{x}) = \begin{pmatrix} x_2 \\ -\dfrac{g}{L}\sin x_1 \end{pmatrix}$$

Where, from the definition of x_1 and x_2, the state variables are explicit in the fixed rule since $x_1 = \theta$, the angular position of the pendulum with respect to the vertical, and $x_2 = \dot{\theta}$, the rotation rate of the pendulum are seen in the function $\mathbf{f}(\mathbf{x})$. Therefore, since the pendulum has (1) a defined state and (2) a fixed rule describing the evolution of the state, it is a dynamical system.

As another example of a dynamical system, consider the amount of money in a bank account. Suppose that the annual interest rate, compounded monthly, is given by r, then the account balance increases by a factor of $(1 + r/12)$ each month. In addition, suppose that a deposit, d, is made every month. In this example, the state, x, is the balance in the account every month. The balance at month $k+1$ is given by

$$x_{k+1} = \left(1 + \frac{r}{12}\right) x_k + d$$

Even though this relationship is given by a discrete, difference relationship, it has both of the components required by a dynamical system: (1) a state and (2) a rule

describing the evolution of the state. Thus, the amount of money in a bank account can be considered a dynamical system.

Finally, consider finding the root of a function $\mathbf{g}(\mathbf{x})$. The root is the value of $\mathbf{x}$ such that the function's value is $\mathbf{0}$. Many numerical methods for finding the root of a function are dynamical systems since they rely on iterative schemes to identify the root [126]. For instance, the bisection method, secant method, function iteration method, and Newton's method are all iterative techniques that satisfy the requirements of a dynamical system. To demonstrate, consider Newton's method of finding a root to the uni-dimensional equation $g(x) = 0$ as shown shown in Fig. 7. An initial guess

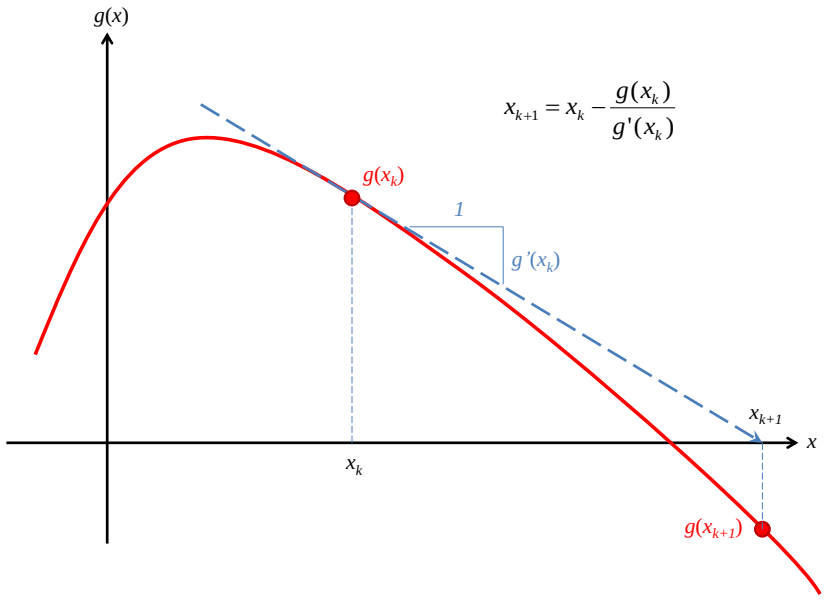

Figure 7: Newton's method for numerically finding the root of a nonlinear equation.

is first taken, x_0. Then $y_0 = g(x_0)$ is computed. If $y_0 = 0$, then x_0 is a root. This, however, is usually not the case. Newton's method approximates the slope of the function at a given point in order to find the root. It is desired to find y_1 such that $y_1 = 0$. At x_0, an approximation for the slope is given by

$$g'(x_0) = \frac{\Delta y}{\Delta x} = \frac{y_1 - y_0}{x_1 - x_0} = \frac{0 - g(x_0)}{x_1 - x_0}$$

When this relationship is rearranged for x_1 the following results

$$x_1 = x_0 - \frac{g(x_0)}{g'(x_0)}$$

This can be generalized for any iterate k

$$x_{k+1} = x_k - \frac{g(x_k)}{g'(x_k)}$$

This relationship has the necessary components to be a dynamical system: (1) a state, in this case x, and (2) a fixed rule describing how x evolves with iteration.

1.4 Previous Use of Dynamical System Concepts in Multidisciplinary Design

Several investigators have applied concepts from dynamical systems in analyzing and designing complex multidisciplinary systems.

One example which couples dynamical system concepts with multidisciplinary design is given by Appa and Argyris in Ref. [127]. They use dynamical system theory to simultaneously optimize the structure and trajectory of an aircraft. System identification is used to characterize in a generalized state the nonlinear CAs of the system using regression or neural network methods. The derivatives of the dynamic properties of the aircraft can also be found using system identification. These are then coupled with the dynamic equations of motion for the system in order to form a functional in terms of the physical state variable and the generalized states. While their work embraces multiple aspects of dynamical systems theory and satisfies the definition of a dynamical system as they define both a state and how that state evolves, they provide little detail on how they transformed the original problem into the state space and their solution methods. Furthermore, their work requires that the design variables appear explicitly in the modeling of the CAs for the system, (*i.e.*, where the model is given by $\mathbf{f}(\mathbf{u}, \mathbf{p})$ instead of $\mathbf{f}(\mathbf{g}(\mathbf{u}), \mathbf{p})$). This functional form prohibits coupling between CAs and is therefore limited in the set of applicable problems.

Smith and Eppinger use stability concepts in the organization of a multidisciplinary design process[128]. Their work decomposes a DSM using eigenvectors in order to minimize the feedback within the design. In this representation each of the links between CAs is given a relative strength for the connection. Then the "modes" are analyzed to identify the strongest connection. Although not explicitly described in their work, by performing a modal analysis on the organization structure, an implicit state is assumed, that of the information communicated between each of the CAs. This state concept is identical to that used in this work. A similar organizational decomposition was made using game theory ideas by Lewis and Mistree[129]. This work iteratively anticipates the dependence of each CA on another and uses that information to decompose the design for CAs that are lightly dependent on each other. This work defines a state as the dependency of each CA on each other.

Others have combined an explicit dynamical system—that of the trajectory of a vehicle—with multidisciplinary design. For instance, Delaurentis developed a methodology that probabilistically designed a multidisciplinary system at multiple levels of the DSM hierarchy[41]. In this work, he employed metamodeling techniques for response surface equations to design a vehicle in order to achieve a system level objective that includes both performance objectives (*e.g.*, range and stability) and system level considerations (*e.g.*, weight). The developed metamodels contain variables for the control system that directly impact the vehicle's dynamical equations of motion which govern the performance of the aircraft. The vehicle's performance as well as other sizing and synthesis components are accounted for, making it a multidisciplinary design; however, the use of dynamical system theory is limited to designing the control system of the aircraft through the explicit equations of motion.

Work by Grant uses optimal control theory in order to simultaneously design the trajectory and vehicle geometry for an entry, descent, and landing system[130, 131]. This work exploits dynamical system theory fully, albeit for a specific system in which

the equations of motion are a function of the vehicle geometry and does not require iteration between the CAs to converge the design. In turn, the problem is collapsed to the design of a *system* as opposed to a general *multidisciplinary design*.

A summary of this previous work with a comparison to the methods presented in this investigation is provided in Table 2.

Table 2: Some previous uses of dynamical system concepts in design.

Investigator	**Description**	**Multidisciplinary**	**Design Relevant State**	**Explicit Dynamical System**	**Design Covergence**	**Design Optimization**	**Stability**	**Control**	**Estimation**
Appa & Argyris[127]	Simultaneously optimized structure and trajectory of an aircraft; model given by $\mathbf{f}(\mathbf{g}(\mathbf{u}), \mathbf{p})$ and limits coupling between CAs	◐	●	●	○	◐	○	●	○
Smith & Eppinger[128]	Decomposes a DSM for an organization based on the eigenstructure	●	◐	○	○	○	◐	○	○
Lewis & Mistree[129]	Uses game theory to decompose an organizational DSM	●	◐	●	◐	○	◐	○	○
Delaurentis[41]	Uses metamodels to design an aircraft considering stability and trajectory constraints	●	○	◐	○	○	◐	◐	○
Grant[130, 131]	Simultaneously performs trajectory and shape optimization; collapses into a single analysis	◐	●	●	○	●	○	●	○

●: Characteristic as used in this study
◐: Characteristic used, but differently than in this study
○: Characteristic not used

1.5 Study Overview and Objectives

A general multidisciplinary design problem features coupling and feedback between CAs. This feedback may lead to convergence issues requiring significant iteration in order to obtain a feasible design.

Because finding a converged multidisciplinary design can be thought of as a multi-dimensional root-finding problem, an iteration scheme can be developed for the state vector, where the subsequent iteration relies on information from prior iterates. The process of finding the root iteratively will be shown to be identical to the that of solving a dynamical system. Therefore, the multidisciplinary design problem can be cast as dynamical system where the state is the iteration-dependent data required by each of the disciplines comprising the design. Casting the multidisciplinary design problem as dynamical system enables leveraging techniques associated with the dynamical system field in order to overcome some of the traditional shortcomings of multidisciplinary design techniques, such as the computational burden required by the iteration and the potentially conflicting objectives between CA-level and system-level optimizations.

Rigorous description for casting the multidisciplinary design problem as a dynamical system, including handling of equality and inequality constraints within the design will be provided. Three areas from dynamical system theory are chosen for detailed investigation: stability analysis, optimal control, and estimation theory. Stability analysis is used to investigate the existence of a solution to the design problem. This analysis can be broadened to investigating the range of initial guesses that provide guaranteed convergence for different iteration schemes. Optimal control techniques allow the requirements associated with the design to be incorporated into the system and allow for constraints that are functions of both the CA outputs and input values to be handled simultaneously. Finally, estimation methods are employed to obtain an evaluation of the robustness of the multidisciplinary design.

These three dynamical system techniques are then combined in a complete methodology for the rapid robust design of a linear multidisciplinary design. The developed robust design methodology allows for uncertainties both within the models as well as the parameters of the multidisciplinary problem. While linear multidisciplinary designs are not common, extension to nonlinear designs is achievable through successive linearization of the design or through an alternate estimation technique. A description of the appropriate domains of applicability for this linear technique is provided in this thesis.

As observed in Table 2, this study is the only one to apply dynamical system theory from the domains of stability, control, and estimation to the general multidisciplinary design problem to address design convergence and optimization. In addition, it is the only one to apply estimation theory to the quantify the uncertainty associated with a design's response.

1.6 Thesis Organization

The remaining portions of this thesis are organized as follows:

- **Chapter 2** provides the theoretical context for this work. Included in this discussion is a definition of the state and discrete dynamical systems which enable the casting of the multidisciplinary design problem in the form of a dynamical system. In addition, the theoretical foundation for several other techniques utilized within this work (*e.g.*, root-finding methods, covariance matrices, matrix norms, and unscented transform) are described. Finally, the chapter concludes with a discussion of how to cast the multidisciplinary design problem as a discrete dynamical system.

- **Chapter 3** demonstrates how to apply various techniques from dynamical system theory to the multidisciplinary design problem. These techniques include using concepts from stability analysis, control theory, and estimation theory.

Stability analysis can be used to determine whether a design is feasible, whether an optimal design exists, the range of initial values that can be used to converge the design, and the rate at which the design will converge. Control theory is able to be used to enforce constraints that are functions of the CA's output and the design variables at the same level in the optimization hierarchy. Finally, techniques with roots in estimation theory can be used to propagate uncertainty through the multidisciplinary design, leading to a way to simultaneously converge the design and quantify the uncertainty associated with that design point. For each of these dynamical system techniques, the theory underlying their use is summarized followed by a discussion of how the technique can be used in context of the multidisciplinary design problem.

- **Chapter 4** integrates the techniques described in Chapter 3 into a rapid robust design methodology for linear multidisciplinary design which is capable of extension to nonlinear multidisciplinary design through the use of successive linearization. Within this chapter are formulations of the rapid robust design methodology using two root-finding techniques—fixed-point iteration and Newton-Raphson iteration.

- **Chapter 5** demonstrates each of the dynamical system techniques developed in illustrative multidisciplinary design problems. This chapter pedagogically progresses from relatively straight-forward analytical examples to more complex practical examples. The chapter concludes with applying the developed methodology to the design of a deployable aerodynamic surface for a strategic system.

- **Chapter 6** discusses the extensibility of the rapid robust design methodology from both computational and accuracy perspectives. The effect of problem scaling on computational cost is considered by examining the number of design

variables, number of CAs, nonlinearity of the CAs, and nonlinearity of the response. In addition to computational cost, the accuracy of applying a method with linear fundamentals to nonlinear problems is examined through nonlinear perturbation analysis to identify the region of applicability for the method.

- **Chapter 7** provides a summary of the thesis and its academic contributions. In addition, various avenues for future work are discussed.

1.7 Academic Contributions

This thesis advances the state-of-the-art in the design and analysis of multidisciplinary systems. The multidisciplinary design problem is recast as a dynamical system enabling new analyses to be performed and for a rapid robust design methodology to be produced. The academic contributions of this research are summarized as follows:

Formulation of the General Multidisciplinary Design Problem as a Dynamical System In Order to Leverage Established Techniques from Dynamical System Theory

The convergence and optimization of a multidisciplinary design are root-finding problems, where the iterative techniques used to find the their solutions meet the requirements of a dynamical system. In turn, this allows the application of established methods from dynamical systems to be applied to multidisciplinary design. Leveraging these techniques from dynamical system theory, the multidisciplinary design process is shown to be more computationally tractable while yielding additional insight into the problem.

Application of the Dynamical System Domain to the Multidisciplinary Design Problem

The applicability of dynamical system techniques to the multidisciplinary design problem will be shown through application of three different areas—stability, control, and estimation. These techniques are chosen for the speed and knowledge they provide relative to traditional MDO techniques as well as their use in formulating a rapid robust design methodology.

Stability Analysis: Stability theory provides insight into the existence of a design based on the convergence procedure being utilized. For linear, constant coefficient systems, stability can be checked through eigenanalysis. For more general designs, the existence of a converged design can be identified through Lyapunov techniques. Lyapunov techniques can also identify domains for which initial guesses result in converged designs as well as to assess information regarding the rate of convergence.

Control Theory: Optimal control techniques allow constraints that are a function of both the CA output and the design variables to be included at the same level of the design hierarchy. This is a departure from many traditional MDO techniques, where only constraints that are an explicit function of the design variables are considered. By allowing for both types of constraints to be considered simultaneously, a coordinated search of potential designs ensues which is capable of providing computational efficiency.

Estimation Techniques: Estimation theory provides a means to obtain a rapid estimate of the mean and variance of the design. These estimates are provided by propagating additional equations alongside the convergence relations. Furthermore, design decomposition can be guided through the use of these techniques.

Development of a Linear Technique for the Rapid Robust Design of a Multidisciplinary System

Integrating these three areas of dynamical system theory together, a procedure for the rapid robust design of a linear multidisciplinary system is produced. This methodology provides a bound on the variance through the use of the matrix two-norm and is applicable to nonlinear designs through successive linearization. The domain of applicability of this rapid robust design methodology is quantified with respect to design complexity, including nonlinearity. This design methodology is also demonstrated on a suite of analytical and practical test problems.

Application of the Multidisciplinary Design Methodology to a Design Example of Relevance to the Entry, Descent, and Landing Community

In addition to other test problems, a design example which obtains robust designs for a deployable device that either increases the range or accuracy of a strategic system is provided. This design example considers both the design of the deployable as well as the selection of a guidance algorithm with comparisons to a contemporary robust design methodology.

CHAPTER II

CASTING THE MULTIDISCIPLINARY DESIGN PROBLEM AS A DYNAMICAL SYSTEM

This chapter provides the theoretical background for casting the multidisciplinary design problem as a dynamical system beginning with a discussion of the enabling theoretical foundations. These include a rigorous definition of the state and a discrete dynamical system. This is followed by a mathematical description of several numerical root-finding schemes and how each satisfies the criterion to be dynamical system. Theoretical foundations for several other techniques utilized within this work are then discussed including the covariance matrix, matrix norms, and a more rigorous discussion of various methods for propagating uncertainty through mathematical mappings. The chapter then concludes with a discussion of how to cast the multidisciplinary design problem as a nested discrete dynamical system where feasible designs are identified and then optimized.

2.1 Enabling Theoretical Foundations

2.1.1 The Concept of a State

The concept of a state is fundamental in transforming the multidisciplinary design problem to a dynamical system. It is a summary of the status of the system at a particular instance.

Definition: State

The *state* consists of the minimum set of parameters that completely summarize the internal status of the dynamical system in the following sense: at any time $t_0 \in \mathcal{T}$ the state $\mathbf{x}(t_0)$ is known, then the output at a future instance in time, $t_1 \in \mathcal{T}$, $\mathbf{y}(t_1)$ where $t_1 > t_0$ can be uniquely determined for a given evolution scheme provided the input $\mathbf{u}_{[t_0,t_1]} \in \mathcal{U}$ is known.

In this work, two states will be considered—one which describes the output of the CAs for the convergence of the design and another which describes the design variables during the optimization of the design.

2.1.2 Mathematical Definition of a Dynamical System

Mathematically, a dynamical system is a set of times $\mathcal{T}$, spaces $\mathcal{U}$, Σ, and $\mathcal{Y}$, and transformations $\mathbf{g} : \mathcal{T}\times\mathcal{T}\times\Sigma\times\mathcal{U} \to \Sigma$ and $\mathbf{h} : \mathcal{T}\times\Sigma\times\mathcal{U}^s \to \mathcal{Y}^t$. The transformations $\mathbf{g}$ and $\mathbf{h}$ are such that[132]

$$\mathbf{x}(t_1) = \mathbf{g}(t_0, t_1, \mathbf{x}(t_0), \mathbf{u}_{[t_0,t_1]})$$

and

$$\mathbf{y}(t_1) = \mathbf{h}(t_1, \mathbf{x}(t_1), \mathbf{u}(t_1))$$

The sextuple, $(\mathcal{T}, \mathcal{U}, \Sigma, \mathcal{Y}, \mathbf{g}, \mathbf{h})$, defines a dynamical system provided the transformations have the following properties:

1. **Identity Property**: for every $t_0, t_1 \in \mathcal{T}$,

$$\mathbf{x}(t_0) = \mathbf{g}(t_0, t_0, \mathbf{x}(t_0), u_{[t_0,t_1]})$$

2. **State Transition Property**: for every $\mathbf{u} \in \mathcal{U}$, $\mathbf{v} \in \mathcal{U}$ such that $\mathbf{u} = \mathbf{v}$ over an interval $[t_0, t_1] \in \mathcal{T}$, then

$$\mathbf{g}(t_0, t_1, \mathbf{x}(t_0), \mathbf{u}_{[t_0,t_1]}) = \mathbf{g}(t_0, t_1, \mathbf{x}(t_0), \mathbf{v}_{[t_0,t_1]})$$

3. **Semigroup Property**: for every $t_0, t_1, t_2 \in \mathcal{T}$ and $t_0 < t_1 < t_2$,

$$\begin{aligned}
\mathbf{x}(t_2) &= \mathbf{g}(t_0, t_2, \mathbf{x}(t_0), \mathbf{u}_{[t_0,t_2]}) \\
&= \mathbf{g}(t_1, t_2, \mathbf{x}(t_1), \mathbf{u}_{[t_1,t_2]}) \\
&= \mathbf{g}(t_1, t_2, \mathbf{g}(t_0, t_1, \mathbf{x}(t_0), \mathbf{u}_{[t_0,t_1]}), \mathbf{u}_{[t_1,t_2]})
\end{aligned}$$

The first of these properties is a statement that $\mathbf{g}$ is an identity transformation whenever the arguments are the same. The second says that this causal dynamical system does not depend on inputs prior to t_0 since those inputs determined $\mathbf{x}(t_0)$ and similarly $\mathbf{x}(t_1)$ does not depend on inputs after t_1. This is referred to as the state transition property. The third property says it is irrelevant how $\mathbf{x}(t_2)$ is computed, whether it be directly from $\mathbf{x}(t_0)$ and $\mathbf{u}_{[t_0,t_2]}$ or if $\mathbf{x}(t_1)$ is obtained first from $\mathbf{x}(t_0)$ and $\mathbf{u}_{[t_0,t_1]}$ and then used to compute $\mathbf{x}(t_2)$ with $\mathbf{u}_{[t_1,t_2]}$.

It is important to note that in the mathematical definition the transformation $\mathbf{g}$ that describes a dynamical system is not required to be described by a differential equation, although this is the case in many instances and fulfills the three required properties.

2.1.3 Discrete Dynamical Systems

The framework developed for this work relies on discrete dynamical systems. That is, a dynamical system of the form

$$\left.\begin{aligned}
\mathbf{x}_{k+1} &= \mathbf{f}(\mathbf{x}_k, \mathbf{u}_k, k) \\
\mathbf{y}_k &= \mathbf{g}(\mathbf{x}_k, \mathbf{u}_k, k)
\end{aligned}\right\} \tag{5}$$

where $\mathbf{x}$ is the state of the system, $\mathbf{f}$ is a function which describes the time evolution of the system, $\mathbf{u}$ is the input into the system, and k is the iterate number. A specific instance of Eq. (5) that is used throughout this work is a linear, discrete dynamical

system, which is given by

$$\left.\begin{aligned} \mathbf{x}_{k+1} &= \mathbf{A}_k\mathbf{x}_k + \mathbf{B}_k\mathbf{u}_k \\ \mathbf{y}_k &= \mathbf{C}_k\mathbf{x}_k + \mathbf{D}_k\mathbf{u}_k \end{aligned}\right\} \tag{6}$$

Graphically, this is shown in the block diagram shown in Fig. 8.

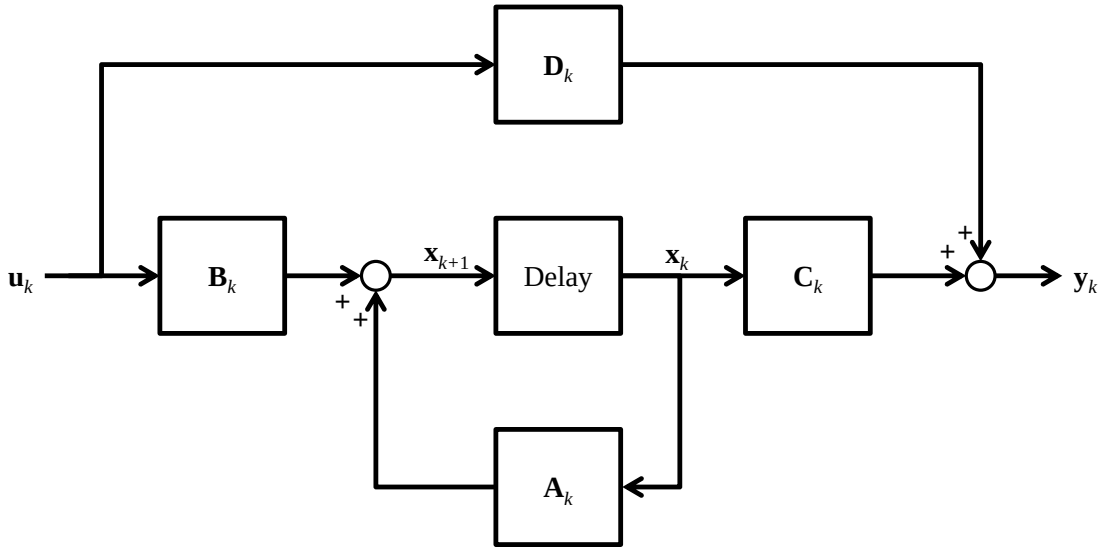

Figure 8: Block diagram of a linear, discrete dynamical system.

2.1.4 Root-Finding Methods

Root-finding methods consider an equation of the form

$$\mathbf{f}(\mathbf{x}) = \mathbf{0} \tag{7}$$

where a root, $\mathbf{x}^*$, that satisfies Eq. (7) (*i.e.*, $\mathbf{f}(\mathbf{x}^*) = \mathbf{0}$) is sought.

2.1.4.1 Fixed-Point Iteration

Fixed-point iteration is a straight-forward method for finding the root of a function. It does not rely on derivative information, and in general has linear convergence properties. The fundamental concept behind the method is that there exists a fixed-point for a transformed form of Eq. (7)

$$\mathbf{x} = \mathbf{g}(\mathbf{x}) \tag{8}$$

where the iteration is prescribed by

$$\mathbf{x}_{k+1} = \mathbf{g}(\mathbf{x_k}) \tag{9}$$

The algorithm is as follows

Algorithm: Fixed-Point Iteration

Transform $\mathbf{f}(\mathbf{x}) = \mathbf{0}$ to $\mathbf{x} = \mathbf{g}(\mathbf{x})$;
Choose an initial guess $\mathbf{x}_0$ in $[\mathbf{a}, \mathbf{b}]$;
for *k=0,1,2,...* **do**
  $\mathbf{x}_{k+1} = \mathbf{g}(\mathbf{x}_k)$;
  if $\| \mathbf{x}_{k+1} - \mathbf{x}_k \| < \epsilon$ **then**
    $\mathbf{x}^* = \mathbf{x}_{k+1}$;
    return $\mathbf{x}^*$;
  else
    continue;
  end
end

Consider the following proposition[133]

Proposition 1. *Define* $\{\mathbf{x}_k\}_0^\infty$ *using* $\mathbf{x}_{k+1} \triangleq \mathbf{g}(\mathbf{x}_k)$ *as described in the algorithm above. If* $\{\mathbf{x}_k\}_0^\infty$ *converges to a limit* $\mathbf{x}^*$ *and the function* $\mathbf{g}$ *is continuous at* $\mathbf{x} = \mathbf{x}^*$*, then the limit,* $\mathbf{x}^*$*, is a root of* $\mathbf{f}(\mathbf{x}) : \mathbf{f}(\mathbf{x}^*) = \mathbf{0}$

Proof. Assume that $\{\mathbf{x}_k\}_0^\infty$ converges to some value $\mathbf{x}^*$. Since $\mathbf{g}$ is continuous, the definition of continuity implies that

$$\lim_{k\to\infty} \mathbf{x}_k = \mathbf{x}^* \Rightarrow \lim_{k\to\infty} \mathbf{g}(\mathbf{x}_k) = \mathbf{g}(\mathbf{x}^*)$$

Therefore, using this fact, the proposition can be proven by noting

$$\mathbf{g}(\mathbf{x}^*) = \lim_{k\to\infty} \mathbf{g}(\mathbf{x}_k) = \lim_{k\to\infty} \mathbf{x}_{k+1} = \mathbf{x}^*$$

Thus, $\mathbf{g}(\mathbf{x}^*) = \mathbf{x}^*$ and since the equation $\mathbf{g}(\mathbf{x}) = \mathbf{x}$ is equivalent to the original one $\mathbf{f}(\mathbf{x}) = \mathbf{0}$, it can be concluded that $\mathbf{f}(\mathbf{x}^*) = \mathbf{0}$. □

This method to find the root is graphically shown in Fig. 9 where two curves are shown, one for $y = g(x)$ and another for $y = x$. These are the two sides of the fixed-point iteration equation.

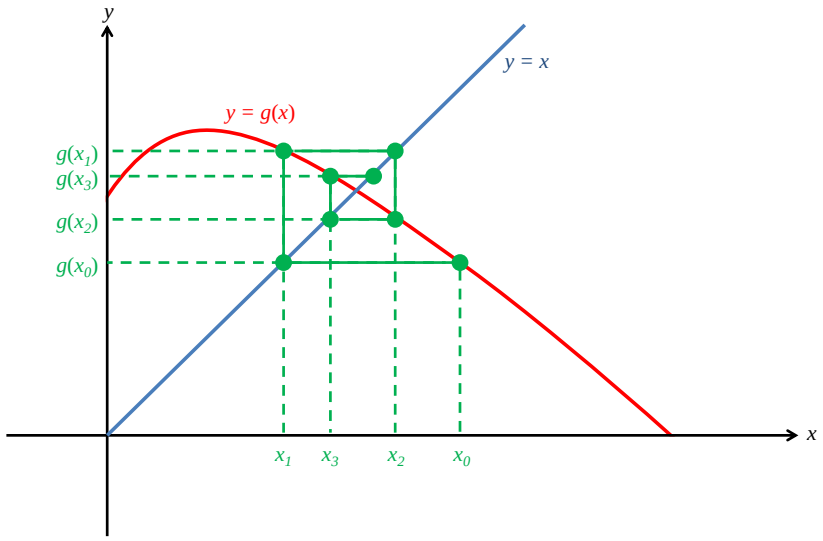

Figure 9: Visual represent ion of the fixed-point iteration root-finding method.

It is important to note that fixed-point iteration inherently fits the definition of a discrete dynamical system described by Eq. (5) with no dependence on $\mathbf{u}_k$ and k. However, it is clear that the iteration scheme meets the criterion of a dynamical system as it (1) has a defined state, the value of the root $\mathbf{x}$, and (2) a fixed-rule that describes its evolution with iteration (time). Furthermore, by inspection $\mathbf{g}(\mathbf{x})$ satisfies the identity and semigroup properties. Since there is no dependence on additional input (*i.e.*, $\mathbf{u}$) the iteration scheme also satisfies the state-transition property.

2.1.4.2 Newton-Raphson Iteration

As briefly described in the previous chapter, Newton-Raphson iteration is a first-order method to root-finding. It has roots in the Taylor series expansion of the function and uses successive linearization, as shown in Fig. 10, to find the root of the function

described by Eq. (7). The iteration scheme is given by

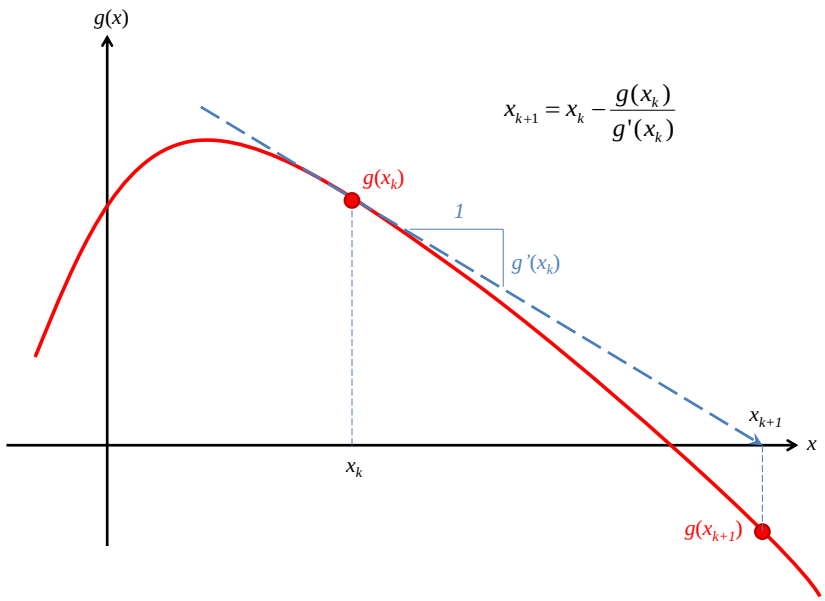

Figure 10: Newton's method for numerically finding the root of a nonlinear equation.

$$\mathbf{x}_{k+1} = \mathbf{x}_k - \left(\frac{\partial \mathbf{f}(\mathbf{x}_k)}{\partial \mathbf{x}_k} \right)^{-1} \mathbf{f}(\mathbf{x}_k) \tag{10}$$

As derivative information is used, it is expected that this method will converge to the root faster than fixed-point iteration. Indeed this is true, as the method converges at quadratic rates; however, ascertaining the derivative information requires additional function evaluations.

The algorithm for Newton-Raphson iteration is found below. Note that there are variants of this algorithm which do not require the computation of the inverse of the Jacobian and instead solve the system directly for the step size using efficient computation methods (*e.g.*, LU decomposition).

Algorithm: Newton-Raphson Iteration

Choose an initial guess $\mathbf{x}_0$ in $[\mathbf{a}, \mathbf{b}]$;
for *k=0,1,2,...* **do**
  $\mathbf{J} = \frac{\partial \mathbf{f}(\mathbf{x}_k)}{\partial \mathbf{x}_k}$;
  $\mathbf{x}_{k+1} = \mathbf{x}_k - \mathbf{J}^{-1}\mathbf{f}(\mathbf{x}_k)$;
  if $\| \mathbf{x}_{k+1} - \mathbf{x}_k \| < \epsilon$ **then**
    $\mathbf{x}^* = \mathbf{x}_{k+1}$;
    return $\mathbf{x}^*$;
  else
    continue;
  end
end

The following proposition describes the convergence of Newton-Raphson iteration to the root[133]

Proposition 2. *Assume that* $\mathbf{f} \in \mathcal{C}^2[\mathbf{a}, \mathbf{b}]$ *and* $\exists \mathbf{x}^* \in [\mathbf{a}, \mathbf{b}]$ *where* $\mathbf{f}(\mathbf{x}^*) = \mathbf{0}$. *If* $\left.\frac{\partial \mathbf{f}}{\partial \mathbf{x}}\right|_{\mathbf{x}^*} \neq \mathbf{0}$, *then* $\exists \boldsymbol{\delta} > \mathbf{0}$ *such that* $\{\mathbf{x}_k\}_0^\infty$ *using*

$$\mathbf{x}_{k+1} = \mathbf{x}_k - \left(\frac{\partial \mathbf{f}(\mathbf{x}_k)}{\partial \mathbf{x}_k}\right)^{-1} \mathbf{f}(\mathbf{x}_k)$$

will converge to $\mathbf{x}^*$ *for any initial approximation* $\mathbf{x}_0 \in [\mathbf{x}^* - \boldsymbol{\delta}, \mathbf{x}^* + \boldsymbol{\delta}]$.

Proof. Consider the first-degree Taylor polynomial and its remainder term

$$\mathbf{f}(\mathbf{x}) = \mathbf{f}(\mathbf{x}_0) + \frac{\partial \mathbf{f}(\mathbf{x}_0)}{\partial \mathbf{x}_0}(\mathbf{x} - \mathbf{x}_0) + \frac{1}{2}(\mathbf{x} - \mathbf{x}_0)^T \frac{\partial^2 \mathbf{f}(\mathbf{x}_0)}{\partial^2 \mathbf{x}_0}(\mathbf{x} - \mathbf{x}_0)$$

Using the fact that $\mathbf{f}(\mathbf{x}^*) = \mathbf{0}$ yields

$$\mathbf{0} = \mathbf{f}(\mathbf{x}_0) + \frac{\partial \mathbf{f}(\mathbf{x}_0)}{\partial \mathbf{x}_0}(\mathbf{x} - \mathbf{x}_0) + \frac{1}{2}(\mathbf{x} - \mathbf{x}_0)^T \frac{\partial^2 \mathbf{f}(\mathbf{x}_0)}{\partial^2 \mathbf{x}_0}(\mathbf{x} - \mathbf{x}_0)$$

If $\mathbf{x}_0$ is close enough to $\mathbf{x}^*$ then the second-order term will be small compared to the rest of the terms

$$\mathbf{0} \approx \mathbf{f}(\mathbf{x}_0) + \frac{\partial \mathbf{f}(\mathbf{x}_0)}{\partial \mathbf{x}_0}(\mathbf{x} - \mathbf{x}_0)$$

Solving for $\mathbf{x}^*$ yields

$$\mathbf{x}^* \approx \mathbf{x}_0 - \left(\frac{\partial \mathbf{f}(\mathbf{x}_0)}{\partial \mathbf{x}_0}\right)^{-1} \mathbf{f}(\mathbf{x}_0)$$

which can be used to define the next approximation, $\mathbf{x}_1$ to the root

$$\mathbf{x}_1 = \mathbf{x}_0 - \left(\frac{\partial \mathbf{f}(\mathbf{x}_0)}{\partial \mathbf{x}_0}\right)^{-1} \mathbf{f}(\mathbf{x}_0)$$

which leads to the general rule

$$\mathbf{x}_{k+1} = \mathbf{x}_k - \left(\frac{\partial \mathbf{f}(\mathbf{x}_k)}{\partial \mathbf{x}_k}\right)^{-1} \mathbf{f}(\mathbf{x}_k)$$

Note that this general recursive relation is analogous to the fixed-point relation $\mathbf{x}_{k+1} = \mathbf{g}(\mathbf{x}_k)$. It can be shown that

$$\begin{aligned}\frac{\partial \mathbf{g}(\mathbf{x})}{\partial \mathbf{x}} &= \mathbf{I} - \left(\frac{\partial \mathbf{f}(\mathbf{x})}{\partial \mathbf{x}}\right)^{-T} \left[\frac{\partial \mathbf{f}(\mathbf{x})}{\partial \mathbf{x}} \frac{\partial \mathbf{f}(\mathbf{x})}{\partial \mathbf{x}} - \frac{\partial^2 \mathbf{f}(\mathbf{x})}{\partial^2 \mathbf{x}} \mathbf{f}(\mathbf{x})\right] \left(\frac{\partial \mathbf{f}(\mathbf{x})}{\partial \mathbf{x}}\right)^{-1} \\ &= \left(\frac{\partial \mathbf{f}(\mathbf{x})}{\partial \mathbf{x}}\right)^{-T} \left[\frac{\partial^2 \mathbf{f}(\mathbf{x})}{\partial^2 \mathbf{x}} \mathbf{f}(\mathbf{x})\right] \left(\frac{\partial \mathbf{f}(\mathbf{x})}{\partial \mathbf{x}}\right)^{-1}\end{aligned}$$

By hypothesis, $\mathbf{f}(\mathbf{x}^*) = \mathbf{0}$ and therefore $\frac{\partial \mathbf{g}(\mathbf{x}^*)}{\partial \mathbf{x}^*} = \mathbf{0}$. Because $\frac{\partial \mathbf{g}(\mathbf{x}^*)}{\partial \mathbf{x}^*} = \mathbf{0}$ and $\mathbf{g}(\mathbf{x})$ is continuous it is possible to find a $\boldsymbol{\delta} > \mathbf{0}$ so that $\| \frac{\partial \mathbf{g}(\mathbf{x})}{\partial \mathbf{x}} \| < 1$ is satisfied on $[\mathbf{x}^* - \boldsymbol{\delta}, \mathbf{x}^* + \boldsymbol{\delta}]$. Therefore, the sequence $\{\mathbf{x}_k\}_0^\infty$ converges to the root $\mathbf{x} = \mathbf{x}^*$ for $\mathbf{x}_0 \in [\mathbf{x}^* - \boldsymbol{\delta}, \mathbf{x}^* + \boldsymbol{\delta}]$ □

The next iterate of Newton-Raphson iteration is only a function of the current iterate, $\mathbf{x}_k$, therefore it forms a discrete dynamical system as described in Eq. (5) with no dependence on $\mathbf{u}_k$ and k. Therefore, as with fixed-point iteration, it can also be shown that Newton-Raphson iteration meets the mathematical requirements of a dynamical system.

2.1.5 The Covariance Matrix

The covariance matrix of a n-dimensional random vector $\mathbf{X}$ is an $n \times n$ matrix defined as follow[59]

$$\boldsymbol{\Sigma} = \mathbb{E}\left[(\mathbf{X} - \mathbb{E}[\mathbf{X}])(\mathbf{X} - \mathbb{E}[\mathbf{X}])^T\right] \tag{11}$$

and can be thought of as a generalization of the scalar variance of a single random variable X with mean μ and variance $\sigma^2 = \mathbb{E}[(X - \mu)^2]$. Note that the covariance

matrix is (1) positive semi-definite and (2) symmetric. The expansion of Eq. (11) gives insight into the terms that comprise the covariance matrix

$$\mathbf{\Sigma} = \begin{pmatrix} \sigma_{X_1}^2 & \rho_{X_1,X_2}\sigma_{X_1}\sigma_{X_2} & \cdots & \rho_{X_1,X_2}\sigma_{X_1}\sigma_{X_n} \\ \rho_{X_1,X_2}\sigma_{X_2}\sigma_{X_1} & \sigma_{X_2}^2 & \cdots & \rho_{X_2,X_n}\sigma_{X_2}\sigma_{X_n} \\ \vdots & \vdots & \ddots & \vdots \\ \rho_{X_1,X_n}\sigma_{X_n}\sigma_{X_1} & \rho_{X_2,X_n}\sigma_{X_n}\sigma_{X_2} & \cdots & \sigma_{X_n}^2 \end{pmatrix} \tag{12}$$

where $\sigma_{X_i}^2$ is the variance of variable X_i and ρ_{X_i,X_j} is the product-moment coefficient (*i.e.*, the correlation coefficient) given by

$$\rho_{X_i,X_j} = \frac{\mathbb{E}\left[(X_i - \mu_{X_i})(X_j - \mu_{X_j})\right]}{\sigma_{X_i}\sigma_{X_j}} \tag{13}$$

The product-moment coefficient is a measure of the dependence of one random variable on another random variable and can vary between -1 and 1. Negative values indicate negative dependence (*i.e.*, an increase in one variable produces a decrease in the other variable), positive values indicate positive dependence (*i.e.*, an increase in one variable produces an increase in the other variable), and zero indicates zero correlation between the two variables. Hence, the covariance matrix captures second-order effects of the distribution with both the variance and dependence of each random variable when taken pairwise with another random variable. For this work, the covariance matrix of interest is either (1) the output of each CA or (2) the output of the entire design. These are used by other CAs within the multidisciplinary system to compute the robustness of the entire design.

2.1.6 Propagating Uncertainty

The computation (or estimation) of the output distribution of a CA or design with uncertain modeling or inputs can be achieved by a multitude of methods as discussed in Chapter 1. For some specific examples, analytical methods could be utilized. For example, when linear operations are conducted on random variables with known mean

and covariance an exact propagation of the uncertainty is possible[59]. However, in general, approximate techniques must be used. In this work, a sampling method, the unscented transform, is pursued. The unscented transform selects the samples so that the moments of the probability distribution can be matched. This leads to more accurate estimates of the probability distributions. In addition, once the multidisciplinary design is formulated as a dynamical system, covariance techniques which implement a Kalman filter can be invoked as shown in Chapter 3.

While the theoretical development of the method in this investigation considers all analyses to be linear (or linearized) such that an analytic propagation is possible, the formulation discussed later allows extension to nonlinear applications.

2.1.6.1 Sample Statistics

Sample statistics describe the statistics of a known set of values. In this methodology, it can be assumed that the sample is the resultant of a number of propagated trials through the analysis. There are two two sample statistics of interest: the sample mean ($\bar{\mathbf{x}}$) and the sample covariance ($\mathbf{S}$). The unbiased estimates of each of these is given by Eqs. (14) and (15), respectively[59].

$$\bar{\mathbf{x}} = \frac{1}{n}\sum_{i=1}^{n}\mathbf{x}_i \tag{14}$$

$$\mathbf{S}_{jk} = \frac{1}{n-1}\sum_{i=1}^{n}(x_{ij} - \bar{x}_j)(x_{ik} - \bar{x}_k) \tag{15}$$

2.1.6.2 The Unscented Transform

The unscented transform approximates a probability distribution by selecting a small number of test points, the sigma points, which are propagated through the analysis to allow estimation of the posterior mean and covariance. While this is similar to Monte Carlo analysis because a trial is propagated through the analysis, by selecting the test points according to the eigenstructure of the covariance matrix, third-order

accurate estimates of the resulting distribution's mean and covariance matrix are achievable with a small number of sigma points[134]. The relative speed and accuracy of computation for the uncertainty propagation leads this technique to be the basis of the Unscented Kalman Filter[135].

Conceptually, the unscented transform can be understood through the following development. Suppose that the output of an analysis, $\mathbf{y}$, is related to the n-dimensional input, $\mathbf{x}$, by the relationship

$$\mathbf{y} = \mathbf{g}(\mathbf{x}) \tag{16}$$

where $\mathbf{x}$ has mean $\bar{\mathbf{x}}$ and covariance $\mathbf{\Sigma}$. The set of trial points are selected based on the solution of the relationship[134]

$$\mathbf{A}\mathbf{A}^T = n\mathbf{\Sigma} \tag{17}$$

There are an infinite number of matrices, $\mathbf{A}$, that satisfy Eq. (17). Two commonly used solutions are the upper triangular matrix found from the Cholesky decomposition and the symmetric square root matrix. A set of $2n$ points, $\mathcal{S} = \{\boldsymbol{\sigma}_i\}_{i=1}^{2n}$, are then selected as the columns of $\pm\mathbf{A}$. The set of trial points are then given by[134]

$$\boldsymbol{\mathcal{X}}_i = \boldsymbol{\sigma}_i + \bar{\mathbf{x}} \tag{18}$$

and are propagated through the CA, Eq. (16)[134]

$$\boldsymbol{\mathcal{Y}}_i = \mathbf{g}(\boldsymbol{\mathcal{X}}_i) \tag{19}$$

. This set can then be used to find the mean and covariance matrix of the analysis' output, which are given by[134]

$$\bar{\mathbf{y}} \approx \frac{1}{2n}\sum_{i=1}^{2n}\boldsymbol{\mathcal{Y}}_i \tag{20}$$

$$\mathbf{\Sigma} \approx \frac{1}{2n}\sum_{i=1}^{2n}\left[\boldsymbol{\mathcal{Y}}_i - \bar{\mathbf{y}}\right]\left[\boldsymbol{\mathcal{Y}}_i - \bar{\mathbf{y}}\right]^T \tag{21}$$

These estimates are third-order accurate, meaning for analyses with polynomial input-output relationships that are less than cubic, the approximation is exact. Hence, for minimal computational expense (two times the function evaluations as the dimensionality of the matrix, $\mathbf{A}$) a very good approximation of both the mean of the output of the analysis (or design) and the output covariance matrix is obtained[134].

2.1.7 Matrix Norms

In order to obtain a singular value that bounds the variance, consider the matrix two-norm which is defined as[136]

$$\| \mathbf{A} \|_2 = \max_{\|\mathbf{x}\|_2=1} \| \mathbf{Ax} \|_2 = \sqrt{\lambda_{\max}(\mathbf{A}^H \mathbf{A})} \tag{22}$$

where $\mathbf{A}^H$ represents the conjugate transpose of a matrix $\mathbf{A}$ and $\lambda_{\max}(\cdot)$ is a function which returns the maximum eigenvalue. The two-norm can be more readily understood in the context of spectral decomposition such that $\mathbf{D} = \mathbf{V}^{-1}\mathbf{AV}$ where $\mathbf{D}$ is at worst a block-diagonal matrix. In the case of real, distinct eigenvalues, the diagonal of matrix $\mathbf{D}$ consists of the eigenvalues. By virtue of the properties of the covariance matrix, $\mathbf{\Sigma}$, the maximum eigenvalue is greater than or equal to the maximum variance. This means that the two-norm provides a bound on the maximum variance.

In two-dimensions, this can be seen in Fig. 11 where the covariance matrix is plotted as an ellipse. In Fig. 11, the axes $\sigma_{X_1}\sigma_{X_2}$ are the standard deviations associated with the covariance matrix, $\mathbf{\Sigma}$. The eigenvectors of the covariance matrix form the alternate set of axes (in blue), $\sigma_{X_1'}\sigma_{X_2'}$. The two-norm is the variance of the "pseudo-variable" that is oriented along the principal eigenvector of the resulting ellipse, which is the magnitude of the semi-major axis of the ellipse. In other words, the two-norm is the radius of the circle which completely encompasses the covariance matrix. An advantageous feature of this norm is that it is always a conservative estimate of the variance of the system.

Another way to view the resulting bound is through the auxiliary circle that is

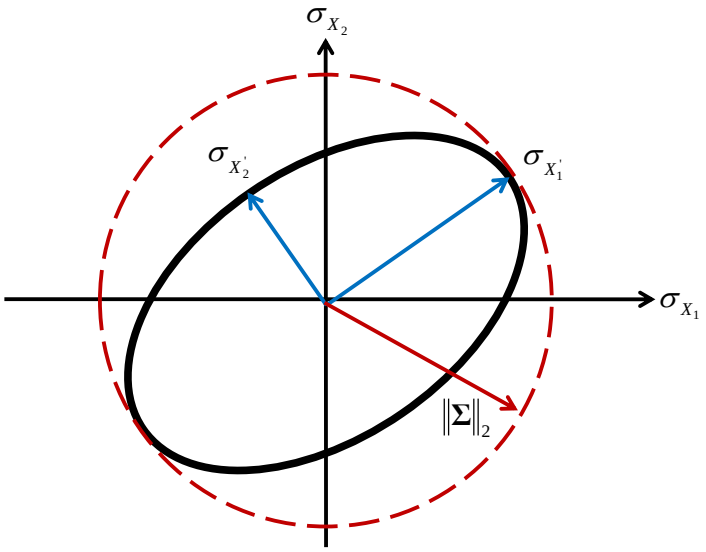

Figure 11: Visual representation of the matrix two-norm.

formed from sweeping through the eccentric anomaly of an elliptical orbit. This auxiliary circle completely encompasses the elliptical orbit and is coincident with the orbit at two points (when the true anomaly is 0° and 180°), much in the same way that the two-norm encompasses the ellipse formed from a covariance matrix and is coincident at two points.

2.2 Multidisciplinary Design as a Dynamical System

2.2.1 Identification of Feasible Designs

Identifying feasible designs in multidisciplinary systems can be thought of as the process of finding the root of a function. Consider a multidisciplinary problem where the analysis variables are described by a multivariable function $\mathbf{f}(\mathbf{u}, \mathbf{p})$ where $\mathbf{u}$ are the design variables and $\mathbf{p}$ are the parameters of the problem. Assume that the requirements of the design are given by only equality constraints that are a function of the performance of the system. The performance of the design is described by a multivariable mapping $\mathbf{g}(\mathbf{f}(\mathbf{u}, \mathbf{p}))$ and the requirements are given by $\mathbf{z}$. In order to

meet the requirements it is necessary to adjust the design variables $\mathbf{u}$ so that

$$\mathbf{z} = \mathbf{g}(\mathbf{f}(\mathbf{u}, \mathbf{p})) \tag{23}$$

The solution $\mathbf{u}^*$ of Eq. (23) is the root of the system. Since identifying feasible designs within the multidisciplinary design problem requires finding the value of $\mathbf{u}$ that satisfies Eq. (23), this process can be thought of as a root-finding problem when an iterative solution method is chosen. As described previously, many of the iterative schemes to find the root of a function, $\mathbf{g}(\mathbf{u})$, can be thought of as a dynamical system. Therefore, finding the feasible designs can be a dynamical system.

2.2.2 Design Optimization

In order for a converged design to be an optimum with respect to some objective function, its performance needs to be evaluated with respect to other potential designs. The general optimization problem is formulated as

$$\left.\begin{array}{lll} \textbf{Minimize}: & \mathcal{J}(\mathbf{u}, \mathbf{p}) & \\ \textbf{Subject to}: & \mathbf{g}_i(\mathbf{u}, \mathbf{p}) \leq \mathbf{0}, & i = 1, \ldots, n_g \\ & \mathbf{h}_j(\mathbf{u}, \mathbf{p}) = \mathbf{0}, & j = 1, \ldots, n_h \\ \textbf{By varying}: & \mathbf{u} & \end{array}\right\} \tag{24}$$

which requires a stationary point of the Lagrangian given as

$$L(\mathbf{u}, \mathbf{p}, \boldsymbol{\lambda}) = \mathcal{J}(\mathbf{u}, \mathbf{p}) + \sum_{i=1}^{n_g} \lambda_i \mathbf{g}_i(\mathbf{u}, \mathbf{p}) + \sum_{j=1}^{n_h} \lambda_{n_g+j} \mathbf{h}_j(\mathbf{u}, \mathbf{p}) \tag{25}$$

to be found. The stationary point of the Lagrangian (Eq. (25)) is the value of $\mathbf{u}$ such that $\nabla_{\mathbf{u}} L(\mathbf{u}, \mathbf{p}, \boldsymbol{\lambda}) = \mathbf{0}$. This is also a root-finding problem and therefore can be thought of as a dynamical system.

2.2.3 Identifying an Optimal Multidisciplinary Design

Multidisciplinary design optimization can be broken down into two steps: (1) identifying feasible designs and (2) identifying the optimal design from the set of feasible

candidates. As discussed, both of these steps are root-finding problems. With the choice of an appropriate iterative numerical root-finding scheme, each of these individual steps can be posed as dynamical systems. When combined together, a nested root-finding problem results. This is shown in Fig. 12

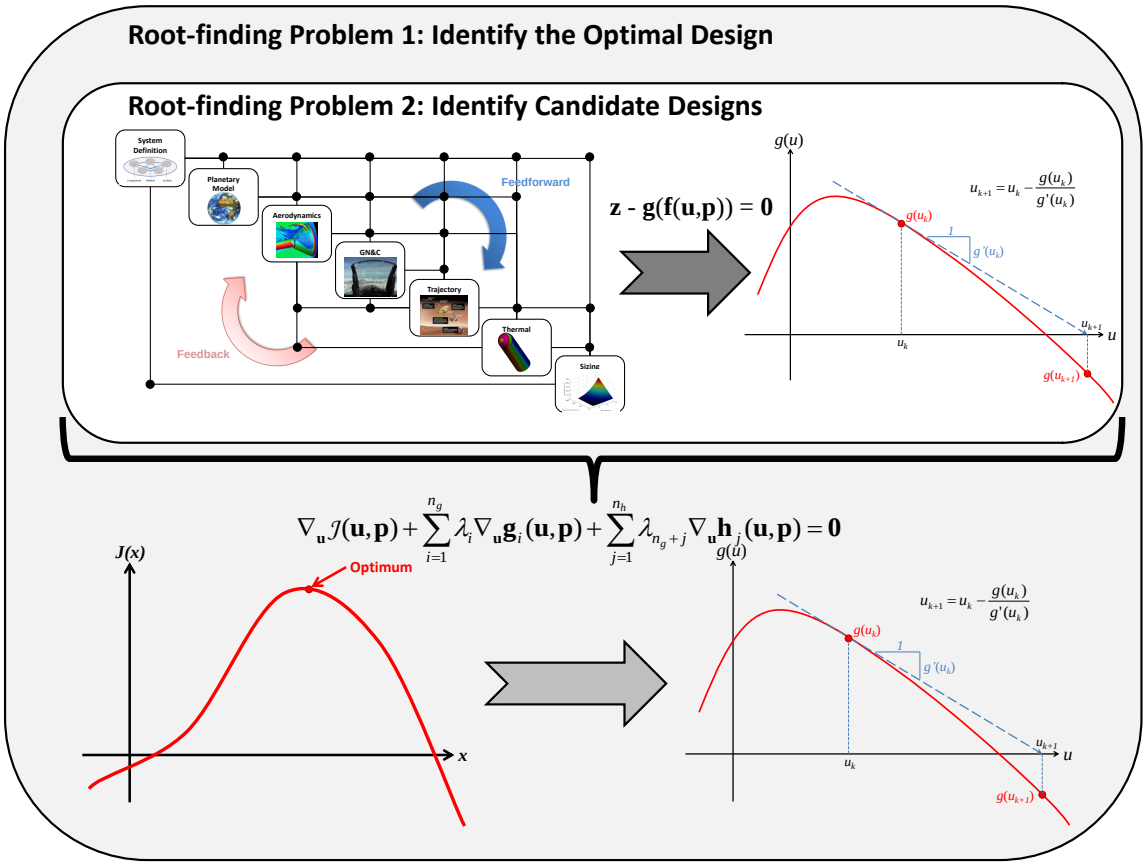

Figure 12: Multidisciplinary design through root-finding.

2.2.4 Analog of Dynamical System Variables and Multidisciplinary Design Variables

The convergence and optimization of a multidisciplinary design problem have been shown to be root-finding problems that can be given by an iterative relationship of the form

$$\mathbf{y}_{k+1} = \mathbf{f}(\mathbf{y}_k, \mathbf{u}_k, k) \tag{26}$$

The iteration equation given in Eq. (26) is the same form given in the definition of a discrete dynamical system equation, Eq. (5). Table 3 shows the analogy between dynamical system variables in Eq. (26) and the variables associated with design. Throughout the remainder of this thesis, this notation is used consistently.

Table 3: Analog between dynamical system variables and design variables.

Variable	**Dynamical System Description**	**Design Description**
$\mathbf{y}$	State	CAs Output
$\mathbf{u}$	Control	Design Variables
k	Iteration #	Design Iteration

2.3 Summary

This chapter provided the theoretical context for viewing the multidisciplinary design problem as a dynamical system. Included in this discussion was a rigorous definition of the state and discrete dynamical systems. This was followed by a description of two numerical root-finding algorithms, fixed-point iteration and Newton-Raphson iteration and it was shown that each of these methods both converge to a root and meet the criterion to be a dynamical system. In particular, the state was shown to be the independent variable and the iteration scheme meets the requirements set forth at the beginning of the chapter to be a discrete dynamical system. In addition, the theoretical foundation for several other techniques utilized within this work such as covariance matrices, matrix norms, and unscented transform were described. Finally, a discussion surrounding how to cast the root-finding problems associated with the multidisciplinary design as a dynamical system ensued. This discussion showed that both steps in design, finding feasible designs and the subsequent optimization are root-finding problems that can be nested within one another to form a single dynamical system.

CHAPTER III

APPLYING DYNAMICAL SYSTEM THEORY TO MULTIDISCIPLINARY DESIGN

This chapter builds on the approach of casting the multidisciplinary design problem as a dynamical system shown in Chapter 2 to apply dynamical system theory. Techniques from dynamical system theory are applied to the multidisciplinary design problem, including concepts from stability analysis, control theory, and estimation theory. Stability analysis is shown to be able to determine whether a design is feasible, whether an optimal design exists, the range of initial values that can be used to converge the design, and the rate at which the design will converge. Control theory enables efficient handling of constraints as it enforces constraints that are functions of the CA's output and the design variables at the same level in the optimization hierarchy. Finally, estimation theory is used to propagate uncertainty through the multidisciplinary design, yielding a method that simultaneously converges the design and quantifies the uncertainty associated with that design point.

3.1 Design Convergence Using Stability Concepts

Concepts from the stability domain of dynamical system theory are applied to multidisciplinary design in order to identify:

1. Whether a feasible design exists (for a given iteration scheme)
2. Whether an optimal design exists (for a given iteration scheme)
3. The range of initial values that can be used to converge the design
4. The rate at which the design will converge

Each of these is an enhancement compared to current MDA/O techniques enabled by viewing the iterative relationships formed in the convergence of the design problem as a dynamical system.

3.1.1 Foundations of Stability Analysis

The concept of stability allows for the identification of feasible designs for given iteration schemes. These iteration schemes can usually be written in the form

$$\mathbf{y}_{k+1} = \mathbf{f}(\mathbf{y}_k, \mathbf{u}_k) \tag{27}$$

where $\mathbf{y}$ is the state of the system, $\mathbf{f}$ is a function which describes the time evolution of the system, $\mathbf{u}$ is the input into the system, and k is the iterate number. A specific instance of Eq. (27) is a linear, discrete dynamical system, which is given by

$$\mathbf{y}_{k+1} = \mathbf{A}_k\mathbf{y}_k + \mathbf{B}_k\mathbf{u}_k \tag{28}$$

For a given initial state, a system is stable if the state does not grow beyond the initial state's magnitude. More rigorously, this is defined in terms of equilibrium points of a system. Consider the discrete dynamical system defined by Eq. (27), the equilibrium point is defined as

Definition: Equilibrium of a Dynamical System

A particular point $\mathbf{y}_e$ is an *equilibrium point* of the dynamical system given by Eq. (27) if the system's state at iterate $k = 0$ is $\mathbf{y}_e$ implies that $\forall k \in \mathbb{Z}_+ \setminus \{0\}$, $\mathbf{f}(\mathbf{y}_e, \mathbf{0}) = \mathbf{y}_e$.

For a linear dynamical system, given by Eq. (28), the equilibrium point is the origin of the system (*i.e.*, $\mathbf{y}_e = \mathbf{0}$).

The equilibrium point's stability is defined with regard to the zero-input discrete

dynamical system given by[132, 137, 138, 139]

$$\left.\begin{aligned} \mathbf{y}_{k+1} &= \mathbf{f}(\mathbf{y}_k, \mathbf{0}) \\ \mathbf{y}_{k=0} &= \mathbf{y}_0 \end{aligned}\right\} \tag{29}$$

Definition: Stability

For the system given by Eq. (29), if $\forall \epsilon > 0$, $\exists \delta(\epsilon, 0) \in (0, \epsilon]$ an equilibrium point of the system is

- *stable* if $\forall k > 0$ and $\| \mathbf{y}_0 \| < \delta$, $\| \mathbf{y}_k \| < \epsilon$
- *asymptotically stable* if
  1. the equilibrium point is stable and
  2. $\exists \delta' \in (0, \epsilon]$ such that whenever $\| \mathbf{y}_0 \| < \delta'$ the state's evolution satisfies $\lim_{k \to \infty} \| \mathbf{y}_k \| = 0$
- *unstable* if it is not stable or asymptotically stable

Figures 13 and 14 demonstrate the concept of equilibrium point stability. Figure 13 shows an intuitive concept of stability while Fig. 14 demonstrates different state trajectories in $\mathbb{R}^2 \times \mathbb{R}$ and $\mathbb{R}^2$. In Fig. 14, asymptotically stable state trajectories are seen to approach the origin as time progresses whereas stable trajectories remain within a given distance, ϵ of the origin.

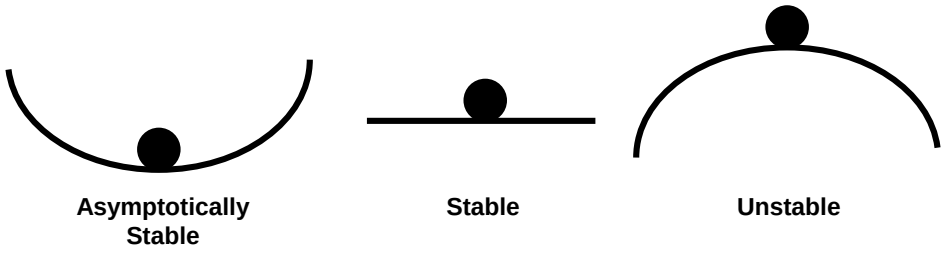

Figure 13: Visualization of the concept of stability.

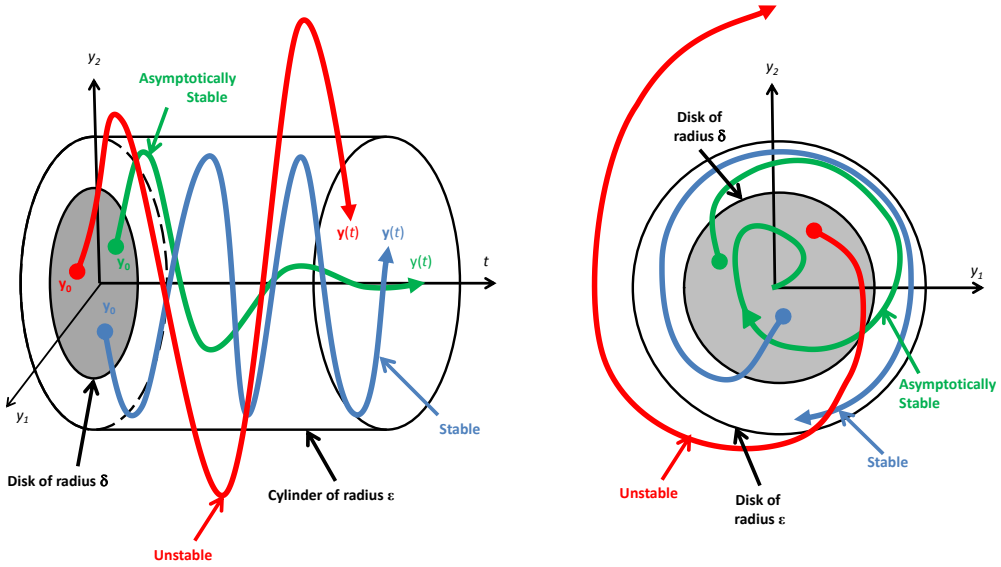

(a) (b)

Figure 14: Visualization of state trajectories in (a) $\mathbb{R}^2 \times \mathbb{R}$ and (b) $\mathbb{R}^2$ showing stability for a continuous dynamical system.

3.1.1.1 Linear Stability Criterion

For discrete, linear systems, that is dynamical systems given by Eq. (28), the solution for the evolution of the state and the output is given by

$$\mathbf{y}_k = \mathbf{\Phi}(k,0)\mathbf{y}_0 + \sum_{j=1}^{k} \mathbf{\Phi}(k,j)\mathbf{B}_{j-1}\mathbf{u}_{j-1} \tag{30}$$

where $\mathbf{\Phi}(k,j)$ is the discrete state transition matrix. This transition matrix is given by

$$\mathbf{\Phi}(k,j) = \mathbf{A}^{k-j} \tag{31}$$

in the case where $\mathbf{A}_k = \mathbf{A}\ \forall k \in \mathbb{Z}_+$, that is when $\mathbf{A}$ is constant. Substituting Eq. (30) and Eq. (31) into Eq. (28) yields[132]

$$\mathbf{y}_{k+1} = \mathbf{A}^{k+1}\mathbf{y}_0 + \sum_{j=1}^{k} \mathbf{A}^{k-j+1}\mathbf{B}_{j-1}\mathbf{u}_{j-1} + \mathbf{B}_k\mathbf{u}_k \tag{32}$$

which is a relationship that depends on the initial condition and the control history. In the unforced case (*i.e.*, $\mathbf{u}_k = \mathbf{0}\ \forall k \in \mathbb{Z}_+$) and by the Cayley-Hamilton theorem,

the stability criterion can be identified. If $\max_i |\lambda_i| > 1$ for any simple root of the characteristic equation

$$\det(\mathbf{A} - \lambda \mathbf{I}) = 0 \tag{33}$$

or $\max_i |\lambda_i| \geq 1$ for any repeated root of Eq. (33) then the system is unstable. This is because the Jordan canonical form of $\mathbf{A}$ has terms that tend to infinity as the iteration proceeds (*i.e.*, $\lim_{k\to\infty} \mathbf{V}^T \mathbf{A}^k \mathbf{V} = \infty$ since diagonal terms of $\mathbf{V}^T\mathbf{A}\mathbf{V}$ are greater than unity). Similarly, if $\max_i |\lambda_i| \leq 1$ for any simple root or $\max_i |\lambda_i| < 1$ for repeated roots of Eq. (33), then the iteration scheme is asymptotically stable[132, 140, 141]. More rigorous proof of this concept is provided in Ref. [140].

3.1.1.2 Lyapunov Stability

Stability of general dynamical systems, including the one formed for design, can be studied using Lyapunov stability theory. This theory lays the foundations to assess the stability characteristics of arbitrary designs and can be leveraged to provide insight about the convergence properties of the design. For instance, Lyapunov stability can be used to ascertain information regarding the convergence rate and what starting iteration values will lead to a converged design for a given root-finding scheme.

Lyapunov stability theory is prevalent for continuous dynamical systems such as the autonomous system

$$\dot{\mathbf{y}} = \mathbf{f}(\mathbf{y}), \quad \forall t \in [0, \infty) \tag{34}$$

for which the origin is an equilibrium point. A Lyapunov function is a continuously differentiable map $V : \mathbb{R}^n \to \mathbb{R}$ such that

1. $V(\mathbf{y}) > 0,\ \mathbf{y} \neq \mathbf{0},\ V(\mathbf{0}) = 0$
2. $\dfrac{d}{dt}\left(V(\mathbf{y}(t))\right) \leq 0, \quad \forall t \in [0, \infty)$

where $\mathbf{y} : [0, \infty) \to \mathbb{R}^n$ is any solution of Eq. (34)[138]. In fact, it has been applied to differential equations such as this since Lyapunov first defined this technique in 1892.

Its use in dynamical systems, defined by difference equations such as those used to converge and optimize designs, is less mature with the first treatment in the literature being attributed to Hahn in 1958[142].

To begin the development of Lyapunov theory for discrete dynamical systems, consider the following definition of a Lyapunov function[142, 139, 141, 143, 144]

Definition: Discrete Lyapunov Function

A mapping $V : \mathbb{R}^n \to \mathbb{R}$ is a *Lyapunov function* for the zero-input autonomous, discrete dynamical system, Eq. (27), (*i.e.*, $\mathbf{f}(\mathbf{y}_k, \mathbf{0})$) at an equilibrium point $\mathbf{y}_e$ of $\mathbf{f}$ if there is an open neighborhood $\mathcal{D}$ at $\mathbf{y}_e$ such that V is continuous on $\mathcal{D}$ and

- $V(\mathbf{y}) > 0 \ \forall \mathbf{y} \in \mathcal{D},\ \mathbf{y} \neq \mathbf{y}_e,\ V(\mathbf{y}_e) = 0$
- $\Delta V = V(\mathbf{y}_{k+1}) - V(\mathbf{y}_k) \leq 0$ whenever $\mathbf{y}_k, \mathbf{y}_{k+1} \in \mathcal{D}$

With this definition, the following theorem can be presented.

Theorem 1 (Lyapunov's Direct Method for Discrete Dynamical Systems)**.** *Consider the following dynamical system*

$$\left.\begin{aligned} \mathbf{y}_{k+1} &= \mathbf{f}(\mathbf{y}_k), \quad \mathbf{y}_k \in \mathcal{S} \subseteq \mathcal{D} \\ \mathbf{f}(\mathbf{0}) &= \mathbf{0} \end{aligned}\right\}$$

where it is assumed that $\mathbf{f} : \mathbb{R}^n \to \mathbb{R}^n$ *is continuous on an open neighborhood* $\mathcal{S}$ *of a fixed-point* $\mathbf{y}_e$ *and that* $V : \mathbb{R}^n \to \mathbb{R}$ *is a Lyapunov function for* $\mathbf{f}$ *at* $\mathbf{u}^*$*, then at* $\mathbf{u}^*$ *the dynamics governed by* $\mathbf{f}$ *are* stable*. If, in addition,*

$$\Delta V = V(\mathbf{y}_{k+1}) - V(\mathbf{y}_k) < 0 \ \textit{whenever} \ \mathbf{y}, \mathbf{y}_{k+1} \in \mathcal{D} \ \textit{and} \ \mathbf{y}_k \neq \mathbf{y}_e$$

then the trajectory governed by $\mathbf{f}$ *are* asymptotically stable *at* $\mathbf{y}_e$*. If* $\mathcal{S} = \mathcal{D} = \mathbb{R}^n$ *and*

$$V(\mathbf{y}_k) \to \infty \ \textit{as} \ \| \mathbf{y}_k \| \to \infty,$$

then the dynamics governed by $\mathbf{f}$ *is* globally asymptotically stable *at* $\mathbf{y}_e$*.*

The proof of this theorem is shown in Appendix A.

A special case of a discrete dynamical system is that of a linear, discrete system with constant coefficients such as that shown in Eq. (28) with $\mathbf{A}_k = \mathbf{A}\ \forall k \in \mathbb{Z}_+$. The zero-input stability in this case can be investigated using a quadratic Lyapunov function of the form

$$V(\mathbf{y}) = \mathbf{y}^T\mathbf{R}\mathbf{y} \tag{35}$$

This form leads to

$$\Delta V(\mathbf{y}) = V(\mathbf{y}_{k+1}) - V(\mathbf{y}_k) = \mathbf{y}^T\left(\mathbf{A}^T\mathbf{R}\mathbf{A} - \mathbf{R}\right)\mathbf{y} = -\mathbf{y}^T\mathbf{S}\mathbf{y} \tag{36}$$

For any given $\mathbf{S} > 0$, which is symmetric there is exactly one solution for a symmetric matrix $\mathbf{R}$ which is the solution of Stein's equation

$$\mathbf{A}^T\mathbf{R}\mathbf{A} - \mathbf{R} = -\mathbf{S} \tag{37}$$

provided that

$$\lambda_i \neq \lambda_j \neq 1, \quad i = 1, 2, \cdots, n,\ j = 1, 2, \cdots, n \tag{38}$$

holds for all eigenvalues λ_i of $\mathbf{A}$. Thus, if there is a solution, $\mathbf{R}$, to Stein's equation, Eq. (37), then the linear system is globally asymptotically stable since $\Delta V < 0$, $\mathcal{S} = \mathcal{D} = \mathbb{R}^n$, and $V(\mathbf{y}_k) \to \infty$ as $\| \mathbf{y}_k \| \to \infty$. For linear, constant coefficient systems, this is equivalent to the results before (*i.e.*, if an $\mathbf{R}$ exists, this implies $|\lambda_i| < 1$ for all eigenvalues).

3.1.1.3 Summary of Stability Conditions

A summary of the conditions to achieve stability for both a general dynamical system (in terms of Lyapunov functions) and a linear, constant coefficient system (in terms of eigenvalue criterion) is listed in Table 4[132, 140, 141].

Table 4: Discrete dynamical system stability criterion.

Classification	**General System Criterion**	**Linear Constant System Criterion**
Unstable		If $\|\lambda_i\| > 1$ for any simple root or $\|\lambda_i\| \geq 1$ for any repeated root
Stable	1. $V(\mathbf{y}) > 0$ 2. $\Delta V \leq 0$	If $\|\lambda_i\| \leq 1$ for any simple root and $\|\lambda_i\| < 1$ for all repeated roots
Asymptotically Stable	1. $V(\mathbf{y}) > 0\ \forall \mathbf{y} \neq \mathbf{0}$ and $V(\mathbf{0}) = 0$ 2. $\Delta V < 0\ \forall \mathbf{y} \neq \mathbf{0}$ (or $\Delta V \leq 0\ \forall \mathbf{y}$ and $\Delta V \neq 0$ for any solution sequence $\{\mathbf{y}_k\}$)	$\|\lambda_i\| < 1$ for all roots (or $\exists \mathbf{R}$ that satisfies $\mathbf{A}^T\mathbf{R}\mathbf{A} - \mathbf{R} = -\mathbf{S}$ with $\mathbf{S} = \mathbf{S}^T > 0$)
Globally Asymptotically Stable	1. $V(\mathbf{y}) > 0\ \forall \mathbf{y} \neq \mathbf{0}$ and $V(\mathbf{0}) = 0$ 2. $\Delta V < 0\ \forall \mathbf{y} \neq \mathbf{0}$ (or $\Delta V \leq 0\ \forall \mathbf{y}$ and $\Delta V \neq 0$ for any solution sequence $\{\mathbf{y}_k\}$) 3. $V(\mathbf{y}) \to \infty$ as $\| \mathbf{y} \| \to \infty$	

3.1.2 The Relationship of Stability to Design Convergence

From the multidisciplinary design perspective, stability of the dynamical system gives information into the convergence characteristics of the design. Asymptotic stability implies that there is a limited region for which the design will converge, whereas global asymptotic stability implies that the design will converge regardless of the design assumptions used to start the convergence procedure. If the dynamical system representing the multidisciplinary design is unstable or stable, it implies that the design will not converge. This is analogous to stating that a contraction mapping exists.

3.1.3 Region of Attraction

The region of attraction to an equilibrium point $\mathbf{y}_e$ of Eq. (29) is the set

$$\mathcal{A} = \{\mathbf{y} : \mathbf{f}^k(\mathbf{y}) \to \mathbf{y}_e \text{ as } k \to \infty\}$$

This can be more readily understood as the set of initial guesses that make the iteration scheme converge (*i.e.*, those that will result in converged designs). The following theorem helps in identifying this region of attraction[145]

Theorem 2 (Region of Attraction)**.** *Assume that* $\phi : \mathbb{R}^n \to \mathbb{R}$ *is continuous and satisfies*

1. $\phi(\mathbf{y}_e) = 0$
2. $\phi(\mathbf{y}),\ \mathbf{y} \neq \mathbf{y}_e$
3. $\phi(\mathbf{y}) \geq a$ *for* $\| \mathbf{y} - \mathbf{y}_e \| \geq b$

where a *and* b *are positive constants and* $\mathbf{y}_e$ *is a fixed-point of* $\mathbf{f} : \mathbb{R}^n \to \mathbb{R}^n$*. Assume also* $\exists w : \mathbb{R}^n \to \mathbb{R}$ *is continuous at* $\mathbf{y}_e$ *with*

1. $w(\mathbf{y}_e) = 0$
2. $w(\mathbf{y}) > 0,\ \mathbf{y} \neq \mathbf{y}_e$
3. $w(\mathbf{f}(\mathbf{y})) - w(\mathbf{y}) = -\phi(\mathbf{y})(1 - w(\mathbf{y}))\ \forall \mathbf{y} \in \mathbb{R}^n$

Then $\mathcal{A} = \{\mathbf{y} : w(\mathbf{y}) < 1\}$ *is the region of attraction.*

The proof of this theorem is found in Appendix A. A function of the form $\phi(\mathbf{y}) = c \| \mathbf{y} - \mathbf{y}_e \|^p$ satisfies the three required conditions for ϕ. Therefore, the problem of finding the domain of attraction becomes a problem of finding the domain for w such that $w(\mathbf{y}) < 1$.

3.1.4 Methods for Identifying the Stability of a System

In general the search of a Lyapunov function $V(\mathbf{y})$ is a difficult one, particularly for nonlinear systems for which the equations describing their evolution may not be known, as would likely be the case in design. However, several techniques for their search exist[137, 138, 139, 140, 141]. An emerging technique that is used in this work

to identify Lyapunov functions is sum-of-squares decomposition. This technique is particularly applicable for polynomial dynamical systems (including Taylor series approximations) and achieves a Lyapunov function by factoring a nonlinear polynomial that is parametrized by unknown variables into a sum-of-squares. The resulting sum-of-squares polynomial is positive definite and can be used to check the difference condition to find if an iteration scheme for the design is convergent.

3.1.4.1 Sum-of-squares Decomposition and Analysis

A polynomial, $f(\mathbf{y})$, $\mathbf{y} \in \mathbb{R}^n$ is said to be a sum-of-squares if there exist polynomials $f_1(\mathbf{y})$,..., $f_m(\mathbf{y})$ such that

$$f(\mathbf{y}) = \sum_{i=1}^{m} f_i^2(\mathbf{y}) \tag{39}$$

This statement is equivalent to the following proposition[146].

Proposition 3. *Let $f(\mathbf{y})$ be a polynomial in $\mathbf{y} \in \mathbb{R}^n$ of degree $2d$. In addition, let $\mathbf{z}(\mathbf{y})$ be a column vector whose entries are all monomials in $\mathbf{y}$ with degree no greater than d. Then $f(\mathbf{y})$ is a sum-of-squares if and only if there exists a positive semi-definite matrix $\mathbf{Q}$ such that*

$$f(\mathbf{y}) = \mathbf{z}^T(\mathbf{y})\mathbf{Q}\mathbf{z}(\mathbf{y}) \tag{40}$$

Using the proposition definition of a sum-of-squares, it can be seen that a sum-of-squares decomposition can be found using semidefinite programming, to search for the $\mathbf{Q}$ matrix satisfying Eq. (40).

What is significant about sum-of-squares decomposition for design applications is that it allows the search of a polynomial Lyapunov function $V(\mathbf{y})$ (*i.e.*, the $f(\mathbf{y})$) with coefficients that are parametrized in terms of some other unknowns. A search for the coefficients that render the polynomial $f(\mathbf{y})$ a sum-of-squares can be performed using semidefinite programming. For example, consider the construction of a Lyapunov function for a nonlinear system where the following procedure can be used:

1. Coefficients can be used to parametrize a set of candidate Lyapunov functions in an affine manner, that is it can determine a set $\mathcal{V} = \{V(\mathbf{y}) : V(\mathbf{y}) = v_0(\mathbf{y}) + \sum_{i=1}^{m} c_i v_i(\mathbf{y})\}$, where the $v_i(\mathbf{y})$'s are monomials in $\mathbf{y}$.

2. Search for a function $V(x) \in \mathcal{V}$ which satisfies $V(\mathbf{y}) - \phi(\mathbf{y})$ and $-\dfrac{\partial V(\mathbf{y})}{\partial \mathbf{y}} f(\mathbf{y})$, where $\phi(\mathbf{y}) > 0$ using semidefinite programing

The semidefinite programming problem above determines the state dependent linear matrix inequalities (LMIs) that govern the problem which are resultants of solving the following convex optimization problem

$$\left.\begin{array}{ll} \textbf{Minimize}: & \displaystyle\sum_{i=1}^{m} a_i c_i \\ \textbf{Subject to}: & \mathbf{F}_0(\mathbf{y}) + \displaystyle\sum_{i=1}^{m} c_i \mathbf{F}_i(\mathbf{y}) \geq 0 \\ \textbf{By varying}: & c_i \end{array}\right\} \tag{41}$$

where $a_i \in \mathbb{R}$ are fixed coefficients, $c_i \in \mathbb{R}$ are decision variables, and $\mathbf{F}_i(\mathbf{y})$ are symmetric matrix functions of the indeterminate $\mathbf{y} \in \mathbb{R}^n$. When $\mathbf{F}_i(\mathbf{y})$ are symmetric polynomial matrices in $\mathbf{y}$ the computationally difficult problem of solving (41) is relaxed according to the following proposition[146]

Proposition 4. *Let* $\mathbf{F}(\mathbf{y})$ *be an* $m \times m$ *symmetric polynomial matrix of degree* $2d$ *in* $\mathbf{y} \in \mathbb{R}^n$. *Furthermore, let* $\mathbf{z}(\mathbf{y})$ *be a column vector whose entries are all monomials in* $\mathbf{y}$ *with degree no greater than* d, *and assume the following:*

(i) $\mathbf{F}(\mathbf{y}) \geq 0 \quad \forall \mathbf{y} \in \mathbb{R}^n$

(ii) $\mathbf{v}^T \mathbf{F}(\mathbf{y}) \mathbf{v}$ *is a sum of squares, with* $\mathbf{v} \in \mathbb{R}^m$

(iii) There exists a positive semi-definite matrix $\mathbf{Q}$ *such that*

$$\mathbf{v}^T \mathbf{F}(\mathbf{y}) \mathbf{v} = (\mathbf{v} \otimes \mathbf{z}(\mathbf{y}))^T \mathbf{Q} (\mathbf{v} \otimes \mathbf{z}(\mathbf{y}))$$

Then (i) $\Leftarrow$ *(ii) and (ii)* $\Leftrightarrow$ *(iii)*

This proposition is proven by Prajna *et al.* in Ref. [146]. However, by applying Proposition 4, it is seen that the solution to the sum-of-squares optimization problem seen in Eq. (42) is also a solution to the state-dependent LMI problem, Eq. (41).

$$\left.\begin{array}{ll} \textbf{Minimize}: & \displaystyle\sum_{i=1}^{m} a_i c_i \\ \textbf{Subject to}: & \mathbf{v}^T \left(\mathbf{F}_0(\mathbf{y}) + \displaystyle\sum_{i=1}^{m} c_i \mathbf{F}_i(\mathbf{y}) \right) \mathbf{v} \text{ is a sum-of-squares polynomial} \\ \textbf{By varying}: & c_i \end{array}\right\} \quad (42)$$

This relaxation of the LMI problem turns the relatively difficult computation problem associated with Eq. (41) to a relatively simple computational problem since semidefinite programming solvers are readily available on multiple platforms[147, 148].

3.1.5 Estimating the Rate of Convergence Based on Lyapunov-like Techniques

For a special case of an exponentially stable system, the rate of convergence can be estimated. The following lemma defines the basis of exponential stability for a discrete dynamical system

Lemma 1. *For a system defined by Eq. (27) if there exists a function* $V(\mathbf{y})$ *with* $V(\mathbf{0}) = 0$ *such that*

1. $V(\mathbf{y}_k) \geq c\phi(\| \mathbf{y}_k \|)$
2. $\Delta V = V(\mathbf{y}_{k+1}) - V(\mathbf{y}_{k+1}) \leq M - \alpha V(\mathbf{y}_k)$

for some $\phi \in \mathcal{K}$ *and constants* $c > 0$, $M \geq 0$, *and* $0 < \alpha < 1$ *then*

1. $c\phi(\| \mathbf{y}_k \|) \leq V(\mathbf{y}_k) \leq (1-\alpha)^k V(\mathbf{y}_0) + M \displaystyle\sum_{i=0}^{k-1} (1-\alpha)^i$
2. $\displaystyle\lim_{k\to\infty} \phi(\| \mathbf{y}_k \|) \leq \frac{M}{c\alpha}$

The proof of this lemma is found by application of a geometric series as shown in Ref. [149]. The two conclusions of this lemma imply that the Lyapunov function provides a bound on how the state converges as a function of iterate and the ultimate bound of the state.

3.1.5.1 Linear Designs

For the zero-input general linear system as defined by Eq. (28) the following theorem yields information regarding the exponential bounds of the design (*i.e.*, how fast the design converges)[150]

Theorem 3 (Linear System Exponential Stability)**.** *The origin of Eq. (28) with* $\mathbf{u}_k = \mathbf{0}\ \forall k \in \mathbb{Z}_+$ *is uniformly (exponentially) asymptotically stable if, and only if, there exists a sequence of nonsingular matrices* $\mathbf{W}_k \in \mathbb{C}^{n\times n}$ *and some matrix norm* $\|\cdot\|$*, with* $\|\ \mathbf{W}_k\ \|$ *and* $\|\ \mathbf{W}_k^{-1}\ \|$ *uniformly bounded, and* $\beta \triangleq \sup_k\{\beta_k\} < 1$ *where* $\beta_k \triangleq \|\ \mathbf{W}_{k+1}\mathbf{A}_k\mathbf{W}_k^{-1}\ \|$*. In this case, given any initial state* $\mathbf{y}_0 \in \mathbb{R}^n$ *and defining* $w \triangleq \sup_k \|\ \mathbf{W}_k^{-1}\ \|$, $\|\ \mathbf{y}_k\ \| \leq \beta^k w \|\ \mathbf{W}_0\mathbf{y}_0\ \|$

Proof of this theorem is found in Appendix A. This theorem says that if the linear system describing the convergence of the design is transformed according to

$$\boldsymbol{\zeta}_k = \mathbf{W}_k\mathbf{y}_k \tag{43}$$

then

$$\boldsymbol{\zeta}_{k+1} = \boldsymbol{\Psi}_k\boldsymbol{\zeta}_k \tag{44}$$

where $\boldsymbol{\Psi}_k \triangleq \mathbf{W}_{k+1}\mathbf{A}_k\mathbf{W}_k^{-1}$. Due to the condition $\beta_k < 1$, $\|\ \boldsymbol{\Psi}_k\ \| < 1$, the transformed system is a contraction mapping.

The computation of the matrix $\mathbf{W}_k$ for the case when $\mathbf{A}_k = \mathbf{A}\ \forall k \in \mathbb{Z}_+$ is significantly more tractable and can be readily achieved by any of the following methods[150]

1. If $\mathbf{A}$ is diagonalizable, $\mathbf{A} = \mathbf{V}\mathbf{D}\mathbf{V}^{-1}$ where $\mathbf{D} \triangleq \text{diag}\{\lambda_i\}$, then choosing $\mathbf{W} = \mathbf{V}^{-1}$ and $\|\cdot\|_2$ gives $\beta = \lambda_{\max}$.

2. For any $\mathbf{A}$, compute $\mathbf{A} = \mathbf{Q}^H\mathbf{U}\mathbf{Q}$, the Schur decomposition and set $\mathbf{W} = \mathbf{\Gamma}\mathbf{U}$ where $\mathbf{\Gamma} = \text{diag}\{1, \gamma, \gamma^2, \cdots, \gamma^{n-1}\}$.

3. Choose a positive definite $\mathbf{S}$ and solve $\mathbf{R} - \mathbf{A}^T\mathbf{R}\mathbf{A} = \mathbf{S}$ to obtain a positive definite $\mathbf{R}$. Then compute the Cholesky factorization $\mathbf{R} = \mathbf{W}^T\mathbf{W}$ to obtain $\mathbf{W}$.

Each of these provide a value of β which can be used as an absolute scale to describe how fast a design will converge as the norm of the state $\| \mathbf{y} \|$ decreases by a factor proportional to β at each iterate.

3.1.5.2 Nonlinear Designs

The methods of linear systems can be extended to nonlinear designs, that is those designs whose iteration is described by Eq. (27). The following theorem provides a sufficient condition for exponential stability and exponential bounds on the state[150].

Theorem 4 (Nonlinear System Exponential Stability)**.** *The origin of Eq. (27) with* $\mathbf{u}_k = \mathbf{0}\ \forall k \in \mathbb{Z}_+$ *is exponentially asymptotically stable if there exists a nonsingular matrix* $\mathbf{W} \in \mathbb{C}^{n\times n}$ *and some matrix norm* $\| \cdot \|$*, such that*

$$\beta \triangleq \sup_k \sup_{\mathbf{v}\in\Omega} \left|\left| \mathbf{W} \left[\frac{\partial \mathbf{f}}{\partial \mathbf{y}}(\mathbf{v}) \right] \mathbf{W}^{-1} \right|\right| < 1$$

for some open convex set $\Omega \in \mathbb{R}^n$ *with* $\mathbf{0} \in \Omega$*. There exists an open set* $\mathcal{X}_s \subseteq \Omega$ *with* $\mathbf{0} \in \mathcal{X}_s$*, and* $\forall \mathbf{y}_0 \in \mathcal{X}_s$*,* $\exists \beta_0 \in [0, \beta]$ *such that* $\| \mathbf{y}_k \| \leq \beta_0^k \kappa(\mathbf{W}) \| \mathbf{y}_0 \|$*, and hence* $\mathcal{X}_s$ *is a domain of exponential stability.*

This is proven in Appendix A. This theorem provides a rate of convergence estimate as long as the associated conditions are met. In this case, the rate of convergence is given as β_0 as the magnitude of the initial state is reduced successively by this amount.

3.2 Design Constraints Using Optimal Control Theory

Optimal control theory may be used to obtain the solution to the general multidisciplinary design problem. The solution procedure is a root-finding problem, however, optimal control techniques can be used to adjoin a tangency condition for constraints that are a function of the input or state. This allows for a general framework that is capable of handling constraints that are functions of the design variables as well as functions of the CA values. As such, constraints are moved to the highest level in the optimization hierarchy.

3.2.1 Continuous Dynamical Systems

To first illustrate the handling of constraints using optimal control theory, consider the general continuous-time optimal control problem given by

$$\left.\begin{array}{ll} \textbf{Minimize}: & \mathcal{J} = \phi(\mathbf{y}(t_f), t_f) + \displaystyle\int_{t_0}^{t_f} \mathcal{L}(\mathbf{y}(t), \mathbf{u}(t), t)dt \\ \textbf{Subject to}: & \dfrac{d\mathbf{y}}{dt} = \mathbf{f}(\mathbf{y}(t), \mathbf{u}(t), t) \\ & \mathbf{u}(t) \in \mathcal{U} \\ & \mathbf{y}(t) \in \Sigma \\ \textbf{By varying}: & \mathbf{u}(t) \end{array}\right\} \tag{45}$$

In Eq. (45), ϕ is the terminal state cost, $\mathcal{L}$ is the transient or path cost, $\mathcal{U}$ is the set of admissible controls, and Σ is the set of admissible states. Suppose that there is a constraint on the state given by

$$\mathbf{s}(\mathbf{y}, t) = 0 \tag{46}$$

Differentiating Eq. (46) with respect to time, one obtains

$$\dot{\mathbf{s}} = \frac{\partial \mathbf{s}}{\partial t} + \frac{\partial \mathbf{s}}{\partial \mathbf{y}} \frac{d\mathbf{y}}{dt} = \mathbf{0} \tag{47}$$

Substituting the state equation into this result yields

$$\dot{\mathbf{s}} = \frac{\partial \mathbf{s}}{\partial t} + \frac{\partial \mathbf{s}}{\partial \mathbf{y}} \mathbf{f}(\mathbf{y}(t), \mathbf{u}(t), t) = \mathbf{0} \tag{48}$$

Equation (48) provides a technique to yield the optimal control, $\mathbf{u}(t)$, that minimizes $\mathcal{J}$ and meets the equality constraint on the state[151, 152]. If the control is not explicit in Eq. (47), then the process of differentiating $\mathbf{s}$ and substituting the state equation is continued until the control is explicit in the equation to form a set of q point relationships $\{\mathbf{s}^{(n)}\}, \quad n = 0, \ldots, q-1$, where n is the order of the derivative. These tangency conditions can be adjoined using Lagrange multipliers to the path cost, $\mathcal{L}$, to solve for the optimal control history.

Inequality constraints of the form

$$\bar{\mathbf{s}}(\mathbf{y}, t) \leq \mathbf{0} \tag{49}$$

can be handled similarly[151, 152]. In this case, the solution process depends on whether or not the state is on the boundary. If it is on the boundary, the same solution process to equality constraints is followed, while for off-boundary solutions, the terms are ignored. This results in a multiple sub-arc solution, although fundamentally the process is identical to the equality constraint case.

3.2.2 Discrete Dynamical Systems

For the discrete optimal control problem posed as[140]

$$\left.\begin{aligned}
&\textbf{Minimize}: && \mathcal{J}(\mathbf{y}, \mathbf{u}) = \sum_{k=0}^{n-1} \mathcal{L}(\mathbf{y}_k, \mathbf{u}_{k+1}, k) \\
&\textbf{Subject to}: && \mathbf{y}_{k+1} = \mathbf{f}(\mathbf{y}_k, \mathbf{u}_{k+1}, k), \quad \forall k \in \{0, \ldots, n-1\} \\
& && \mathbf{u}_k \in \mathcal{U}(\mathbf{y}_{k-1}), \quad \forall k \in \{1, \ldots, n\} \\
& && \mathbf{y}_k \in \Sigma, \quad \forall k \in \{0, \ldots, n-1\} \\
&\textbf{By varying}: && \mathbf{u}_k, \quad \forall k \in \{1, \ldots, n\}
\end{aligned}\right\} \tag{50}$$

where the restrictions on the domain of $\mathbf{u}_k$ and $\mathbf{y}_k$ provide an opportunity to introduce constraints on the design variables and CA's output, respectively. Similarly to the continuous optimal control problem, the constraints are appended to the objective

function through Lagrange multipliers, which, in turn, ensure the satisfaction of the constraints.

The discrete optimal control solution satisfies the following necessary conditions. First, assume the following regarding the analysis domain:

1. $\mathcal{U}$ is defined for each $\mathbf{y} \in \Sigma$ by equality and inequality constraints of the form

$$\mathbf{g}(\mathbf{y}, \mathbf{u}) \leq \mathbf{0}; \quad \mathbf{g} \in \mathbb{R}^{q_k \times 1} \tag{51}$$

$$\mathbf{h}(\mathbf{y}, \mathbf{u}) = \mathbf{0}; \quad \mathbf{h} \in \mathbb{R}^{k_k \times 1} \tag{52}$$

2. Σ is defined by the equality and inequality constraints of the form

$$\mathbf{w}(\mathbf{y}) = \mathbf{0}; \quad \mathbf{w} \in \mathbb{R}^{r_k \times 1} \tag{53}$$

$$\boldsymbol{\omega}(\mathbf{y}) \leq \mathbf{0}; \quad \boldsymbol{\omega} \in \mathbb{R}^{p_k \times 1} \tag{54}$$

3. There exists convex cones, $\mathcal{P}^{(i)}$ and $\mathcal{Q}^{(i)}$ with vertices at $\mathbf{y}_k$ that cover Σ for all $k = 0, 1, \ldots, n$

4. There exists a scalar $\psi_0 \leq 0$ and vectors

$$\boldsymbol{\psi}_k = [\psi_{1,k}, \ldots, \psi_{n,k}]^T, \quad \forall k \in \{1, \ldots, n\} \tag{55}$$

$$\boldsymbol{\gamma}_k = [\gamma_{1,k}, \ldots, \gamma_{k_k,k}]^T, \quad \forall k \in \{1, \ldots, n\} \tag{56}$$

$$\boldsymbol{\lambda}_k = [\lambda_{1,k}, \ldots, \lambda_{q_k,k}]^T, \quad \forall k \in \{1, \ldots, n\} \tag{57}$$

$$\boldsymbol{\mu}_k = [\mu_{1,k}, \ldots, \mu_{r_k,k}]^T, \quad \forall k \in \{0, \ldots, n\} \tag{58}$$

$$\boldsymbol{\nu}_k = [\nu_{1,k}, \ldots, \nu_{p_k,k}]^T, \quad \forall k \in \{0, \ldots, n\} \tag{59}$$

$$\mathbf{b}^{(i)}, \quad i = 1, \ldots, n \quad \forall k \in \{0, \ldots, n\} \tag{60}$$

such that the direction of $\mathbf{b}^{(i)}$ lies in the dual cone $\mathcal{D}(\mathcal{P}^{(i)})$

5. Let a scalar function $H_k(\mathbf{y}, \mathbf{u})$ be defined as

$$H_k(\mathbf{y}, \mathbf{u}) = \psi_0 \mathcal{L}(\mathbf{y}, \mathbf{u}, k) + \boldsymbol{\psi}_k^T \mathbf{f}(\mathbf{y}, \mathbf{u}, k) + \boldsymbol{\gamma}_k^T \mathbf{h}(\mathbf{y}, \mathbf{u}) + \boldsymbol{\lambda}_k^T \mathbf{g}(\mathbf{y}, \mathbf{u}) \tag{61}$$

The necessary conditions for an optimal control to exist are then given by:

1. If $\psi_0 = 0$ then for at least one k at least one of the vectors $\boldsymbol{\psi}_k$, $\boldsymbol{\gamma}_k$, $\boldsymbol{\lambda}_k$, $\boldsymbol{\mu}_k$, $\boldsymbol{\nu}_k$, or $\mathbf{b}^{(i)}$ is non-zero

2. For all $k = 0, \ldots, n$ and any vector $\boldsymbol{\delta}\mathbf{y}$ whose direction lies in the intersection of the cones $\mathcal{Q}^{(i)}$, the following inequality holds

$$\left(-\boldsymbol{\psi}_k + \frac{\partial H_{k+1}(\mathbf{y}, \mathbf{u})}{\partial \mathbf{y}} + \boldsymbol{\mu}_k^T \frac{\partial \mathbf{w}(\mathbf{y})}{\partial \mathbf{y}} + \boldsymbol{\nu}_k^T \frac{\partial \boldsymbol{\omega}(\mathbf{y})}{\partial \mathbf{y}} - \sum_{i=1}^{n_k} \mathbf{b}^{(i)} \right)^T \boldsymbol{\delta}\mathbf{y} \leq 0$$

   where it is assumed that $\boldsymbol{\psi}_0 = \mathbf{0}$ and $H_{n+1} = 0$

3. $\dfrac{\partial H(\mathbf{y}_{k-1}, \mathbf{u}_k)}{\partial \mathbf{u}} = \mathbf{0}, \quad \forall k \in \{1, \ldots, n\}$

4. $\lambda_{\alpha,k} \leq 0$, $\lambda_{\alpha,k} g_k^\alpha(\mathbf{y}_{k-1}, \mathbf{u}_k) = 0$ $\forall \alpha \in \{1 \ldots, q_k\}$ and $k \in \{1, \ldots, n\}$

5. $\nu_{\alpha,k} \leq 0$, $\nu_{\alpha,k} \omega_k^\alpha(\mathbf{y}_k) = 0$ $\forall \alpha \in \{1, \ldots, p_k\}$ and $k \in \{0, \ldots, n\}$

The proof of these conditions minimizing $\mathcal{J}(\mathbf{y}, \mathbf{u})$ is found in Ref. [140]. Note that the process of adjoining the tangents of the state and control constraints to the objective functional in the second criteria is nearly identical to that of the continuous case with the additional requirement that the space is convex.

3.2.3 Solution Methods

The discrete problem as posed is a nonlinear programming (NLP) problem, which has many known solution techniques, including gradient methods, quadratic programming, sequential quadratic programming, and interior-point methods[153, 140, 154].

Direct methods to the continuous problem also approach the solution procedure to the optimal control problem as a discretized problem, giving rise to an NLP. However, unlike the discrete formulation described previously, the direct solution to the continuous problem may require the use of penalty functions for constraints. Alternatively, indirect methods would approximate the discrete problem as a continuous

problem (*i.e.*, taking the step size caused by the iteration to zero) and then solve the resulting boundary value problem. This allows the constraints to be handled directly using Lagrange multipliers. The validity of viewing the discrete problem as a continuous problem has been shown to work well for multidisciplinary design problems, as the solution set is in general more restrictive (including continuity requirements on the constraints) than the discrete problem; however, solutions may not always exist[155, 156, 132, 157]. This is further shown in Chapter 5.

A comparison of the different solution methods is shown in Table 5.

Table 5: Comparison of solution techniques.

	Advantages	**Disadvantages**
Direct Methods	Large Region of Attraction Large Number of NLP Solvers	Computationally Intensive Convexity Requirement Use of Penalty Functions
Indirect Methods	Fast Convergence Solution Optimality Exact Solution of Constraints	Small Region of Attraction Solutions May Not Exist

3.2.4 Solution Search Coordination

By accommodating both design variables and CA constraints at the same level in the optimization hierarchy, a reduced design space can be searched which eliminates the design region with conflicting constraints. This is shown schematically in Fig. 15.

In Fig. 15(a), the design region resulting from traditional optimization where constraints are only a function of design variables is shown which implies that there is a relatively large feasible region. While in Fig. 15(b) the feasible region that actually exists is shown as it accounts for all possible constraints in the problem. This is the region that is searched by approaching this problem from the optimal control perspective.

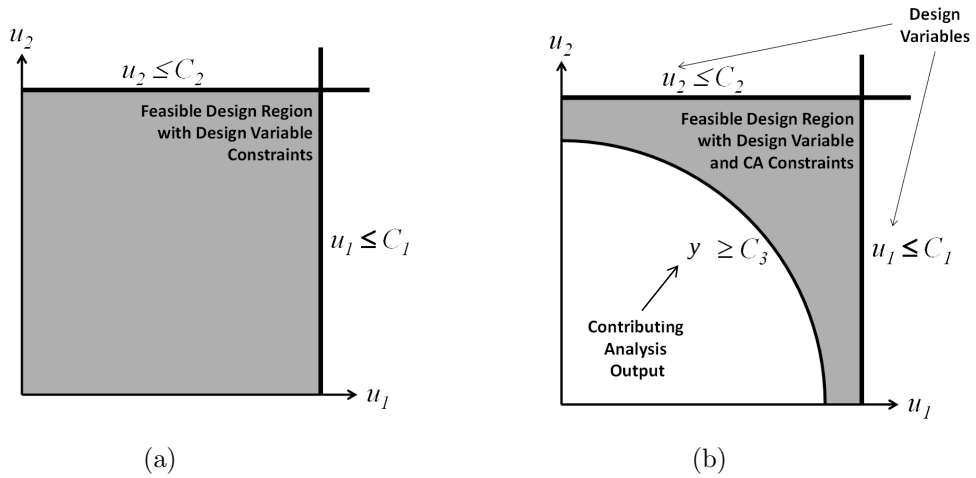

Figure 15: Feasible design space accounting for (a) design variable constraints only and (b) design variable and contributing analysis constraints.

3.3 Propagating Uncertainty Using Estimation Theory

Feedback within a multidisciplinary design problem leads to significantly longer analysis times. Several methods have been developed to eliminate feedback within the design. The traditional approach to eliminate the feedback within the design-analysis cycle is to enforce a constraint in the *converged* design that the estimated value of the feedback variable is within a given tolerance of the value resulting from the subsequent CA. This is an effective technique for deterministic analysis and design; however, increasing the number of constraints can be computationally time consuming for robustness assessment and robust design. A novel technique which applies concepts from estimation theory to this challenge is the use of the Kalman filter. This approach is particularly applicable to the robustness analysis problem as the final quantities being sought are the mean and the variance of an objective function. This approach has not been implemented previously because the Kalman filter is typically implemented with respect to a dynamical system and the multidisciplinary analysis and design problem is traditionally concerned with algebraic quantities. This use of the Kalman filter in this fashion is analogous to linear covariance methods described

in Refs. [82, 83, 84] and Appendix A.

3.3.1 The Discrete Kalman Filter

The Kalman filter can be thought of as a two step process, one which predicts the state (*e.g.*, the output of the CAs) and then an update step which corrects these estimates based on the dynamics of the system. The prediction step is given by the following equations[82, 135, 158, 159, 160, 161, 162]

$$\hat{\mathbf{y}}_{k|k-1} = \mathbf{F}_k \hat{\mathbf{y}}_{k-1|k-1} + \mathbf{B}_k \mathbf{u}_k \tag{62}$$

$$\mathbf{\Sigma}_{k|k-1} = \mathbf{F}_k \mathbf{\Sigma}_{k-1|k-1} \mathbf{F}_k^T + \mathbf{Q}_k \tag{63}$$

where the notation $j|k$ represents the estimate at j given observations up to and including k. Furthermore, the value of $\hat{\mathbf{y}}_{0|0}$ is the initial mean state and $\mathbf{\Sigma}_{0|0}$ is the initial covariance matrix of the state values. The correction step is governed by the following equations[82, 135, 158, 159, 160, 161, 162]

$$\tilde{\mathbf{x}}_k = \mathbf{z}_k - \mathbf{H}_k \hat{\mathbf{y}}_{k|k-1} \tag{64}$$

$$\mathbf{S}_k = \mathbf{H}_k \mathbf{\Sigma}_{k|k-1} \mathbf{H}_k^T + \mathbf{R}_k \tag{65}$$

$$\mathbf{K}_k = \mathbf{\Sigma}_{k|k-1} \mathbf{H}_k^T \mathbf{S}_k^{-1} \tag{66}$$

$$\hat{\mathbf{y}}_{k|k} = \hat{\mathbf{y}}_{k|k-1} + \mathbf{K}_k \tilde{\mathbf{x}}_k \tag{67}$$

$$\mathbf{\Sigma}_{k|k} = \left(\mathbf{I} - \mathbf{K}_k \mathbf{H}_k\right) \mathbf{\Sigma}_{k|k-1} \tag{68}$$

where the final (*a posteriori*) estimate of the state is given by $\hat{\mathbf{y}}_{k|k}$ with covariance matrix given by $\mathbf{\Sigma}_{k|k}$.

3.3.2 Formulating the Multidisciplinary Design Problem in a Form Compatible with the Kalman Filter

The root-finding problem has been shown to be a dynamical system which can be defined by the relation

$$\mathbf{y}_k = \mathbf{f}(\mathbf{y}_{k-1}), \quad \forall k \in \mathbb{Z}_+ \setminus \{0\} \tag{69}$$

where $\mathbf{f}(\mathbf{y}_{k-1})$ is the output value of the CAs on the $k^{\text{th}} - 1$ iteration. For random variables in a linear system, this can be written in the form

$$\mathbf{y}_k = \mathbf{F}_k \mathbf{y}_{k-1} + \mathbf{w}_{k-1}, \quad \forall k \in \mathbb{Z}_+ \setminus \{0\} \tag{70}$$

where $\mathbf{w}_{k-1}$ is the noise associated with the model. For a linear multidisciplinary design, Eq. (70) can also be written as

$$\mathbf{y}_k = \mathbf{F}_k \mathbf{y}_{k-1} + \mathbf{B}_k \mathbf{u}_k + \mathbf{w}_{k-1} \tag{71}$$

which allows for inputs into the CA that are not outputs of other CAs, $\mathbf{u}_k$. When coupled with an equation of the form

$$\mathbf{z}_k = \mathbf{H}_k \mathbf{y}_k + \mathbf{v}_k \tag{72}$$

and when it is assumed that $\mathbf{w}_{k-1} \sim \mathcal{N}(\mathbf{0}, \mathbf{Q}_{k-1})$ and $\mathbf{v}_{k-1} \sim \mathcal{N}(\mathbf{0}, \mathbf{R}_{k-1})$, Eqs. (71) and (72) define the dynamical system needed for a Kalman filter[158, 159, 160, 161]. The noise parameter, $\mathbf{w}_{k-1}$, gives the opportunity to account for random variables within the linearization of the input-output relationship, that is random variables associated with the matrix $\mathbf{F}$. In this work, the Kalman filter is used as a data fusion technique to give an optimal unbiased statistical estimate of the output of the CAs as the design is converging.

The power in implementing the Kalman filter in multidisciplinary design analysis lies in the ability to obtain a continuous estimate in iterate of both the mean and covariance of each CA's output in the multidisciplinary design by propagating a system of seven equations until the design converges.

3.3.3 Using the Covariance Matrix to Guide Design Decomposition

As one of the outputs of the Kalman filter is the estimated covariance at iteration k this information could be used to ascertain the correlation coefficient between variables. Provided the covariance estimate, $\mathbf{\Sigma}$, has the form of Eq. (12) and can be

represented as

$$\boldsymbol{\Sigma} = \{\boldsymbol{\Sigma}_{ij}\} \tag{73}$$

then the representative correlation (or product-moment) coefficients are given by

$$\rho_{ij} = \frac{\boldsymbol{\Sigma}_{ij}}{\sqrt{\boldsymbol{\Sigma}_{ii}}\sqrt{\boldsymbol{\Sigma}_{jj}}}, \quad i \neq j \tag{74}$$

where $\rho_{ij} \in [-1, 1]$. What is important about the correlation coefficient is that it gives a relative measure of how variable j depends on variable i. In particular as $|\rho_{ij}| \to 1$ the importance of variable i on the response of variable j increases. This gives a meaningful way to ascertain the importance of each CA and variables on other CAs and variables. For design decomposition, it may be acceptable to neglect the feedback variables with small correlation coefficient magnitudes.

3.4 Summary

This chapter provides the theory behind application of three techniques from dynamical system theory to the multidisciplinary design problem. Stability analysis was shown to be useful in determining whether a design is feasible, whether an optimal design exists, the range of initial values that can be used to converge the design, and the rate at which the design will converge. Control theory is shown to be capable of enforcing constraints that are functions of the CA's output and the design variables at the same level in the optimization hierarchy. Finally, estimation theory is shown to be capable of propagating uncertainty through the multidisciplinary design, providing a method to simultaneously converge the design and quantify the uncertainty associated with each design point.

CHAPTER IV

DEVELOPMENT OF A FRAMEWORK FOR THE RAPID ROBUST DESIGN OF MULTIDISCIPLINARY SYSTEMS

This chapter takes the foundations set forth in Chapter 2 to view the multidisciplinary design problem as a dynamical system to develop a comprehensive rapid robust design framework for linear designs that utilizes dynamical system theory. This methodology uses the three techniques described in Chapter 3, stability analysis, control theory, and estimation theory as an ensemble. A framework is developed for two different root-finding techniques—fixed-point iteration and Newton-Raphson iteration, although it is extensible to other numerical root-finding methods that are recursive. A discussion is also provided about how to extend this inherently linearly framework to nonlinear multidisciplinary design through successive linearization.

4.1 A Rapid Design Robustness Analysis Framework

The cumulative contribution of this work is the ability to rapidly obtain a bound on the robustness of a multidisciplinary system by posing the multidisciplinary design problem as a dynamical system. In particular, a methodology that rapidly obtains the mean and a bound on the variance of a multidisciplinary design's response is developed. The theoretical development of this methodology is restricted to linear multidisciplinary designs. This implies a CA whose output, $\mathbf{y}$, can be functionally represented as a linear combination of the inputs into the CA, $\mathbf{x}$, and an offset, $\mathbf{b}$, or $\mathbf{y} = \mathbf{A}\mathbf{x} + \mathbf{b}$. While this may seem to be a restrictive framework in which to operate, as in many engineering analyses, linearization can be employed to allow the CAs to fit this functional form. With the mean and variance bound found, traditional measures

of design robustness can be obtained (*e.g.*, the mean, variance, MSD, etc.). Many robustness assessment techniques, particularly those associated with NLP solutions, require solution of a large number of trials. These trials consist of input variables being drawn from distributions and then converging the design through iteration in order to obtain the performance for that trial. The robustness of the design is then ascertained by repeating this process until the output distribution is formed. The methodology developed in this work circumvents the time intensive process of propagating individual trials to obtain the output distribution by using the mean and covariance matrix (the typical quantities needed to define robustness) directly and then derives a bound on the response's variance. With such a technique in place to obtain estimates on the mean and variance, the design robustness may be directly traded early in the design process.

A general multidisciplinary design features coupling between CAs. This may lead to convergence issues, potentially requiring significant iteration in order to converge on a design. As discussed previously, the iteration scheme implemented to find the solution to the multidisciplinary design can be cast as a dynamical system where the state is the output of each of the CAs and the fixed rule describing its evolution is the method used to find the root of the design. In order to examine the existence of a solution, the first application of this new perspective of multidisciplinary design is used—stability analysis. If the dynamical system described by an iteration scheme is asymptotically stable, there exists at least some solution to the multidisciplinary design.

Another enabling technique for this methodology is in the handling of the multidisciplinary design requirements. These are generally written as equality and inequality constraints that are functions of the state. The iteration scheme implicitly handles the compatibility constraints within the multidisciplinary design, a general statement that each CA in a converged design must use the same information. Other constraints

must be handled by more explicit techniques. By viewing the multidisciplinary design as a dynamical system, design constraints are able to be handled through similar techniques as state and control constraints in optimal control, where the constraints are added to the objective function. Adjoining these constraints allows the design variables to appear explicitly in the objective function formulation. This method allows for simultaneous handling of constraints of the outputs of each CA, which are the coupling variables in the design, as well as the design variables.

The last of the the dynamical system techniques employed in this work to obtain a rapid assessment of the design robustness is the use of an estimation technique traditionally applied to state estimation, the Kalman filter. The Kalman filter is a statistical estimation technique for linear dynamical systems which combines measurements to estimate the true dynamics of the system. The multidisciplinary design utilization of the Kalman filter allows for the mean (or nominal) and the covariance matrix of each CA's output to be found simultaneously as a function of iterate number. In this sense, the propagation of the filter equations can be used to converge the design and provide estimates of robustness instead of requiring convergence for each Monte Carlo sample, as in traditional robustness analysis.

Two additional techniques from non-traditional design fields are also used in the methodology. The first of these is the unscented transform, which is a statistical transformation that gives accurate estimates of the first two moments of the output probability distribution of a CA while only evaluating a small sample of carefully chosen points, the sigma points. This technique, is similar to a Monte Carlo; however, third order accuracy of the mean and covariance matrix is maintained for any functional form of the CA despite the small number of trials (sigma points) evaluated. The last enabling technique used in this work is the two-norm of a matrix. The matrix two-norm provides a conservative bound for the output covariance variance, as it finds the principal eigenvalue (*i.e.*, the "variance" along the principal direction

of the covariance matrix). This quantity gives a bound on the variance and, as shown later, can be used as a direct surrogate for the variance for fixed distributions as the observed error remains identical.

4.2 A Rapid Robust Design Methodology

The following section describes a rapid robust design methodology that implements a matrix-norm to obtain a bound on the variance of a multidisciplinary system which can be decomposed into CAs.

4.2.1 Formulation with Fixed-Point Iteration

Step 1: Decompose the Design

A general multidisciplinary design can be decomposed into multiple CAs. Each of these CAs represents an analysis that contributes to the entire design. For example, consider the design or analysis of an entry system. It may be desired for the entry system to be evaluated with respect to its payload capability and landing accuracy. Many different analyses must be conducted in order to obtain this information. This information flow is shown in Fig. 16, where one such representation of each of the analyses that must be conducted to design an entry system is shown[163]. In this case, the entry system is decomposed into seven CAs. The responses of these CAs allow the payload capability as well as the landed accuracy to be assessed. Each CA in Fig. 16 (*i.e.*, the blocks) represents an input-output relationship. For instance, inputs into the aerodynamics analysis include the configuration of the entry system and planetary body where it is to operate; outputs include the force coefficients of the vehicle as a function of Mach number and attitude. This relationship may be known analytically; however, it is more likely that this CA would represent a computational analysis that is linked into the design process. This decomposition is also analogous to that required by other MDO techniques, such as SSA, OBD, and CO and therefore requires no additional upfront computational time.

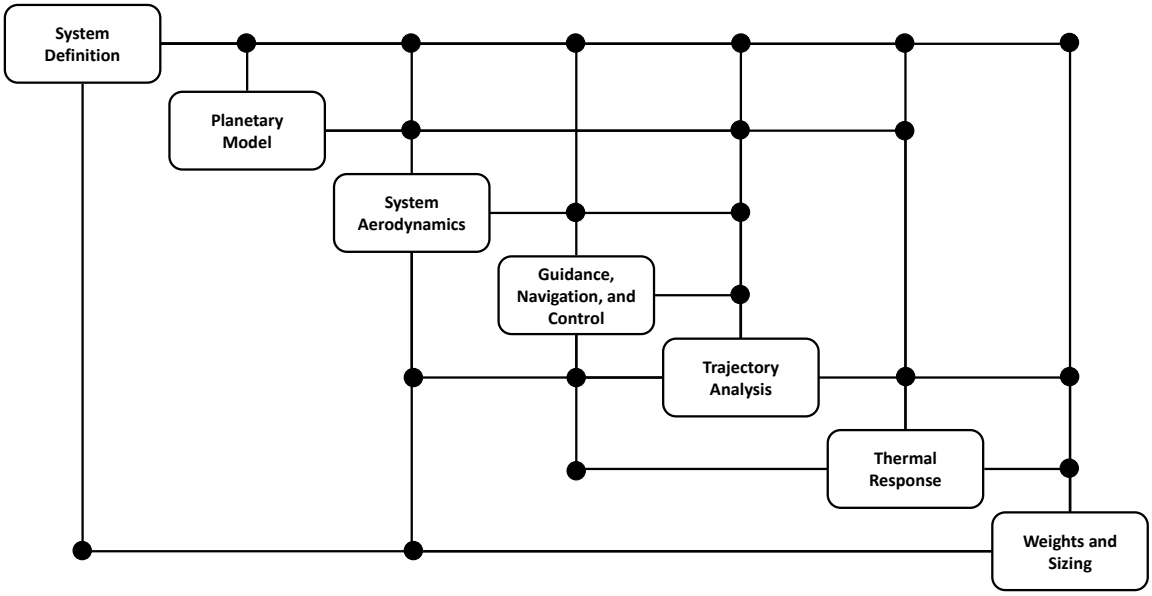

Figure 16: The decomposition of an entry system into a Design Structure Matrix.

In the theoretical development underlying this work, it is assumed that each of the n CAs are linear and algebraic. This limitation will be addressed subsequently. That is, the output of the CA is of the form

$$\mathbf{y_j} = \mathbf{A_j y} + \mathbf{B_j u_d} + \mathbf{C_j u_p} + \mathbf{d_j} \tag{75}$$

where $\mathbf{y_j} \in \mathbb{R}^{l_j}$, $\mathbf{y} \in \mathbb{R}^m$ is the concatenated output from all of the CAs (*e.g.*, if $\mathbf{y_1}$, $\mathbf{y_2}$ through $\mathbf{y_n}$ are the outputs of the n CAs in a multidisciplinary design, $\mathbf{y} = \left(\mathbf{y_1}^T\ \mathbf{y_2}^T\ \cdots\ \mathbf{y_n}^T\right)^T$), $\mathbf{u_d} \in \mathbb{R}^d$ are the deterministic system-level inputs into the design, $\mathbf{u_p} \in \mathbb{R}^p$ are the probabilistic system-level inputs into the design, and $\mathbf{d_j} \in \mathbb{R}^{l_j}$ is the bias associated with the model. This implies $\mathbf{A_j} \in \mathbb{R}^{l_j \times m}$, $\mathbf{B_j} \in \mathbb{R}^{l_j \times d}$, $\mathbf{C_j} \in \mathbb{R}^{l_j \times p}$, and that $\sum_{j=1}^{n} l_j = m$.

For general designs where the CAs may not be linear, the required functional form can be achieved through linearization where $\mathbf{A_j} = \left.\frac{\partial \mathbf{g}}{\partial \mathbf{y}}\right|_{\tilde{\mathbf{y}}}$, $\mathbf{B_j} = \left.\frac{\partial \mathbf{g}}{\partial \mathbf{u_d}}\right|_{\tilde{\mathbf{u}}_\mathbf{d}}$, $\mathbf{C_j} = \left.\frac{\partial \mathbf{g}}{\partial \mathbf{u_p}}\right|_{\tilde{\mathbf{u}}_\mathbf{p}}$, and

$$\mathbf{d_j} = -\left(\mathbf{A_j}\tilde{\mathbf{y}} + \mathbf{B_j}\tilde{\mathbf{u}}_\mathbf{d} + \mathbf{C_j}\tilde{\mathbf{u}}_\mathbf{p}\right)$$

when the input-output relationship for the CA is given by $\mathbf{y_j} = \mathbf{g}\left(\mathbf{y}, \mathbf{u_d}, \mathbf{u_p}\right)$ and $\tilde{(\cdot)}$

is the value of $(\cdot)$ about which the function is linearized. During the iteration, $\tilde{(\cdot)}$ is the value of $(\cdot)$ from the prior iteration.

Step 2: Identify the Random Variables and their Distributions

In the design and analysis of a complex multidisciplinary system, it is unlikely that each of the models and inputs are deterministic; instead, many are likely to be probabilistic and account for unknowns in the modeling and in the operating conditions . In order to propagate these uncertainties through the design to estimate the robustness, the probabilistic variables must be identified.

The random variables associated with the uncertainty within the design are handled in two different ways in this work depending on where the random variable is functionally located. Functionally, the uncertainty resulting from inputs into the CA refers to uncertainties associated with $\mathbf{u_p}$, whereas uncertainty associated with the physical modeling pertain to $\mathbf{A_j}$, $\mathbf{B_j}$, $\mathbf{C_j}$, or $\mathbf{d_j}$. In the first instance, the mean is propagated in the $\hat{\mathbf{y}}_{k|k}$ term of the filter equations and the covariance is propagated in the $\mathbf{\Sigma}_{k|k}$ term of the filter equations. In the second case, the mean is again accounted for in the $\hat{\mathbf{y}}_{k|k}$ term of the equations; however, the covariance is accounted for in the $\mathbf{Q}_k$ term of the filter. In the components of the Kalman filter mentioned, the notation $k|k$ refers to the k^{th} iteration of the filter given all previous information regarding the convergence of the system.

Due to the the propagation within the Kalman filter there is an assumption that the uncertainties associated with the model are Gaussian. For symmetrical probability distributions (*i.e.*, probability distributions centered about the mean), this is not an overly strong assumption since the first two moments are the only terms being approximated. However, for asymmetric probability distributions, this becomes a restrictive assumption that is a limitation of this technique.

Step 3: Form the Iterative Equations

In order to implement the discrete Kalman filter, a causal, discrete dynamical system must be formed. The process of converging the multidisciplinary design through root solving leads to an inherent dynamical system. This root is typically sought out using an iterative technique. For example, fixed-point iteration, defined in Eq. (69) uses the previous iteration's solution as an input to the current iteration. For this work, $\mathbf{f}(\cdot)$ is the concatenation of the input-output relationships for the CAs (*e.g.*, if $\mathbf{f_1}(\cdot)$, $\mathbf{f_2}(\cdot)$ through $\mathbf{f_n}(\cdot)$ describe the input-output relationship for each of the n CAs, $\mathbf{f}(\cdot) = \left(\mathbf{f_1}^T(\cdot)\ \mathbf{f_2}^T(\cdot)\ \cdots\ \mathbf{f_n}^T(\cdot)\right)^T$). In the framework described here, where the multidisciplinary design consists solely of linear CAs, the fixed-point iteration relationship becomes tractable

$$\mathbf{y}_k = \mathbf{\Lambda}\mathbf{y}_{k-1} + \boldsymbol{\beta}\mathbf{u_d} + \boldsymbol{\gamma}\mathbf{u_p} + \boldsymbol{\delta}, \quad \forall k \in \{1, 2, ...\} \tag{76}$$

where it is assumed that $\mathbf{\Lambda} = \begin{pmatrix} \mathbf{A_1} \\ \vdots \\ \mathbf{A_n} \end{pmatrix} \in \mathbb{R}^{m\times m}$, $\boldsymbol{\beta} = \begin{pmatrix} \mathbf{B_1} \\ \vdots \\ \mathbf{B_n} \end{pmatrix} \in \mathbb{R}^{m\times d}$, $\boldsymbol{\gamma} = \begin{pmatrix} \mathbf{C_1} \\ \vdots \\ \mathbf{C_n} \end{pmatrix} \in \mathbb{R}^{m\times p}$, and $\boldsymbol{\delta} = \begin{pmatrix} \mathbf{d_1} \\ \vdots \\ \mathbf{d_n} \end{pmatrix} \in \mathbb{R}^m$.

Step 4: Ensure a Solution Exists

Since the iterative system defined by Eq. (76) is a discrete, linear, dynamical system, the existence of a solution to the multidisciplinary design problem is given solely by the stability of the system. In particular, if the system is asymptotically stable, a converged design exists for some initial guess of the CA outputs and if it is globally asymptotically stable, a design exists for all initial guesses of the CA outputs.

For cases where $\mathbf{\Lambda}$ is a constant matrix, finding the eigenvalues of the matrix $\mathbf{\Lambda}$ determines the existence of a design solution. Should all of these eigenvalues have

moduli less than unity (*i.e.*, $|\lambda_i| < 1$) the dynamical system is globally asymptotically stable and the multidisciplinary system will converge regardless of the initial guess for the output of the CAs. However, should this not be the case, and at least one eigenvalue has a modulus greater than or equal to unity (*i.e.*, $|\lambda_i| \geq 1$), a contraction mapping does not exist for the choice of root-finding schemes and the design will not converge.

When $\mathbf{\Lambda}$ is a varying matrix or even a nonlinear mapping, a Lyapunov function technique can be used to investigate the stability (and convergence) of the design. In this case, for asymptotic stability, a positive-definite function is sought whose difference between iterates in some region around the origin is negative definite. As described in Chapter 3, the search for a Lyapunov function can be accomplished using several methods, including some numerical based techniques. A sum-of-squares analysis can be performed by expanding $\mathbf{g}(\mathbf{y}, \mathbf{u_d}, \mathbf{u_p})$ in a sufficiently high-order Taylor Series. This expansion can then be used in the semidefinite programming problem as described in Eq. (42).

Step 5: Estimate the Mean Output and the Covariance

The mean output of the multidisciplinary system and the associated covariance matrix are found by propagating the Kalman filter equations, Eqs. (62)-(68) until convergence. In order to accomplish this, the iterative system formed in Eq. (76) needs to be transformed to the form needed in Kalman filter, Eq. (71). This is a relatively straightforward process when the following substitutions are made

$$\mathbf{F}_{k-1} = \mathbf{\Lambda}, \quad \forall k \in \{1, 2, ...\} \tag{77}$$

$$\mathbf{B}_{k-1} = \begin{pmatrix} \boldsymbol{\beta} & \boldsymbol{\gamma} & \mathbf{I_{m \times m}} \end{pmatrix}, \quad \forall k \in \{1, 2, ...\} \tag{78}$$

$$\mathbf{u}_{k-1} = \begin{pmatrix} \mathbf{u_d} \\ \mathbf{u_p} \\ \boldsymbol{\delta} \end{pmatrix}, \quad \forall k \in \{1, 2, ...\} \tag{79}$$

The mean state, that is the output of the analyses, ($\hat{\mathbf{y}}_{0|0}$) and the covariance matrix associated with the state ($\mathbf{\Sigma}_{0|0}$) are initialized by the relations

$$\hat{\mathbf{y}}_{0|0} = \mathbf{y_0} \tag{80}$$

$$\mathbf{\Sigma}_{0|0} = \mathbf{\Sigma_0} \tag{81}$$

In this work, $\mathbf{y_0}$ and $\mathbf{\Sigma_0}$ are found by assuming a starting value for the coupled CA and an input covariance matrix associated with the parameters of the problem. These values are then propagated through each CA of a serial (*i.e.*, uncoupled) design structure matrix using the unscented transform technique. The concatenated output of each of the CAs is then used to form $\mathbf{y_0}$ and the covariance matrix $\mathbf{\Sigma_0}$, which will initially be a block diagonal matrix. The last parameter which need to be identified in order to estimate the mean output and the covariance of the system is the covariance matrix associated with the model, $\mathbf{Q}$. This is a block diagonal matrix composed of the variances and covariances associated with $\mathbf{A_j}$, $\mathbf{B_j}$, $\mathbf{C_j}$, and $\mathbf{d_j}$. Note that the iteration starts from an infeasible design point as the compatibility constraints are not met and moves to a converged design which meets the design constraints using Step 7.

The iterates are then found by by propagating the filter equations, Eqs. (62)-(68), with $\mathbf{H}_{k-1} = \mathbf{I_{m\times m}} \quad \forall k \in \{1, 2, ...\}$ and $\mathbf{R}_{k-1} = \mathbf{0} \quad \forall k \in \{1, 2, ...\}$ until the design convergence criterion is met. These are the values used by Geller to assess state-only uncertainty using linear covariance analysis[84]. These values also enable the estimate to approach the Cramer-Rao lower bound.

The exact convergence criterion can be of several forms, the two criterion used within this work are an absolute tolerance of the state and a relative tolerance of the

state. These are demonstrated in the following relations

$$\| \hat{\mathbf{y}}_{k|k} - \hat{\mathbf{y}}_{k-1|k-1} \|_2 \leq \epsilon_1 \tag{82}$$

$$\frac{\| \hat{\mathbf{y}}_{k|k} - \hat{\mathbf{y}}_{k-1|k-1} \|_2}{\| \hat{\mathbf{y}}_{k-1|k-1} \|_2} \leq \epsilon_2 \tag{83}$$

Step 6: Identify the Mean and Variance Bound of the Objective Function Assume the design objective is a linear combination of the outputs of linear CAs, that is

$$r = \mathbf{M}\mathbf{y}^* \tag{84}$$

where $r \in \mathbb{R}$ is the design objective value, $\mathbf{M} \in \mathbb{R}^{1\times q}$ is a matrix describing the linear combination of the pertinent CA outputs, and $\mathbf{y}^* \in \mathbb{R}^q$ is the vector of pertinent CA responses that contribute to the design objective. An estimate of the mean and variance bound for the design objective can be found as follows

$$\bar{r} = \mathbf{M}\hat{\mathbf{y}}^*_{n|n} \tag{85}$$

$$\sigma_r^2 \leq \| \boldsymbol{\Sigma}_{\boldsymbol{y}^*{}_{n|n}} \|_2 \, \mathbf{M}\mathbf{1}_q \tag{86}$$

where it is assumed the n iterations have occurred and $\boldsymbol{\Sigma}_{\boldsymbol{y}^*{}_{n|n}}$ is the reduced covariance matrix associated with only the variables associated with $\mathbf{y}^*$ (*i.e.*, the rows and columns of the variables not pertinent in the design objective are eliminated from $\boldsymbol{\Sigma}_{\boldsymbol{y}_{n|n}}$). Additionally, the notation $\mathbf{1}_q \in \mathbb{R}^{q\times 1}$ is the unity vector of length q (*i.e.*, $\mathbf{1}_q = (1\ 1\ 1 \cdots\ 1)^T \in \mathbb{R}^{q\times 1}$).

More generally, a first-order expansion of an objective function that is of the form

$$r = g(\mathbf{y}^*) \tag{87}$$

can be made. The linearized objective function, Eq. (87), about $\mathbf{y}^*_{\mathbf{nom}}$ is then given by

$$\tilde{r} = \frac{\partial g}{\partial \mathbf{y}^*}\mathbf{y}^* - \frac{\partial g}{\partial \mathbf{y}^*}\mathbf{y}^*_{\mathbf{nom}} = \mathbf{N}\mathbf{y}^* + b \tag{88}$$

which leads to the results

$$\bar{r} \approx \mathbf{N}\hat{\mathbf{y}}^*_{n|n} + b \tag{89}$$

$$\sigma_r^2 \approx \| \mathbf{\Sigma}_{\boldsymbol{y}^* n|n} \|_2 \, \mathbf{N}\mathbf{1}_q^T \tag{90}$$

where it is assumed that $\mathbf{N} \in \mathbb{R}^{1\times q}$.

Step 7: Optimize for Uncertainty and Ensure Constraints are Met

Formulating the output of Step 6 in terms of the mean and variance allows for an optimal control problem to be setup where the objective function is defined by

$$\mathcal{J} = \mathbf{M}\left(\alpha\hat{\mathbf{y}}^*_{n|n} + \beta \, \| \, \mathbf{\Sigma}_{\boldsymbol{y}^*_{n|n}} \, \|_2 \, \mathbf{1}_q^T\right) \tag{91}$$

and α and β are weights on the relative components that can be varied to find different compromised optimal designs. The problem is then to seek out the control, $\mathbf{u}$, that minimizes $\mathcal{J}$. In this case the control is constant (since they are parameters of the problem) and given by $\mathbf{u_d}$. The requirements outside of the compatibility constraints are then handled by adjoining the set of convex constraints to the objective function and identifying an optimum that satisfies the necessary conditions outlined previously.

Step 8: Evaluate the Quality of the Robustness Estimate

The quality of the robustness estimate can be evaluated by using the unscented transform to get a higher-order estimate of the mean and the covariance of the output. This step, however, may be time consuming and may not be desirable to perform in all instances, particularly if the design is known to be linear, as the propagation by the Kalman filter through a linear system is exact. The procedure to obtain this estimate is as follows:

1. Identify the uncertain parameters for the problem and form the initial covariance matrix for these parameters

2. Identify the m (or $m+1$ if an alternate form of the unscented transform is used) sigma points based on the eigenstructure of the initial covariance matrix to satisfy Eq. (17)

3. Propagate each of these sigma points through the design until convergence

4. Record the objective function for each sigma point propagation

5. Compute the scalar mean and variance from the composite results for each of the objective function values via Eqs. (20) and (21)

4.2.2 Formulation with Newton-Raphson Iteration

When formulating the rapid robust design methodology using Newton-Raphson iteration defined by Eq. (10) only Steps 3 and 5 need modification. This is true when considering the substitution of any root-finding scheme that is defined by a recursive sequence. As described in Chapter 2, fixed-point iteration is formed by a relation of the form

$$\mathbf{y} = \mathbf{g}(\mathbf{y}) \Rightarrow \mathbf{f}(\mathbf{y}) = \mathbf{g}(\mathbf{y}) - \mathbf{y} = \mathbf{0}$$

where it is desired to find the root, $\mathbf{y}^*$, of a function $\mathbf{f}(\mathbf{y}) = \mathbf{g}(\mathbf{y}) - \mathbf{y}$. Comparing this result to the iteration relationship used when applying fixed-point iteration for design defined by Eq. (76) means that

$$\mathbf{g}(\mathbf{y}) = \boldsymbol{\Lambda}\mathbf{y} + \boldsymbol{\beta}\mathbf{u_d} + \boldsymbol{\gamma}\mathbf{u_p} + \boldsymbol{\delta}$$

and

$$\mathbf{f}(\mathbf{y}) = \mathbf{g}(\mathbf{y}) - \mathbf{y} \Rightarrow \mathbf{f}(\mathbf{y}) = \boldsymbol{\Lambda}\mathbf{y} + \boldsymbol{\beta}\mathbf{u_d} + \boldsymbol{\gamma}\mathbf{u_p} + \boldsymbol{\delta} - \mathbf{y}$$

Therefore, the form required by Newton iteration, Eq. (10), is

$$\begin{aligned}\mathbf{y}_k = \mathbf{y}_{k-1} - \left(\frac{\partial \mathbf{f}(\mathbf{y}_{k-1})}{\partial \mathbf{y}_{k-1}}\right)^{-1} [(\boldsymbol{\Lambda} - \mathbf{I_{m\times m}})\,\mathbf{y}_{k-1} \\ + \boldsymbol{\beta}\mathbf{u_d} + \boldsymbol{\gamma}\mathbf{u_p} + \boldsymbol{\delta}], \quad \forall k \in \{1, 2, ...\}\end{aligned} \tag{92}$$

When $\mathbf{\Lambda}$, $\boldsymbol{\beta}$, $\boldsymbol{\gamma}$, and $\boldsymbol{\delta}$ are independent of the CA output, $\mathbf{y}$, the Jacobian is given by

$$\frac{\partial \mathbf{f}(\mathbf{y})}{\partial \mathbf{y}} = \mathbf{\Lambda} - \mathbf{I_{m\times m}}$$

In the linear case, this prescribes the root in a single iteration as

$$\mathbf{y}_k = \mathbf{y}^* = -\left(\mathbf{\Lambda} - \mathbf{I_{m\times m}}\right)^{-1}\left(\boldsymbol{\beta}\mathbf{u_d} + \boldsymbol{\gamma}\mathbf{u_p} + \boldsymbol{\delta}\right) \tag{93}$$

provided that $\det(\mathbf{\Lambda} - \mathbf{I_{m\times m}}) \neq 0$. However, in the general case $\mathbf{\Lambda}$, $\boldsymbol{\beta}$, $\boldsymbol{\gamma}$, and $\boldsymbol{\delta}$ could be functions of $\mathbf{y}$. Provided $\mathbf{f} = (\mathbf{f}_1 \cdots \mathbf{f}_n)^T$ is analytic in the complex domain, it is suggested that the matrix of partial derivatives be found using complex step differentiation[164, 165]

$$\frac{\partial \mathbf{f}}{\partial \mathbf{y}} \approx \begin{pmatrix} \dfrac{\Im\left(\mathbf{f}_1(y_1 + ih)\right)}{h} & \cdots & \dfrac{\Im\left(\mathbf{f}_1(y_m + ih)\right)}{h} \\ \vdots & \ddots & \vdots \\ \dfrac{\Im\left(\mathbf{f}_n(y_m + ih)\right)}{h} & \cdots & \dfrac{\Im\left(\mathbf{f}_n(y_m + ih)\right)}{h} \end{pmatrix} \tag{94}$$

By using the complex step differentiation a machine-precision approximation of the derivative is obtained that is independent of the step size. The modifications to Steps 3 and 5 required to utilize Newton-Raphson iteration instead of fixed-point iteration are shown below.

Step 3: Form the Iterative Equations

The iteration scheme required to converge the design is given by

$$\begin{aligned} \mathbf{y}_k = &\left[\mathbf{I_{m\times m}} - \left(\frac{\partial \mathbf{f}(\mathbf{y}_{k-1})}{\partial \mathbf{y}_{k-1}}\right)^{-1}\left(\mathbf{\Lambda} - \mathbf{I_{m\times m}}\right)\right]\mathbf{y}_{k-1} \\ &- \left(\frac{\partial \mathbf{f}(\mathbf{y}_{k-1})}{\partial \mathbf{y}_{k-1}}\right)^{-1}\left[\boldsymbol{\beta}\mathbf{u_d} + \boldsymbol{\gamma}\mathbf{u_p} + \boldsymbol{\delta}\right] \end{aligned} \tag{95}$$

Step 5: Estimate the Mean Output and the Covariance

In order to propagate the Kalman filter equations, Eqs. (62)-(68), a dynamical system needs to be formed. These follow from comparing comparing Eq. (95) to Eq. (71)

as was done in the case of fixed-point iteration. The following results after this comparison

$$\mathbf{F}_{k-1} = \mathbf{I}_{\mathbf{m}\times\mathbf{m}} - \left(\frac{\partial \mathbf{f}(\mathbf{y}_{k-1})}{\partial \mathbf{y}_{k-1}}\right)^{-1} (\boldsymbol{\Lambda} - \mathbf{I}_{\mathbf{m}\times\mathbf{m}}), \quad \forall k \in \{1, 2, ...\} \tag{96}$$

$$\mathbf{B}_{k-1} = \begin{pmatrix} \boldsymbol{\beta}^T \left(\frac{\partial \mathbf{f}(\mathbf{y}_{k-1})}{\partial \mathbf{y}_{k-1}}\right)^{-T} \\ \boldsymbol{\gamma}^T \left(\frac{\partial \mathbf{f}(\mathbf{y}_{k-1})}{\partial \mathbf{y}_{k-1}}\right)^{-T} \\ \left(\frac{\partial \mathbf{f}(\mathbf{y}_{k-1})}{\partial \mathbf{y}_{k-1}}\right)^{-T} \end{pmatrix}^T, \quad \forall k \in \{1, 2, ...\} \tag{97}$$

$$\mathbf{u}_{k-1} = \begin{pmatrix} \mathbf{u_d} \\ \mathbf{u_p} \\ \boldsymbol{\delta} \end{pmatrix}, \quad \forall k \in \{1, 2, ...\} \tag{98}$$

4.3 Summary

This chapter took the techniques described in Chapter 3 to develop an eight step methodology to rapidly obtain a robust design. The steps of this methodology are shown below

1. Decompose the design
2. Identify the random variables in the design and their distributions
3. Form the iterative equations
4. Ensure a solution exists
5. Estimate the mean output and the covariance of the design
6. Identify the mean and variance bound of the objective function
7. Optimize for uncertainty and ensure constraints are met
8. Evaluate the quality of the robustness estimate for nonlinear designs

While the theoretical development is restricted to linear systems due to the Kalman filter being utilized, extensions via successive linearization to nonlinear designs were discussed. The flexibility of the methodology to accommodate different numerical root-finding algorithms was also demonstrated through formulation of an alternate methodology with Newton iteration. Note that there is no additional upfront computational time compared to other MDO techniques.

CHAPTER V

DEMONSTRATION OF DYNAMICAL SYSTEM THEORY APPLIED TO THE MULTIDISCIPLINARY DESIGN PROBLEM

This chapter demonstrates the dynamical system techniques developed to illustrative multidisciplinary design problems. This begins with an analytical, linear example that describes the accuracy of the estimation technique to propagate uncertainty within the design as well as a quantization of its performance relative to industry-standard techniques. Then the methods to find the region of initial guesses required to converge the design (*i.e.*, make the design asymptotically stable) and examine the rate of convergence are demonstrated. Then three robust design applications are presented. One linear, analytical example and two nonlinear applications. The last application shows the application of the developed methodology to a practical problem relevant to the entry, descent, and landing community, the design of a deployable device to increase the range or accuracy of an existing strategic system. For each of these design applications comparison is made to traditional techniques.

5.1 Accuracy of the Mean and Variance Estimate

To show the accuracy of the mean and variance estimate provided by the rapid robust design methodology, consider the coupled, linear two CA system shown in Fig. 17. For this analysis, assume that there are two components to the probabilistic parameter vector and the two output vectors, that is $\mathbf{u_p} \in \mathbb{R}^2$, $\mathbf{y_1} \in \mathbb{R}^2$, and $\mathbf{y_2} \in \mathbb{R}^2$, which, in turn, implies $\mathbf{A'_1} \in \mathbb{R}^{2\times2}$, $\mathbf{B'_1} \in \mathbb{R}^2$, $\mathbf{C'_1} \in \mathbb{R}^{2\times2}$, $\mathbf{A'_2} \in \mathbb{R}^{2\times2}$, and $\mathbf{B'_2} \in \mathbb{R}^2$. Also, let the distribution of the probabilistic parameter input be given by a multivariate

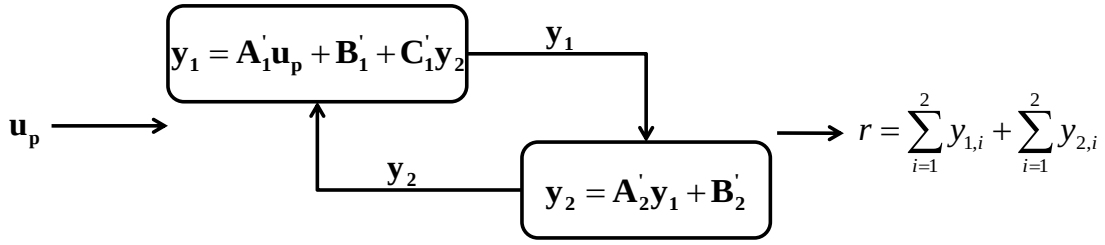

Figure 17: Two-contributing analysis multidisciplinary design.

normal, $\mathbf{u_p} \sim \mathcal{N}(\boldsymbol{\mu}_{\mathbf{u_p}}, \boldsymbol{\Sigma}_{\mathbf{u_p}})$.

The effectiveness of the rapid robustness assessment methodology (*i.e.*, Steps 1 - 6 of the rapid robust design methodology described in Chapter 4) will be demonstrated by letting the mean of the probabilistic input, $\boldsymbol{\mu}_{\mathbf{u_p}}$, and the components of the covariance matrix $\sigma_{y_1}^2$, $\sigma_{y_2}^2$, and $\rho_{y_1 y_2}$ vary between given ranges. The maximum error between the response obtained from the robustness assessment methodology and an analytical propagation is then reported for a multitude of points within the design space.

5.1.1 Analytical Solution

As this is a multidisciplinary analysis consisting of two linear CAs, there is a single simultaneous solution for $\mathbf{y_1}$ and $\mathbf{y_2}$ which is found to be

$$\left.\begin{aligned} \mathbf{y_1} &= (\mathbf{I_{2\times 2}} - \mathbf{C_1'A_2'})^{-1} (\mathbf{A_1'u_p} + \mathbf{B_1'} + \mathbf{C_1'B_2'}) \\ \mathbf{y_2} &= \mathbf{A_2'} (\mathbf{I_{2\times 2}} - \mathbf{C_1'A_2'})^{-1} (\mathbf{A_1'u_p} + \mathbf{B_1'} + \mathbf{C_1'B_2'}) + \mathbf{B_2'} \end{aligned}\right\}$$

which implies that whenever $\mathbf{I_{2\times 2}} - \mathbf{C_1'A_2'}$ is non-singular, a unique solution exists for $\mathbf{y_1}$ and $\mathbf{y_2}$. Since the only uncertainty in this analysis is given by the probabilistic input vector, $\mathbf{u_p}$, which is defined as a multivariate normal, the distribution of the output for each CA can be found exactly. These are given by

$$\left.\begin{aligned} \mathbf{y_1} &\sim \mathcal{N}\left(\boldsymbol{\mu}_{\mathbf{y_1}}, \boldsymbol{\Sigma}_{\mathbf{y_1}}\right) \\ \mathbf{y_2} &\sim \mathcal{N}\left(\boldsymbol{\mu}_{\mathbf{y_2}}, \boldsymbol{\Sigma}_{\mathbf{y_2}}\right) \end{aligned}\right\}$$

where

$$\begin{aligned}\boldsymbol{\mu}_{\mathbf{y_1}} &= \left(\mathbf{I_{2\times 2}} - \mathbf{C_1'A_2'}\right)^{-1}\mathbf{A_1'}\boldsymbol{\mu}_{\mathbf{u_p}} + \left(\mathbf{I_{2\times 2}} - \mathbf{C_1'A_2'}\right)^{-1}\left(\mathbf{B_1'} + \mathbf{C_1'B_2'}\right)\\ \boldsymbol{\Sigma}_{\mathbf{y_1}} &= \left(\mathbf{I_{2\times 2}} - \mathbf{C_1'A_2'}\right)^{-1}\mathbf{A_1'}\boldsymbol{\Sigma}_{\mathbf{u_p}}\mathbf{A_1'}^{T}\left(\mathbf{I_{2\times 2}} - \mathbf{C_1'A_2'}\right)^{-T}\end{aligned}$$

and

$$\begin{aligned}\boldsymbol{\mu}_{\mathbf{y_2}} &= \mathbf{A_2'}\left(\mathbf{I_{2\times 2}} - \mathbf{C_1'A_2'}\right)^{-1}\mathbf{A_1'}\boldsymbol{\mu}_{\mathbf{u_p}} + \mathbf{A_2'}\left(\mathbf{I_{2\times 2}} - \mathbf{C_1'A_2'}\right)^{-1}\left(\mathbf{B_1'} + \mathbf{C_1'B_2'}\right) + \mathbf{B_2'}\\ \boldsymbol{\Sigma}_{\mathbf{y_2}} &= \mathbf{A_2'}\left(\mathbf{I_{2\times 2}} - \mathbf{C_1'A_2'}\right)^{-1}\mathbf{A_1'}\boldsymbol{\Sigma}_{\mathbf{u_p}}\mathbf{A_1'}^{T}\left(\mathbf{I_{2\times 2}} - \mathbf{C_1'A_2'}\right)^{-T}\mathbf{A_2'}^{T}\end{aligned}$$

Since both of the output distributions from the CAs are also multivariate normal, the components of the response

$$r = \sum_{i=1}^{2} y_{1,i} + \sum_{i=1}^{2} y_{2,i}$$

can be found exactly by summing the components of mean components of $\boldsymbol{\mu}_{\mathbf{y_1}}$ and $\boldsymbol{\mu}_{\mathbf{y_2}}$ to find the mean of the response and adding the appropriate variances from the covariance matrices $\boldsymbol{\Sigma}_{\mathbf{y_1}}$ and $\boldsymbol{\Sigma}_{\mathbf{y_2}}$. That is

$$r \sim \mathcal{N}\left(\sum_{i=1}^{2}\boldsymbol{\mu}_{\mathbf{y_1},i} + \sum_{i=1}^{2}\boldsymbol{\mu}_{\mathbf{y_2},i}, \sum_{i=1}^{2}\lambda(\boldsymbol{\Sigma}_{\mathbf{y_1}})|_i + \sum_{i=1}^{2}\lambda(\boldsymbol{\Sigma}_{\mathbf{y_2}})|_i\right)$$

where $\boldsymbol{\mu}_{\mathbf{y_1},i}$ is the i^{th} component of $\mathbf{y_1}$, $\boldsymbol{\mu}_{\mathbf{y_2},i}$ is the i^{th} component of $\mathbf{y_2}$, and $\lambda(\cdot)|_i$ is the i^{th} eigenvalue of the matrix argument.

5.1.2 Rapid Robustness Assessment Methodology

To assess the performance of the robustness estimate provided by the rapid robust design methodology, the first six steps outlined in Chapter 4 will be followed. These steps obtain an estimate of the output mean and a bound on the variance provided by the two-norm of the covariance matrix obtained by propagating the dynamical system through a Kalman filter.

Step 1: Decompose the Design

The problem as given has already been decomposed into the representative contributing analyses; however, it is still necessary to identify each of the terms in Eq. (75).

For the first CA, $\mathbf{y_1}$, the functional form is as follows

$$\mathbf{y_1} = \begin{pmatrix} \mathbf{0} & \mathbf{C_1'} \end{pmatrix} \mathbf{y} + \begin{pmatrix} \mathbf{0} \end{pmatrix} \mathbf{u_d} + \begin{pmatrix} \mathbf{A_1'} \end{pmatrix} \mathbf{u_p} + \mathbf{B_1'}$$

Similarly, for the second CA, the functional form is given by

$$\mathbf{y_2} = \begin{pmatrix} \mathbf{A_2'} & \mathbf{0} \end{pmatrix} \mathbf{y} + \begin{pmatrix} \mathbf{0} \end{pmatrix} \mathbf{u_d} + \begin{pmatrix} \mathbf{0} \end{pmatrix} \mathbf{u_p} + \mathbf{B_2'}$$

Hence,

$$\mathbf{A_1} = \begin{pmatrix} \mathbf{0} & \mathbf{C_1'} \end{pmatrix} \quad \mathbf{B_1} = \begin{pmatrix} \mathbf{0} \end{pmatrix}$$

$$\mathbf{C_1} = \begin{pmatrix} \mathbf{A_1'} \end{pmatrix} \quad \mathbf{d_1} = \mathbf{B_1'}$$

$$\mathbf{A_2} = \begin{pmatrix} \mathbf{A_2'} & \mathbf{0} \end{pmatrix} \quad \mathbf{B_2} = \begin{pmatrix} \mathbf{0} \end{pmatrix}$$

$$\mathbf{C_2} = \begin{pmatrix} \mathbf{0} \end{pmatrix} \quad \mathbf{d_2} = \mathbf{B_2'}$$

Step 2: Identify the Random Variables and their Distributions

There is only one set of random variables in this example, that of the probabilistic input variable, $\mathbf{u_p}$. This is given in the problem description as a multivariate normal distribution, $\mathbf{u_p} \sim \mathcal{N}(\boldsymbol{\mu}_{\mathbf{u_p}}, \boldsymbol{\Sigma}_{\mathbf{u_p}})$. Later, the two defining parameters of the multivariate normal will be given numerical values.

Step 3: Form the Iterative Equations

In order to use the Kalman filter to simultaneously estimate the robustness and converge the design, the iterative equations described in Eq. (76) for fixed-point iteration need to be formed. Through analogy of variables, the matrices are given by

$$\boldsymbol{\Lambda} = \begin{pmatrix} \mathbf{A_1} \\ \mathbf{A_2} \end{pmatrix} = \begin{pmatrix} \mathbf{0} & \mathbf{C_1'} \\ \mathbf{A_2'} & \mathbf{0} \end{pmatrix}$$

$$\boldsymbol{\beta} = \begin{pmatrix} \mathbf{B_1} \\ \mathbf{B_2} \end{pmatrix} = \begin{pmatrix} \mathbf{0} \\ \mathbf{0} \end{pmatrix}$$

$$\boldsymbol{\gamma} = \begin{pmatrix} \mathbf{C_1} \\ \mathbf{C_2} \end{pmatrix} = \begin{pmatrix} \mathbf{A_1'} \\ \mathbf{0} \end{pmatrix}$$

$$\boldsymbol{\delta} = \begin{pmatrix} \mathbf{d_1} \\ \mathbf{d_2} \end{pmatrix} = \begin{pmatrix} \mathbf{B_1'} \\ \mathbf{B_2'} \end{pmatrix}$$

Step 4: Ensure a Solution Exists

In this problem, the components of $\boldsymbol{\Lambda}$, $\boldsymbol{\beta}$, $\boldsymbol{\gamma}$, and $\boldsymbol{\delta}$ are yet to be defined. However, they are constant coefficients. This implies that the likelihood of finding a solution is dependent entirely on the matrix $\boldsymbol{\Lambda}$, providing a constraint to the values which will be examined in this design space analysis. Expanding $\boldsymbol{\Lambda}$ allows the characteristic equation to be found

$$\boldsymbol{\Lambda} = \begin{pmatrix} 0 & 0 & C_1 & C_2 \\ 0 & 0 & C_3 & C_4 \\ A_1 & A_2 & 0 & 0 \\ A_3 & A_4 & 0 & 0 \end{pmatrix}$$

Therefore, the characteristic equation is given by

$$\det(\boldsymbol{\Lambda} - \lambda \mathbf{I_{4\times 4}}) = \begin{vmatrix} -\lambda & 0 & C_1 & C_2 \\ 0 & -\lambda & C_3 & C_4 \\ A_1 & A_2 & -\lambda & 0 \\ A_3 & A_4 & 0 & -\lambda \end{vmatrix} = 0$$

which can be solved in order to ensure that the modulus of each of the eigenvalues is less than one for repeated roots or less than or equal to one for simple roots.

Step 5: Estimate the Mean Output and the Covariance

The equations formed in the prior step can then be propagated through the Kalman filter defined by Eqs. (62)-(68) with

$$\mathbf{F}_{k-1} = \mathbf{\Lambda}, \quad \forall k \in \{1, 2, ...\}$$

$$\mathbf{B}_{k-1} = \begin{pmatrix} \boldsymbol{\beta} & \boldsymbol{\gamma} & \mathbf{I_{4\times 4}} \end{pmatrix}, \quad \forall k \in \{1, 2, ...\}$$

$$\mathbf{u}_{k-1} = \begin{pmatrix} \mathbf{u_d} \\ \mathbf{u_p} \\ \boldsymbol{\delta} \end{pmatrix}, \quad \forall k \in \{1, 2, ...\}$$

where in this example $\mathbf{u_d} = \mathbf{0}$ and $\mathbf{u_p} = \mathbb{E}(\mathbf{u_p}) = \boldsymbol{\mu}_{\mathbf{u_p}}$. In this example, the matrix $\mathbf{Q}$ is the null matrix since the only uncertain parameters of the problem are associated with the input parameters, not the model. The unscented transform is used on an uncoupled system with the distribution described in Step 2 in order to identify $\mathbf{y_0}$ and $\mathbf{\Sigma_0}$, the initial output mean and covariance for each design. A design is considered converged when the absolute difference between iteration estimates is less than 1×10^{-4} or the relative difference is less than 1×10^{-6}.

Step 6: Identify the Mean and Variance Bound of the Objective Function

Upon convergence the value of $\mathbf{y}$, the state variable in the problem, is the mean response for each of the components of the output CAs. The matrix $\mathbf{M}$ is simply a 1×4 vector of ones, $\mathbf{1}_4^T$, since $\mathbf{y}^* = \mathbf{y}$, that is, it is the entire state vector. Therefore,

$$\bar{r} = \mathbf{1}_4^T \hat{\mathbf{y}}_{n|n}$$

The estimate for the variance (*i.e.*, the variance bound) in this case is simply

$$\sigma_r^2 \leq \sum_{i=1}^{4} \parallel \mathbf{\Sigma}_{n|n} \parallel_2 = 4 \parallel \mathbf{\Sigma}_{n|n} \parallel_2$$

5.1.3 Analysis Results

In order to assess a large variety of problems, a parametric sweep of the design variables was performed to identify the maximum errors in the design space. To perform this parameter sweep, the problem's parameters were varied independently as shown in Table 6 where the distribution of each variable was assumed to be uniform and a 100,000 case Monte Carlo analysis was conducted.

Table 6: Parameter ranges to assess the validity of the rapid robust design methodology.

Parameter	Distribution
σ_1^2	$\mathcal{U}(0, 100)$
σ_2^2	$\mathcal{U}(0, 100)$
$\rho_{y_1 y_2}$	$\mathcal{U}(-1, 1)$
$\mathbf{A_1'}$	$\begin{pmatrix} \mathcal{U}(-1,1) & \mathcal{U}(-1,1) \\ \mathcal{U}(-1,1) & \mathcal{U}(-1,1) \end{pmatrix}$
$\mathbf{B_1'}$	$\begin{pmatrix} \mathcal{U}(-1,1) \\ \mathcal{U}(-1,1) \end{pmatrix}$
$\mathbf{C_1'}$	$\begin{pmatrix} \mathcal{U}(-1,1) & \mathcal{U}(-1,1) \\ \mathcal{U}(-1,1) & \mathcal{U}(-1,1) \end{pmatrix}$
$\mathbf{A_2'}$	$\begin{pmatrix} \mathcal{U}(-1,1) & \mathcal{U}(-1,1) \\ \mathcal{U}(-1,1) & \mathcal{U}(-1,1) \end{pmatrix}$
$\mathbf{B_2'}$	$\begin{pmatrix} \mathcal{U}(-1,1) \\ \mathcal{U}(-1,1) \end{pmatrix}$

In order to guarantee convergence of the design, constraints were imposed on the parameters to ensure that all of the eigenvalues of the matrix $\mathbf{\Lambda}$ had modulus less than unity. To ensure realizable covariance matrices, that is a matrix that is symmetric and positive definite, the components of the covariance (*e.g.*, variance and correlation coefficient) were determined independently and then combined to form the covariance matrix.

In addition to the parameters shown in Table 6, the effect of the mean of the probabilistic parameters was conducted by analyzing three different cases–one where the mean was $\boldsymbol{\mu}_{\mathbf{u_p}} = (0\ 0)^T$, one where the mean was $\boldsymbol{\mu}_{\mathbf{u_p}} = (100\ 0)^T$, and one

where the mean was $\boldsymbol{\mu}_{\mathbf{u_p}} = (100\ 100)^T$. The results were then compared with results propagated analytically resulting in Figs. 18-20.

It is observed from these results that the mean error is less than 0.08% for all of the cases examined. This is a result of the system being linear and the Kalman filter propagating results exactly for a linear system. Therefore the error in the mean is solely a result of the convergence criterion being utilized. For each case, there is seen to be a rise in the standard deviation error near the origin. This is because the nominal mean goes to zero causing a rise in the in the percent error near this point.

The rapid robustness assessment methodology is observed to provide a consistent conservative bound on the variance as seen in Figs. 18-20 since all of the percent error values are positive. It is also interesting to note that the error in mean and standard deviation, regardless of the mean of the input, appears to be close to the same order of magnitude. As the mean input value increases, the magnitude of the mean response and standard deviation of that response increases, which causes a decrease in the percent error. Furthermore, it is observed that the maximum error approaches a limit of less than 40%. This limit is a function of the two-norm being used. This limit is described and related to the dimensionality of the problem in Chapter 6. In analyzing the data, the largest errors are caused for weakly coupled systems, that is systems where $\mathbf{C}_\mathbf{1}'$ is small. This can be explained since $\mathbf{C}_\mathbf{1}'$ being small leads to a larger domain of values that lead to a converged design. Additionally, since the interplay between $\mathbf{y_1}$ and $\mathbf{y_2}$ is reduced, the iterations to achieve convergence is reduced in these cases.

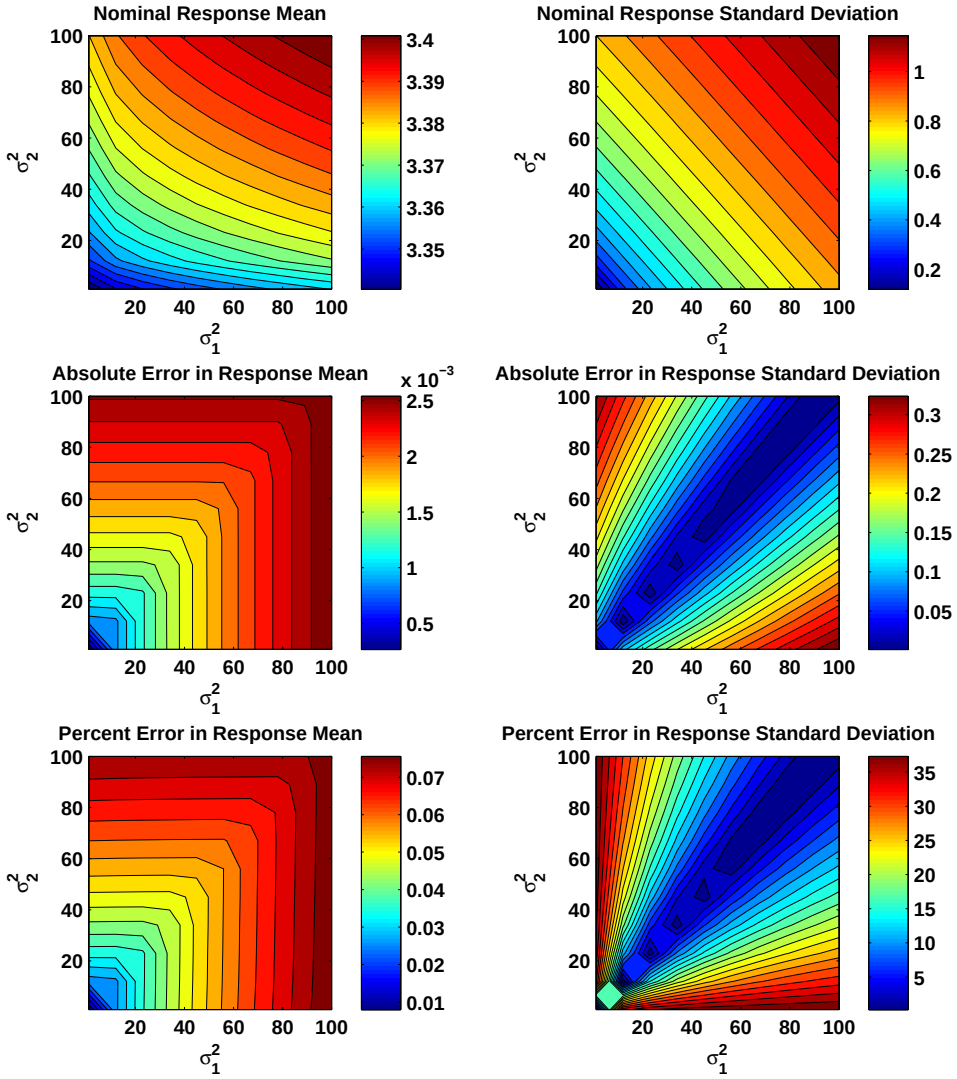

Figure 18: Maximum error for a two contributing analysis multidisciplinary design with $\boldsymbol{\mu}_{\mathbf{u_p}} = (0\ 0)^T$.

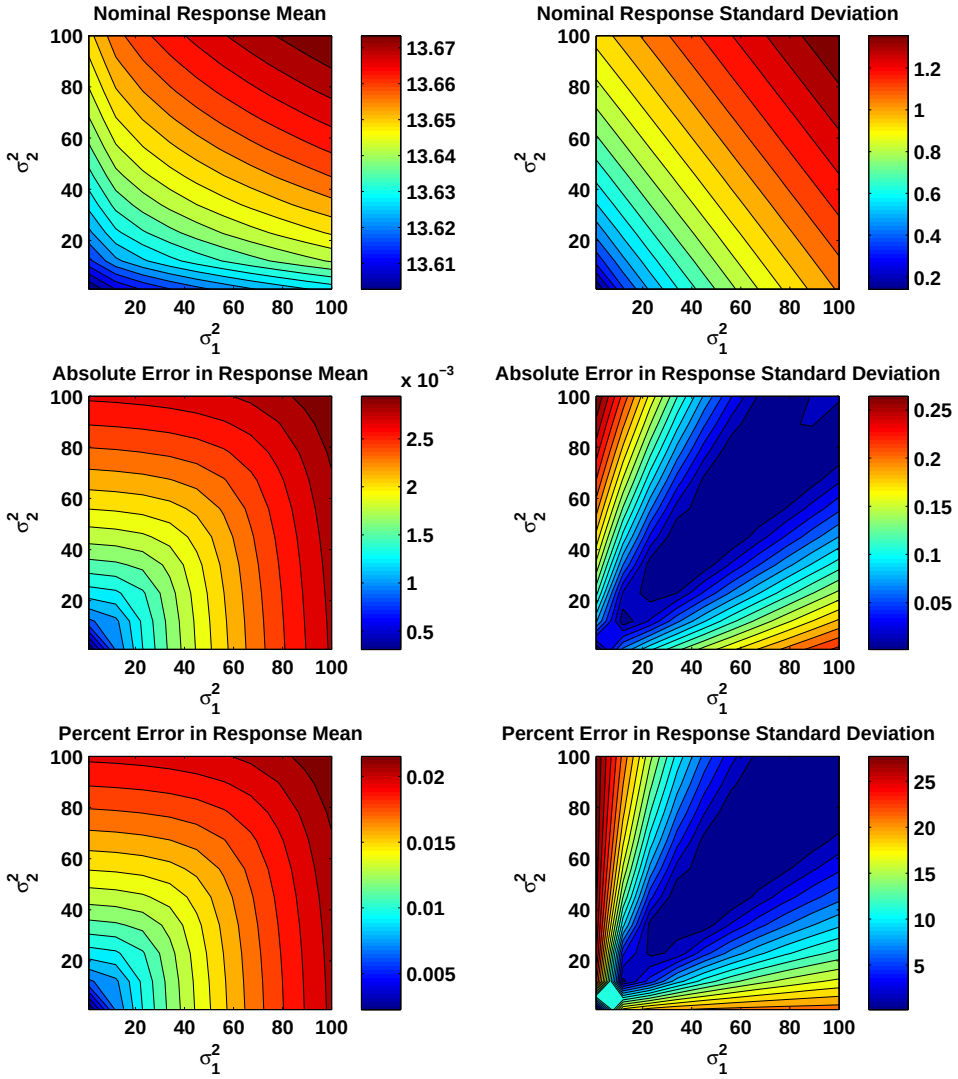

Figure 19: Maximum error for a two contributing analysis multidisciplinary design with $\boldsymbol{\mu}_{\mathbf{u_p}} = (100\ 0)^T$.

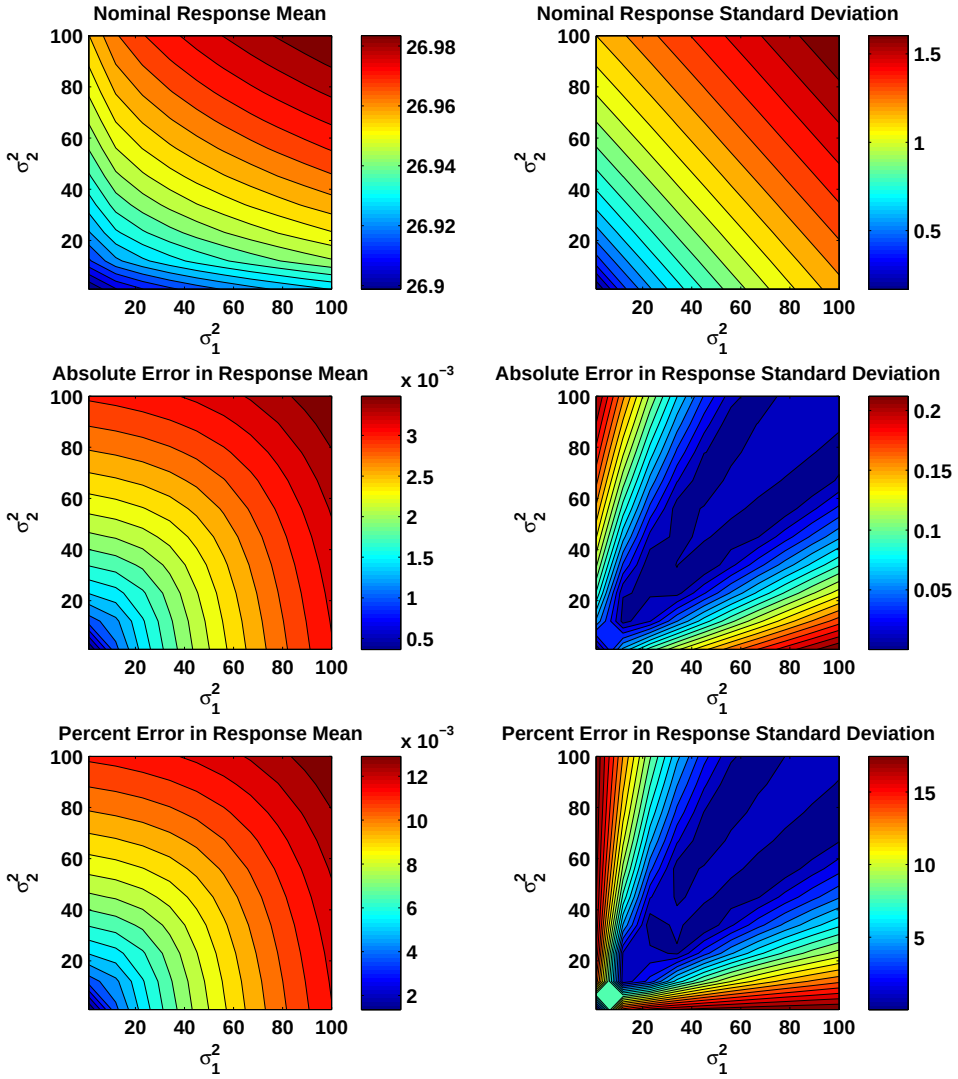

Figure 20: Maximum error for a two contributing analysis multidisciplinary design with $\boldsymbol{\mu}_{\mathbf{u_p}} = (100\ 100)^T$.

5.2 Analysis of a Linear, Two Contributing Analysis Design

The errors associated with the rapid linear robustness technique are compared to more commonly used methods to propagate uncertainty, namely a 10,000 case Monte Carlo analysis, the unscented transform, and fast probability integration. For the data presented, specific numerical values were utilized for the various problem matrices and vectors. These are given by

$$\mathbf{A_1'} = \begin{pmatrix} 0.25 & 0 \\ 0 & 0.5 \end{pmatrix} \quad \mathbf{B_1'} = \begin{pmatrix} 1 \\ 1 \end{pmatrix} \quad \mathbf{C_1'} = \begin{pmatrix} 1 & 0 \\ 0 & 1 \end{pmatrix}$$

$$\mathbf{A_2'} = \begin{pmatrix} 0.25 & 0 \\ 0 & 0.25 \end{pmatrix} \quad \mathbf{B_2'} = \begin{pmatrix} 1 \\ 1 \end{pmatrix}$$

The errors between the rapid linear robustness analysis technique and traditional analysis methods for these values are shown in Figs. 21-23.

The advantages of the rapid robust analysis technique are elucidated in the Table 7 where the four techniques are compared to analytic propagation of the uncertainty. This table reports the maximum error from a parameter sweep of $\sigma^2_{u_{p,1}}$, $\sigma^2_{u_{p,2}}$, and $\rho_{u_{p,1}u_{p,2}}$ across the range of values in Table 6 with $\boldsymbol{\mu}_{\mathbf{u_p}} = (0\ 0)^T$. It can be seen that the rapid robust analysis technique provides a slightly improved level of accuracy relative to the other contemporary methods in estimating the mean. The error in standard deviation is larger than the other techniques (three times greater than the unscented transform); however, this error is less than 3% and is acceptable for conceptual design studies. These levels of accuracy are obtained for less than one-third the number of CA evaluations compared to the unscented transform and orders of magnitude fewer CA evaluations relative to Monte Carlo and fast probability integration. For problems in which the CA function evaluation time is large or the model for each CA needs to be built in real-time, this provides a large execution time benefit.

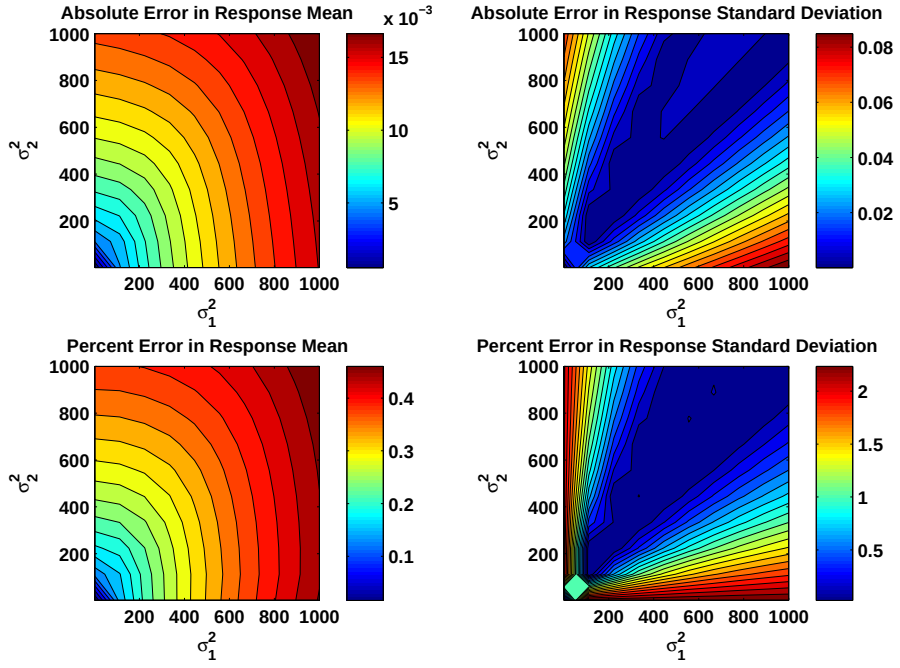

Figure 21: Mean and variance error between the rapid linear robustness analysis technique and Monte Carlo analysis.

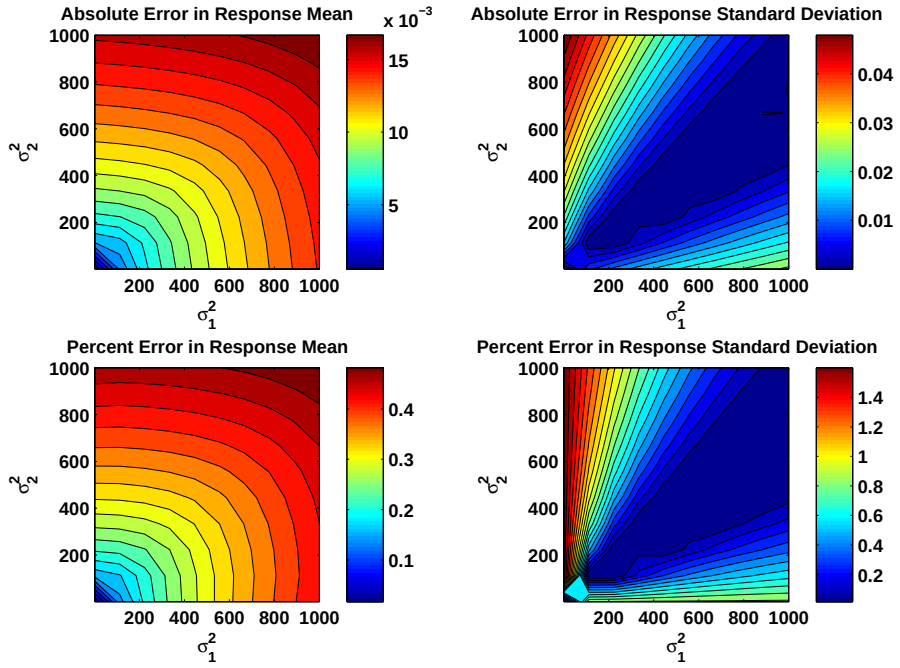

Figure 22: Mean and variance error between the rapid linear robustness analysis technique and the unscented transform.

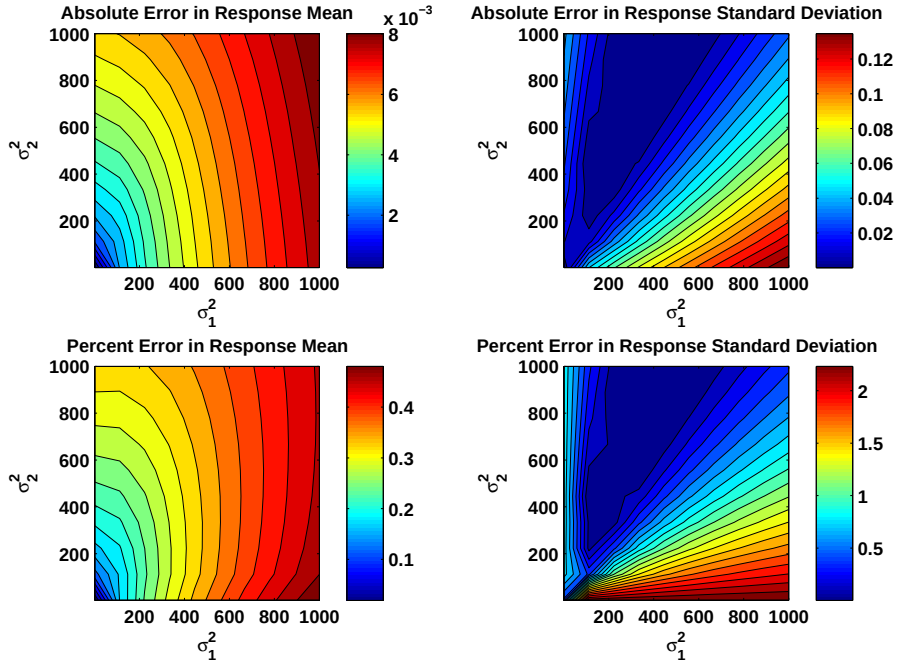

Figure 23: Mean and variance error between the rapid linear robustness analysis technique and fast probability integration.

Table 7: Comparison of the performance of the rapid robustness assessment method with other multidisciplinary uncertainty assessment techniques.

	Rapid Robust Design Methodology	**Monte Carlo**	**Unscented Transform**	**Fast Probability Integration**
Maximum Percent Discrepancy in Mean Relative to Analytic Propagation, %	0.07843	0.10234	0.18458	0.10357
Maximum Percent Discrepancy in Standard Deviation Relative to Analytic Propagation, %	2.4583	0.02939	0.80879	0.14299
Number of CA Evaluations, -	140	109,954	435	2,349

5.3 Region and Rate of Convergence for a Nonlinear, Two Contributing Analysis System

Consider the design of a cantilever beam with a fixed load of 4 N applied to the tip as shown in Fig. 24.

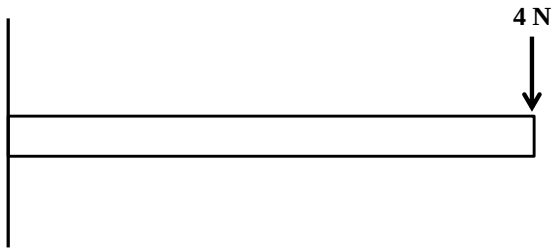

Figure 24: Cantilever beam with a tip load.

The design of such a cantilever beam can be described by the DSM in Fig. 25.

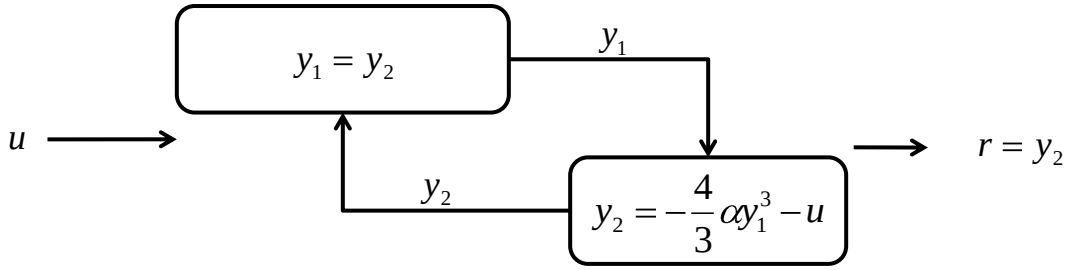

Figure 25: Nonlinear two contributing analysis design.

In Fig. 25, y_1 represents the length of the beam (a surrogate for the cost), y_2 is a simplified relation for the maximum deflection of the beam, α parametrizes the material properties characterizing the elasticity and cross-sectional parameters of the beam, and u is a design variable governing the unloaded deflection.

For this design, the fixed-point iteration relations are defined by

$$\left.\begin{aligned} y_{1,k+1} &= y_{2,k} \\ y_{2,k+1} &= -\frac{4}{3}\alpha y_{1,k}^3 - u \end{aligned}\right\}$$

The matrix $\mathbf{W}$ can be chosen (arbitrarily) to be

$$\mathbf{W} = \begin{pmatrix} 1 & 2 \\ 0 & 2 \end{pmatrix}$$

and defining

$$a \triangleq 24\alpha y_1^2$$

it is shown that $\beta < 1$ for $a \in [-1.9, 1.4]$, which shows the origin is exponentially asymptotically stable for any finite α. With $\alpha = 0.1$ the domain of attraction (*i.e.*, the range of initial values that can be given to converge the design) is

$$\mathcal{A} = \{\mathbf{y}| \ -0.89 < y_1 < 0.89\}$$

Choosing $V(\mathbf{y}) =\| \ \mathbf{W}\mathbf{y} \ \|_2$ it can be shown that $\mathcal{X}_s = \{\mathbf{y}|V(\mathbf{y}) < 0.63\} \subset \mathcal{A}$. Therefore, by choosing $\| \ \mathbf{y}_0 \ \|_2 < 0.2$ (*i.e.*, $\mathbf{y}_0 \in \mathcal{X}_s$) then $\beta_0 = 0.56$ shows that the iteration is bounded by

$$\| \ \mathbf{y}_k \ \|_2 < 0.9(0.56)^k$$

Which means that the function exponentially reduces by a factor greater than 50% for each iteration ($\beta = 0.56$).

5.4 Rapid Robust Design of a Linear, Three Contributing Analysis System

Consider the linear, three CA system shown in Fig. 26 where each CA is scalar. In

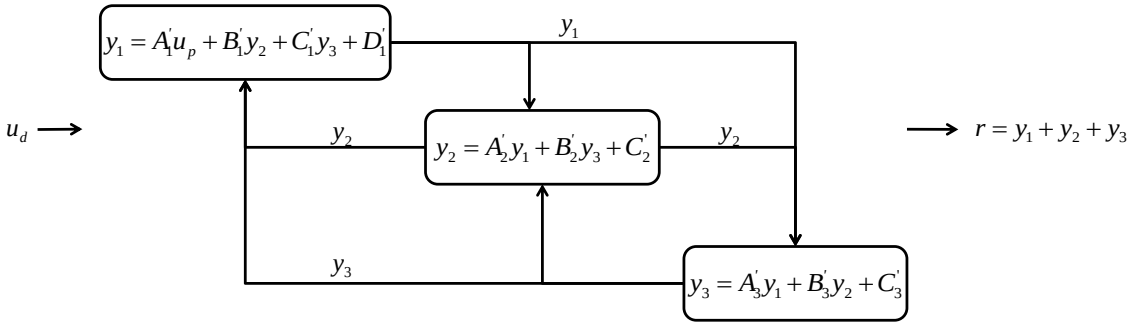

Figure 26: Three contributing analysis multidisciplinary design.

this case, it is desired to find $u_d \in \mathbb{R}$ that minimizes the summation of the CAs output while being within the unit cube centered at the origin. In other words

$$\left.\begin{array}{ll} \textbf{Minimize}: & [\mathcal{J}_{mean}\ \mathcal{J}_{var}] \\ \textbf{Subject to}: & y_1, y_2, y_3 \in [-1, 1] \\ \textbf{By varying}: & u_d \end{array}\right\}$$

where

$$\mathcal{J}_{mean} = \bar{y}_1 + \bar{y}_2 + \bar{y}_3$$

and

$$\mathcal{J}_{var} = \sigma_{y_1}^2 + \sigma_{y_2}^2 + \sigma_{y_3}^2$$

When using the rapid robust design methodology, $\sigma_{y_i}^2 = \| \Sigma_{\mathbf{y}^*} \|_2$.

5.4.1 Applying the Rapid Robust Design Methodology

Step 1: Decompose the Design

The problem as given has already been decomposed into the representative contributing analyses; however, it is still necessary to identify each of the terms in Eq. (75). For the first CA, $\mathbf{y_1}$, the functional form of the CA is as follows

$$y_1 = \begin{pmatrix} 0 & B_1' & C_1' \end{pmatrix} \mathbf{y} + \begin{pmatrix} A_1' \end{pmatrix} u_d + \begin{pmatrix} \mathbf{0} \end{pmatrix} \mathbf{u_p} + D_1'$$

Similarly, for the second CA, the functional form is given by

$$y_2 = \begin{pmatrix} A_2' & 0 & B_2' \end{pmatrix} \mathbf{y} + \begin{pmatrix} 0 \end{pmatrix} u_d + \begin{pmatrix} \mathbf{0} \end{pmatrix} \mathbf{u_p} + C_2'$$

and the third CA

$$y_3 = \begin{pmatrix} A_3' & B_3' & 0 \end{pmatrix} \mathbf{y} + \begin{pmatrix} 0 \end{pmatrix} u_d + \begin{pmatrix} \mathbf{0} \end{pmatrix} \mathbf{u_p} + C_3'$$

Hence,

$$\mathbf{A_1} = \begin{pmatrix} 0 & B_1' & C_1' \end{pmatrix} \quad \mathbf{B_1} = \begin{pmatrix} A_1' \end{pmatrix} \quad \mathbf{C_1} = \begin{pmatrix} \mathbf{0} \end{pmatrix} \quad \mathbf{d_1} = D_1'$$

$$\mathbf{A_2} = \begin{pmatrix} A_2' & 0 & B_2' \end{pmatrix} \quad \mathbf{B_2} = \begin{pmatrix} 0 \end{pmatrix} \quad \mathbf{C_2} = \begin{pmatrix} \mathbf{0} \end{pmatrix} \quad \mathbf{d_2} = C_2'$$

$$\mathbf{A_3} = \begin{pmatrix} A'_3 & B'_3 & 0 \end{pmatrix} \quad \mathbf{B_3} = \begin{pmatrix} 0 \end{pmatrix} \quad \mathbf{C_3} = \begin{pmatrix} \mathbf{0} \end{pmatrix} \quad \mathbf{d_3} = C'_3$$

Step 2: Identify the Random Variables and their Distributions

In this example, suppose that there is uncertainty in the component of the third CA's model that acts on the the CA output. This uncertainty is given as a normal distribution, $A'_3 \sim \mathcal{N}(\mu_{A'_3}, \sigma^2_{A'_3})$ and $B'_3 \sim \mathcal{N}(\mu_{B'_3}, \sigma^2_{B'_3})$.

Step 3: Form the Iterative Equations

For this example, the fixed-point iteration equations described in Eq. (76) are

$$\boldsymbol{\Lambda} = \begin{pmatrix} \mathbf{A_1} \\ \mathbf{A_2} \\ \mathbf{A_3} \end{pmatrix} = \begin{pmatrix} 0 & B'_1 & C'_1 \\ A'_2 & 0 & B'_2 \\ A'_3 & B'_3 & 0 \end{pmatrix}$$

$$\boldsymbol{\beta} = \begin{pmatrix} \mathbf{B_1} \\ \mathbf{B_2} \\ \mathbf{B_3} \end{pmatrix} = \begin{pmatrix} A'_1 \\ 0 \\ 0 \end{pmatrix}$$

$$\boldsymbol{\gamma} = \begin{pmatrix} \mathbf{C_1} \\ \mathbf{C_2} \\ \mathbf{C_3} \end{pmatrix} = \begin{pmatrix} \mathbf{0} \\ \mathbf{0} \\ \mathbf{0} \end{pmatrix}$$

$$\boldsymbol{\delta} = \begin{pmatrix} \mathbf{d_1} \\ \mathbf{d_2} \\ \mathbf{d_2} \end{pmatrix} = \begin{pmatrix} D'_1 \\ C'_2 \\ C'_3 \end{pmatrix}$$

Step 4: Ensure a Solution Exists

In this problem, the variables are yet to be quantified. However, they are constant coefficients which allows the characteristic equation to be expressed as

$$\det(\boldsymbol{\Lambda} - \lambda \mathbf{I_{3\times 3}}) = -\lambda^3 + \lambda(A'_2 B'_1 - A'_3 C'_1) + A'_3 B'_1 B'_2 + A'_2 B'_3 C'_1 = 0$$

which can be solved in order to ensure that the modulus of each of the eigenvalues is less than one for repeated roots or less than or equal to one for simple roots.

Step 5: Estimate the Mean Output and the Covariance

The equations formed in the prior step can then be propagated through the Kalman filter defined by Eqs. (62)-(68) with

$$\mathbf{F}_{k-1} = \mathbf{\Lambda}, \quad \forall k \in \{1, 2, ...\}$$

$$\mathbf{B}_{k-1} = \begin{pmatrix} \boldsymbol{\beta} & \boldsymbol{\gamma} & \mathbf{I_{3\times 3}} \end{pmatrix}, \quad \forall k \in \{1, 2, ...\}$$

$$\mathbf{u}_{k-1} = \begin{pmatrix} \mathbf{u_d} \\ \mathbf{u_p} \\ \boldsymbol{\delta} \end{pmatrix}, \quad \forall k \in \{1, 2, ...\}$$

where in this example $\mathbf{u_d} = u_d$ and $\mathbf{u_p} = \mathbf{0}$. Since there are uncertainties with the model, the matrix $\mathbf{Q}$ is given by

$$\mathbf{Q}_{k-1} = \begin{pmatrix} 0 & 0 & 0 \\ 0 & 0 & 0 \\ 0 & 0 & A_3'\sigma^2_{A_3'}\hat{y}_{1,k-1|k-1} + B_3'\sigma^2_{B_3'}\hat{y}_{2,k-1|k-1} \end{pmatrix}, \quad \forall k \in \{1, 2, ...\}$$

Note that this implies that the state uncertainty can be no less than the uncertainty associated with the model. The unscented transform is used on an uncoupled system with the distribution described in Step 2 in order to identify $\mathbf{y_0}$ and $\mathbf{\Sigma_0}$, the initial output mean and covariance for each design. A design is considered converged when the absolute difference between iteration estimates is less than 1×10^{-4} or the relative difference is less than 1×10^{-6}.

Step 6: Identify the Mean and Variance Bound of the Objective Function

Upon convergence the value of $\mathbf{y}$, the state variable in the problem, is the mean

response for each of the components of the output CAs. The matrix $\mathbf{M}$ is simply a 1×3 vector of ones, $\mathbf{1}_3^T$, since $\mathbf{y}^* = \mathbf{y}$, that is, it is the entire state vector. Therefore,

$$\bar{r} = \mathbf{1}_3^T \hat{\mathbf{y}}_{n|n}$$

The estimate for the variance (*i.e.*, the variance bound) in this case is simply

$$\sigma_r^2 \leq \sum_{i=1}^{3} \parallel \mathbf{\Sigma}_{n|n} \parallel_2 = 3 \parallel \mathbf{\Sigma}_{n|n} \parallel_2$$

Step 7: Optimize for Uncertainty and Ensure Constraints are Met

Formulating the output of Step 6 in terms of the mean and variance allows for an optimal control problem to be setup for the system design, where the objective function is defined by

$$\mathcal{J} = \alpha \mathbf{1}_3^T \hat{\mathbf{y}}_{n|n} + 3\beta \parallel \mathbf{\Sigma}_{\boldsymbol{y}^* n|n} \parallel_2$$

and α and β are weights on the relative components and can be varied. The design space and constraints in this problem are inherently convex therefore the constraints can be directly formulated as

$$\mathbf{g}(\mathbf{y}, \mathbf{u}) = \begin{pmatrix} y_1 - 1 \\ y_2 - 1 \\ y_3 - 1 \\ -y_1 - 1 \\ -y_2 - 1 \\ -y_3 - 1 \end{pmatrix} = \begin{pmatrix} \mathbf{I_{3\times 3}} \\ -\mathbf{I_{3\times 3}} \end{pmatrix} \mathbf{y} - \mathbf{1_6} \leq \mathbf{0}_6$$

Additionally, there is an equality constraint for the control that states

$$\mathbf{h}(\mathbf{y}, \mathbf{u}) = \mathbf{u}_k - \mathbf{u}_{k-1} = \mathbf{0}, \quad \forall k \in 1, \ldots, n$$

Therefore, the Hamiltonian in the optimal control problem is given by

$$H_k(\mathbf{y},\mathbf{u}) = \psi_0\left(\alpha\hat{\mathbf{y}}_{n|n} + 3\beta \parallel \mathbf{\Sigma}_{\boldsymbol{y}^*{}_{n|n}} \parallel_2\right) + \boldsymbol{\gamma}^T\left(\begin{pmatrix}\mathbf{I_{3\times 3}}\\ -\mathbf{I_{3\times 3}}\end{pmatrix}\hat{\mathbf{y}}_{n|n} - \mathbf{1_6}\right) + \boldsymbol{\lambda}^T\left(\mathbf{u}_k - \mathbf{u}_{k-1}\right)$$

where the terms in this relation can be computed numerically. The optimal control conditions listed in Chapter 3 can then be used to compute the value of u_d for a chosen value of α and β.

5.4.2 Design Results

The parameters used within the models for each of the cases examined are shown in Table 8 where the values without distributions are assumed to be deterministic.

Table 8: Parameters for the robust design of a three contributing analysis system.

Parameter	**Case 1**	**Case 2**
$\boldsymbol{\Lambda}$	$\begin{pmatrix}0 & 1 & 1\\ 1 & 0 & 1\\ \mathcal{N}(1,1) & \mathcal{N}(1,1) & 0\end{pmatrix}$	$\begin{pmatrix}0 & 1/3 & 1/3\\ 1/3 & 0 & 1/3\\ \mathcal{N}(1/3,1) & \mathcal{N}(1/3,1) & 0\end{pmatrix}$
$\boldsymbol{\beta}$	$\begin{pmatrix}1\\0\\0\end{pmatrix}$	$\begin{pmatrix}1\\0\\0\end{pmatrix}$
$\boldsymbol{\gamma}$	$\begin{pmatrix}0\\0\\0\end{pmatrix}$	$\begin{pmatrix}0\\0\\0\end{pmatrix}$
$\boldsymbol{\delta}$	$\begin{pmatrix}0\\0\\0\end{pmatrix}$	$\begin{pmatrix}0\\0\\0\end{pmatrix}$

5.4.2.1 Case 1: Divergent Design

In the first case, the nominal eigenvalues of $\boldsymbol{\Lambda}$ are found to be

$$\lambda = \{-1, -1, 2\}$$

Hence, since $|\lambda_{\max}| \geq 1 \ \forall \lambda_i, \ i \in \{1, 2, 3\}$ there is not a feasible design to be found with the iteration scheme. This is shown in Fig. 27 where the objective function value exponentially diverges. Despite fixed-point iteration not being able to find a

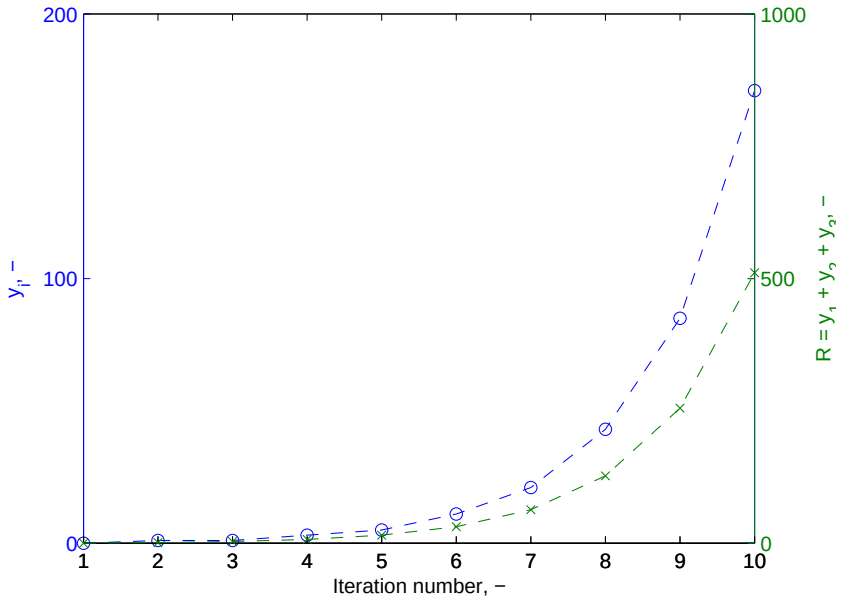

Figure 27: Divergent behavior demonstrated by the fixed-point iteration system ($u_d = 1$).

solution, a feasible design does exist. The feasible designs are characterized by the equation

$$\mathbf{y} = \begin{pmatrix} 0 \\ -1/2 \\ -1/2 \end{pmatrix} u_d$$

which implies that the deterministic optimum is found with $u_d = 2$ which is also the robust optimum for this problem for an equally weighted objective function. This example demonstrates the need for alternative iteration schemes to be investigated. However, it should be noted that the conditions outlined in Chapter 3 accurately describe the behavior of the dynamical system resulting from the multidisciplinary design as outlined.

5.4.2.2 *Case 2: Convergent Design*

In the second case, the nominal eigenvalues of $\mathbf{\Lambda}$ (see Table 8) are substantially different,

$$\lambda = \{-1/3, -1/3, 2/3\}$$

This implies that a feasible solution should be able to be found since $|\lambda_{\max}| = 2/3 \leq 1$. This fact is demonstrated in Fig. 28 where the objective function value converges for an arbitrary value of u_d.

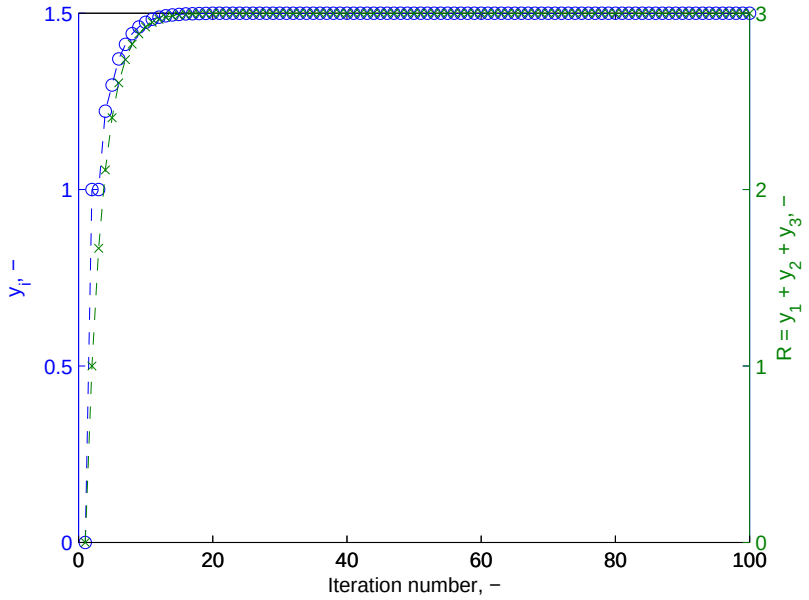

Figure 28: Convergent behavior demonstrated by the fixed-point iteration system ($u_d = 1$).

Candidate designs for this multidisciplinary system are shown in Fig. 29 for both the rapid robust design methodology (in green) as well as an exact propagation (in blue). Values for the exact propagation show the variance of the response, σ_r^2, against the mean response, whereas the rapid robust design methodology show the value $3 \parallel \mathbf{\Sigma}_{n|n} \parallel_2$ against the mean response. It should be also noted that the values of u_d for each method for three design points are presented on the figure for comparison between the two methods.

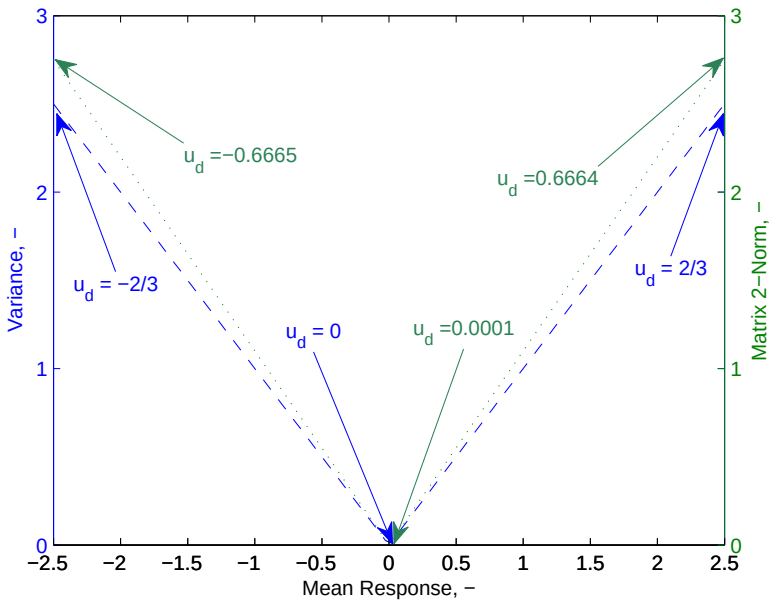

Figure 29: Optimal robust designs found using an exact propagation of uncertainty (blue) and approximate bounding method (green).

Depending on the overall ability to handle uncertainty, the designer should choose optimal solutions located on the the Pareto frontier. The Pareto optimal solutions are located with $u_d \in [-2/3, 0]$ with the mean response $\bar{r} \in [-2.5, 0]$. In addition, when examining Fig. 29 several important characteristics about the rapid robust design methodology are clear:

1. The values for the approximate method produce optimal values of u_d that are within 1% of the exact values.

2. The bounding method provided a conservative bound for the variance of the multidisciplinary design.

3. The method was capable of producing the same range of mean response as the exact propagation.

5.4.2.3 Deterministic Solutions

Several different approaches to finding the optimum were considered for the deterministic version of this problem given as

$$\left.\begin{aligned} &\textbf{Minimize}: && \mathcal{J} = y_1 + y_2 + y_3 \\ &\textbf{Subject to}: && y_1, y_2, y_3 \in [-1, 1] \\ &\textbf{By varying}: && u_d \end{aligned}\right\}$$

with $\mathbf{u_p} = \mathbf{0}$. These approaches include solving this design problem as a discrete optimal control problem, a direct optimal control problem, and an indirect optimal control problem. For the discrete and direct optimal control problem, the optimal design is found using the Sparse Nonlinear Optimization (SNOPT), an NLP solver which uses a sequential quadratic programming algorithm[166]. A boundary value problem solver using collocation was used to solve the indirect problem. The solutions obtained for each of these techniques along with the number of DSM iterations is shown in Table. 9.

Table 9: Design results for the linear, three contributing analysis system.

Method	u_d^*	$\mathcal{J}^*$	**DSM Iterations**
Discrete	-0.6665	2.499	21
Continuous, Direct	-0.6645	2.478	26
Continuous, Indirect	-0.6666	2.500	16

5.5 Rapid Robust Design of a Two Bar Truss

Consider the planar truss which consists of two elements with a vertical load at the mutual joint, as shown in Fig. 30 (adapted from Ref. [167]).

For this problem, it is desired to find the vertical position of nodes 2 and 3, h_2 and h_3, that minimize the weight of the truss while ensuring that the structure will not fail due to Euler buckling or yielding with some factor of safety given fixed values for the material properties, E, σ_y, and ρ, the load, f, and the bar geometry, r_1 and

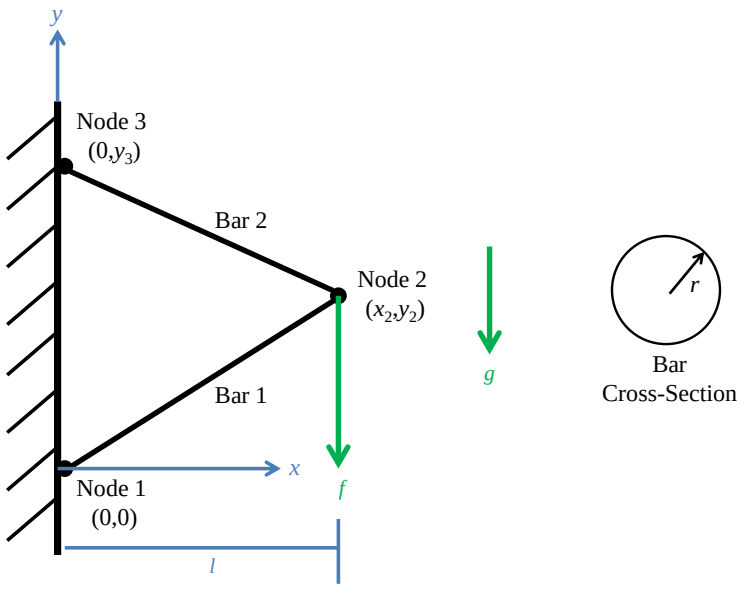

Figure 30: Two bar truss with a load at the mutual joint.

r_2. The horizontal position of node 2 is constrained to be l. In standard form, the problem is written as

$$\left.\begin{array}{ll} \textbf{Minimize}: & [\bar{m}\ \sigma_m^2] \\ \textbf{Subject to}: & g_1(h_2,h_3) = |T_1(h_2,h_3)| - \pi r_1^2 \sigma_y \leq 0 \\ & g_2(h_2,h_3) = |T_2(h_2,h_3)| - \pi r_2^2 \sigma_y \leq 0 \\ & g_3(h_2,h_3) = -T_1(h_2,h_3) - \dfrac{\pi^2 E I_1}{L_1^2} \leq 0 \\ & g_4(h_2,h_3) = -T_2(h_2,h_3) - \dfrac{\pi^2 E I_2}{L_2^2} \leq 0 \\ \textbf{By varying}: & h_2, h_3 \end{array}\right\}$$

where $\bar{m}$ is the mean mass of the bars and the variance of the mass, σ_m^2, for the rapid robust design methodology is given by $\| \Sigma_{\mathbf{y}^*} \|_2$. In these relations, the mass is given by

$$m = \rho\pi g\left(r_1^2 L_1 + r_2^2 L_2\right) = \rho\pi g\left(r_1^2\sqrt{l^2+h_2^2} + r_2^2\sqrt{l^2+(h_3-h_2)^2}\right)$$

L_1 and L_2 are the lengths of the two bars, respectively, I_1 and I_2 are the moments of inertia of the two bars ($I_i = \dfrac{1}{4}mr_i^2$), and $T_1(h_2,h_3)$ and $T_2(h_2,h_3)$ are the tensions

in the two bars. In this formulation both the objective function and constraints are nonlinear with respect to the design variables. Numerical values for this problem are shown in Table 10.

Table 10: Parameters for the two-bar truss problem.

Parameter	Description	Nominal Value	Distribution
E	Young's Modulus	200×10^6 kN/m^2	–
σ_y	Yield Strength	250×10^3 kN/m^2	$\mathcal{N}(250 \times 10^3, 625 \times 10^6)$
ρ	Density	7850 kg/m^3	$\mathcal{N}(7850, 100)$
l	Length	5 m	–
r_1	Radius of Bar 1	30 mm	–
r_2	Radius of Bar 2	5 mm	–
f	Applied Force	3.5 kN	$\mathcal{N}(3.5, 0.49)$
g	Gravitational Acceleration	9.81 m/s^2	–

5.5.1 Applying the Rapid Robust Design Methodology

Step 1: Decompose the Design

Two analyses must occur in order to design the two bar truss: a structural analysis and a sizing of the bars constituting the truss. Although not explicit in the problem statement, the mass of the bars also provide a load through their weight. Hence, this is a coupled analysis problem since the structural analysis depends on the sizing of each of the bars. The coupled DSM is shown in Fig. 31.

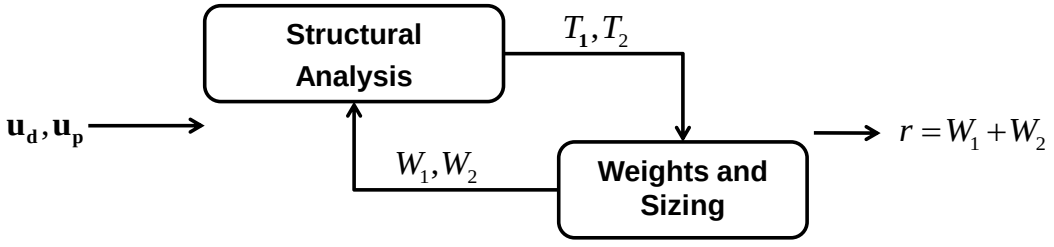

Figure 31: Two bar truss design structure matrix.

The inputs into the design problem are the deterministic and probabilistic parameters of the problem whose values are shown in Table 10. In particular,

$$\mathbf{u_d} = \begin{pmatrix} E & l & r_1 & r_2 & g & y_2 & y_3 \end{pmatrix}^T$$

and

$$\mathbf{u_p} = \begin{pmatrix} \sigma_y & \rho & f \end{pmatrix}^T$$

The structural analysis CA feeds the forces seen in each of the members of the truss to the weights and sizing module. These can be found through the static equilibrium equations and are found by solving the linear equations

$$\begin{pmatrix} \frac{l}{L_1} & 0 & 1 & 0 & 0 & 0 \\ -\frac{y_2}{L_1} & 0 & 0 & 1 & 0 & 0 \\ -\frac{l}{L_1} & \frac{l}{L_2} & 0 & 0 & 0 & 0 \\ -\frac{y_2}{L_1} & \frac{y_3 - y_2}{L_2} & 0 & 0 & 0 & 0 \\ 0 & \frac{l}{L_2} & 0 & 0 & 1 & 0 \\ 0 & \frac{y_3 - y_2}{L_2} & 0 & 0 & 0 & 1 \\ 0 & 0 & 1 & 0 & 0 & 0 \\ 0 & 0 & 0 & 1 & 0 & 0 \\ 0 & 0 & 0 & 0 & 1 & 0 \\ 0 & 0 & 0 & 0 & 0 & 1 \end{pmatrix} \begin{pmatrix} T_1 \\ T_2 \\ R_{1x} \\ R_{1y} \\ R_{3x} \\ R_{3y} \end{pmatrix} = \begin{pmatrix} 0 \\ 0 \\ 0 \\ -\frac{l}{2y_3}(W_1 + W_2 + 2f) \\ f\left(1 + \frac{y_2}{y_3}\right) \\ 0 \\ 0 \\ f \\ \frac{l}{2y_3}(W_1 + W_2 + 2f) \\ f\left(1 + \frac{y_2}{y_3}\right) + W_1 + W_2 \end{pmatrix}$$

for the tensions. The weights and sizing CA computes the weights of each of the bars based on the relationship

$$\mathbf{y_2} = \begin{pmatrix} W_1 \\ W_2 \end{pmatrix} = \begin{pmatrix} \pi \rho g r_1^2 L_1 \\ \pi \rho g r_2^2 L_2 \end{pmatrix}$$

Both relationships defined by the CAs rely on the lengths of the bars, which are given

by

$$\begin{aligned} L_1 &= \sqrt{l^2 + y_2^2} \\ L_2 &= \sqrt{l^2 + (y_3 - y_2)^2} \end{aligned}$$

This is a realistic example in which the CAs are nonlinear. Therefore, in order to apply the developed methodology, a Taylor series expansion about a nominal value (chosen to be the previous iterate's mean value) must be conducted. Functionally, this means that Eq. (5.5.1) can be expanded as follows

$$\mathbf{y_1} = \begin{pmatrix} T_1 \\ T_2 \end{pmatrix} \approx \begin{pmatrix} \left.\frac{\partial T_1}{\partial \mathbf{u_d}}\right|_{\hat{\mathbf{u}}_\mathbf{d}} (\mathbf{u_d} - \hat{\mathbf{u}}_\mathbf{d}) + \left.\frac{\partial T_1}{\partial \mathbf{u_p}}\right|_{\boldsymbol{\mu}_{\mathbf{u_p}}} (\mathbf{u_p} - \boldsymbol{\mu}_{\mathbf{u_p}}) + \left.\frac{\partial T_1}{\partial \mathbf{y}}\right|_{\hat{\mathbf{y}}} (\mathbf{y} - \hat{\mathbf{y}}) \\ \left.\frac{\partial T_2}{\partial \mathbf{u_d}}\right|_{\hat{\mathbf{u}}_\mathbf{d}} (\mathbf{u_d} - \hat{\mathbf{u}}_\mathbf{d}) + \left.\frac{\partial T_2}{\partial \mathbf{u_p}}\right|_{\boldsymbol{\mu}_{\mathbf{u_p}}} (\mathbf{u_p} - \boldsymbol{\mu}_{\mathbf{u_p}}) + \left.\frac{\partial T_2}{\partial \mathbf{y}}\right|_{\hat{\mathbf{y}}} (\mathbf{y} - \hat{\mathbf{y}}) \end{pmatrix}$$

Similarly, Eq. (5.5.1) can be expanded as

$$\mathbf{y_2} = \begin{pmatrix} W_1 \\ W_2 \end{pmatrix} \approx \begin{pmatrix} \pi \rho g r_1^2 \frac{\hat{y}_2}{\sqrt{l^2 + \hat{y}_2^2}} (y_2 - \hat{y}_2) \\ \pi \rho g r_2^2 \left(\frac{\hat{y}_2 - \hat{y}_3}{\sqrt{l^2 + (\hat{y}_2 - \hat{y}_3)^2}} (y_2 - \hat{y}_2) + \frac{\hat{y}_3 - \hat{y}_2}{\sqrt{l^2 + (\hat{y}_2 - \hat{y}_3)^2}} (y_3 - \hat{y}_3) \right) \end{pmatrix}$$

Therefore, in the form of Eq. (75)

$$\mathbf{A_1} = \left(\left.\frac{\partial T_1}{\partial \mathbf{y}}\right|_{\hat{\mathbf{y}}} \right) \quad \mathbf{B_1} = \left(\left.\frac{\partial T_1}{\partial \mathbf{u_d}}\right|_{\hat{\mathbf{u}}_\mathbf{d}} \right)$$

$$\mathbf{C_1} = \left(\left.\frac{\partial T_1}{\partial \mathbf{u_p}}\right|_{\boldsymbol{\mu}_{\mathbf{u_p}}} \right)$$

$$\mathbf{d_1} = - \left(\left.\frac{\partial T_1}{\partial \mathbf{u_d}}\right|_{\hat{\mathbf{u}}_\mathbf{d}} \hat{\mathbf{u}}_\mathbf{d} + \left.\frac{\partial T_1}{\partial \mathbf{u_p}}\right|_{\boldsymbol{\mu}_{\mathbf{u_p}}} \boldsymbol{\mu}_{\mathbf{u_p}} + \left.\frac{\partial T_1}{\partial \mathbf{y}}\right|_{\hat{\mathbf{y}}} \hat{\mathbf{y}} \right)$$

$$\mathbf{A_2} = \left(\left.\frac{\partial T_2}{\partial \mathbf{y}}\right|_{\hat{\mathbf{y}}} \right) \quad \mathbf{B_2} = \left(\left.\frac{\partial T_2}{\partial \mathbf{u_d}}\right|_{\hat{\mathbf{u}}_\mathbf{d}} \right)$$

$$\mathbf{C_2} = \left(\left.\frac{\partial T_2}{\partial \mathbf{u_p}}\right|_{\boldsymbol{\mu}_{\mathbf{u_p}}} \right)$$

$$\mathbf{d_2} = -\left(\left.\frac{\partial T_2}{\partial \mathbf{u_d}}\right|_{\hat{\mathbf{u}}_\mathbf{d}} \hat{\mathbf{u}}_\mathbf{d} + \left.\frac{\partial T_2}{\partial \mathbf{u_p}}\right|_{\boldsymbol{\mu}_{\mathbf{u_p}}} \boldsymbol{\mu}_{\mathbf{u_p}} + \left.\frac{\partial T_2}{\partial \mathbf{y}}\right|_{\hat{\mathbf{y}}} \hat{\mathbf{y}} \right)$$

Step 2: Identify the Random Variables and their Distributions

All of the random variables in this example are associated with the parameters and not with the model itself. As shown in Table 10, the values are given by $\sigma_y \sim \mathcal{N}(250 \times 10^3, 625 \times 10^6)$, $\rho \sim \mathcal{N}(7850, 100)$, and $f \sim \mathcal{N}(3.5, 0.49)$.

Step 3: Form the Iterative Equations

In order to use the Kalman filter to simultaneously estimate robustness and converge the design, the iterative equations described in Eq. (76) for fixed-point iteration need to be formed. Through analogy of variables, the matrices are given by

$$\boldsymbol{\Lambda} = \begin{pmatrix} \mathbf{A_1} \\ \mathbf{A_2} \end{pmatrix} = \begin{pmatrix} \mathbf{0} & \left.\frac{\partial T_1}{\partial \mathbf{y_2}}\right|_{\hat{\mathbf{y}}} \\ \left.\frac{\partial T_2}{\partial \mathbf{y_1}}\right|_{\hat{\mathbf{y}}} & \mathbf{0} \end{pmatrix}$$

$$\boldsymbol{\beta} = \begin{pmatrix} \mathbf{B_1} \\ \mathbf{B_2} \end{pmatrix} = \begin{pmatrix} \left.\frac{\partial T_1}{\partial \mathbf{u_d}}\right|_{\hat{\mathbf{u}}_\mathbf{d}} \\ \left.\frac{\partial T_2}{\partial \mathbf{u_d}}\right|_{\hat{\mathbf{u}}_\mathbf{d}} \end{pmatrix}$$

$$\boldsymbol{\gamma} = \begin{pmatrix} \mathbf{C_1} \\ \mathbf{C_2} \end{pmatrix} = \begin{pmatrix} \left.\frac{\partial T_1}{\partial \mathbf{u_p}}\right|_{\boldsymbol{\mu}_{\mathbf{u_p}}} \\ \left.\frac{\partial T_2}{\partial \mathbf{u_p}}\right|_{\boldsymbol{\mu}_{\mathbf{u_p}}} \end{pmatrix}$$

$$\boldsymbol{\delta} = \begin{pmatrix} \mathbf{d_1} \\ \mathbf{d_2} \end{pmatrix} = \begin{pmatrix} -\left(\left.\frac{\partial T_1}{\partial \mathbf{u_d}}\right|_{\hat{\mathbf{u}}_\mathbf{d}} \hat{\mathbf{u}}_\mathbf{d} + \left.\frac{\partial T_1}{\partial \mathbf{u_p}}\right|_{\boldsymbol{\mu}_{\mathbf{u_p}}} \boldsymbol{\mu}_{\mathbf{u_p}} + \left.\frac{\partial T_1}{\partial \mathbf{y}}\right|_{\hat{\mathbf{y}}} \hat{\mathbf{y}} \right) \\ -\left(\left.\frac{\partial T_2}{\partial \mathbf{u_d}}\right|_{\hat{\mathbf{u}}_\mathbf{d}} \hat{\mathbf{u}}_\mathbf{d} + \left.\frac{\partial T_2}{\partial \mathbf{u_p}}\right|_{\boldsymbol{\mu}_{\mathbf{u_p}}} \boldsymbol{\mu}_{\mathbf{u_p}} + \left.\frac{\partial T_2}{\partial \mathbf{y}}\right|_{\hat{\mathbf{y}}} \hat{\mathbf{y}} \right) \end{pmatrix}$$

where the numerical values for each of these matrices is evaluated at each subsequent iteration at the appropriate nominal values.

Step 4: Ensure a Solution Exists

While this problem is posed as a linear system, the matrix $\mathbf{\Lambda}$ varies with iteration. This requires a Lyapunov analysis to be conducted in order to identify the stability of the system. For this example, this analysis was completed simultaneously with the convergence by numerically solving a matrix Riccati equation. A positive definite matrix, $\mathbf{R}$, for the quadratic problem was able to be found that satisfies the relationship

$$\mathbf{\Lambda}_k^T \mathbf{R}_k \mathbf{\Lambda}_k - \mathbf{R}_k = -\mathbf{S}_k$$

for $\mathbf{S}_k > 0$. Since a solution for $\mathbf{R}_k$ was able to be found when $\mathbf{S}_k = \mathbf{I_{4\times 4}}$ for each iterate, this enables a Lyapunov function of the form

$$V_k(\mathbf{y}) = \mathbf{y}_k^T \mathbf{R}_k \mathbf{y}_k$$

to be formed which shows asymptotic stability for a linear, time varying, discrete system.

The stability of this problem was also analyzed by using a sum-of-squares Lyapunov function technique as outlined in Chapter 3 where a tenth-order polynomial about $\mathbf{y}_0$ was formed. Applying SOSTOOLS, a semi-definite programming algorithm, to this problem yielded a polynomial solution to Eq. (42), that also satisfies the requirements of a Lyapunov function.

The modulus of the eigenvalues show similar conclusions regarding the asymptotic stability as Lyapunov stability as shown in Fig. 32.

Step 5: Estimate the Mean Output and the Covariance

The equations formed in the prior step can then be propagated through the Kalman filter defined by Eqs. (62)-(68) with

$$\mathbf{F}_{k-1} = \mathbf{\Lambda}, \quad \forall k \in \{1, 2, ...\}$$

$$\mathbf{B}_{k-1} = \begin{pmatrix} \boldsymbol{\beta} & \boldsymbol{\gamma} & \mathbf{I_{4\times 4}} \end{pmatrix}, \quad \forall k \in \{1, 2, ...\}$$

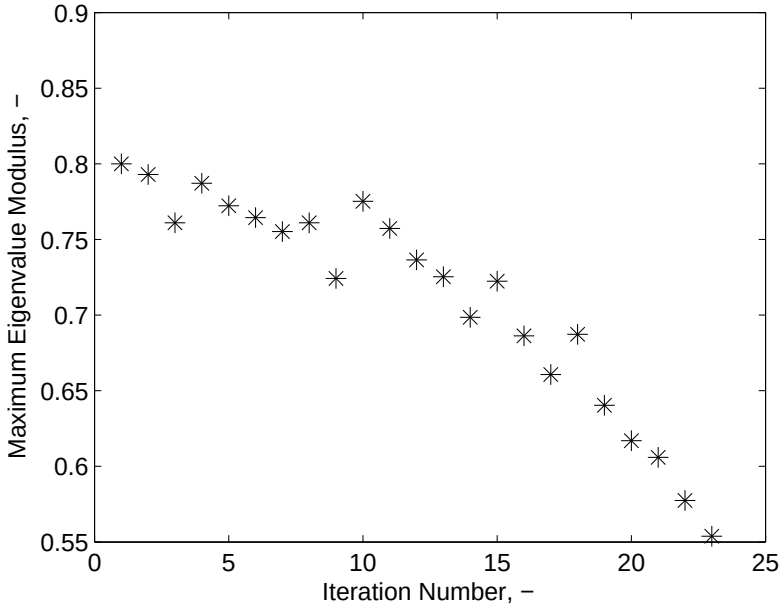

Figure 32: History of the modulus of the maximum eigenvalue of the two bar truss system with iteration.

$$\mathbf{u}_{k-1} = \begin{pmatrix} \mathbf{u_d} \\ \mathbf{u_p} \\ \boldsymbol{\delta} \end{pmatrix}, \quad \forall k \in \{1, 2, ...\}$$

where in this example $\mathbf{u_d} = \begin{pmatrix} E & l & r_1 & r_2 & g & y_2 & y_3 \end{pmatrix}^T$ and $\mathbf{u_p} = \mathbb{E}(\mathbf{u_p}) = \boldsymbol{\mu}_{\mathbf{u_p}}$. In this example, the matrix $\mathbf{Q}$ is the null matrix since the only uncertain parameters of the problem are associated with the input parameters, not the model. The unscented transform is used on an uncoupled system with the distribution described in Step 2 in order to identify $\mathbf{y_0}$ and $\boldsymbol{\Sigma_0}$, the initial output mean and covariance for each design. A design is considered converged when the absolute difference between iteration estimates is less than 1×10^{-4} or the relative difference is less than 1×10^{-6}.

Step 6: Identify the Mean and Variance Bound of the Objective Function Upon convergence, the value of $\mathbf{y}$, the state variable in the problem, is the mean response for each of the components of the output CAs. In this example, the matrix

$\mathbf{M}$ is given by

$$\mathbf{M} = \begin{pmatrix} 0 & 0 & 1 & 1 \end{pmatrix}$$

since the objective is the weight of truss $W_1 + W_2$, the two elements of the second CA output. Therefore,

$$\bar{r} = \begin{pmatrix} 0 & 0 & 1 & 1 \end{pmatrix} \hat{\mathbf{y}}_{n|n}$$

The estimate for the variance (*i.e.*, the variance bound) in this case is two times the two-norm of the entire estimated covariance matrix

$$\sigma_r^2 \leq \sum_{i=1}^{2} \parallel \mathbf{\Sigma}_{\mathbf{y}^*{}_{n|n}} \parallel_2 = 2 \parallel \mathbf{\Sigma}_{\mathbf{y}^*{}_{n|n}} \parallel_2$$

.

Step 7: Optimize for Uncertainty and Ensure Constraints are Met

Formulating the output of Step 6 in terms of the mean and variance allows for an optimal control problem to be setup for the system's design, where the objective function is defined by

$$\mathcal{J} = \alpha \begin{pmatrix} 0 & 0 & 1 & 1 \end{pmatrix} \hat{\mathbf{y}}_{n|n} + 2\beta \parallel \mathbf{\Sigma}_{\boldsymbol{y}^*{}_{n|n}} \parallel_2$$

and α and β allow different weighting on the mean and variance. The constraints for this problem as given are

$$\mathbf{g}(\mathbf{y}, \mathbf{u}) = \begin{pmatrix} g_1(\mathbf{y}, \mathbf{u}) \\ g_2(\mathbf{y}, \mathbf{u}) \\ g_3(\mathbf{y}, \mathbf{u}) \\ g_4(\mathbf{y}, \mathbf{u}) \end{pmatrix} = \begin{pmatrix} |T_1(\mathbf{u})| - \pi r_1^2 \sigma_y \\ |T_2(\mathbf{u})| - \pi r_2^2 \sigma_y \\ -T_1(\mathbf{u}) - \dfrac{\pi^2 E I_1}{L_1^2} \\ -T_2(\mathbf{u}) - \dfrac{\pi^2 E I_2}{L_2^2} \end{pmatrix}$$

Additionally, there is an equality constraint for the control that states

$$\mathbf{h}(\mathbf{y}, \mathbf{u}) = \mathbf{u}_k - \mathbf{u}_{k-1} = \mathbf{0}, \quad \forall k \in 1, \ldots, n$$

Therefore, the Hamiltonian in the optimal control problem is given by

$$H_k(\mathbf{y}, \mathbf{u}) = \psi_0 \left(\alpha \begin{pmatrix} 0 & 0 & 1 & 1 \end{pmatrix} \hat{\mathbf{y}}_{n|n} + 2\beta \parallel \mathbf{\Sigma}_{\boldsymbol{y}^*{}_{n|n}} \parallel_2 \right) + \boldsymbol{\gamma}^T \mathbf{h} + \boldsymbol{\lambda}^T \mathbf{g}$$

where the terms in this relation can be computed numerically. The optimal control conditions listed in Chapter 3 can then be used to compute the values of y_2 and y_3 for a chosen value of α and β.

5.5.2 Design Results

As mentioned at the beginning of this section, the formulation of this problem is based on work in Ref. [167]. This work showed the deterministic optimal design to be as shown in Fig. 33 which also shows the minimum variance robust design found in this work[167]. This positions the vertical positions of the nodes, (y_2^*, y_3^*), at $(0.751, 9.970)$

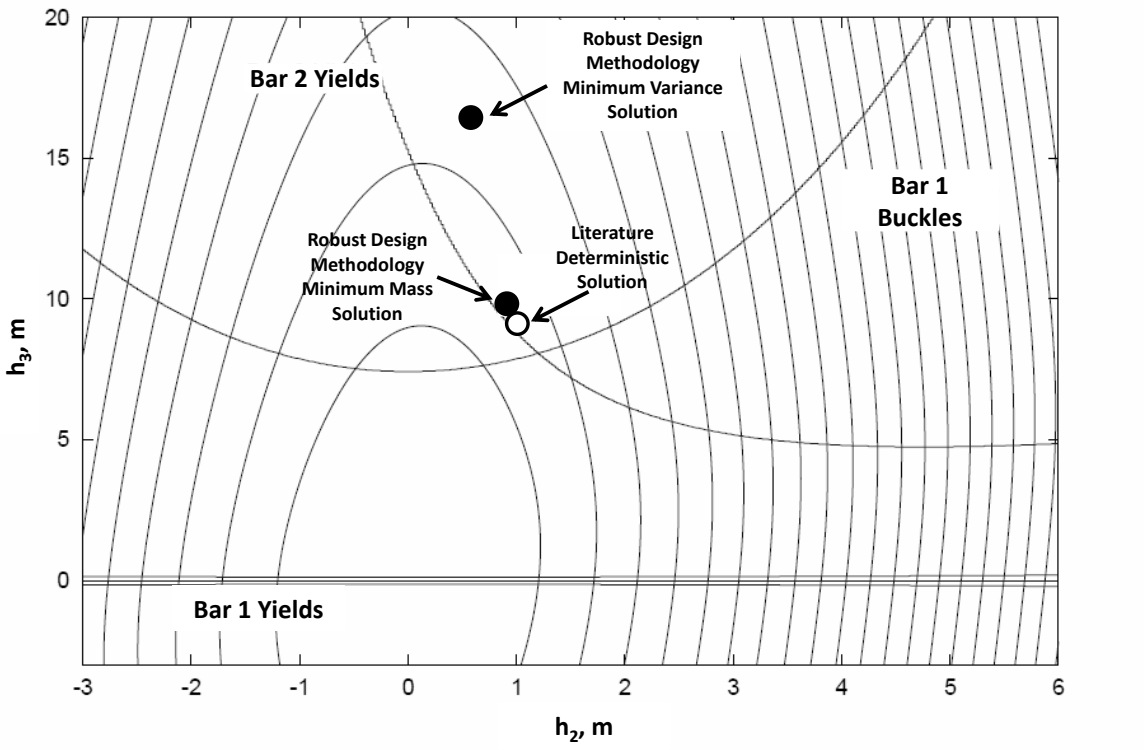

Figure 33: Deterministic and robust design of a two bar truss with a load at the mutual joint.

m with an objective function value of $\mathcal{J} = 291.092$ N. The deterministic case of this analysis (*i.e.*, when $\alpha = 1$ and $\beta = 0$) yields a very similar result with (y_2^*, y_3^*) at $(0.746, 9.991)$ m with an objective function value of $\mathcal{J} = 291.151$ N which implies that the method developed achieves an accurate numerical result even in the case of

nonlinear problems.

The variation in terms of mean and variance for this problem is shown in Fig. 34.

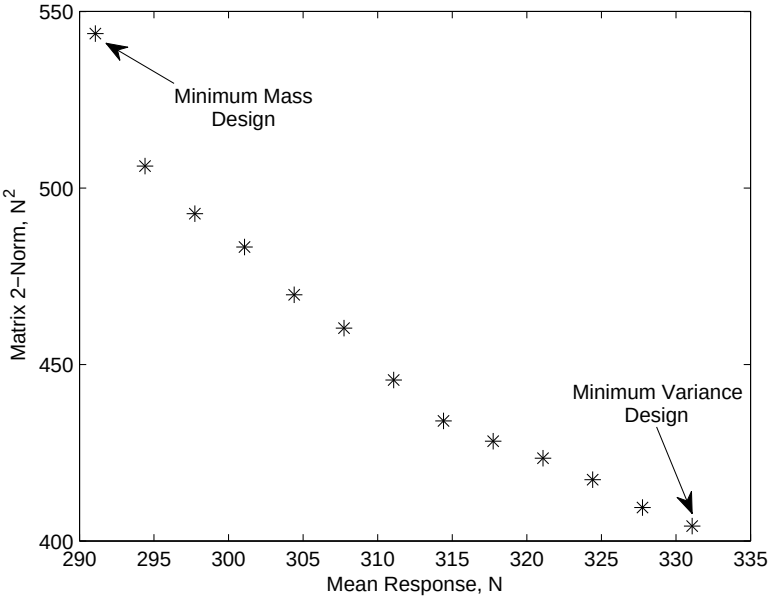

Figure 34: Variation of $2||\mathbf{\Sigma}_{\mathbf{y}^*}||_2$ with the mean objective function for the design of a two bar truss with a load at the mutual joint.

From this figure, the deterministic optimum is the minimum mean solution; however, it is not the minimum variance solution. This minimum variance design is approximately 39 N heavier.

5.6 Rapid Robust Design of a Deployable for Strategic Vehicles

As the demands on the performance of entry, descent, and landing (EDL) systems increase, additional technologies will be needed in order to enable the desired mission sets. Deployable devices are one such technology, reducing or eliminating the maximum diameter constraint placed on the entry vehicle shape by the launch or boost vehicle. Relaxation or elimination of this constraint provides an aerodynamic performance advantage enabling a broad spectrum of next-generation missions for both

civilian and national defense applications. Some examples of previously investigated deployable systems are discussed in Refs. [168, 169, 170, 171, 172, 173, 174, 175, 176, 177, 178, 179, 180, 181, 182].

Deployables are usually thought to be drag enhancing devices to reduce the ballistic coefficient of a system. However, for strategic vehicles, the inclusion of a deployable device may also improve controllability, enhance constraint margins, and lead to new concepts of operations. Boost-glide systems are typically mid- to high-L/D systems that use a boost phase to achieve a desired state and then manage their energy to glide to their desired target. Deployables could be added to existing strategic systems leading to an evolved boost-glide mission set through increased range and accuracy. This work robustly designs deployable systems for a representative strategic system in order to examine this evolved boost-glide mission set.

5.6.1 Performance Impact of a Deployable System

In general, the performance of a vehicle is strongly characterized by the ballistic coefficient, β, and the lift-to-drag ratio, L/D [183]. Figure 35 shows the 1σ miss distance to a surface target and achievable range as a function of L/D for a range of β. The results seen in Fig. 35 are the product of solving the optimal control problem where the control is the orientation and magnitude of the net aerodynamic force vector at Earth from an initial state of $h_0 = 155$ km, $v_0 = 6.2$ km/s, and $\gamma_0 = -9.6°$. It was assumed that the aerodynamic force vector could be oriented freely and non-continuously within a reachable cone having a half-angle defined by the maximum L/D. The objective function to be maximized for this optimization problem is either accuracy (in the case of Fig. 35(a)) or range (in the case of Fig. 35(b)).

In Fig. 35, it is seen that the miss distance is relatively insensitive to ballistic coefficient; however, there is a strong, nonlinear dependence on L/D for values less

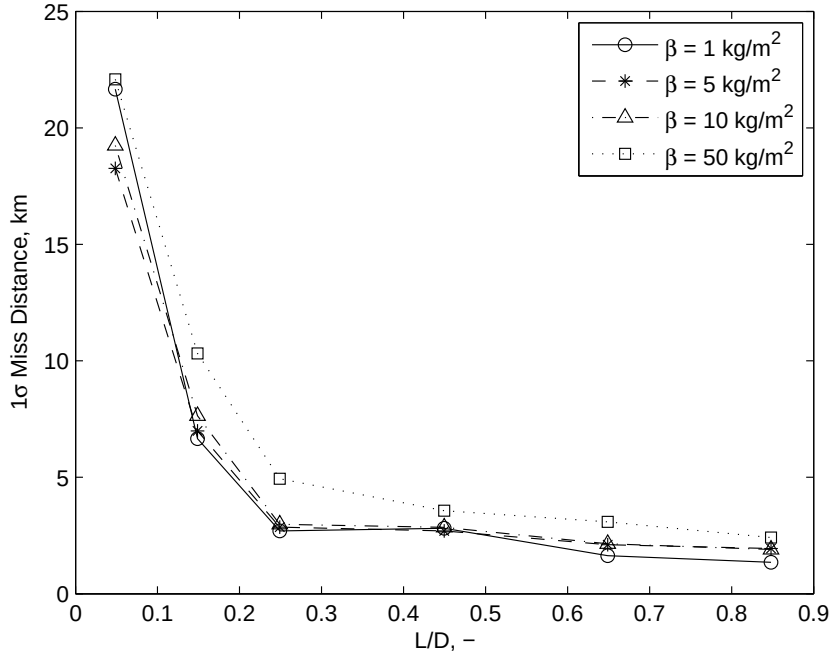

(a)

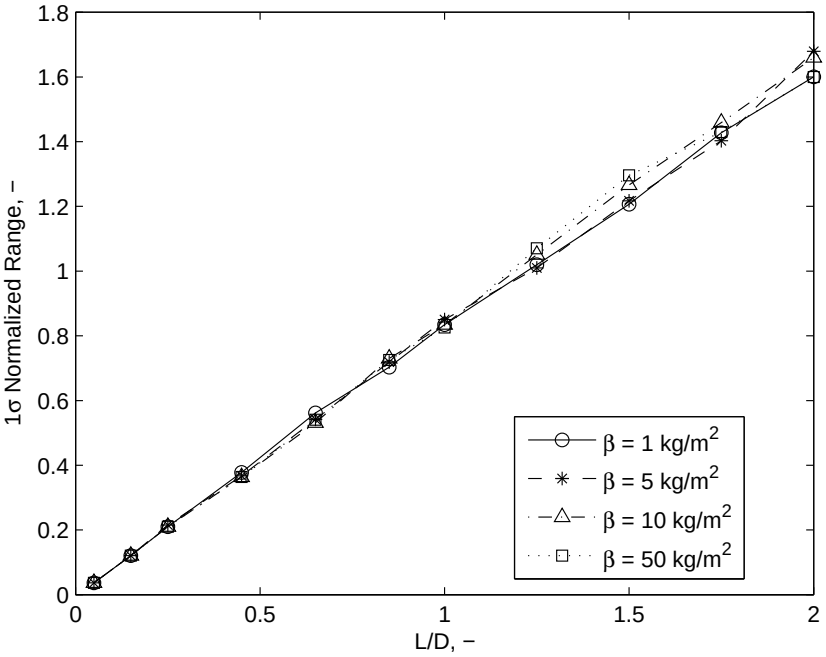

(b)

Figure 35: Variation of (a) miss distance and (b) range showing sensitivity to lift-to-drag ratio and insensitivity to ballistic coefficient.

than 0.3 with limited additional improvement beyond this point. A strong, near-linear dependence on L/D is seen for range capability. Like with the accuracy, there is little sensitivity to the ballistic coefficient.

There is a large design space of deployable concepts. This investigation will limit the design to a single concept—that of deployable chines, which are shown in Fig. 36. In this investigation, the root chord is fixed at $2d$.

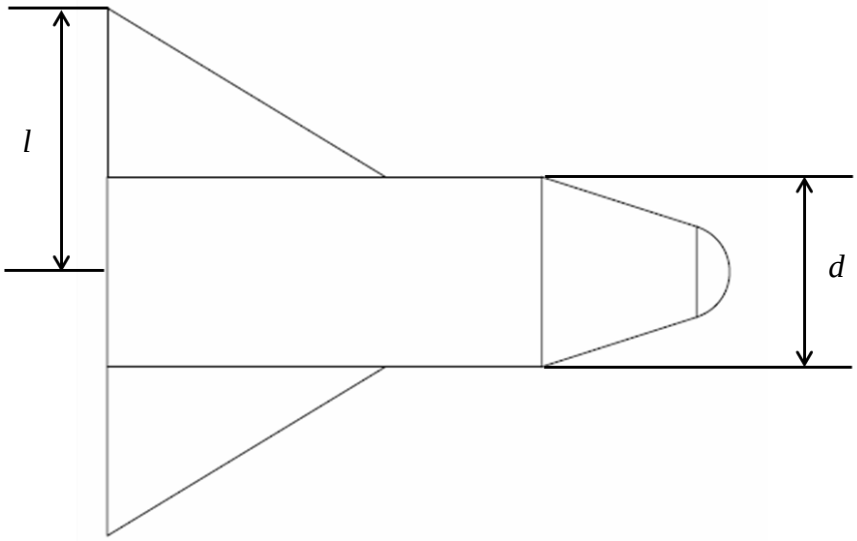

Figure 36: Geometry of the deployable device.

Chines have the potential to increase the L/D performance of the system [184, 185, 186, 187]. This effect is shown in Fig. 37 where the improvement over a representative baseline's L/D is plotted against a non-dimensional size, l/d—the ratio of the distance from the centerline of the vehicle to tip chord of the deployable to the baseline vehicle's diameter.

Figure 35 implies that from a performance perspective, the vehicle should have as much L/D as possible while Fig. 37 indicates that in order to maximize the L/D of the system, the deployable should be as large as possible. However, the larger the deployable the more massive it is, which negatively impacts the performance of the system. Therefore, a multiobjective design problem is formulated where the mass

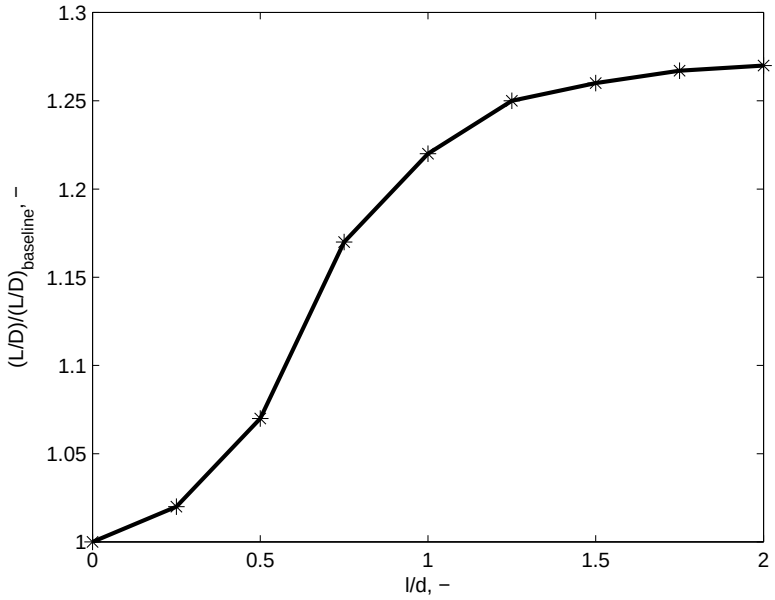

Figure 37: Increase in the maximum lift-to-drag ratio of the entry system for a single-delta deployable as a function of deployable size.

Table 11: Baseline strategic vehicle aerodynamics

Parameter	**Value**
$(L/D)_{\max}$	1.02
$\alpha\|_{(L/D)_{\max}}$	22.5°
$C_L\|_{(L/D)_{\max}}$	0.864
$C_D\|_{(L/D)_{\max}}$	0.849

of the decelerator is traded with the performance of the system (either accuracy or range).

5.6.2 Baseline Strategic System Characteristics

The rapid robust design methodology is used to design a deployable system that could be added to a representative baseline strategic system to potentially improve its performance. The baseline system is shown in Fig. 38 and selected characteristics describing its aerodynamics are shown in Table 11.

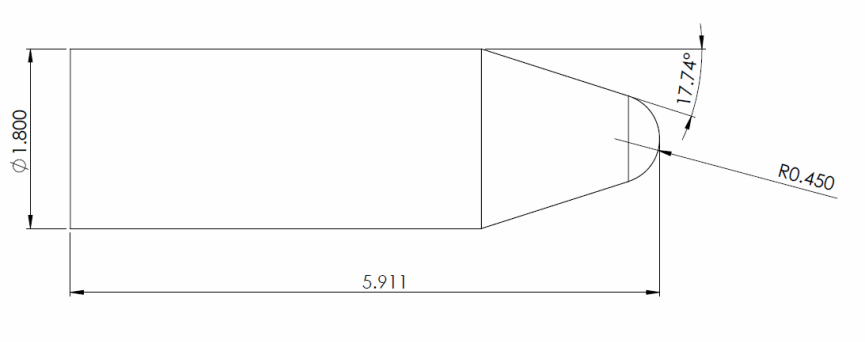

Figure 38: Baseline strategic vehicle characteristics.

5.6.3 Modeling

This design can be decomposed into seven CAs as shown in Fig. 39. The models for each of these CAs will be discussed in the discussion that follows.

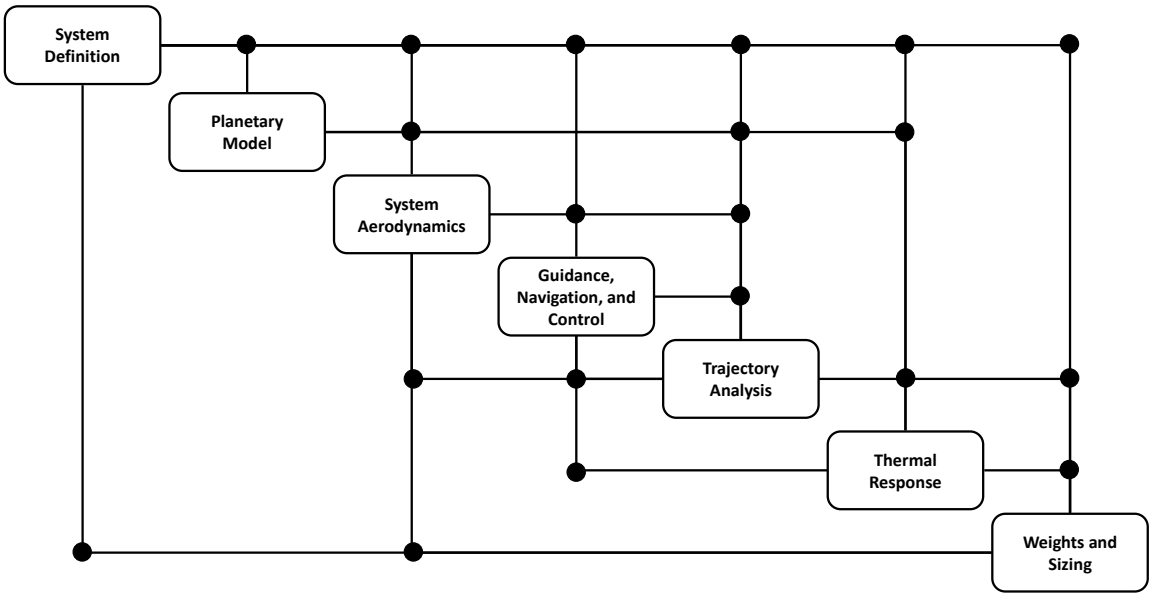

Figure 39: Design structure matrix for the design of a deployable for a strategic system.

5.6.3.1 Planetary Model

This analysis assumes an inverse square law gravity field and an exponential atmospheric density profile for Earth.

5.6.3.2 System Aerodynamics

For this investigation, a hypersonic aerodynamics analysis of the baseline strategic system along with the deployable was performed using a Newtonian impact model. These results were generated with a first-order industry standard tool, the configuration based aerodynamics (CBAero) tool [188]. The conditions at the maximum lift-to-drag ratio, $(L/D)_{\max}$, were then regressed as a function of the size of the deployable (*e.g.*, $C_L(l/d)$, $C_D(l/d)$, etc.) for use in the design of the deployable system. The deployable is assumed to be a single-delta shape as shown in Fig. 36.

5.6.3.3 Guidance, Navigation, and Control

Two different guidance schemes are considered in this work: bank-to-steer guidance and acceleration control.

Bank-to-Steer Guidance

Bank-to-steer guidance has been used on missions such as Apollo and the Mars Science Laboratory [189, 190]. This control technique rotates the lift vector around the velocity vector. In the downrange direction, control is provided by varying the amount of vertical lift, which is proportional to the cosine of the bank angle, σ. Crossrange control is provided by bank reversals since both σ and $-\sigma$ provide the same $(L/D)_{vert}$.

Acceleration Control

Acceleration control is a bounding technique which controls the direction of the aerodynamic acceleration vector assuming that the magnitude of the acceleration is equal to that produced by drag at zero angle of attack. This is consistent with a system where drag is reduced as lift is produced. The direction of the acceleration vector is allowed to freely vary within a cone with half-angle θ_c defined by the lift-to-drag ratio

of the system

$$\theta_c = \tan^{-1}\left(\frac{L}{D}\right) = \tan^{-1}\left(\frac{C_L}{C_D}\right) \tag{99}$$

Mathematically, the commanded acceleration is given by

$$\mathbf{a_c} = \frac{D_{\max}}{m}\hat{\mathbf{u}} = \frac{\rho v^2 C_D|_{\alpha=0^\circ} A}{2m}\frac{\mathbf{u}}{\parallel \mathbf{u} \parallel} \tag{100}$$

with the constraint that

$$\cos^{-1}\left(\frac{\hat{\mathbf{u}}^T\mathbf{v}}{v}\right) \leq \theta_c \tag{101}$$

Implementation

During propagation of the trajectory, an optimal control trajectory is obtained for the remainder of the trajectory at frequency of 0.5 Hz. This optimal control is predicted using GPOPS, a pseudospectral optimal control software [191, 192, 193, 194, 195]. In the case where the range is to be maximized, the objective function used in GPOPS is given by

$$\mathcal{J} = -s_f = -s(t_f) \tag{102}$$

Similarly, when the accuracy is to be maximized, the objective function is given as

$$\mathcal{J} = d_{miss}^2 = \left(\mathbf{r}(t_f) - \mathbf{r_T}\right)^T \left(\mathbf{r}(t_f) - \mathbf{r_T}\right) \tag{103}$$

which is equivalent to minimizing the miss distance.

5.6.3.4 Trajectory Analysis

In addition to Cartesian equations of motion, an additional equation for the range of the system is also propagated. This equation for the range is given by

$$\dot{s} = v\cos(\gamma) \tag{104}$$

These equations were propagated from the initial state using a fixed-step, fourth-order, Runge-Kutta propagator until the system reached the surface ($h = 0$).

5.6.3.5 Thermal Response

The Sutton-Graves approximation for stagnation point heating is used [196].

$$\dot{q}_s = k_s \sqrt{\frac{\rho}{r_n}} v^3 \tag{105}$$

For this analysis, $r_n = 0.25$ m and the nominal value of the Sutton-Graves constant, k_s, for Earth, 1.74153×10^{-4} kg$^{1/2}$m$^{-1/2}$ is used.

5.6.3.6 Weights and Sizing

Deployable Structure

The sizing of the deployable's structure is based on work by Krivoshapko for ellipsoidal shell pressure vessels where analytical relationships for the meridional and parallel stresses and critical buckling pressure are given in terms of the geometry of the ellipsoid [197].

$$\sigma_\phi = \frac{p}{2b\delta} \sqrt{r^2(b^2 - a^2) + a^4} \tag{106}$$

$$\sigma_\beta = \frac{p}{2b\delta} \frac{2r^2(b^2 - a^2) + a^4}{\sqrt{r^2(b^2 - a^2) + a^4}} \tag{107}$$

$$p_{cr} = \frac{16E\delta^4}{a^2\sqrt{3(1-\nu^2)}} \left[1 + \left(\frac{z}{a}\right)^{1/2} \sqrt{\frac{193(1-4\delta^2)}{16\delta\sqrt{12(1-\nu^2)}}} \right] \tag{108}$$

In this work, the thickness, δ, is chosen based on minimum thickness resulting from Eqs. (106), (107), and (108) when a factor of safety of 1.3 is applied. The value of the internal pressure, p, is chosen such that it is twice the maximum dynamic pressure experienced. The dimensions of the ellipsoid are such that it produces a minimum volume deployable. The deployable's mass is determined by the following relationship

$$m_{structure} = \frac{3\sqrt{3}l^2 z \delta \rho_d}{4} \tag{109}$$

which includes an increase in mass of 50% to account for deployable systems and design immaturity.

Deployable TPS System

A first-order relationship determined by Laub and Venkatapathy uses heat load as the sole parameter to determine the thermal protection system (TPS) mass fraction [198]. This approximate relation is used in this investigation to size the TPS material for the deployable. The model uses historical United States planetary missions at Venus, Earth, Mars, and Jupiter with ablative TPS to regress TPS mass fraction against the integrated heat load. These missions have integrated heat loads ranging from approximately 3×10^3 J/cm^2 to 2×10^5 J/cm^2 (the trajectories analyzed in this investigation have heat loads that are approximately 7-12 $\times 10^3$ J/cm^2). The derived mass model for the TPS is given by [198]

$$m_{TPS} = \left(9.1 \times 10^{-4} Q^{0.51575}\right) m_0 \tag{110}$$

where Q is the integrated heat load in J/cm^2 and m_0 is the initial mass.

Deployable Mass

The total deployable's mass is the addition of the structural mass (including deployable system mass and margin) and the TPS system.

$$m_{deploy} = m_{structure} + m_{TPS} \tag{111}$$

5.6.4 Problem Setup

The setup of the design problem posed is presented below. First, the parameters used within the models is presented, then the problem constraints are introduced, and finally the optimization problem is formed.

5.6.4.1 Design Parameters

The solutions presented subsequently are based on the deterministic and probabilistic parameters shown in Table 12.

Table 12: Parameter values for the design.

Parameter	Description	Nominal Value	Distribution
μ_g	Gravitational Parameter	3.986×10^5 km^3/m^2	$\mathcal{N}(\tilde{\mu}_g, 10^6)$
ρ_0	Surface Atmospheric Density	1.225 kg/m^3	$\mathcal{N}(\tilde{\rho}_0, 0.01)$
H	Scale Height	7.116 km	$\mathcal{N}(\tilde{H}, 4)$
k_{C_L}	Lift Coefficient Multiplier	1	$\mathcal{N}(\tilde{k}_{C_L}, 0.0625)$
k_{C_D}	Drag Coefficient Multiplier	1	$\mathcal{N}(\tilde{k}_{C_D}, 0.0625)$
m_0	Initial Mass	5,000 kg	—
h_0	Initial Altitude	155 km	—
v_0	Initial Velocity Magnitude	6,200 m/s	$\mathcal{N}(\tilde{v}_0, 40000)$
γ_0	Initial Flight Path Angle	$-9.6°$	$\mathcal{N}(\tilde{\gamma}_0, 0.04)$
θ_0	Initial Latitude	Design Variable	$\mathcal{N}(\tilde{\theta}_0, 0.0625)$
ϕ_0	Initial Longitude	Design Variable	$\mathcal{N}(\tilde{\phi}_0, 0.0625)$
ψ_0	Initial Heading Angle	90°	$\mathcal{N}(\tilde{\psi}_0, 4)$
h_T	Target Altitude	0 m	—
ϕ_T	Target Longitude	0°	—
θ_T	Target Latitude	10.354°	—
k_s	Sutton-Graves Constant	$1.74153 \times 10^{-4} \sqrt{\frac{\text{kg}}{\text{m}}}$	$\mathcal{N}(\tilde{k}_s, 1 \times 10^{-8})$
r_n	Stagnation Radius	0.25 m	$\mathcal{N}(\tilde{r}_n, 0.0025)$
ρ_d	Material Density	1.3 g/cm^2	$\mathcal{N}(\tilde{\rho}_d, 0.01)$
E	Young's Modulus	3,000 MPa	$\mathcal{N}(\tilde{E}, 90000)$
σ_t	Tensile Strength	60 MPa	$\mathcal{N}(\tilde{\sigma}_t, 100)$
ν	Poisson Ratio	0.4	—

5.6.4.2 Design Constraints

Several practical design constraints exist in this design space. These include:

1. A limitation on the size of the deployable: $l/d \in [0.0, 2.0]$

2. A limitation on the mass of the deployable: $m_{deploy} \leq 5,000$ kg

3. A restriction that the range must be greater than the range with no deployable:

$s_f \geq s_{f,baseline}$

4. A restriction that the accuracy must be greater than the accuracy with no deployable: $d_{miss} \leq d_{miss,baseline}$

5. A restriction that the heating must be consistent with anticipated deployable ablative TPS materials: $\dot{q}_s \leq 100$ W/cm^2

Each of these constraints are appended to the objective function.

5.6.4.3 Standard Form of the Optimization Problem

The optimization problem, in standard form, is given by

$$\left.\begin{array}{ll} \textbf{Minimize}: & [\mathcal{J}_{mass} \quad -\mathcal{J}_{range}] \text{ or } [\mathcal{J}_{mass} \quad \mathcal{J}_{accuracy}] \\ \textbf{Subject to}: & g_1(l/d, \theta_0, \phi_0) = -l/d \leq 0 \\ & g_2(l/d, \theta_0, \phi_0) = l/d - 2 \leq 0 \\ & g_3(l/d, \theta_0, \phi_0) = m_{deploy}(l/d) - 5000 \leq 0 \\ & g_4(l/d, \theta_0, \phi_0) = s_{f,baseline} - s_f(l/d) \leq 0 \\ & g_5(l/d, \theta_0, \phi_0) = d_{miss}(l/d, \theta_0, \phi_0) - d_{miss,baseline} \leq 0 \\ & g_6(l/d, \theta_0, \phi_0) = \dot{q}_s(l/d) - 100 \leq 0 \\ \textbf{By varying}: & l/d, \theta_0, \phi_0 \end{array}\right\}$$

where

$$\mathcal{J}_{mass} = \frac{\bar{m}_{deploy}}{m_0} + \frac{\sigma^2_{m_{deploy}}}{m_0^2}$$

$$\mathcal{J}_{range} = \frac{\bar{s_f}}{s_{f,baseline}} - \frac{\sigma^2_{s_f}}{s^2_{f,baseline}}$$

$$\mathcal{J}_{accuracy} = \frac{\bar{d}_{miss}}{d_{miss,baseline}} + \frac{\sigma^2_{d_{miss}}}{d^2_{miss,baseline}}$$

In terms of the rapid robust design methodology, the quantity $\frac{\sigma_x^2}{x^2}$ can be replaced with $\frac{\| \boldsymbol{\Sigma}_{\boldsymbol{y}^*_{\boldsymbol{x}}} \|_2}{x^2}$ for the quantity x, where x can be m_0, s_f, or d_{miss}. Pareto frontier solutions

were identified by an additive weighting technique where the aggregate objective function was of the form

$$\mathcal{J} = \alpha \mathcal{J}_{mass} - \beta \mathcal{J}_{range} \tag{112}$$

in the case where the mass and range was being investigated or

$$\mathcal{J} = \alpha \mathcal{J}_{mass} + \beta \mathcal{J}_{accuracy} \tag{113}$$

in the case where the mass and accuracy was being investigated.

5.6.5 Applying the Rapid Robust Design Methodology

Step 1: Decompose the Design

This problem has already been decomposed into the representative CAs; however, to match the terms required by Eq. (75), these are described in terms of the matrices

$$\begin{aligned}\mathbf{y_j} = &\left.\frac{\partial \mathbf{g_j}}{\partial \mathbf{y}}\right|_{\tilde{\mathbf{y}}} \mathbf{y} + \left.\frac{\partial \mathbf{g_j}}{\partial \mathbf{u_d}}\right|_{\tilde{\mathbf{u}}_\mathbf{d}} \mathbf{u_d} + \left.\frac{\partial \mathbf{g_j}}{\partial \mathbf{u_p}}\right|_{\tilde{\mathbf{u}}_\mathbf{p}} \mathbf{u_p} \\ &- \left(\left.\frac{\partial \mathbf{g_j}}{\partial \mathbf{y}}\right|_{\tilde{\mathbf{y}}} \tilde{\mathbf{y}} + \left.\frac{\partial \mathbf{g_j}}{\partial \mathbf{u_d}}\right|_{\tilde{\mathbf{u}}_\mathbf{d}} \tilde{\mathbf{u}}_\mathbf{d} + \left.\frac{\partial \mathbf{g_j}}{\partial \mathbf{u_p}}\right|_{\tilde{\mathbf{u}}_\mathbf{p}} \tilde{\mathbf{u}}_\mathbf{p} \right), \quad \forall j = \{1, 2, \ldots, 7\}\end{aligned}$$

where the CA's output is nominally described by the expression

$$\mathbf{y_j} = \mathbf{g_j}(\mathbf{y}, \mathbf{u_d}, \mathbf{u_p})$$

Step 2: Identify the Random Variables and their Distributions

There are 15 random variables that are used in this design problem as specified in Table 12. Except for the material properties (*i.e.*, ρ_d, E, and σ_t) the random variables are treated as uncertain inputs, $\mathbf{u_p}$, in the design problem.

Step 3: Form the Iterative Equations

For this example, fixed-point iteration is used to converge the design as described in Eq. (76). In these terms, the equations are given by

$$\boldsymbol{\Lambda} = \begin{pmatrix} \dfrac{\partial \mathbf{g_1}}{\partial \mathbf{y}}\Big|_{\tilde{\mathbf{y}}} \\ \vdots \\ \dfrac{\partial \mathbf{g_7}}{\partial \mathbf{y}}\Big|_{\tilde{\mathbf{y}}} \end{pmatrix}$$

$$\boldsymbol{\beta} = \begin{pmatrix} \dfrac{\partial \mathbf{g_1}}{\partial \mathbf{u_d}}\Big|_{\tilde{\mathbf{u}}_\mathbf{d}} \\ \vdots \\ \dfrac{\partial \mathbf{g_7}}{\partial \mathbf{u_d}}\Big|_{\tilde{\mathbf{u}}_\mathbf{d}} \end{pmatrix}$$

$$\boldsymbol{\gamma} = \begin{pmatrix} \dfrac{\partial \mathbf{g_1}}{\partial \mathbf{u_p}}\Big|_{\tilde{\mathbf{u}}_\mathbf{p}} \\ \vdots \\ \dfrac{\partial \mathbf{g_7}}{\partial \mathbf{u_p}}\Big|_{\tilde{\mathbf{u}}_\mathbf{p}} \end{pmatrix}$$

$$\boldsymbol{\delta} = -\begin{pmatrix} \dfrac{\partial \mathbf{g_1}}{\partial \mathbf{y}}\Big|_{\tilde{\mathbf{y}}} \tilde{\mathbf{y}} + \dfrac{\partial \mathbf{g_1}}{\partial \mathbf{u_d}}\Big|_{\tilde{\mathbf{u}}_\mathbf{d}} \tilde{\mathbf{u}}_\mathbf{d} + \dfrac{\partial \mathbf{g_1}}{\partial \mathbf{u_p}}\Big|_{\tilde{\mathbf{u}}_\mathbf{p}} \tilde{\mathbf{u}}_\mathbf{p} \\ \vdots \\ \dfrac{\partial \mathbf{g_7}}{\partial \mathbf{y}}\Big|_{\tilde{\mathbf{y}}} \tilde{\mathbf{y}} + \dfrac{\partial \mathbf{g_7}}{\partial \mathbf{u_d}}\Big|_{\tilde{\mathbf{u}}_\mathbf{d}} \tilde{\mathbf{u}}_\mathbf{d} + \dfrac{\partial \mathbf{g_7}}{\partial \mathbf{u_p}}\Big|_{\tilde{\mathbf{u}}_\mathbf{p}} \tilde{\mathbf{u}}_\mathbf{p} \end{pmatrix}$$

Step 4: Ensure a Solution Exists

A sum-of-squares analysis using a tenth-order Taylor series polynomial was performed using SOSTOOLS. As a result of this analysis, an asymptotically stable system was able to be identified for the nominal parameters, using fixed point iteration.

Step 5: Estimate the Mean Output and the Covariance

The equations formed in the prior step can then be propagated through the Kalman filter defined by Eqs. (62)-(68) with

$$\mathbf{F}_{k-1} = \boldsymbol{\Lambda}, \quad \forall k \in \{1, 2, ...\}$$

$$\mathbf{B}_{k-1} = \begin{pmatrix} \boldsymbol{\beta} & \boldsymbol{\gamma} & \mathbf{I}_{\mathbf{7}\times\mathbf{7}} \end{pmatrix}, \quad \forall k \in \{1, 2, ...\}$$

$$\mathbf{u}_{k-1} = \begin{pmatrix} \mathbf{u_d} \\ \mathbf{u_p} \\ \boldsymbol{\delta} \end{pmatrix}, \quad \forall k \in \{1, 2, ...\}$$

where in this example $\mathbf{u_d} = u_d$ and $\mathbf{u_p} = \mathbf{0}$. Since there are uncertainties with the model, the matrix $\mathbf{Q}$ is not null and the appropriate elements are populated with the model uncertainties. The unscented transform is used on an uncoupled system with the distribution described in Step 2 (and Table 12) in order to identify $\mathbf{y_0}$ and $\mathbf{\Sigma_0}$, the initial output mean and covariance for each design. A design is considered converged when the absolute difference between iteration estimates is less than 1×10^{-4} or the relative difference is less than 1×10^{-6}.

Step 6: Identify the Mean and Variance Bound of the Objective Function

Upon convergence the mean values of m_{deploy}, s_f, and d_{miss} (*e.g.*, $\bar{m}_{deploy}$, $\bar{s}_f$, and $\bar{d}_{miss}$) can be calculated using the output of the converged Kalman filter equations from Step 5. The mass is an output of the weights and sizing CA while the mass and miss distance are outputs from the trajectory CA. The estimate for the variance (*i.e.*, the variance bound) in this case is simply

$$\sigma_r^2 \leq \| \mathbf{\Sigma}_{\boldsymbol{y_x^*}} \|_2$$

where x in y_x^* is either the deployable mass, m_{deploy}, the range, s_f, or the miss distance d_{miss}.

Step 7: Optimize for Uncertainty and Ensure Constraints are Met

Formulating the output of Step 6 in terms of the mean and variance allows for an optimal control problem to be setup for the system design, where the objective function

is defined by either

$$\mathcal{J} = \alpha \mathcal{J}_{mass} - (1-\alpha)\mathcal{J}_{range} = \alpha \left(\frac{\bar{m}_{deploy}}{m_0} + \frac{\| \mathbf{\Sigma}_{m_{deploy}} \|_2}{m_0^2} \right) - (1-\alpha) \left(\frac{\bar{s_f}}{s_{f,baseline}} - \frac{\| \mathbf{\Sigma}_{s_f} \|_2}{s_{f,baseline}^2} \right)$$

or

$$\mathcal{J} = \alpha \mathcal{J}_{mass} + (1-\alpha)\mathcal{J}_{range} = \alpha \left(\frac{\bar{m}_{deploy}}{m_0} + \frac{\| \mathbf{\Sigma}_{m_{deploy}} \|_2}{m_0^2} \right) + (1-\alpha) \left(\frac{\bar{d}_{miss}}{d_{miss,baseline}} + \frac{\| \mathbf{\Sigma}_{d_{miss}} \|_2}{d_{miss,baseline}^2} \right)$$

In these relationships $\alpha \in [0,1]$ is used to identify the Pareto frontier.

The constraints can be formulated as both a function of the design variable (l/d) and of the CA output (m_{deploy}, s_f, d_{miss}, and $\dot{q}_s$) as

$$\mathbf{g}(\mathbf{y},\mathbf{u}) = \begin{pmatrix} -l/d \\ l/d - 2 \\ m_{deploy} - 5000 \\ s_{f,baseline} - s_f \\ d_{miss} - d_{miss,baseline} \\ \dot{q}_s - 100 \end{pmatrix} \leq \mathbf{0}_{6\times 1}$$

Additionally, there is an equality constraint for the control that states

$$\mathbf{h}(\mathbf{y},\mathbf{u}) = \mathbf{u}_k - \mathbf{u}_{k-1} = \mathbf{0}, \quad \forall k \in 1,\ldots,n$$

Therefore, the Hamiltonian in the optimal control problem is given by either

$$H_k(\mathbf{y},\mathbf{u}) = \psi_0 \alpha \left(\frac{\bar{m}_{deploy}}{m_0} + \frac{\| \mathbf{\Sigma}_{m_{deploy}} \|_2}{m_0^2} \right) - (1-\alpha) \left(\frac{\bar{s_f}}{s_{f,baseline}} - \frac{\| \mathbf{\Sigma}_{s_f} \|_2}{s_{f,baseline}^2} \right) + \boldsymbol{\gamma}^T \mathbf{g}(\mathbf{y},\mathbf{u}) + \boldsymbol{\lambda}^T (\mathbf{u}_k - \mathbf{u}_{k-1})$$

or

$$H_k(\mathbf{y},\mathbf{u}) = \psi_0 \alpha \left(\frac{\bar{m}_{deploy}}{m_0} + \frac{\| \mathbf{\Sigma}_{m_{deploy}} \|_2}{m_0^2} \right) - (1-\alpha) \left(\frac{\bar{d}_{miss}}{d_{miss,baseline}} + \frac{\| \mathbf{\Sigma}_{d_{miss}} \|_2}{d_{miss,baseline}^2} \right) + \boldsymbol{\gamma}^T \mathbf{g}(\mathbf{y},\mathbf{u}) + \boldsymbol{\lambda}^T (\mathbf{u}_k - \mathbf{u}_{k-1})$$

where the terms in these relations can be computed numerically. The discrete optimal control conditions listed in Chapter 3 can then be used to compute the value of u_d for a chosen value of α.

5.6.6 Design Results

The results of the sizing of the deployable aerodynamic surface are presented in the sections that follow.

5.6.6.1 Single-Delta Design Solutions

Converged, optimal deployable designs for the single-delta configuration are shown in Figs. 40 and 41. The points denoted with circles correspond to optimal designs found using the rapid robust multidisciplinary design methodology and points denoted with an 'x' correspond to optimal designs found using a multi-objective particle swarm optimizer (MOPSO) wrapped around a Monte Carlo simulation. The 1σ robustness estimate provided by the Monte Carlo is the result of increasing the number of samples until the change was less than 0.1%.

Correlation between the MOPSO results and those obtained through the rapid robust design methodology is seen in both Figs. 40 and 41. The discrepancy in values can be attributed to the conservatism provided by the rapid robust design methodology with respect to the estimation of the variance as well as the inherent linearity of the methodology. The variance bound approximates the variance in the response of the design (*i.e.*, the 1σ mass, range, or accuracy) with the largest eigenvalue of the propagated covariance matrix, which is conservative and is seen throughout the results. In addition, the sequential linearization procedure to accommodate nonlinearities introduces errors in the resulting solutions. These are discussed further in Chapter 6. However, these shortcomings are within those accepted by the conceptual design community and are compensated for by the additional speed of the methodology.

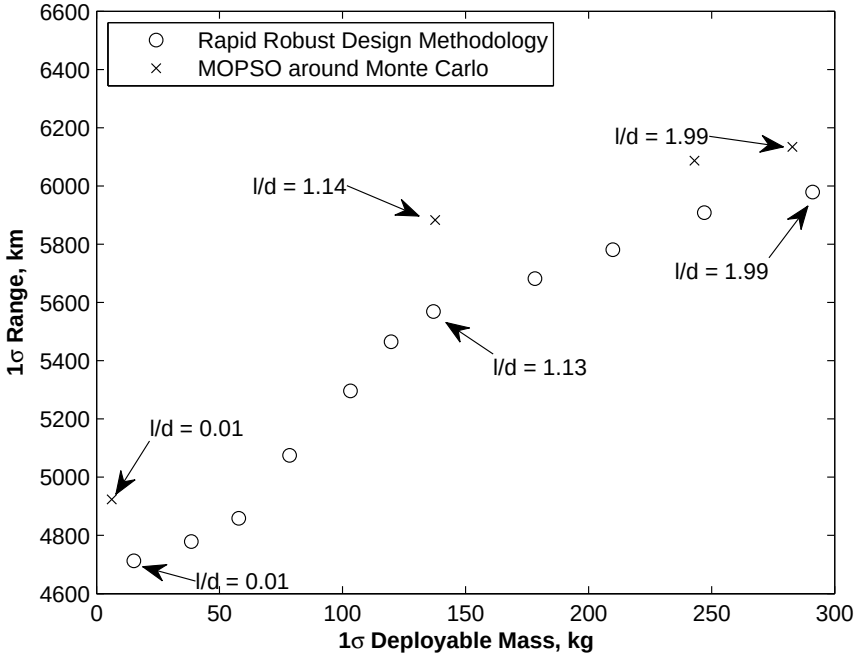

(a)

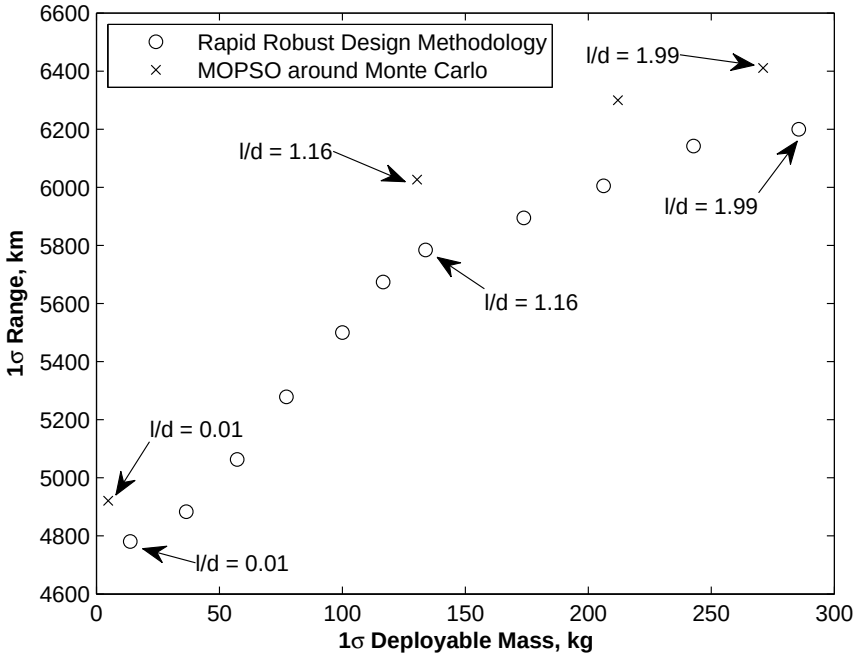

(b)

Figure 40: Design solutions for range comparing the rapid robust design methodology and a multiobjective particle swarm optimizer for a (a) bank-to-steer guidance algorithm and the (b) acceleration control guidance algorithm.

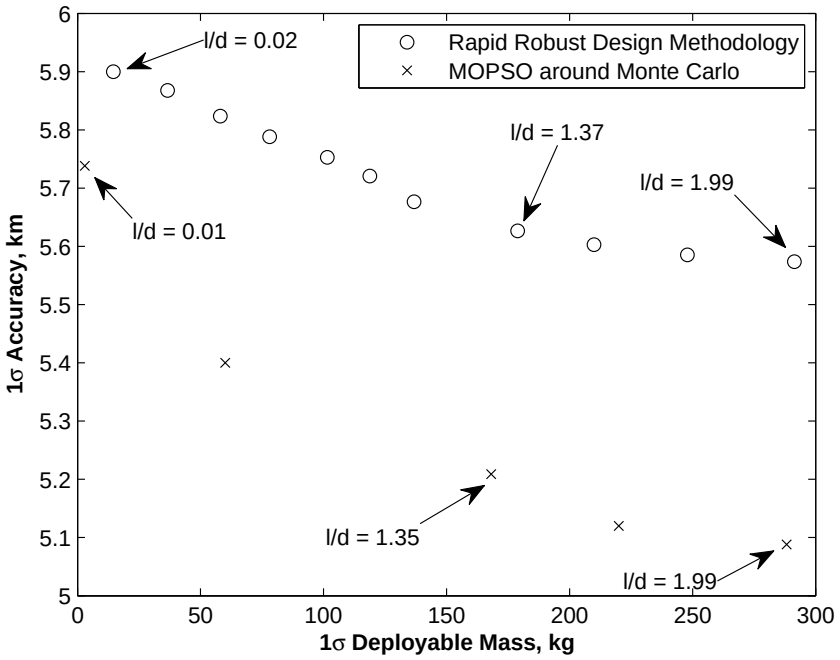

(a)

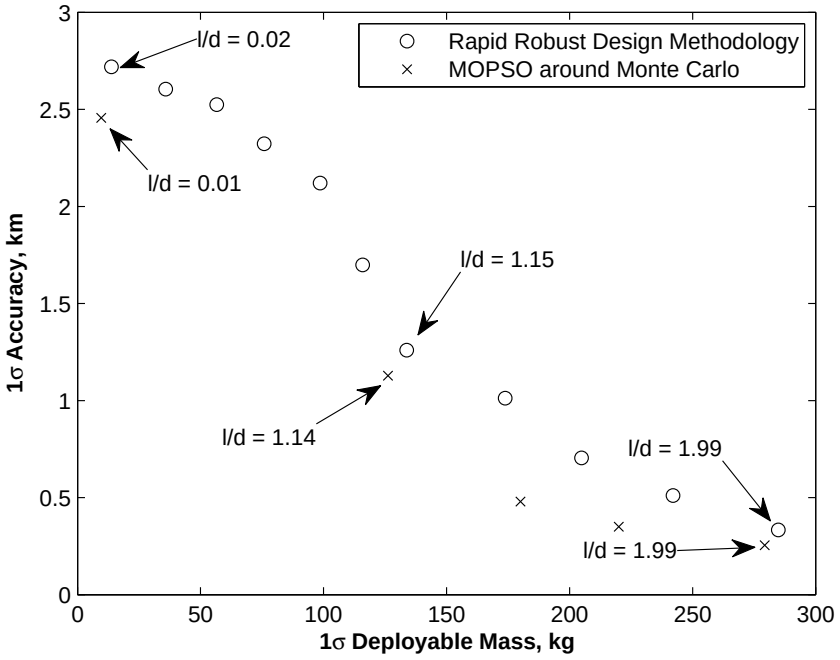

(b)

Figure 41: Design solutions for accuracy comparing the rapid robust design methodology and a multiobjective particle swarm optimizer for a (a) bank-to-steer guidance algorithm and the (b) acceleration control guidance algorithm.

Figure 40 demonstrates that the larger the deployable's mass, the more range capability the strategic system can achieve. In fact, for an approximately 300 kg deployable, the range is improved over 1,200 km (an improvement of greater than 25%). The range is seen insensitive to the two guidance algorithms considered. This is due to the fact that the trajectory for maximum range is largely a full-lift up trajectory which is equally capable of being flown by a bank-to-steer algorithm and the acceleration control method. For an equally weighted objective function between range and mass, the optimal design has an l/d of 1.16 ($m_{deploy} = 139$ kg), regardless of the guidance algorithm.

Figure 41 demonstrates that the larger the deployable is, the more accurate the system will be. For an approximately 300 kg deployable, the accuracy is capable of being improved by an order of magnitude from the baseline strategic system (from 2.8 km to 0.3 km). Unlike range, the accuracy of the system is sensitive to the guidance algorithm. For the bank-to-steer algorithm, the control is nearly saturated with a miss distance of about 5.5 km across all deployable sizes. However, using acceleration control, improvement is consistently seen with a larger deployables (with larger L/D). For an equally weighted objective function between range and mass using acceleration control, the optimal design has a l/d of 1.14 ($m_{deploy} = 131$ kg).

A significant advantage of the rapid robust design methodology is computational runtime. This is shown in Table 13 where the number of iterations required to obtain the results shown in Figs. 40 and 41 is provided.

Despite returning approximately four times as many optimal solutions as the MOPSO approach, the number of analysis iterations of the rapid robust design methodology is an order of magnitude less (with runtimes less than 5%) than the MOPSO. In addition, the probabilistic results obtained by this new methodology are within 10% of those obtained using the MOPSO, with the vast majority having errors less than 3% the MOPSO values.

Table 13: Computational comparison between MOPSO and the Rapid Robust Design Methodology.

	Range		**Accuracy**	
	Rapid Robust Design Methodology	*MOPSO*	*Rapid Robust Design Methodology*	*MOPSO*
Number of DSM Iterations, -	24,962	710,108	28,616	841,094
Computational Runtime, hours	2.2	69.7	2.4	85.7

Center of Gravity Considerations

The results presented thus far allow for the center of gravity (CG) to be positioned anywhere, including outside the outer mold line of the vehicle. This is not practical. As shown in Fig. 42, when limiting the CG to be within the vehicle, as l/d increases, the maximum L/D achievable diminishes to a point where it is actually less than the baseline system.

In order to achieve trim conditions with practical values of CG position, a body flap was added to the baseline system. This body flap was assumed to be a flat surface that was 25% of the vehicle's length. Figure 43 shows that the body flap deflection angle in order to achieve maximum L/D. Note that the deflection angle remains less than 30° for all deployable sizes considered.

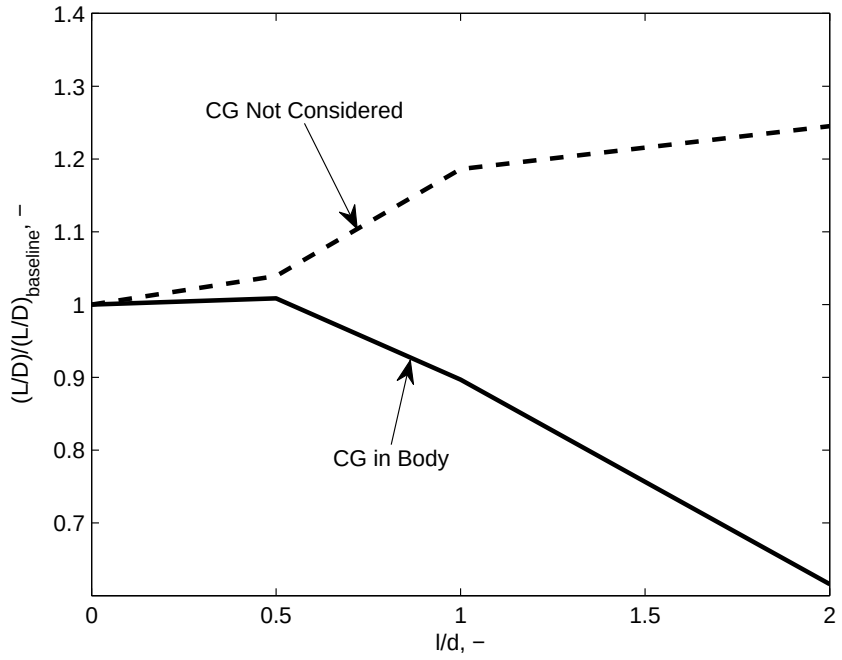

(a)

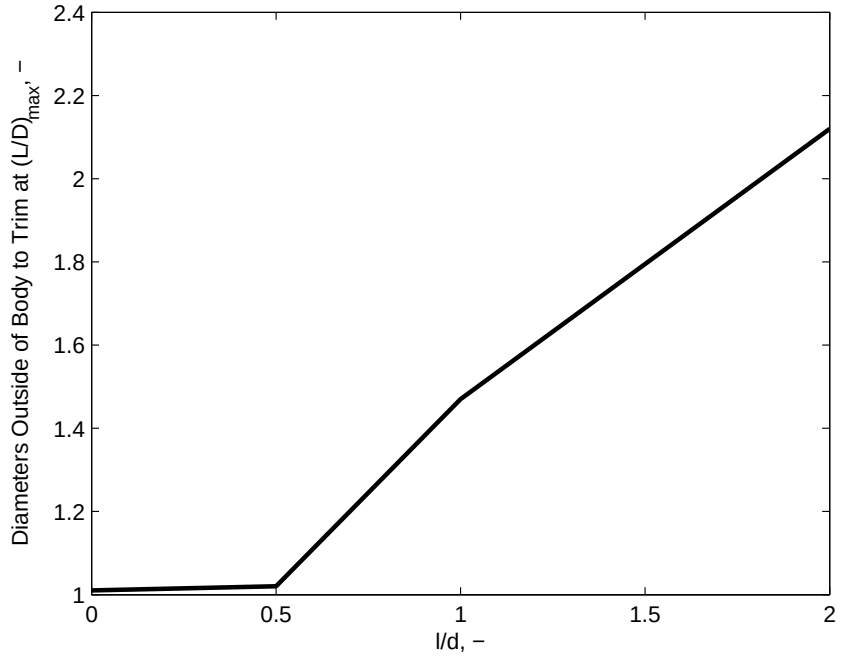

(b)

Figure 42: The (a) impact on L/D of constraining the CG position to be within the vehicle and (b) the normalized (relative to the vehicle's diameter) distance outside the vehicle the CG needs to be to achieve $(L/D)_{\max}$.

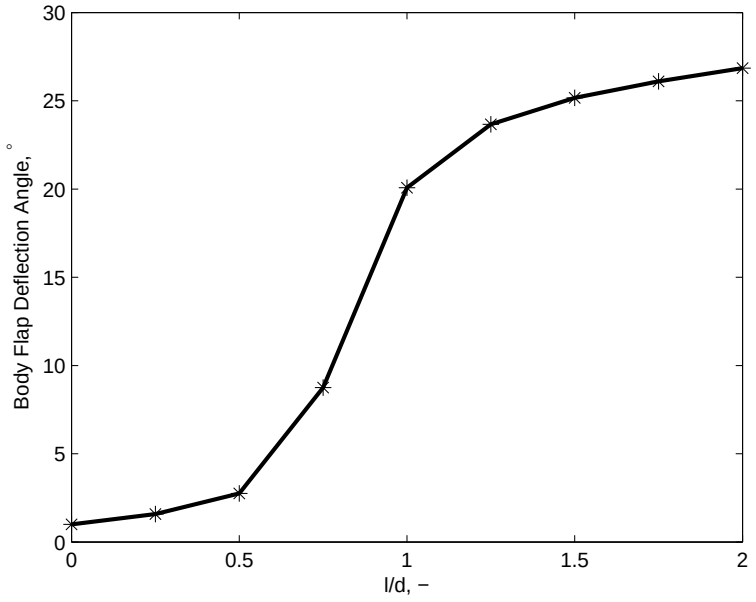

Figure 43: Body flap deflection angle required to trim the vehicle at the theoretical maximum L/D.

5.6.6.2 Alternative Configuration

An additional deployable configurations were assessed to identify whether an improvement in L/D can be obtained without the inclusion of a body flap. This configuration is shown in Fig. 44.

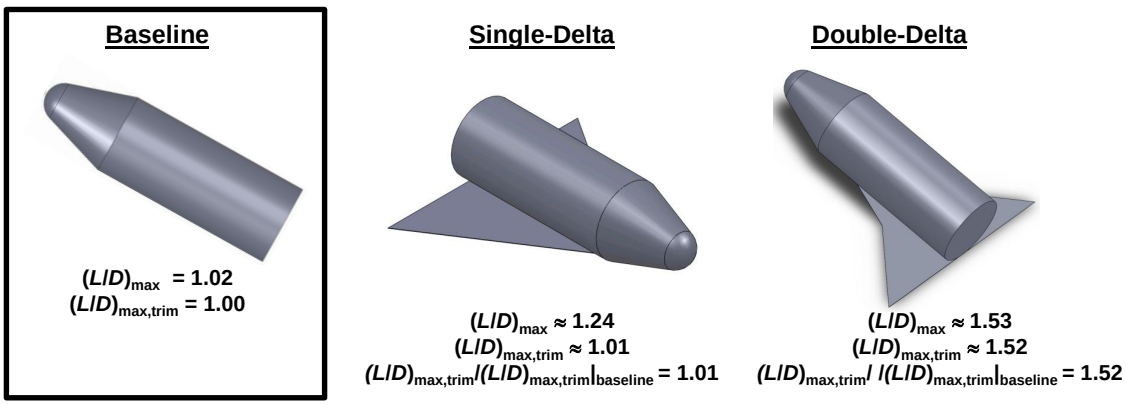

Figure 44: Comparison of investigated deployable concepts showing the maximum achievable L/D accounting for trim considerations.

While the single-delta deployable concept previously described does not provide

improvement in performance without the addition of a body flap, the double-delta configuration provides a significant increase in L/D (52%) relative to the baseline strategic vehicle while maintaining an appropriate CG position. The large performance improvement of the double-delta configuration without the use of a body flap can be explained by the aerodynamic force of the deployable being located farther aft than in the single-delta concept. The mean aerodynamic center of the baseline vehicle is located close to the cylinder cap beneath the nose cone. The lift of the double-delta deployable is sufficiently far aft to provide a sufficient restoring moment to allow the vehicle to trim, whereas this is not the case for the single-delta configuration. For the double-delta, the CG to trim at L/D_{max} shifts aft as l/d increases resulting in a l/d maximum of 2.0.

The trim angle of attack for these vehicles is significant ($\sim 20°$), providing another advantage of the double-delta—less drag area. This enables a larger L/D increase relative to the single-delta configuration discussed previously. However, this is traded for a more complex shape which would be more difficult to manufacture and deploy in flight.

5.6.6.3 Double-Delta Design Solutions

Converged, optimal double-delta deployable designs are shown in Figs. 45 and 46. As before, there is strong correlation between the MOPSO results and those obtained through this methodology. However, in this case, as shown in Fig. 45, the range performance is significantly improved for larger deployables. For an approximately 300 kg deployable, the range is improved over 2,400 km (an improvement that is twice that of the single-delta with a body flap configuration). Furthermore, the range capability insensitivity to guidance algorithm is persistent in the double-delta configuration, since the trajectory is again largely full-lift up. For an equally weighted objective function between range and mass, the optimal design has a l/d of 1.19,

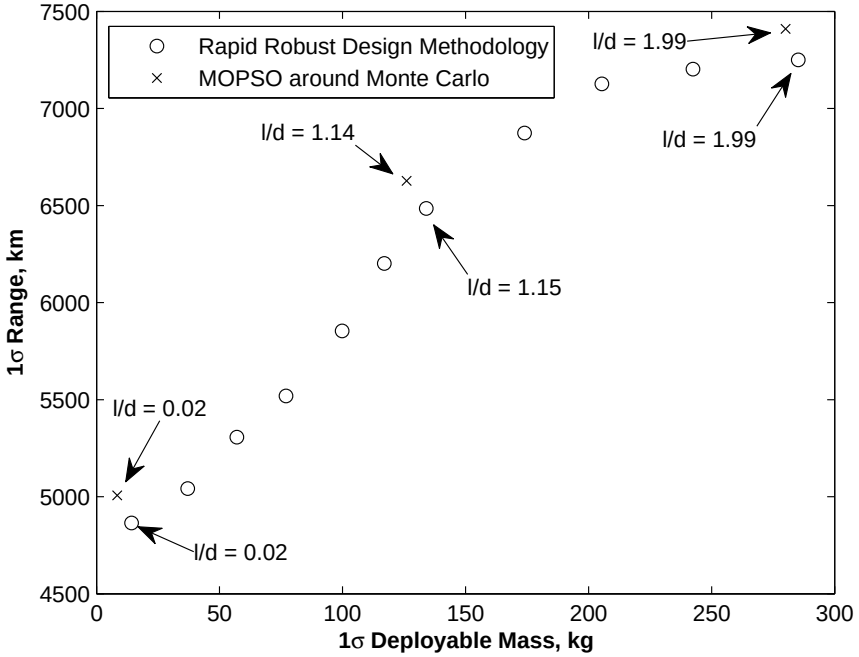

(a)

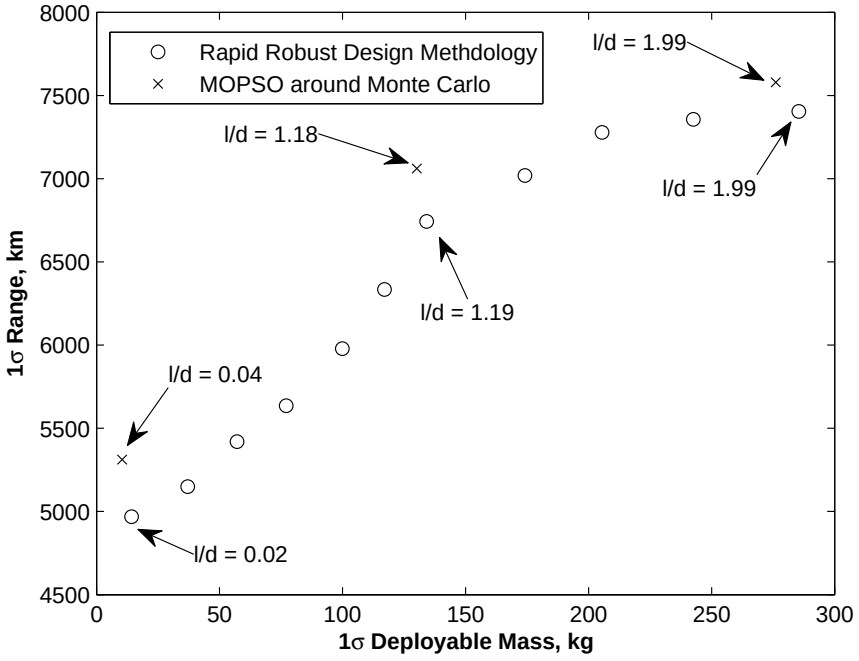

(b)

Figure 45: Design solutions for range comparing the rapid robust design methodology and a multiobjective particle swarm optimizer for a (a) bank-to-steer guidance algorithm and the (b) acceleration control guidance algorithm for the double-delta configuration.

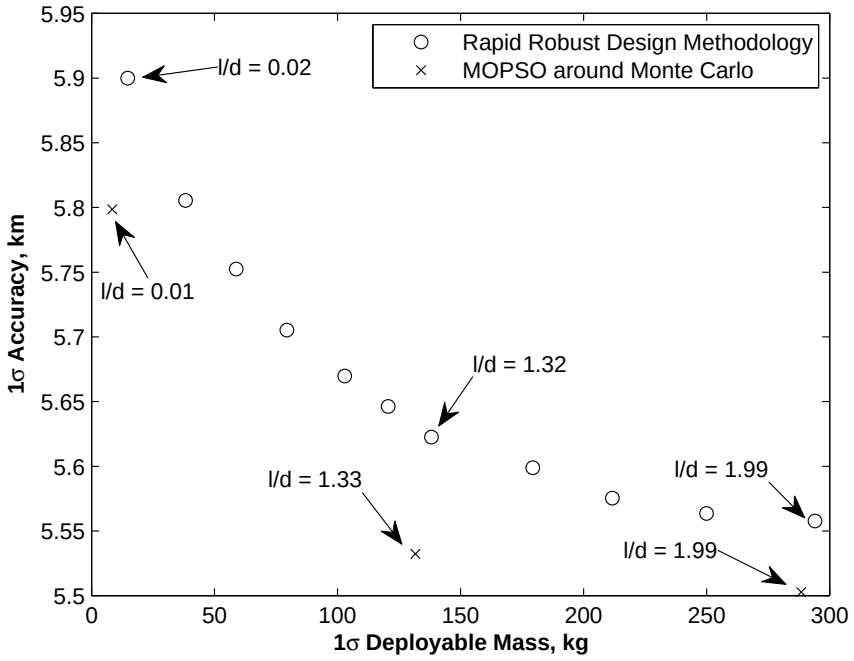

(a)

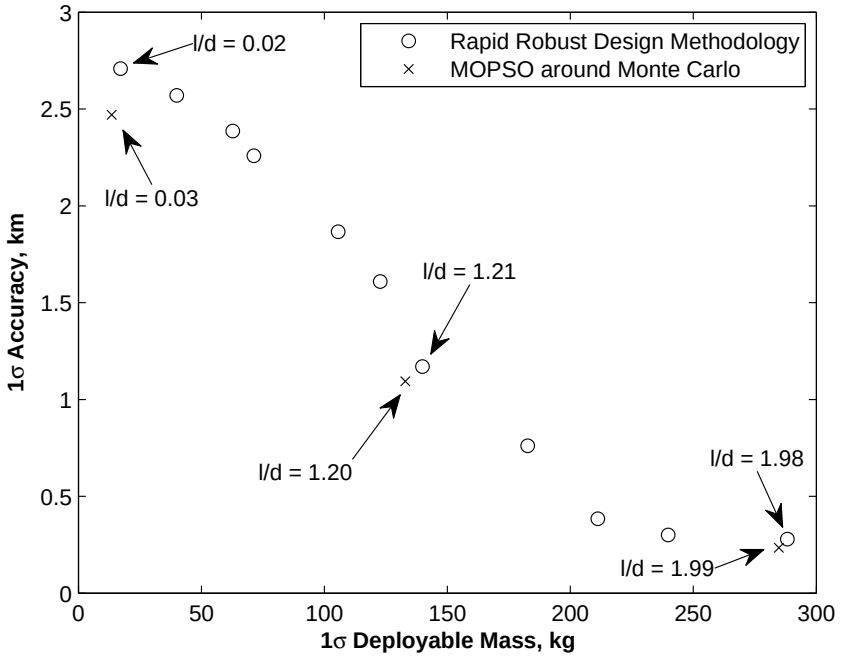

(b)

Figure 46: Design solutions for accuracy comparing the rapid robust design methodology and a multiobjective particle swarm optimizer for a (a) bank-to-steer guidance algorithm and the (b) acceleration control guidance algorithm for the double-delta configuration.

regardless of the guidance algorithm ($m_{deploy} = 148$ kg).

Figure 46 shows trends for the double-delta that are similar to those observed for the single-delta configuration—the larger the deployable is, the more accurate the system. When considering accuracy, however, the performance gain of the double-delta configuration is not as great compared to range benefits. For an approximately 300 kg deployable, the 1σ accuracy is 0.2 km for the double-delta configuration, compared to 0.3 km for the single-delta. However, the double-delta configuration is characterized by a faster rate of improving accuracy as the deployable increases in size (from an l/d of 0 to l/d of 2.0) compared to the single-delta and a body flap is not required in order to achieve these performance gains. Again, 1σ accuracy of the system is sensitive to the guidance algorithm, with the bank-to-steer guidance demonstrating saturated qualities. For an equally weighted objective function between range and mass using acceleration control, the optimal design has a l/d of 1.2 ($m_{deploy} = 149$ kg).

The computational runtime advantage (factor of 30) of the rapid robust design methodology is shown in Table 14 where accuracies acceptable to conceptual design are shown to be achievable.

Table 14: Computational comparison between MOPSO and the Rapid Robust Design Methodology.

	Range		**Accuracy**	
	Rapid Robust Design Methodology	*MOPSO*	*Rapid Robust Design Methodology*	*MOPSO*
Number of DSM Iterations, -	26,842	642,132	33,534	713,124
Computational Runtime, hours	2.3	59.6	2.8	64.2

5.6.7 Conclusions

The rapid robust design methodology was implemented to optimize the design of a deployable system for a strategic system. This methodology was shown to provide similar results to traditional Monte Carlo methods with solutions within 10% for less than 5% of the computational time.

Two deployable configurations were investigated—a single-delta and a double-delta. For a 300 kg deployable, the single-delta configuration was shown to provide an increase in 1σ range of more than 1,200 km (25%) and a reduction in 1σ miss distance from 2.5 km to 0.5 km (500%) over the baseline strategic system. For this configuration, a body flap is required for physical realizable CG positions. A 300 kg double-delta is able to increase the baseline system's 1σ range by over 2,400 km (50%) and reduce the 1σ miss distance by an order of magnitude (to less than 0.25 km) without the use of a body flap.

In addition to configuration, the effect of guidance algorithm was investigated using a bank-to-steer algorithm and a bounding guidance algorithm. The range results were insensitive to guidance algorithm selection. However, when accuracy is considered, guidance algorithm selection was shown to have a large effect as the bank-to-steer algorithm's control was shown to be nearly saturated with marginal performance gains across the deployable sizes investigated.

5.7 Summary

This chapter demonstrated the use of dynamical system theory in multidisciplinary design through several applications of increasing complexity. A probabilistic performance assessment of the robustness methodology as well as example robust design problems were provided, demonstrating application of dynamical system theory to multidisciplinary design. The probabilistic assessment showed that the robustness assessment methodology had maximum errors relative to exact values less than 1%

on the mean objective value and less than approximately 35% in standard deviation for a large design space. In addition, for specific values of the CAs, a comparison between traditional uncertainty quantification techniques and the rapid robustness assessment methodology demonstrated significant computational advantages of the developed methodology. The capability of stability theory to provide ranges of initial values to start the iteration was demonstrated along with the capability to compute the rate at which the design will converge. Through the design examples, application to nonlinear and practical problems were demonstrated. For the two-bar truss, the successive linearization procedure showed a minimal mass design that is consistent with that found in the literature while rapidly characterizing both optimal and robust designs. The computational advantages of the technique was also demonstrated in robust design of a deployable aerodynamic surface for a strategic system. Families of comparable designs for this large, highly nonlinear problem were found 25 times faster than using Monte Carlo methods coupled with traditional multiobjective optimization techniques.

CHAPTER VI

COMPUTATIONAL PERFORMANCE OF THE RAPID ROBUST DESIGN METHODOLOGY

This chapter describes the range of applicability for the rapid robust design methodology from a computational perspective. This includes an analysis of the computational cost associated with design complexity. The accuracy of the linear rapid robust design methodology is considered for general problems using nonlinear perturbation analysis, providing a basis to identify the region in which the successive linearization procedure is valid. A discussion of the conservatism resulting from use of the matrix two-norm as a bound on design variance is also provided.

6.1 Computational Effect of Increasing the Design Complexity on the Rapid Robust Design Methodology

The previous chapter demonstrated the use of the rapid robust design methodology on several example applications ranging from analytical problems to a problem relevant to the EDL community. For these problems, the number of function evaluations were reduced by a factor that approached thirty relative to traditional Monte Carlo methods wrapped in an evolutionary optimizer. The following sections examine the effect of design complexity on the number of function evaluations required to obtain a solution. Quantitatively defining the complexity of the design is a matter of debate amongst experts[199, 200, 201, 202]. In this investigation, the following definition will be employed.

Definition: Design Complexity

Design complexity is the relative difficulty in obtaining an optimal design.

In the sections that follow, design complexity is used in the structural sense[201]. In terms of the MDO problem, structural design complexity is comprised of components such as the number of design variables, the number of CAs, the nonlinearity of the CAs, and the nonlinearity of the response function. For the rapid robust design methodology developed in this work, the effect of each of these components are first examined individually, then several overall evaluation criterion are applied. Some of these overall evaluation criterion also evaluate the strength of coupling between the CAs.

6.1.1 Test Problem Definition

To assess the effect of increasing design complexity on the computational efficiency of the rapid robust design methodology, a generalized test problem was formulated. This test problem is shown in Fig. 47.

The DSM in Fig. 47 is fully coupled and can be functionally represented as

$$\mathbf{y}_i = \mathbf{f}(\mathbf{y}_1, \mathbf{y}_2, \cdots, \mathbf{y}_{i-1}, \mathbf{y}_{i+1}, \cdots, \mathbf{y}_{n-1}, \mathbf{y}_n, \mathbf{u}) \tag{114}$$

where in this case $\mathbf{f}(\cdot)$ and each CA are scalar functions. The function in Eq. (114) is represented as an q^{th}-order polynomial

$$\begin{aligned}&\mathbf{f}(\mathbf{y}_1,\mathbf{y}_2, \cdots, \mathbf{y}_{i-1}, \mathbf{y}_{i+1}, \cdots, \mathbf{y}_{n-1}, \mathbf{y}_n, \mathbf{u}) = \\ &\quad \sum_{j_1=1}^{q}\sum_{j_2=1}^{q}\cdots\sum_{j_{n-1}=1}^{q}\sum_{j_n=1}^{q}\left[a(j_1, j_2, \cdots j_{n-1}, j_n) y_1^{j_1} y_2^{j_2} \cdots y_{n-1}^{j_{n-1}} y_n^{j_n} + \sum_{i=1}^{d+p} u_i\right]\end{aligned} \tag{115}$$

Similarly, the response function is a r^{th}-order polynomial consisting of the outputs for each of the contributing analysis

$$r = \sum_{j_1=1}^{r}\sum_{j_2=1}^{r}\cdots\sum_{j_{n-1}=1}^{r}\sum_{j_n=1}^{r} b(j_1, j_2, \cdots j_{n-1}, j_n) y_1^{j_1} y_2^{j_2} \cdots y_{n-1}^{j_{n-1}} y_n^{j_n} \tag{116}$$

In each case the coefficients, are given by

$$a(j_1, j_2, \cdots j_{n-1}, j_n) = \begin{cases} \mathcal{U}(-1, 1), & j_i \neq i \\ 0, & j_i = i \end{cases} \tag{117}$$

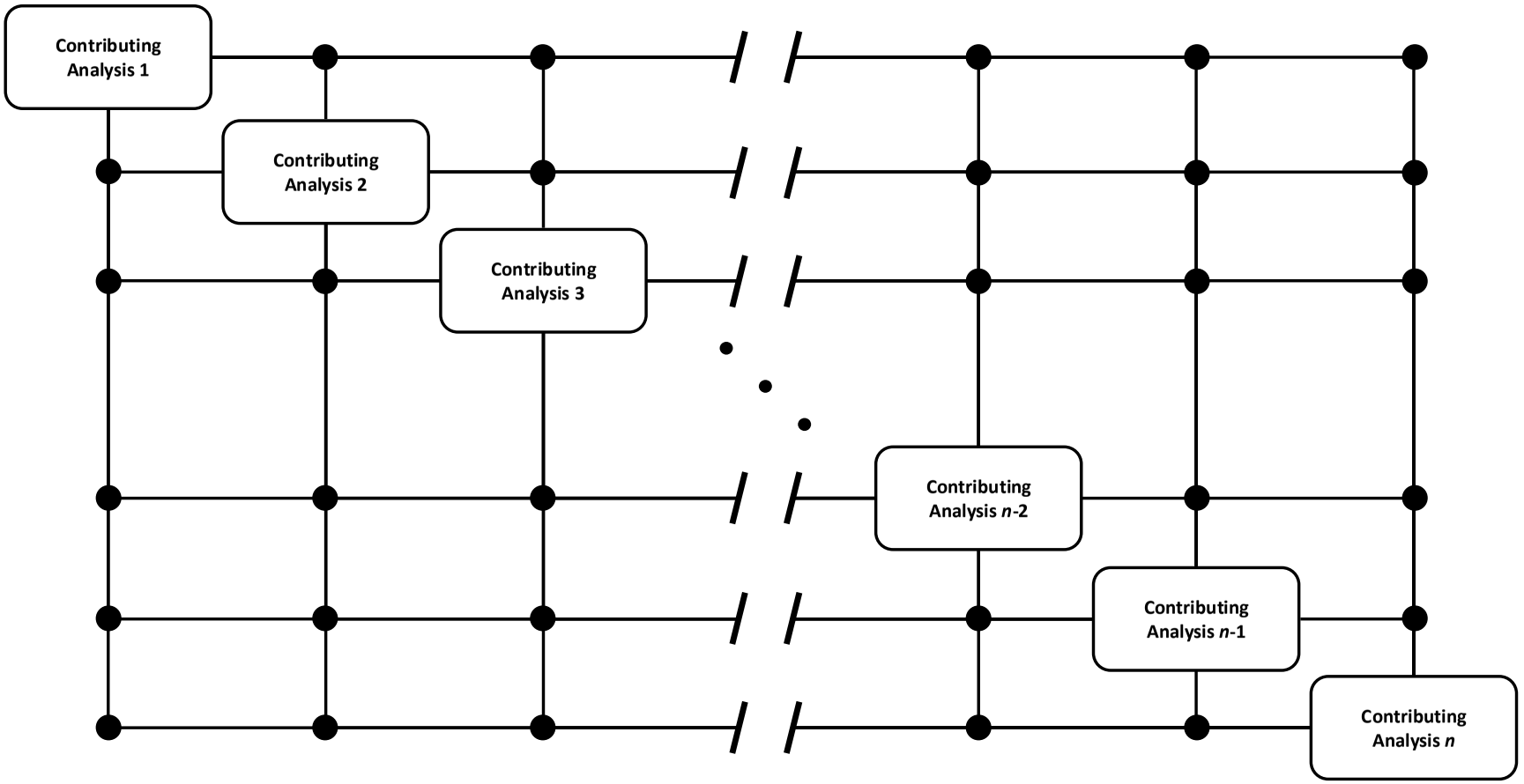

Figure 47: General design structure matrix for analyzing the effect of design complexity.

and

$$b(j_1, j_2, \cdots j_{n-1}, j_n) \sim \mathcal{U}(-1, 1) \tag{118}$$

which are sampled before evaluating for each design. The inputs, $\mathbf{u} \in \mathbb{R}^{d+p}$, are prescribed by

$$u_i = \begin{cases} u_{d_i}, & i \leq d \\ \mathcal{N}(0, 100), & d < i \leq d + p \end{cases} \tag{119}$$

where u_{d_i} are assumed to be design variables, $d \geq 1$, and $p \geq 1$.

The unconstrained robust design problem is given by

$$\left.\begin{array}{ll} \textbf{Minimize}: & \mathcal{J} = \bar{r} + \sigma_r \\ \textbf{By varying}: & \mathbf{u_d} \end{array}\right\}$$

where $\bar{r}$ is the sample mean of r and σ_r is the sample standard deviation (or its estimate, $\sqrt{\| \mathbf{\Sigma_y} \|_2}$, in the case of the rapid robust design methodology).

6.1.2 Individual Sensitivities

The individual effect of the number of design variables, number of CAs, nonlinearity of the CAs, and nonlinearity of the response are discussed below. In each case the number of function evaluations is compared to a Newton-based solution where the uncertainties are provided by a Monte Carlo simulation, FPI, or unscented transform. In the case of the Monte Carlo, the number of samples was continually increased until the change in the variance estimate was less than 1%.

Table 15 shows the parameters used to analyze each scenario used when examining the individual effects of the increase in complexity while Fig. 48 shows the computational cost as each of these parameters are varied. For each sensitivity analysis, the number of probabilistic parameters, p, was fixed at 10.

Table 15: Parameters used to examine the individual effect of complexity parameters on the design.

Parameter	**Description**	**# of Design Variables**	**# of CAs**	**CA Non-linearity**	**Response Nonlinearity**
d	# of design variables	Variable	1	1	1
n	# of CAs	10	Variable	10	10
q	Order of the CAs	1	1	Variable	1
r	Order of the response	1	1	1	Variable

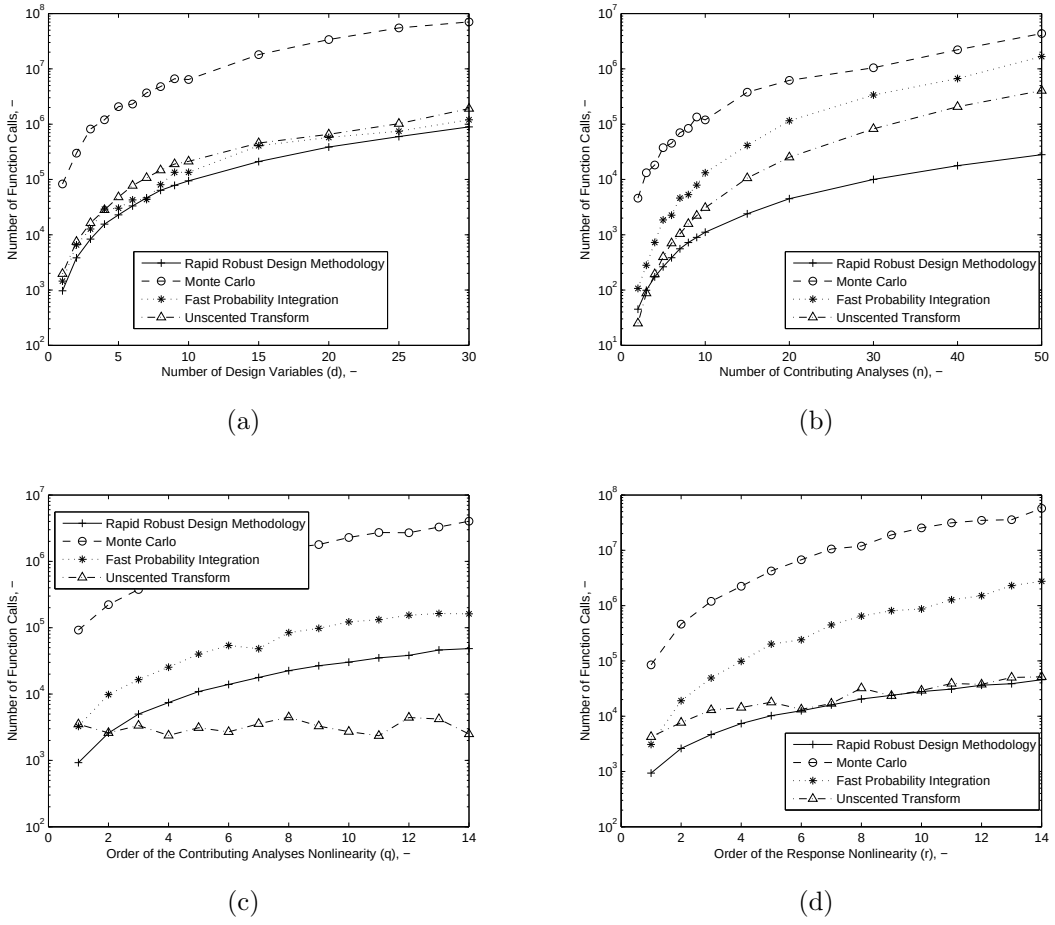

Figure 48: Increase in computational cost with (a) number of design variables, (b) number of contributing analyses, (c) nonlinearity of the CAs, and (d) nonlinearity of the response.

6.1.2.1 *Effect of Number of Design Variables*

In this case, the number of design variables, d, is varied while the other parameters were held constant as shown in Table 15. Figure 48(a) shows that each of the methods exhibit algebraic growth with number of design variables (*i.e.*, the number of function calls goes as $\mathcal{O}(n^c)$ for some c). As a Newton optimization algorithm is being utilized, this is expected. It is also observed that the Monte Carlo solutions have an order of magnitude more function evaluations compared to the other techniques considered. This is expected since the rapid robust design methodology, FPI, and unscented transform require a fixed number of function evaluations to obtain the mean and the variance.

6.1.2.2 *Effect of Number of Contributing Analyses*

The number of CAs is representative of the complexity of the problem domain. To analyze this effect on the number of function calls, the number of CAs, n, is varied while the other parameters were held constant as shown in Table 15. As seen in Fig. 48(b), each of the methods exhibit approximately algebraic growth with the number of CAs. The increase in the number of function calls is a result of the fixed-point iteration requiring an increasing number of iterations in order to reach the convergence tolerance. For larger designs (greater than 20 CAs), the rate of function call growth with number of CAs is similar between each of the methods. However, for small designs (less than 20 CAs) the rapid robust design methodology is observed to have the slowest rate of growth.

6.1.2.3 *Effect of Contributing Analysis Nonlinearity*

The effect of CA nonlinearity was assessed by varying the maximum degree of the polynomial defined in Eq. (115), q. Each of the ten CAs' order is varied simultaneously so that each polynomial has the same number of terms. The other parameters used in this analysis are shown in Table 15. Figure 48(c) shows that the rapid robust

design methodology and FPI again exhibit algebraic growth with the number of CAs due to the fact that they rely on successive linearization to approximate the system. Since the unscented transform does not depend on the linearity of the CAs and propagates the same number of samples based on the dimensionality of the problem $(n + d + p)$, it has no sensitivity to the nonlinearity of the CAs. The Monte Carlo exhibits algebraic growth initially, with exponential growth (*i.e.*, number of functions calls $\sim \mathcal{O}(c^q)$) for highly nonlinear systems. This can be attributed to the fact that the Monte Carlo simulation ensures that the change in the variance estimate is less than 1%, requiring additional sampling for more nonlinear designs.

6.1.2.4 Effect of Response Nonlinearity

The effect of response nonlinearity was assessed by varying the maximum degree of the polynomial defined in Eq. (116), r. The parameters used in this analysis are shown in Table 15 while the variation in the number of function calls required to obtain a robust design is shown in Fig. 48(d). The variation in the number of function calls required by the rapid robust design methodology and unscented transform as the response nonlinearity is increased is similar. Both of the techniques exhibit quasi-linear growth behavior for increasing nonlinearity, while the Monte Carlo and FPI exhibit an algebraic increase in the number of function calls.

6.1.3 Overall Complexity Metrics

An overall complexity index could also be used to measure the performance of the rapid robust design methodology compared to traditional methods. Four different metrics are considered—an algebraic metric, a Jacobian metric, a force-based clustering metric, and an input-output graphical based metric. In addition providing information about the structure of the design problem, the Jacobian and the force based clustering metric also account for the functional relationship within the design. That is to say, in addition to topological considerations in the design, these metrics

account for how strongly coupled the design is or what the mapping between the input and output looks like.

6.1.3.1 Algebraic Metric

The algebraic metric combines the four individual metrics discussed previously—the number of design variables, the number of CAs, the nonlinearity of the CAs, and the order of the response. The metric considered is defined as follows

$$\mathcal{C}_a = dr\left(\sum_{i=1}^{n} q_i\right) \tag{120}$$

where q_i is the order of the i^{th} CA. In this metric, the size and the order of the CAs are combined into a single value, the summation of the order of each CA; however, for a linear design, this reduces to the number of CAs.

6.1.3.2 Jacobian Metric

The Jacobian metric augments the algebraic metric with the addition of the order of the matrix of partial derivatives between the input and output of the design. Specifically, this metric is defined as

$$\mathcal{C}_J = \mathcal{C}_a \sum_{i=1}^{d} \mathcal{O}\left(\frac{\partial r}{\partial \mathbf{u_d}}\right)_i = dr\left(\sum_{i=1}^{n} q_i\right)\left(\sum_{i=1}^{d} \mathcal{O}\left(\frac{\partial r}{\partial \mathbf{u_d}}\right)_i\right) \tag{121}$$

The Jacobian captures the sensitivity of the output to perturbations in the input and is used in many optimization algorithms (*e.g.*, steepest-descent).

6.1.3.3 Force-Based Clustering Metric

Force-based clustering is a graphical method that can be used to reorder a design into a structured DSM and simultaneously provides information on the strength of the connection between CAs[30]. This method works by modeling the connections between CAs with an attractive force that clusters CAs with strong linkages, pulling CAs that use the same information together. Decomposing the problem in this way arranges the DSM in the "lowest energy" state, which can be used to measure the

strength of the connections between the CAs. This complexity index augments the algebraic metric with the summation of these forces once the DSM is arranged in the minimal energy state.

$$\mathcal{C}_{fbc} = \mathcal{C}_a \mathcal{J}_{fbc} = dr \mathcal{J}_{fbc} \left(\sum_{i=1}^{n} q_i \right) \tag{122}$$

where $\mathcal{J}_{fbc}$ is the sum of the edges of the force-based clustering graph when decomposed.

6.1.3.4 Input-Output Graph Metric

The last metric considered is a graphical technique based on the topology of the design. In this method the net information flow through each CA is considered. That is the difference between the number of output variables to the number of used input variables is utilized,

$$\begin{aligned} \mathcal{C}_{io} &= \mathcal{C}_a \sum_{i=1}^{n} \left(\dim(\mathbf{y}_{i,\text{out}}) - \dim(\mathbf{y}_{i,\text{in}}) \right) \\ &= dr \left(\sum_{i=1}^{n} q_i \right) \left(\sum_{i=1}^{n} \left(\dim(\mathbf{y}_{i,\text{out}}) - \dim(\mathbf{y}_{i,\text{in}}) \right) \right) \end{aligned} \tag{123}$$

where $\mathbf{y}_{i,\text{out}}$ and $\mathbf{y}_{i,\text{in}}$ are the number of output variables and used input variables, respectively.

6.1.3.5 Correlation Between Computational Cost and Complexity

The use of each of these techniques is demonstrated in Fig. 49 for nine representative designs. These designs varied from a linear, weakly coupled three CA system with a single input to a nonlinear design with 20 CAs, five design variables, and a highly nonlinear response. Each design case is shown in Table 16 where the number of probabilistic parameters, p, is assumed to be 5 for each case.

From Fig. 49, it is observed that the number of function calls generally increase for each metric. However, the number of function calls does not monotonically increase with the Jacobian augmented metric. Furthermore, as seen by the same complexity

Table 16: Design cases used to evaluate the overall complexity metrics.

Parameter	Case 1	Case 2	Case 3	Case 4	Case 5	Case 6	Case 7	Case 8	Case 9
n	3	3	3	3	3	10	10	20	20
q	1	2	1	5	5	1	5	1	5
r	1	1	2	1	5	1	5	1	5
d	1	1	1	5	5	1	5	1	5

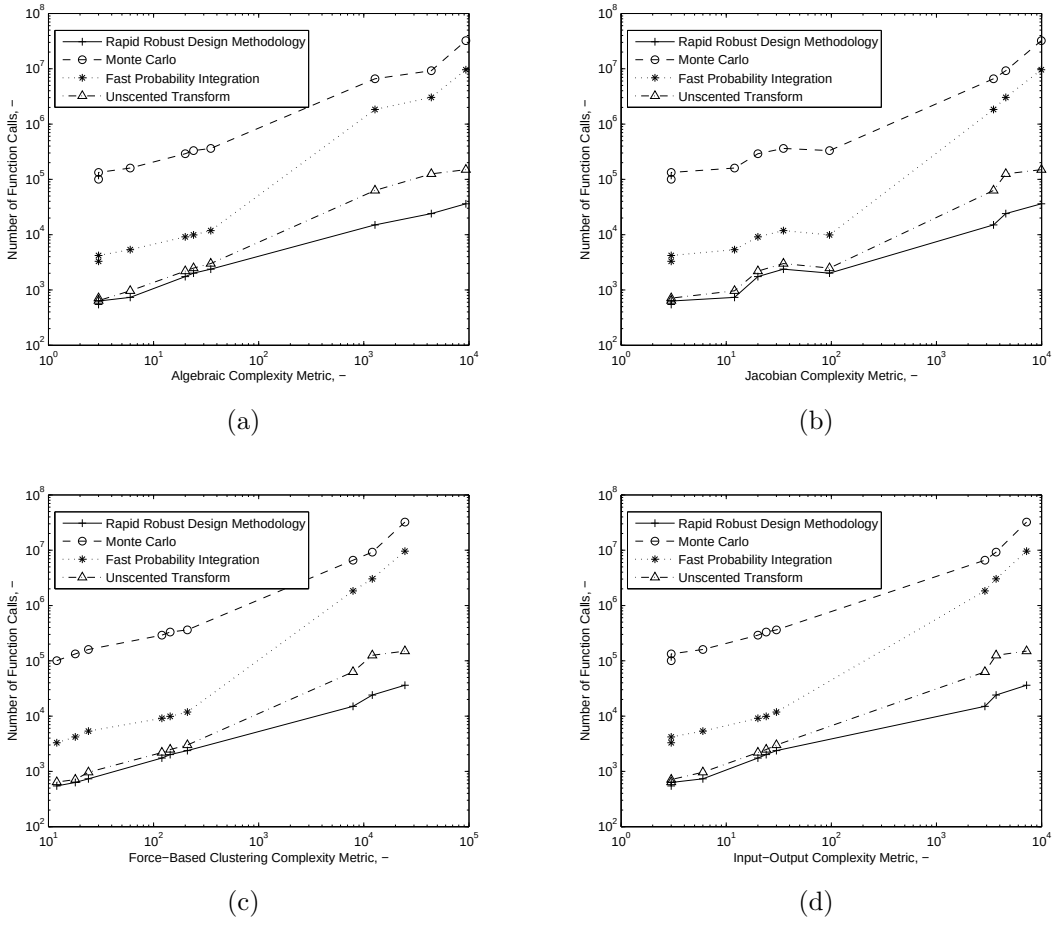

Figure 49: Increase in computational cost with complexities using the (a) algebraic complexity metric, (b) Jacobian complexity metric, (c) force-based clustering metric, and (d) input-output metric.

value resulting in multiple number of function calls, all metrics except force-based clustering provided multiple values for the number of function calls for low complexity designs. This makes the force-based clustering metric the most promising for

evaluation of design complexity. However, this metric is also the most computationally intensive and requires the reorganization of the DSM. In cases where this is not tractable, the input-output metric can be used as an alternative.

6.1.4 Computational Speed of the Rapid Robust Design Methodology

Figures 48 and 49 show favorable computational performance of the rapid robust design methodology compared to the more traditional design methodologies such as Monte Carlo simulation using a gradient-based optimization algorithm. The rapid robust design methodology scales favorably with the number of design variables and number of CAs, and its scaled performance was only met or exceeded by the unscented transform with respect to the nonlinearity of the CAs and response. Across the range of problems investigated, optimum designs were achieved using the rapid robust design methodology with fewer function calls than the traditional techniques evaluated with at least an order of magnitude less function evaluations compared to FPI and Monte Carlo methods). This implies that the rapid robust design methodology scales well with increasingly complex designs.

6.2 The Accuracy of a Linear Technique

The rapid robust design methodology developed in this investigation is based on linear system theory. However, in Chapter 4 this methodology was extended to nonlinear problems through successive linearization. In Chapter 5 results for the highly nonlinear deployable aerodynamic surface example show reasonable accuracy (1σ errors less than 10%) relative to full nonlinear propagation.

The extent of nonlinearity that the rapid robust design methodology can accommodate can be analyzed through a perturbation analysis. That is a nonlinearity is added to the converged linear system. This analysis is common in orbital mechanics and in control applications. For instance in orbital mechanics, this type of analysis is

common when dealing with perturbations (*e.g.*, drag, gravity, etc.) in the Clohessy-Wilshire equations of relative motion[203]. For control applications, it is common to linearize around a trajectory and assess the effect of nonlinear perturbations to linear matrix propagation[137].

For this analysis, two different designs were considered, one with three CAs and another with ten CAs. In each case the first $n-1$ CAs are scalar, linear, and fully coupled, while the last is assumed to be a scalar, linear function with a nonlinear perturbation term given by $g(\mathbf{y})$. This is shown in Figs. 50 and 51.

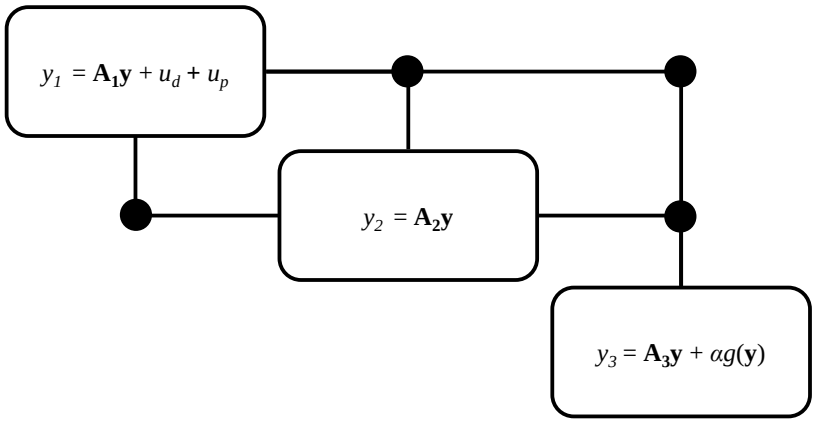

Figure 50: Three contributing analysis design structure matrix for nonlinearity analysis.

For these designs, the iteration equations (based on fixed-point iteration) is given by

$$\mathbf{y}_k = \mathbf{\Lambda y}_{k-1} + \boldsymbol{\beta}\mathbf{u_d} + \boldsymbol{\gamma}\mathbf{u_p} + \boldsymbol{\delta}_{k-1}$$

where

$$\mathbf{\Lambda} = \left(\mathbf{A_1}^T \ \cdots \mathbf{A_n}^T \right)^T$$

$$\boldsymbol{\beta} = \boldsymbol{\gamma} = \left(1 \ 0 \ \cdots \ 0 \right)^T_{1\times n}$$

and

$$\boldsymbol{\delta} = \boldsymbol{\gamma} = \left(\alpha g(\mathbf{y}_{k-1}) \ 0 \ \cdots \ 0 \right)^T_{n\times 1}$$

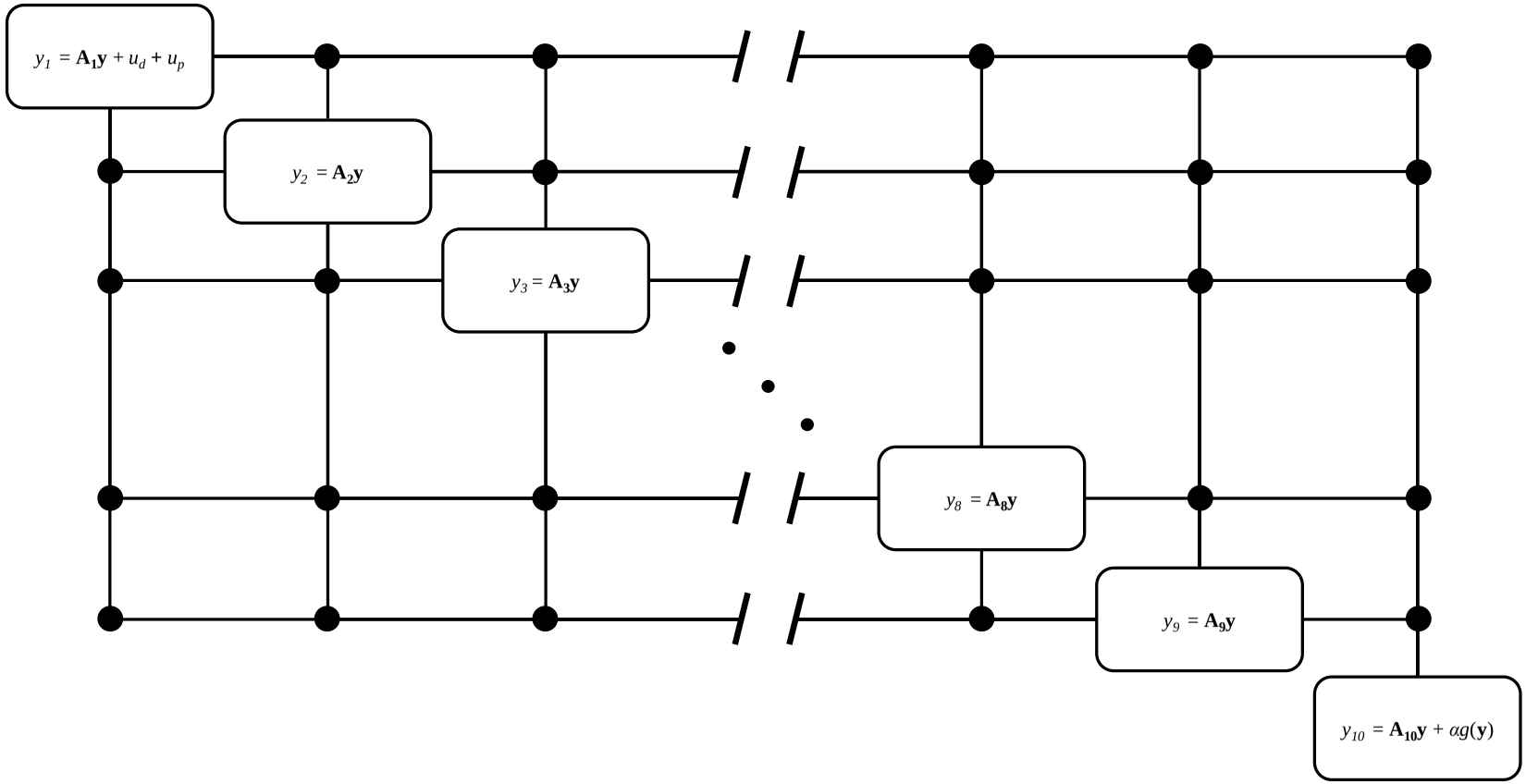

Figure 51: Ten contributing analysis design structure matrix for nonlinearity analysis

The values of $\mathbf{\Lambda}$ are given by

$$\mathbf{\Lambda}_{ij} = \begin{cases} 0, & i = j \text{ or } j = n \\ \dfrac{1}{2}, & \text{otherwise} \end{cases}$$

In addition, the inputs, $\mathbf{u} = (u_d \; u_p)^T \in \mathbb{R}^2$, are prescribed by

$$\begin{aligned} u_1 &= u_d \\ u_2 &\sim \mathcal{N}(0, 100) \end{aligned}$$

and the response is the value of the last CA,

$$r = y_n$$

Finally, the nonlinearity is prescribed by one of three different functions

$$g(\mathbf{y}) = \begin{cases} g_1(\mathbf{y}) &= \sin\left(\displaystyle\sum_{i=1}^{n-1} y_i\right) \\ g_2(\mathbf{y}) &= \ln\left(\displaystyle\sum_{i=1}^{n-1} y_i\right) \\ g_3(\mathbf{y}) &= \Re(-1)^{\left(\displaystyle\sum_{i=1}^{n-1} y_i\right)} \end{cases}$$

Although the apparent nonlinearity analyzed is only present in the final CA, the functional form presented accommodate a large number of nonlinearities throughout the CAs within the design. A nonlinearity within coupled CAs amplify upon each other until the design converges. As such, this modifies the value of α and potentially leads to combinations of the three prototypical (or other) nonlinearity functions. However, in each of these cases, the design's response can be modeled as a Taylor series expansion consisting of a linear term (*e.g.*, the $\mathbf{Ay}$ term in r) plus nonlinear terms (*e.g.*, the $\alpha g(\mathbf{y})$ in r).

Solutions to the robust optimization problem given by

$$\left.\begin{array}{ll} \textbf{Minimize}: & \mathcal{J} = \bar{y}_n + \sigma_{y_n} \\ \textbf{Subject to}: & y_i \geq 1 \quad \forall i \in \{1, \ldots, n\} \\ \textbf{By varying}: & u_d \end{array}\right\}$$

are found using a gradient based optimizer. In this problem, since there is only one probabilistic variable the two-norm provides directly the variance of the response used (*i.e.*, $\sigma_r = \sqrt{\| \mathbf{\Sigma} \|_2}$).

A solution is first found for a fully linear design (*i.e.*, $\alpha = 0$), y^*_{lin}. The weight on the nonlinearity is then varied to obtain the results seen in Fig. 52.

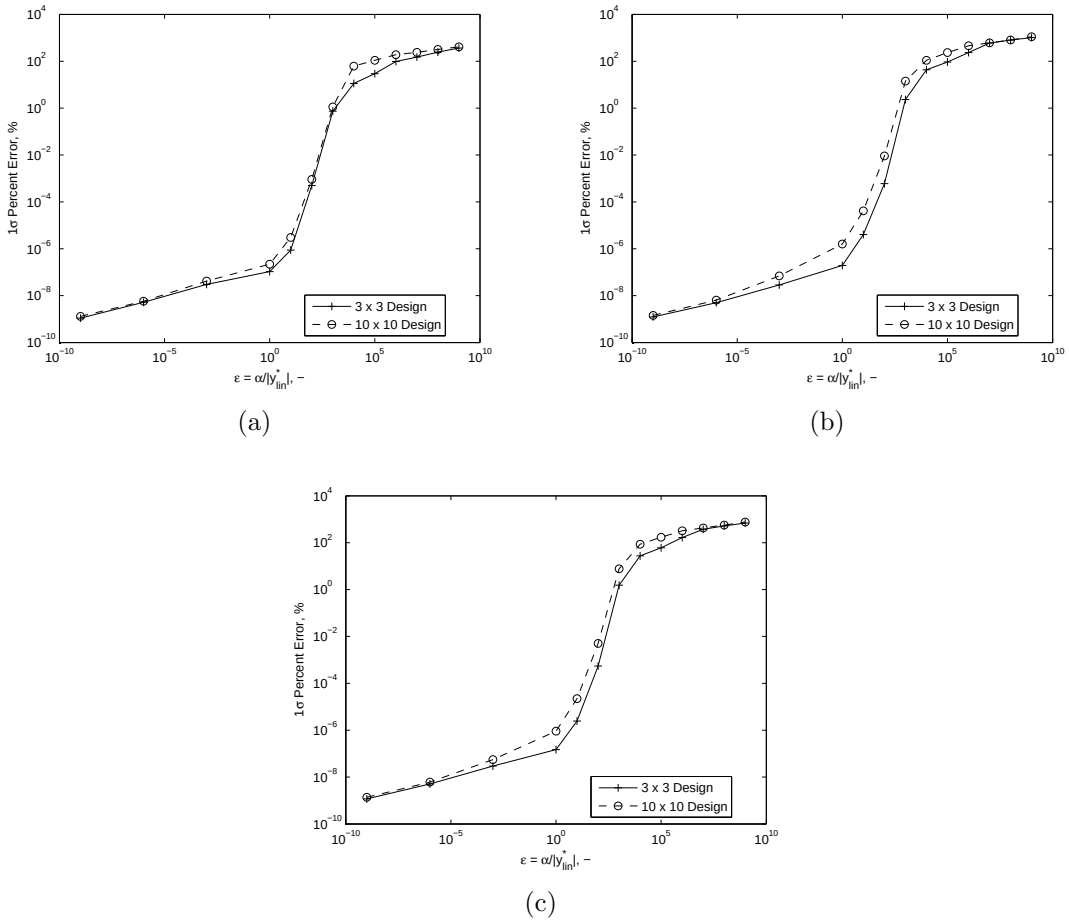

Figure 52: Variation in the computed accuracy of the rapid robust design methodology with the degree of nonlinearity. Three different nonlinear functions are shown, (a) $\sin(y)$, (b) $\ln(y)$, and (c) $(-1)^y$.

In Fig. 52, the error, defined as the percent difference in $\mathcal{J}$ between the Monte Carlo solution after the variance difference is less than 1% and the rapid robust design methodology, is plotted on a log-log plot as a function of ϵ

$$\epsilon = \frac{\alpha}{|y^*_{lin}|}$$

a normalized value of the perturbation. This normalized value of the perturbation can be thought of as an amplitude relative to nominal design response.

The analysis shows a consistent trend, once the amplitude of the nonlinearity is of the same order as the nominal response (*i.e.*, $\epsilon \sim 1$), the error increases significantly and once it is more than three orders of magnitude the error is greater than 10%. However, after this divergence point, the rate of growth of the error is similar to that prior to the divergence point. This result is independent of the size of the design and the perturbation function. Therefore, to keep the errors associated with the rapid robust design methodology consistent with that expected in the conceptual design phase (*i.e.*, $< 10\%$), one must keep the nonlinear part of the analysis to less than three orders of magnitude relative to the nominal linear response. This is not a very stringent requirement as shown in Fig. 53, which shows Fig. 52(b) with the nonlinearities associated with the single-delta deployable design examples found in Chapter 5 for an equally weighted objective function.

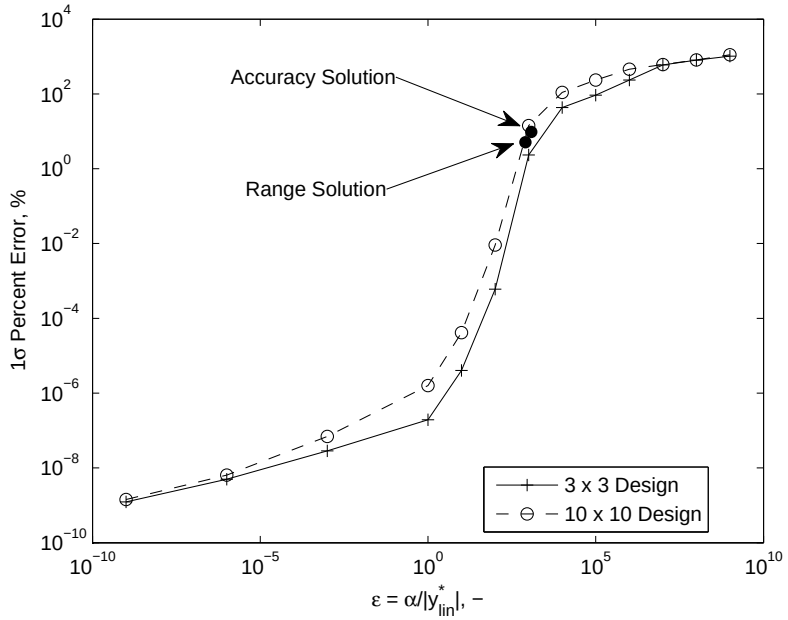

Figure 53: Nonlinear perturbation analysis using the function $g_2(y) = \ln(y)$ with the errors associated with the deployable design example superimposed.

This example had nonlinearities in each of the CAs, yet still was able to achieve a robust design solution that is acceptable for conceptual design. The largest contributor to this nonlinearity is the trajectory propagation coupled with guidance (contributing over 60% to the overall nonlinearity of the design). .

6.3 Conservatism of the Matrix Two-Norm

In Chapter 5, an asymptotic error of approximately 40% was observed when sweeping the design space of a linear design with two CAs. Each of the CAs had two output variables (*i.e.*, $\dim(\mathbf{y}) = 4$) and there were two probabilistic inputs into the design. For linear systems, the Kalman filter propagates the uncertainty exactly, therefore, this error is a function of the matrix two-norm being used to obtain a bound on the variance. This section quantifies this error as a function of the geometry of the matrix two-norm. The matrix two-norm was defined in Chapter 2 as

$$\| \mathbf{A} \|_2 = \max_{\|\mathbf{x}\|_2=1} \| \mathbf{Ax} \|_2 = \sqrt{\lambda_{\max}(\mathbf{A}^H\mathbf{A})}$$

which, in practical terms means that the matrix two-norm returns a value equal to the maximum variance of the design.

Geometrically, consider the geometry shown in Fig. 54 for the matrix two-norm where x and y are the projection of $\sigma_{X_1'}$ on the σ_{X_1} axis and $\sigma_{X_2'}$ on the σ_{X_2} axis, respectively.

In this figure, the matrix two-norm approximates σ_{X_1} with $\sigma_{X_1'}$. The error in this approximation is a maximum when $\theta = 45^\circ$ (*i.e.*, $\cos^{-1}(\hat{\boldsymbol{\sigma}}_{X_1}^T \hat{\boldsymbol{\sigma}}_{X_1'}) = 45^\circ$). The percent error due to this approximation is given by

$$\epsilon_{\%} = 100\left(\frac{\sigma_{X_1'} - x}{x}\right) = 100\left(\frac{\sigma_{X_1'}}{x} - 1\right)$$

where by geometry

$$x = \sigma_{X_1'} \cos\theta$$

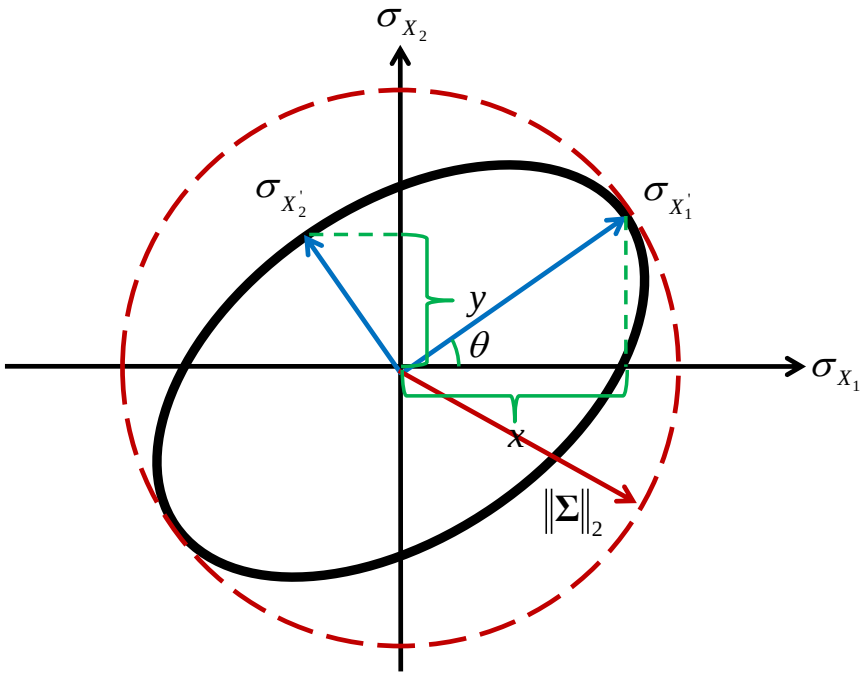

Figure 54: Two-dimensional geometry associated with the matrix two-norm.

Therefore, the expression for error can be reduced to

$$\epsilon_{\%} = 100\left(\frac{1}{\cos\theta} - 1\right)$$

When substituting in $\theta = 45°$, this yields a percent error of 41.42% in the estimation of the standard deviation for the two-dimensional problem of Fig. 54. This result can be generalized to accommodate growth in the dimensionality of the covariance matrix. As the dimensionality of the covariance matrix increases, the value of $\epsilon_{\%}$ decreases due to changes in the geometry of the design space changing θ. This is shown in Fig. 55.

In Fig. 55, for the case of four CA outputs, as was used in Chapter 5, this error produces a 37.8% error, which is the error observed in the parameter sweep in Figs. 18-20. Even with a large number of design variables, the two-norm approximation to the standard deviation produces a $20 - 25\%$ conservative approximation. However, this will only be achieved in cases where there is loose coupling between CAs.

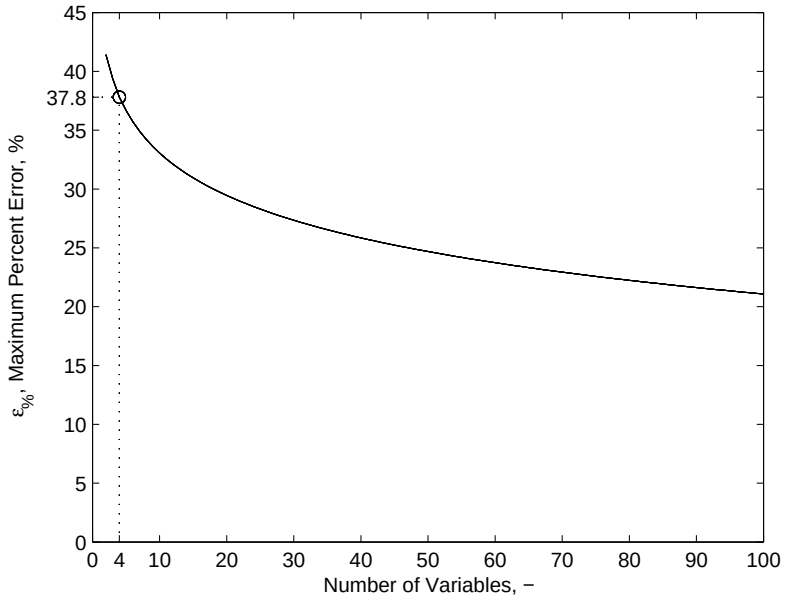

Figure 55: Maximum percent error due to the matrix two-norm approximation as a function of the dimensionality of the problem.

6.4 Summary

This chapter discusses the limitations and extensibility of the rapid robust design methodology from computational and accuracy perspectives. The effect of problem scaling on computational cost was considered two different ways. The first examined individual effects such as the number of design variables, nonlinearity of the CAs, and nonlinearity on the computational cost. The second considered computational cost through development of several potential complexity metrics. Relative to traditional robust design methods, the rapid robust design methodology developed within this thesis scaled better with the size of the problem and had performance that exceeded the traditional techniques examined. In addition to computational cost, the accuracy of applying a method with linear fundamentals to nonlinear problems was examined through nonlinear perturbation analysis to identify the region of applicability for the method. For a wide variety of problems if the magnitude of nonlinearity is less than 1,000 times that of the nominal linear response, the error associated with applying

successive linearization will result in 1σ errors in the response less than 10% compared to the full nonlinear error. Conservatism due to the use of the matrix two-norm was also examined through assessment of the asymptotic error that was first observed in Chapter 5. This error was shown to be the result of design geometry and is reduced as the dimensionality of $\mathbf{y}$ (*i.e.*, the number of outputs from the CAs) increases.

CHAPTER VII

SUMMARY AND FUTURE WORK

7.1 Summary of Academic Contributions

This thesis advances the state-of-the-art in the analysis and design of multidisciplinary systems by developing and applying concepts from dynamical systems theory to the conceptual design process. Three techniques from dynamical system theory—stability analysis, constraint handling, and estimation theory—are shown to provide advantages compared to traditional design techniques. Building on these techniques, a rapid robust design methodology is developed for linear multidisciplinary design. While the developed methodology is inherently linear, it was shown to be applicable to nonlinear engineering problems through successive linearization.

7.1.1 Formulation of the General Multidisciplinary Design Problem as a Dynamical System In Order to Leverage Established Techniques from Dynamical System Theory

The design of multidisciplinary systems requires analyses from numerous disciplines in order to achieve a set of objectives. A converged candidate design is one in which each of the disciplines uses the same information, has a common set of assumptions, and satisfies the problem constraints. An optimal design can be selected from the set of converged candidates. These processes are traditionally computationally burdensome. By leveraging advances in dynamical system theory, solution of the multidisciplinary design process is shown to be more computationally tractable as well as yielding robustness insight into the problem.

Finding a converged multidisciplinary design can be thought of as a multidimensional root-finding problem (*e.g.*, the process of finding $\mathbf{x}^*$ such that $\mathbf{f}(\mathbf{x}^*) = \mathbf{0}$). In

this case, the $\mathbf{x}$ being sought are the outputs of each of the CAs in the design and the function, $\mathbf{f}(\cdot)$, is the difference between the assumed values of the CAs output and the actual values of the output. The solution process to identify the roots of the design can be framed as an iterative one, where the subsequent iteration relies on information from prior iterates. Since a dynamical system is defined by two characteristics: (1) a state and (2) a fixed-rule describing the evolution of the state, the root-finding iteration scheme can be thought of as a dynamical system, where the CAs output is the state and the root-finding scheme is the fixed-rule.

7.1.2 Application of the Dynamical System Domain to the Multidisciplinary Design Problem

Three dynamical system techniques were investigated for the benefits they could provide to multidisciplinary design as well as their use as an ensemble in development of a rapid robust design methodology.

7.1.2.1 Stability Analysis

Typically, there is little indication beyond designer experience at the beginning of the design-analysis cycle regarding the existence of a converged design that meets the design specifications. Such was the case in the NASA Constellation program where select requirements were relaxed or ignored[204]. Stability theory can be used to rectify this problem by providing insight into the existence of a design based on the convergence procedure being utilized. For a design to exist, it was shown that when using iterative convergence techniques (*e.g.*, fixed-point iteration), the iteration scheme used to converge the design must be asymptotically stable. For linear, constant coefficient systems, this was shown to be readily checked through evaluation of the eigenvalues. However, for more general designs, existence of a converged design was shown to be obtainable through the use of Lyapunov techniques. These techniques were shown to be able to identify domains for which initial guesses result in

converged, feasible designs as well as to access the rate of convergence. This allows *a priori* knowledge regarding the design space, specifically whether a design is capable of being found as well as how fast it can be found. Lyapunov techniques rely on identification of a Lyapunov function for analysis. Identifying this Lyapunov function, in general, can be challenging; however, this work demonstrated that sum-of-squares analysis can be used to obtain this function. This technique allows a Lyapunov function to be found for systems (including those with unknown variables) that can be factored into a sum-of-squares. This is shown to be computationally efficient through application of standard semi-definite programming tools. For exponentially stable designs, it was shown that further analysis can be applied to the Lyapunov function to identify the rate at which the design will converge.

7.1.2.2 Control Theory

Optimal control techniques were demonstrated in this thesis to allow equality and inequality constraints to be included in the design procedure. These techniques allow for the consideration of design variable constraints and constraints on the output of each CA to be considered at the same level in the design hierarchy. This is a departure from the majority of MDO techniques, where only constraints that are a function of the design variables are considered explicitly at the system level. By applying these constraints at the same level in the optimization hierarchy, a coordinated search of the design space ensues which may lead to efficiency in the design process.

7.1.2.3 Estimation Techniques

Estimation theory is used in this work to obtain a rapid estimate of the mean and variance of the design. The Kalman filter, when modified to resemble those formed in linear covariance analysis, is propagated alongside the iteration relationship, providing a simultaneous estimate of the mean and covariance of the CAs' output. This was shown to have significant computational advantages as opposed to traditional

uncertainty quantification techniques such as Monte Carlo simulation, the unscented transform, and FPI. To achieve this estimate requires propagating seven additional equations as opposed to traditional methods which require drawing from a distribution and converging the design for that set of uncertainty values or building successive approximate functions to the response. Furthermore, since the correlation coefficient for each output of the CAs can be obtained directly from the resulting covariance matrix it can be used to guide design decomposition. In this approach, correlation coefficients larger in magnitude are more significant in the response and as such should always be included. However, variables with smaller correlation coefficient magnitudes may be eliminated from the feedback structure of a design.

7.1.3 Development of a Linear Technique for the Rapid Robust Design of a Multidisciplinary System

A method for robustness assessment and identification of a robust design that bounds the variance using a matrix norm of the covariance matrix was also developed in this thesis. This technique was developed for linear systems and was shown to be readily extensible to nonlinear systems. This methodology was applied to a wide variety of problems that ranged from algebraic examples to aerospace applications, demonstrating the broad applicability of the developed techniques to a number of fields. Significant computational performance gains of the developed technique were demonstrated with a reduction in the number of function calls by a factor of two when compared to the unscented transform and more than an order of magnitude when compared to FPI and Monte Carlo techniques with minimal sacrifices to the accuracy ($< 3\%$). It was shown that the methodology could accommodate nonlinearity with an order of magnitude less than 100 times the nominal value of the CA response. Finally, conservatism associated with use of the matrix two-norm showed that the error bounding the variance is a result of geometry and is reduced as the number of outputs from the CAs increases.

7.1.4 Application of the Multidisciplinary Design Robustness Methodology to a Design Example of Relevance to the Entry, Descent, and Landing Community

A design example which obtains robust designs for a deployable device that either increases the range or accuracy of a strategic system was discussed. This design example considered the impact of the geometry of the deployable aerodynamic surface as well as the selection of a guidance algorithm. Agreement between the designs obtained using the rapid robust design methodology and through utilization of a Monte Carlo was observed.

7.1.5 Traceability of Each Contribution

The support for each of the contributions described above is provided in the chapters indicated in Table 17

Table 17: Traceability of academic contributions.

Academic Contribution	Chapter 2	Chapter 3	Chapter 4	Chapter 5	Chapter 6
Formulation of the general multidisciplinary design problem as a dynamical system in order to leverage established techniques from dynamical system theory	✓	✓	✓	–	–
Application of the dynamical system domain to the multidisciplinary design problem	–	✓	✓	✓	✓
Development of a linear technique for the rapid robust design of a multidisciplinary system	–	–	✓	✓	✓
Application of the multidisciplinary design robustness methodology to a design example of relevance to the the entry, descent, and landing community	–	–	–	✓	–

7.2 Advantages of Viewing the Multidisciplinary Design Problem as a Dynamical System

Viewing the multidisciplinary design problem as a dynamical systems improves the design knowledge, broadens the computational tools, and reduces the computational burden in the design-analysis cycle.

- **Increase in Design Knowledge**: Applying stability theory allows the identification of whether or not a feasible design exists for a given iteration scheme and knowledge regarding how that design is approached. *A priori* knowledge of this information can be used by the designer to examine the design space sensitivities as well as gives an estimate of the time to obtain a design. In addition, this information can be leveraged in a distributed work environment to provide an estimate of the level of accuracy that is achievable for a given number of data transfers.

- **Broadens Computational Tools**: Using optimal control theory allows for constraints that are functions of both the CA output and the design variables to be considered at the same level of the optimization hierarchy. This allows the search for an optimal solution from a reduced design space, potentially enabling efficiencies in the design process. Estimation theory can also be used in a manner similar to linear covariance analysis to provide an estimate of the mean and covariance of the CA's output (and their effect on the design response) at the same time as the design is found.

- **Reduces Computational Burden**: Several solution methods that are primarily used within the dynamical system community were described within this thesis. These include sum-of-squares analysis for stability analysis, use of discrete and continuous optimal control solutions, and the Kalman filter. Efficient solution procedures for these methods exist, such as those described in

Refs. [147, 131, 205]. As shown in Chapters 5 and 6, application of these methods can provide solutions faster than those of current MDO techniques.

These advantages along with the comparable accuracy complement the existing conceptual design techniques such as surrogate modeling and design of experiments.

7.3 Limitations of the Rapid Robust Design Methodology

The rapid robust design methodology developed in Chapter 4 has several limitations due to the assumptions associated with its development. These include:

1. **Linear technique**: The application of the Kalman filter is exact only for linear dynamical systems. However, as in this methodology, the Kalman filter can be extended to nonlinear systems through successive linearization which may induce an error in the estimate of the mean and covariance of the response. As shown in Chapters 5 and 6, this is not a strong limitation of the technique. The successive linearization procedure induces errors that are less than 1% as long as the nonlinear perturbation is less than the magnitude of the linear CAs' response.

2. **Scalar objective function**: As formulated, the rapid robust design methodology requires a single, scalar objective function. As mentioned in Chapter 1, design is usually a multi-objective problem. Therefore in order to account for the multi-objective nature of design an aggregate objective function such as

$$\mathcal{J} = \sum_{\Omega} w_i \mathcal{J}_i^n \tag{124}$$

needs to be formed in order to seek the Pareto frontier. In Eq. (124), Ω is the set of objective functions, w_i are weights on the objective functions, $\mathcal{J}_i$ is the individual objective function, and $n \in \mathbb{R}_+ \cup \{\infty\} \setminus 0$ is the power of the objective function. A limitation of this technique is that aggregate objective functions

are known to omit concave parts of the frontier, which limits the techniques ability to find to full set of Pareto optimal designs[206].

3. **Iteration scheme**: If the application of the stability analysis portion of the rapid robust design methodology fails to show at least asymptotic stability it does not necessarily mean that a design does not exist. Instead, it implies that for the given iteration scheme chosen, a design cannot be found. In these instances alternative iteration schemes should be investigated.

4. **Variance bound**: The matrix two-norm of the covariance matrix was invoked in order to meet the scalar objective function limitation presented in this methodology. While the two-norm provides a conservative bound on the variance of the design's response with estimates that are no more than 42% that of the actual design response's standard deviation, it is provides a source of error in the solutions of the rapid robust design methodology.

5. **Gaussian uncertainties**: The derivation of the Kalman filter assumes Gaussian distributions of the uncertainties[158]. Since the Kalman filter is utilized in this work, the Gaussian distribution assumption is also applicable to this work.

7.4 Suggestions for Future Work

The work presented within this thesis has shown the applicability of dynamical systems techniques to the multidisciplinary design problem. In particular three areas of dynamical system theory were explored as they relate to the the development of a rapid robust multidisciplinary design methodology. Some suggested avenues for future work are described below—additional dynamical systems techniques that have potential applicability to the multidisciplinary design problem and potential techniques to extend and overcome some of the limitations of the rapid robust design methodology.

7.4.1 Additional Dynamical Systems Techniques

The formulation of the multidisciplinary design problem as a dynamical system lends itself to application of a large variety of dynamical systems techniques. These techniques can be used to analyze and extend knowledge regarding the multidisciplinary design problem. In addition, these methods could be used to formalize already existing procedures and methodologies within the multidisciplinary analysis and optimization community.

The stability aspect of dynamical system theory was discussed in Chapter 3 where convergence conditions for constant coefficient, linear designs were identified using eigenvalue analysis and more general designs were identified using Lyapunov theory. However, Lyapunov theory has its limitations. In particular, if a Lyapunov function cannot be found, then nothing can be said regarding whether the design will ultimately converge. While this proved not to be an issue for any of the example problems examined within this thesis, this characteristic ultimately limits the utility of Lyapunov theory. Analyzing the invariant manifolds associated with converged designs is one possible path to overcome the shortcoming of Lyapunov theory. By identifying the stable invariant manifold, a path to a converged design can be identified and as long as the iteration intersects this manifold, convergence can be assured[207]. This technique is commonly used within the astrodynamics community to identify transfers within the three-body problem[208].

Convergence properties of multidisciplinary designs were analyzed in this work for a specific subset of problems—design iterations that can be shown to be exponentially stable through Lyapunov analysis. However, other information about convergence behavior can be identified through alternative means. For example, Fourier analysis, which is used in computational fluid dynamics to identify the convergence properties of finite difference solutions to partial differential equations, could be employed[209]. Similarly, for linear systems, the z-transform can be used to transform the analysis

domain. In particular, the stability of a system in the z-plane can be determined by looking at its trace in the z-plane. Namely, if all of the poles of the transfer function lie within the unit circle then the discrete system is stable[210, 141, 132]. Furthermore, for this restricted class of systems, additional characteristics such as rise time and overshoot can be characterized.

It was observed in Chapters 3 and 5 that indirect and direct continuous optimal control solutions provided similar results as the discrete optimal control problem. The reason for this is the more restrictive conditions associated with the solution to the continuous problem which are a subset of the discrete optimal control problem. However, the issue of time-horizon was not addressed, which can be further investigated. Another area for further exploration within the control world is how to ensure that the constraints are convex. For the problems examined in Chapter 5, the constraints were convex by formulation. However, for general design problems this may not be achievable requiring techniques such as second-order cone theory to be used to convexify the constraint[211, 212].

Finally, in the area of estimation theory additional methods to propagate uncertainty could be incorporated. For this work, theoretical development was restricted to linear designs which lend themselves to the use of the Kalman filter. However, design is nonlinear, as demonstrated in Chapters 5 and 6. While the techniques developed within this thesis were shown yield accurate estimates of the mean and covariance for all but the most nonlinear of designs, other estimation techniques may be more efficient and more accurate. These estimation techniques include the Extended Kalman filter, which formalizes the successive linearization process implemented in this work, the Unscented Kalman filter, which uses the unscented transform instead of the linearized dynamics to propagate the uncertainty, and the particle filter, which propagates a small number of samples to obtain the mean and variance at each iteration[162, 213]. In addition, the rapid assessment of uncertainty allows

the contributors to the design's uncertainty to be examined rapidly. This could be accomplished in a traditional manner by perturbing the design variables to obtain the sensitivities. However, as the full covariance analysis is available to the designer, the individual CA response contributions to the uncertainty can be readily ascertained as is performed in Ref. [84].

While this work was limited to the multidisciplinary design problem, dynamical system theory has potential application in the design and optimization community at large. For instance, stability analysis could be applied to an optimization algorithm directly to identify whether or not the algorithm will obtain an optimal design and the speed at which it can do so. As such, this information can be leveraged in the design of optimization algorithms to ensure solutions are obtained efficiently. Similarly, these techniques have further applicability to traditional MDO techniques such as optimizer based decomposition, where the optimizer handles the design convergence, allowing knowledge regarding the behaviors of these methodologies to be obtained and leveraged.

In addition, the dynamical system field is rich with elements that could be used to study design including chaos theory, ergodic theory, functional analysis, graph theory, and topology theory. Each of these areas has numerous techniques that offer potential to better understand the design problem.

7.4.2 Extending the Use of the Rapid Robust Design Methodology

In the derivation of the methodology, a strong underlying assumption of employing the Kalman filter in the analysis is that the uncertain inputs and parameters are Gaussian distributed. This is because the Kalman filter only propagates the first and second moments (*i.e.*, the mean and variance) which fully describe the normal distribution. This assumption also holds well for symmetric probability distributions; however, for asymmetric distributions it breaks down relatively rapidly[214]. Methods

such as a particle filtering enable the propagation of various probability distributions, but they do so at the expense of computational speed. A potential solution to this problem would be to borrow from control theory and look at implementing a robust or stochastic control algorithm[215, 216]. These techniques use assumptions of the behavior of noise variables to make sure that a solution is reached. Alternatively, investigation of a Gaussian-mixture type formulation (as is done in Ref. [98]) may allow for a broader class of uncertainties to be accommodated within the developed framework.

As formulated in this dissertation, the rapid robust design methodology lends itself to potential integration with an integrated design environment such as Phoenix Integration's ModelCenter or Simulia's iSIGHT[217, 218]. These environments provide a general wrapping environment to provide a design analysis and optimization framework for various types of CAs that can be substituted and changed. In such an environment, the rapid robust design methodology could be readily applied to provide computationally tractable, robust optimal designs for arbitrary designs with CAs provided by standalone applications.

Another avenue for future work would be to add the capability to analyze a combination of algebraic and dynamical CAs. For aerospace applications this capability could be used to simultaneously design the guidance, navigation, and control (GN&C) system with the trajectory and the vehicle. The design of the GN&C system is usually accomplished subsequent to the preliminary design of the vehicle resulting in significant iteration to approach an optimal design with respect to the true system metrics. By pulling forward the GN&C design such that it is conducted simultaneously with other aspects of the vehicle design, CA interactions are appropriately modeled. Synthesis of the vehicle characteristics simultaneously with the GN&C system may allow a robust solution to be obtained that improves aspects of the trajectory through modification of vehicle characteristics and vice-versa.

APPENDIX A

SELECT MATHEMATICAL CONCEPTS

A.1 Probability and Statistics

A.1.1 Probability Space and Random Variables

Probability space is a model for real world situations in which the outcome is assigned according to some probability. It is a measure space such that the measure of the whole space is equal to unity and is defined as[219]

Definition: Probability Space

Probability space is a triple, $(\Omega, \mathcal{F}, P)$, consisting of the following elements:

- **Sample space** (Ω): a representation of all possible outcomes ($\Omega \neq \varnothing$)
- **Event space** ($\mathcal{F}$): a collection of subsets of Ω such that
  - The null set is an element of the event space: $\varnothing \in \mathcal{F}$
  - The event space is closed under complements: if $A \in \mathcal{F}$, then $(\Omega \backslash A) \in \mathcal{F}$
  - The event space is closed under countable unions: if $A_i \in \mathcal{F}$ for $i = 1, 2, ...$, then $(\cup A_i) \in \mathcal{F}$
- **Probability measure** (P): A function $P : \mathcal{F} \rightarrow [0, 1]$ such that
  - The probability measure is non-negative: $P(A) \geq 0, \quad \forall A \in \mathcal{F}$
  - The probability measure is countably additive: $P(A_i \cup A_j) = P(A_i) + P(A_j)$ if $A_i \cap A_j = \varnothing, \quad \forall A_i, A_j \in \mathcal{F}$
  - The measure of the entire sample space is unity: $P(\Omega) = 1$

With the concept of probability space defined, the formal definition of random variables can be given[220].

Definition: Random Variable

Let $(\Omega, \mathcal{F}, P)$ be a probability space and (Y, Σ) be a measurable space. Then a *random variable* X is a measurable function $X : \Omega \to Y$.

A random variable can be interpreted as the preimages of the well-behaved subsets of Y (the elements of Σ) are events (*i.e.*, elements of $\mathcal{F}$), are are assigned a probability by P. Or, more simply, a random variable is a function whose domain is the sample space and maps events to real numbers.

A.1.2 Univariate Probability Density and Distribution Functions

For an univariate discrete random variable, a probability distribution assigns a probability for each of value of the random variable, while for a continuous univariate random variable, the probability distribution gives the probability of the value falling within a particular interval. Formally, a univariate probability distribution is defined as[220]

Definition: Probability Distribution

For a random variable, $X : \Omega \to Y$, a *probability distribution* is the pushforward measure $X_*P = PX^{-1}$ on (Y, Σ).

More tangibly, for real-valued random variables, the probability of a random variable X being in the interval $(-\infty, x]$ is given by the cumulative distribution function

$$F(x) = P(X \leq x), \quad \forall x \in \mathbb{R} \tag{A.1.1}$$

A.1.2.1 Discrete Random Variables

For discrete probability distributions (*i.e.*, the sample space, Ω, consists entirely of values that are in a countable predefined set), the probability is characterized by a

probability mass function, $f(x)$, which is defined by the relationship

$$\sum_{x\in\Omega} P(X=x) = \sum_{x\in\Omega} f(x) = 1 \tag{A.1.2}$$

In addition, the probability mass function has the property

$$0 \leq f(x) \leq 1 \tag{A.1.3}$$

The cumulative distribution function associated with discrete random variables is such that there are jump discontinuities. Between these jump discontinuities, since there is no additional probability as defined in Eq. (A.1.1), the value of the function is constant.

A.1.2.2 Continuous Random Variables

For continuous random variables (*i.e.*, the sample space, Ω, can consist of any subset $\mathbb{R}$), the cumulative distribution function is defined in terms of an integral instead of a summation as shown in Eq. (A.1.4)

$$F(x) = P(X \leq x) = \int_{-\infty}^{x} f(u)du \tag{A.1.4}$$

where $f(x)$ is the probability density function. The probability density function gives the probability of a given value and is defined in terms of the cumulative distribution function as

$$f(x) = \frac{d}{dx}F(x) \tag{A.1.5}$$

Since the cumulative distribution function is a strictly increasing function, the probability density function, $f(x)$, is a non-negative function whose integral over the entire sample space is equal to unity.

A.1.3 Multivariate Probability Density and Distribution Functions

Assume n ($n < \infty$) random variables $X_1, X_2, \ldots, X_n$ are defined on the same probability space $(\Omega, \mathcal{F}, P)$. The cumulative distribution function of this *bivariate* distribution

is given by[220]

$$F(x_1, x_2, \ldots, x_n) = P(X_1 \leq x_1, X_2 \leq x_2, \ldots, X_n \leq x_n) \tag{A.1.6}$$

Similarly, the probability mass function (density function if Ω is continuous) is given by

$$f(x_1, x_2, \ldots, x_n) = P(X_1 = x_1, X_2 = x_2, \ldots, X_n = x_n) \tag{A.1.7}$$

where the usual properties of the probability mass (density) function hold. That is to say the properties in Table A.1 hold where $A \subset \Omega$..

Table A.1: Multivariate mass and density function properties.

Discrete	**Continuous**
$f(x_1, x_2, \ldots, x_n) \in [0, 1]$	$f(x_1, x_2, \ldots, x_n) \geq 0$
$\sum_{\Omega} f(x_1, x_2, \ldots, x_n) = 1$	$\int_{\Omega} f(x_1, x_2, \ldots, x_n) d\Omega = 1$
$P(X_1, X_2, \ldots, X_n \in A) = \sum_{A} f(x_1, x_2, \ldots, x_n)$	$P(X_1, X_2, \ldots, X_n \in A) = \int_{A} f(x_1, x_2, \ldots, x_n) dA$

A.1.4 Characteristics of Univariate Distributions

A.1.4.1 Mathematical Expectation

The mathematical expectation of a probability distribution is a fundamental characteristic[59].

Definition: Mathematical Expectation

If $f(x)$ is the probability mass (density) function for a random variable X of the discrete (continuous) type, then the *mathematical expectation* of a function $u(x)$ is defined as

$$\mathbb{E}[u(x)] = \sum_{x \in \Omega} u(x) f(x)$$

for discrete distributions and

$$\mathbb{E}[u(x)] = \int_{-\infty}^{\infty} u(x) f(x) dx$$

for continuous distributions provided they exist and are finite.

From this definition, it is clear to see that the expectation is a linear operator.

A.1.4.2 The Moment Generating Function

For the majority of distributions whose densities are given analytically, it is useful to consider the moment generating function[59].

Definition: Moment Generating Function

The *moment generating function* for a distribution whose probability mass (density) function is defined by $f(x)$ is given by

$$M(t) = \mathbb{E}(e^{tX})$$

provided it exists and is finite for some $t \in [-h, h]$.

To examine the impact of the moment generating function, consider the discrete case where the sample space Ω consists of $\{\omega_1, \omega_2, \omega_3, \ldots\}$ then

$$M(t) = e^{t\omega_1} f(\omega_1) + e^{t\omega_2} f(\omega_2) + e^{t\omega_3} f(\omega_3) + \ldots$$

and hence the coefficient of $e^{t\omega_i}$ is the probability

$$f(\omega_i) = P(X = \omega_i)$$

Therefore, since this probability is prescribed only to this distribution, the moment generating function describes a unique distribution, if it exists.

A.1.4.3 The Mean

The mean (or average) is a fundamental quantity that describes the expected value of the distribution, it is also the first moment.

Definition: Mean

The *mean* of a random variable X is given by

$$\mu = \mathbb{E}[X]$$

This is also expressed in terms of the moment generating function (when it exists) as

$$\mu = \frac{dM}{dt}(0)$$

A.1.4.4 The Variance

The variance is another measure of central tendency that describes the spread of values from the mean of the distribution.

Definition: Variance

The *variance* of a random variable X is given by

$$\sigma^2 = \mathbb{E}[(X - \mu)^2]$$

This is also expressed in terms of the moment generating function (when it exists) as

$$\sigma^2 = \frac{d^2M}{dt^2}(0) - \left[\frac{dM}{dt}(0)\right]^2$$

A larger variance (standard deviation) implies that the spread of the distribution is larger than that of a smaller variance.

A.1.5 Confidence Interval

Definition: Confidence Interval

The *confidence interval* is an interval estimate to indicate how likely it is that an estimated random variable will lie between the two bounds.

Mathematically, the $p^{\text{th}}\%$ confidence interval is given by

$$p = P\left[l(X) < w < u(X)\right] \tag{A.1.8}$$

where the $p^{\text{th}}\%$ confidence interval is denoted by the endpoints, $L = l(X)$ and $U = u(X)$, and is given by (L, U). Intuitively, the wider the confidence interval the higher the confidence level as more of the distribution lies within the interval.

A.2 Filtering and Estimation Methods

A.2.1 The Discrete Kalman Filter

For dynamics given by

$$\left.\begin{aligned} \mathbf{y}_k &= \mathbf{F}_k\mathbf{y}_{k-1} + \mathbf{B}_k\mathbf{u}_k + \mathbf{w}_{k-1} \\ \mathbf{z}_k &= \mathbf{H}_k\mathbf{y}_k + \mathbf{v}_k \end{aligned}\right\} \tag{A.2.1}$$

the Kalman filter gives a way to estimate the mean state and covariance. Here $\mathbf{w}_{k-1}$ is the noise associated with the model and $\mathbf{v}_{k-1} \sim \mathcal{N}(\mathbf{0}, \mathbf{R}_{k-1})$ is the noise assoicated with the measurement. The Kalman filter can be thought of as a two step process, one which predicts the state (*e.g.*, the output of the CAs) and then an update step which corrects these estimates based on the dynamics of the system. The prediction step is given by the following equations[82, 135, 158, 159, 160, 161, 162]

$$\hat{\mathbf{y}}_{k|k-1} = \mathbf{F}_k\hat{\mathbf{y}}_{k-1|k-1} + \mathbf{B}_k\mathbf{u}_k \tag{A.2.2}$$

$$\mathbf{\Sigma}_{k|k-1} = \mathbf{F}_k\mathbf{\Sigma}_{k-1|k-1}\mathbf{F}_k^T + \mathbf{Q}_k \tag{A.2.3}$$

where the notation $j|k$ represents the estimate at j given observations up to and including k. Furthermore, the value of $\hat{\mathbf{y}}_{0|0}$ is the initial mean state and $\mathbf{\Sigma}_{0|0}$ is the

initial covariance matrix of the state values. The correction step is governed by the following equations[82, 135, 158, 159, 160, 161, 162]

$$\begin{aligned}
\tilde{\mathbf{x}}_k &= \mathbf{z}_k - \mathbf{H}_k \hat{\mathbf{y}}_{k|k-1} && \text{(A.2.4)} \\
\mathbf{S}_k &= \mathbf{H}_k \boldsymbol{\Sigma}_{k|k-1} \mathbf{H}_k^T + \mathbf{R}_k && \text{(A.2.5)} \\
\mathbf{K}_k &= \boldsymbol{\Sigma}_{k|k-1} \mathbf{H}_k^T \mathbf{S}_k^{-1} && \text{(A.2.6)} \\
\hat{\mathbf{y}}_{k|k} &= \hat{\mathbf{y}}_{k|k-1} + \mathbf{K}_k \tilde{\mathbf{x}}_k && \text{(A.2.7)} \\
\boldsymbol{\Sigma}_{k|k} &= (\mathbf{I} - \mathbf{K}_k \mathbf{H}_k) \boldsymbol{\Sigma}_{k|k-1} && \text{(A.2.8)}
\end{aligned}$$

A.2.2 The Discrete Extended Kalman Filter

The extended Kalman filter requires state transition and observation models of the form

$$\left.\begin{aligned}
\mathbf{y}_k &= \mathbf{f}(\mathbf{y}_{k-1}, \mathbf{u}_{k-1}) + \mathbf{w}_{k-1} \\
\mathbf{z}_k &= \mathbf{h}(\mathbf{y}_k) + \mathbf{v}_k
\end{aligned}\right\} \qquad \text{(A.2.9)}$$

Like the Kalman filter, the extended Kalman filter is also a two step process with a prediction step and an update step. The prediction step is given by the following equations[135, 160, 161, 162]

$$\begin{aligned}
\hat{\mathbf{y}}_{k|k-1} &= \mathbf{f}(\hat{\mathbf{y}}_{k-1|k-1}, \mathbf{u}_{k-1}) && \text{(A.2.10)} \\
\boldsymbol{\Sigma}_{k|k-1} &= \mathbf{F}_{k-1} \boldsymbol{\Sigma}_{k-1|k-1} \mathbf{F}_{k-1}^T + \mathbf{Q}_{k-1} && \text{(A.2.11)}
\end{aligned}$$

The update step is governed by the following equations[135, 160, 161, 162]

$$\begin{aligned}
\tilde{\mathbf{x}}_k &= \mathbf{z}_k - \mathbf{h}(\hat{\mathbf{y}}_{k|k-1}) && \text{(A.2.12)} \\
\mathbf{S}_k &= \mathbf{H}_k \boldsymbol{\Sigma}_{k|k-1} \mathbf{H}_k^T + \mathbf{R}_k && \text{(A.2.13)} \\
\mathbf{K}_k &= \boldsymbol{\Sigma}_{k|k-1} \mathbf{H}_k^T \mathbf{S}_k^{-1} && \text{(A.2.14)} \\
\hat{\mathbf{y}}_{k|k} &= \hat{\mathbf{y}}_{k|k-1} + \mathbf{K}_k \tilde{\mathbf{x}}_k && \text{(A.2.15)} \\
\boldsymbol{\Sigma}_{k|k} &= (\mathbf{I} - \mathbf{K}_k \mathbf{H}_k) \boldsymbol{\Sigma}_{k|k-1} && \text{(A.2.16)}
\end{aligned}$$

where the state transition and observation matrices are given by

$$\mathbf{F}_{k-1} = \left.\frac{\partial \mathbf{f}}{\partial \mathbf{y}}\right|_{\hat{\mathbf{y}}_{k-1|k-1},\mathbf{u}_{k-1}} \tag{A.2.17}$$

$$\mathbf{H}_{k} = \left.\frac{\partial \mathbf{h}}{\partial \mathbf{y}}\right|_{\hat{\mathbf{y}}_{k|k-1}} \tag{A.2.18}$$

A.2.3 The Unscented Kalman Filter

Assuming nonlinear dynamics given by

$$\left.\begin{aligned} \mathbf{y}_k &= \mathbf{f}(\mathbf{y}_{k-1}, \mathbf{u}_{k-1}) + \mathbf{w}_{k-1} \\ \mathbf{z}_k &= \mathbf{h}(\mathbf{y}_k) + \mathbf{v}_k \end{aligned}\right\} \tag{A.2.19}$$

the unscented Kalman filter also has a prediction and correction step. This filter is typically used when the predict and update functions, $\mathbf{f}$ and $\mathbf{h}$ are highly nonlinear. For this filter, the state is augmented with the mean and covariance of the process noise. The prediction step is given by the following equations[213]

$$\mathbf{y}^a_{k-1|k-1} = \left(\hat{\mathbf{y}}^T_{k-1|k-1}\ \mathbb{E}(\mathbf{w}^T_k)\right)^T \tag{A.2.20}$$

$$\mathbf{\Sigma}^a_{k-1|k-1} = \begin{pmatrix} \mathbf{\Sigma}_{k-1|k-1} & \mathbf{0} \\ \mathbf{0} & \mathbf{Q}_k \end{pmatrix} \tag{A.2.21}$$

Provided the dimension of of the augmented states is n, then a set of $2n+1$ sigma points are provided by the following equations

$$\boldsymbol{\chi}^0_{k-1|k-1} = \mathbf{x}^a_{k-1|k-1} \tag{A.2.22}$$

$$\boldsymbol{\chi}^i_{k-1|k-1} = \mathbf{x}^a_{k-1|k-1} + \left(\sqrt{(n+\lambda)\mathbf{\Sigma}^a_{k-1|k-1}}\right)_i, \quad i = 1, \ldots, n \tag{A.2.23}$$

$$\boldsymbol{\chi}^i_{k-1|k-1} = \mathbf{x}^a_{k-1|k-1} - \left(\sqrt{(n+\lambda)\mathbf{\Sigma}^a_{k-1|k-1}}\right)_i, \quad i = n+1, \ldots, 2n \tag{A.2.24}$$

where $\left(\sqrt{(n+\lambda)\mathbf{\Sigma}^a_{k-1|k-1}}\right)_i$ is the i^{th} column of the matrix square root of $(n+\lambda)\mathbf{\Sigma}^a_{k-1|k-1}$ and λ is given by

$$\lambda = \alpha^2(n+\kappa) - n \tag{A.2.25}$$

The variables α and κ control the spread of the sigma points and β is related to the distribution of $\mathbf{y}$. Typical values are $\alpha = 10^{-3}$, $\kappa = 0$, and $\beta = 2$ when $\mathbf{y}$ is Gaussian. The sigma points are propagated through the propagation function

$$\boldsymbol{\chi}^i_{k|k-1} = \mathbf{f}\left(\boldsymbol{\chi}^i_{k-1|k-1}\right), \quad i = 0, \ldots, 2n \tag{A.2.26}$$

The predicted state and covariance are then given by

$$\hat{\mathbf{y}}_{k|k-1} = \sum_{i=0}^{2n} w^i_m \boldsymbol{\chi}^i_{k|k-1} \tag{A.2.27}$$

$$\boldsymbol{\Sigma}_{k|k-1} = \sum_{i=0}^{2n} w^i_c \left(\boldsymbol{\chi}^i_{k|k-1} - \hat{\mathbf{y}}_{k|k-1}\right)\left(\boldsymbol{\chi}^i_{k|k-1} - \hat{\mathbf{y}}_{k|k-1}\right) \tag{A.2.28}$$

where the weights w^i_m and w^i_c are given by

$$w^0_m = \frac{\lambda}{n+\lambda} \tag{A.2.29}$$

$$w^0_c = \frac{\lambda}{n+\lambda} + (1 - \alpha^2 + \beta) \tag{A.2.30}$$

$$w^i_m = w^i_c = \frac{1}{2(n+\lambda)}, \quad i = 1, \ldots, 2n \tag{A.2.31}$$

The update step is governed by the following equations[213]

$$\mathbf{y}^a_{k|k-1} = \left(\hat{\mathbf{y}}^T_{k|k-1}\ \mathbb{E}(\mathbf{v}^T_k)\right)^T \tag{A.2.32}$$

$$\boldsymbol{\Sigma}^a_{k|k-1} = \begin{pmatrix} \boldsymbol{\Sigma}_{k|k-1} & \mathbf{0} \\ \mathbf{0} & \mathbf{R}_k \end{pmatrix} \tag{A.2.33}$$

A set of $2n+1$ sigma points are provided by the following equations

$$\boldsymbol{\chi}^0_{k|k-1} = \mathbf{x}^a_{k|k-1} \tag{A.2.34}$$

$$\boldsymbol{\chi}^i_{k|k-1} = \mathbf{x}^a_{k|k-1} + \left(\sqrt{(n+\lambda)\boldsymbol{\Sigma}^a_{k|k-1}}\right)_i, \quad i = 1, \ldots, n \tag{A.2.35}$$

$$\boldsymbol{\chi}^i_{k|k-1} = \mathbf{x}^a_{k|k-1} - \left(\sqrt{(n+\lambda)\boldsymbol{\Sigma}^a_{k|k-1}}\right)_i, \quad i = n+1, \ldots, 2n \tag{A.2.36}$$

The sigma points are propagated through the function

$$\boldsymbol{\gamma}^i_k = \mathbf{h}\left(\boldsymbol{\chi}^i_{k|k-1}\right), \quad i = 0, \ldots, 2n \tag{A.2.37}$$

With the weights defined in the prediction step, the weighted sigma points are then used to produce the predicted measurement and the measurement correction

$$\hat{\mathbf{z}}_{k|k-1} = \sum_{i=0}^{2n} w_m^i \boldsymbol{\gamma}_k^i \tag{A.2.38}$$

$$\boldsymbol{\Sigma}_{\mathbf{z}_k\mathbf{z}_k} = \sum_{i=0}^{2n} w_c^i \left(\boldsymbol{\gamma}_k^i - \hat{\mathbf{z}}_k\right)\left(\boldsymbol{\gamma}_k^i - \hat{\mathbf{z}}_k\right)^T \tag{A.2.39}$$

The matrix

$$\boldsymbol{\Sigma}_{\mathbf{y}_k\mathbf{z}_k} = \sum_{i=0}^{2n} w_c^i \left(\boldsymbol{\chi}_{k|k-1}^i - \hat{\mathbf{x}}_{k|k-1}\right)\left(\boldsymbol{\gamma}_k^i - \hat{\mathbf{z}}_k\right)^T \tag{A.2.40}$$

is used to compute the gain

$$\mathbf{K}_k = \boldsymbol{\Sigma}_{\mathbf{y}_k\mathbf{z}_k}\boldsymbol{\Sigma}_{\mathbf{z}_k\mathbf{z}_k}^{-1} \tag{A.2.41}$$

which is used to compute the updated state

$$\hat{\mathbf{y}}_{k|k} = \hat{\mathbf{y}}_{k|k-1} + \mathbf{K}_k(\mathbf{z}_k - \hat{\mathbf{z}}_k) \tag{A.2.42}$$

$$\boldsymbol{\Sigma}_{k|k} = \boldsymbol{\Sigma}_{k|k-1} - \mathbf{K}_k\boldsymbol{\Sigma}_{\mathbf{z}_k\mathbf{z}_k}\mathbf{K}_k^T \tag{A.2.43}$$

A.3 Uncertainty Propagation Techniques

A.3.1 Analytic Propagation in Linear Systems

Consider an input-output relationship for an analysis of the following form[59]

$$\mathbf{Y} = \mathbf{A}\mathbf{X} \tag{A.3.1}$$

where $\mathbf{A}$ is a scalar matrix and $\mathbf{X}$ is a vector of random variables with mean $\boldsymbol{\mu}_{\mathbf{X}}$ and covariance matrix $\boldsymbol{\Sigma}_{\mathbf{X}}$. The mean for this combination is given by

$$\boldsymbol{\mu}_{\mathbf{Y}} = \mathbf{A}\boldsymbol{\mu}_{\mathbf{X}} \tag{A.3.2}$$

and the covariance for this linear relationship is given by

$$\boldsymbol{\Sigma}_{\mathbf{Y}} = \mathbf{A}\boldsymbol{\Sigma}_{\mathbf{X}}\mathbf{A}^T \tag{A.3.3}$$

Hence, if the mean and covariance of the input variables are known, the mean and covariance matrix of the output of the analysis can be determined analytically for the case of a linear input-output relationship.

A.3.2 Fast Probability Integration

The Advanced Mean Value (AMV) probability integration approximates the cumulative distribution function for a response function that is assumed to be continuous and smooth[78]. A complex Taylor series expansion of the response function, r, exists of the form[78]

$$\begin{aligned} r(\mathbf{x}) &= r(\mu) + \sum_{i=1}^{n} \left(\frac{\partial r}{\partial x_i} \right) (x_i - \mu_i) + H(\mathbf{x}) \\ &= a_0 + \sum_{i=1}^{n} a_i x_i + H(\mathbf{x}) \\ &= r_{\mathrm{mv}}(\mathbf{x}) + H(\mathbf{x}) \end{aligned} \tag{A.3.4}$$

The coefficients to the Taylor series a_i are found through numerical differentiation.

If the response function is nearly linear, the $H(\mathbf{x})$ term can be neglected. This results in the mean and variance of the linearized response function to be give by

$$\begin{aligned} \mu_r &= a_0 + \sum_{i=1}^{n} a_i \mu_{x_i} \\ \sigma_R^2 &= \sum_{i=1}^{n} a_i^2 \sigma_{x_i}^2 \end{aligned} \tag{A.3.5}$$

If the linearity of the response does not hold, the higher-order terms denoted by $H(\mathbf{x})$ need to be estimated. This involves estimating the function value for user-defined set of cumulative distribution function values based on the response function linear expansion, r_{mv}.

A.3.3 Cramer-Rao Lower Bound

The Cramer-Rao lower bound states that covariance matrix, $\boldsymbol{\Sigma}$, in terms of its parameters, $\boldsymbol{\theta}$, is bounded from below by the expression

$$\boldsymbol{\Sigma} \geq \mathbf{I}^{-1}(\boldsymbol{\theta}) \tag{A.3.6}$$

where the elements of the Fisher information matrix, $\mathbf{I}(\boldsymbol{\theta})$, are given by

$$[\mathbf{I}(\boldsymbol{\theta})]_{ij} = -\mathbb{E}\left[\frac{\partial^2}{\partial \theta_i \partial \theta_j} \ln \boldsymbol{\ell}(\mathbf{x}; \theta) \right] \tag{A.3.7}$$

and the parameter estimation likelihood function is given by $\boldsymbol{\ell}(\mathbf{x};\theta)$. Dependent on the form of the distribution, this equation can be simplified. For example, suppose $\mathbf{X}$ is an n-dimensional random variable distributed as a multivariate normal distribution (*i.e.*, $\mathbf{X} \sim \mathcal{N}(\boldsymbol{\mu}(\boldsymbol{\theta}), \boldsymbol{\Sigma}_{\mathbf{X}}(\boldsymbol{\theta}))$), then the Fisher information index is given by

$$[\mathbf{I}(\boldsymbol{\theta})]_{ij} = \frac{\partial \boldsymbol{\mu}^T}{\partial \theta_i} \boldsymbol{\Sigma}_{\mathbf{X}}^{-1} \frac{\partial \boldsymbol{\mu}}{\partial \theta_j} + \frac{1}{2} \mathrm{tr} \left(\boldsymbol{\Sigma}_{\mathbf{X}}^{-1} \frac{\partial \boldsymbol{\Sigma}_{\mathbf{X}}}{\partial \theta_i} \boldsymbol{\Sigma}_{\mathbf{X}}^{-1} \frac{\partial \boldsymbol{\Sigma}_{\mathbf{X}}}{\partial \theta_j} \right) \tag{A.3.8}$$

In this case, the parameters, $\boldsymbol{\theta}$, are the input variables into the analysis where each element of the mean and covariance matrix can be thought of as a estimated parameter.

A.3.4 Linear Covariance Methods

Linear covariance methods which has been used in the development of guidance, navigation, and control (GN&C) systems. GN&C subsystems are governed by dynamic equations (either differential or difference) and are composed of the system dynamics, sensors, and actuators. As such, consider the following development of the linear covariance equations, which has application in GN&C system and follows that by Geller in Ref. [82].

A.3.4.1 Nonlinear Modeling

Consider a general set of dynamical equations for the truth model,

$$\dot{\mathbf{x}} = \mathbf{f}(\mathbf{x}, \hat{\mathbf{u}}, t) + \mathbf{w} \tag{A.3.9}$$

where $\mathbf{x} \in \mathbb{R}^n$ is a vector of true states, $\hat{\mathbf{u}} \in \mathbb{R}^{n_{\hat{u}}}$ is a vector of control commands, and $\mathbf{w} \in \mathbb{R}^n$ is a vector of zero-mean white noise processes with covariance given by

$$\mathbb{E}\left[\mathbf{w}(t)\mathbf{w}^T(t')\right] = \boldsymbol{\Sigma}_{\mathbf{w}}(t)\delta(t-t') \tag{A.3.10}$$

where $\boldsymbol{\Sigma}_{\mathbf{w}}$ is the strength of the white signal noise and $\delta(t-t')$ is the Dirac delta function.

Sensors can be divided into two categories: (1) inertial sensors for navigation state update (*e.g.*, gyros and accelerometers) and (2) non-inertial sensors for navigation state update (*e.g.*, cameras, LiDAR, radar). The inertial sensors are propagated by continuous nonlinear equations of the form

$$\tilde{\mathbf{y}} = \mathbf{c}\left(\mathbf{x}, t\right) + \boldsymbol{\eta} \tag{A.3.11}$$

where $\tilde{\mathbf{y}} \in \mathbb{R}^{n_y}$ is a vector of continuous measurements at time t. Additionally, the inertial sensors provide discrete measurements, $\boldsymbol{\Delta}\tilde{\mathbf{y}}_j \in \mathbb{R}^{n_{\Delta y}}$, at time t_j

$$\boldsymbol{\Delta}\tilde{\mathbf{y}}_j = \boldsymbol{\Delta}\mathbf{c}\left(\mathbf{x}_j, t_j\right) + \boldsymbol{\Delta}\boldsymbol{\eta}_j \tag{A.3.12}$$

The noninertial sensors provide a vector of measurements, $\tilde{\mathbf{z}}_k \in \mathbb{R}^{n_z}$, at time t_k, where the measurements are given by

$$\tilde{\mathbf{z}}_k = \mathbf{h}\left(\mathbf{x}_k, t_k\right) + \boldsymbol{\nu}_k \tag{A.3.13}$$

The covariance of the noise for each of the classes of sensors is given by

$$\mathbb{E}\left[\boldsymbol{\eta}(t)\boldsymbol{\eta}^T(t')\right] = \boldsymbol{\Sigma}_{\boldsymbol{\eta}}\delta(t - t') \tag{A.3.14}$$

$$\mathbb{E}\left[\boldsymbol{\Delta}\boldsymbol{\eta}_j\boldsymbol{\Delta}\boldsymbol{\eta}_{j'}^T\right] = \boldsymbol{\Sigma}_{\boldsymbol{\Delta}\boldsymbol{\eta}}(t_j)\delta_{jj'} \tag{A.3.15}$$

$$\mathbb{E}\left[\boldsymbol{\nu}_k\boldsymbol{\nu}_{k'}^T\right] = \boldsymbol{\Sigma}_{\boldsymbol{\nu}}(t_k)\delta_{kk'} \tag{A.3.16}$$

The instantaneous corrections to the state vector as a result of performing an impulsive maneuver (such as those resulting from Lambert targeting in a rendezvous scenario) are allowed using this framework. A correction at time t_c is represented as

$$\mathbf{x}_c^+ = \mathbf{x}_c^- + \mathbf{d}\left(\mathbf{x}_c^-, \boldsymbol{\Delta}\hat{\mathbf{u}}_c, t_c\right) + \boldsymbol{\Delta}\mathbf{w}_c \tag{A.3.17}$$

Where $\mathbf{d}\left(\mathbf{x}_c^-, \boldsymbol{\Delta}\hat{\mathbf{u}}_c, t_c\right) : \mathbb{R}^n \times \mathbb{R}^{n_{\hat{u}}} \times \mathbb{R} \mapsto \mathbb{R}^n$, is a function of the true state before the maneuver, $\mathbf{x}_c^-$, the vector of instantaneous commanded controls, $\boldsymbol{\Delta}\hat{\mathbf{u}}_c$, and the time the maneuver is performed, t_j.

The navigation state and the state covariance matrix are propagated according to the following relationships

$$\dot{\hat{\mathbf{x}}} = \hat{\mathbf{f}}\left(\hat{\mathbf{x}}, \hat{\mathbf{u}}, \tilde{\mathbf{y}}, t\right) \tag{A.3.18}$$

$$\dot{\hat{\mathbf{P}}} = \left[\hat{\mathbf{F}}_{\hat{\mathbf{x}}} + \hat{\mathbf{F}}_{\tilde{\mathbf{y}}}\hat{\mathbf{C}}_{\hat{\mathbf{x}}}\right]\hat{\mathbf{P}} + \hat{\mathbf{P}}\left[\hat{\mathbf{F}}_{\hat{\mathbf{x}}} + \hat{\mathbf{F}}_{\tilde{\mathbf{y}}}\hat{\mathbf{C}}_{\hat{\mathbf{x}}}\right]^T + \hat{\mathbf{F}}_{\tilde{\mathbf{y}}}\hat{\boldsymbol{\Sigma}}_{\boldsymbol{\eta}}\hat{\mathbf{F}}_{\tilde{\mathbf{y}}}^T + \hat{\boldsymbol{\Sigma}}_{\mathbf{w}} \tag{A.3.19}$$

where $\hat{\mathbf{x}} \in \mathbb{R}^{\hat{n}}$ is the navigation state where $\hat{n} \leq n$. The matrices $\hat{\mathbf{F}}_{(\cdot)}$ and $\hat{\mathbf{C}}_{(\cdot)}$ are Jacobian matrices indicated by

$$\hat{\mathbf{F}}_{(\cdot)} = \frac{\partial \hat{\mathbf{f}}}{\partial(\cdot)} \tag{A.3.20}$$

$$\hat{\mathbf{C}}_{(\cdot)} = \frac{\partial \hat{\mathbf{c}}}{\partial(\cdot)} \tag{A.3.21}$$

where the partial derivatives are evaluated along the nominal trajectory. Noise from inertial instrument measurements and unmodeled accelerations are accounted by the inclusion of $\hat{\boldsymbol{\Sigma}}_{\boldsymbol{\eta}}$ and $\hat{\boldsymbol{\Sigma}}_{\mathbf{w}}$, respectively, in Eq. (A.3.19).

The navigation state and state covariance updates are provided by the relationships

$$\hat{\mathbf{x}}_k^+ = \hat{\mathbf{x}}_k^- + \hat{\mathbf{K}}(t_k)\left[\hat{\mathbf{z}}_k - \hat{\mathbf{h}}\left(\hat{\mathbf{x}}_k, t_k\right)\right] \tag{A.3.22}$$

$$\begin{aligned}\hat{\mathbf{P}}(t_k^+) = \left[[\mathbf{I}]_{\hat{n}\times\hat{n}} - \hat{\mathbf{K}}(t_k)\hat{\mathbf{H}}_{\hat{\mathbf{x}}}(t_k)\right]\hat{\mathbf{P}}(t_k^-)\left[[\mathbf{I}]_{\hat{n}\times\hat{n}} - \hat{\mathbf{K}}(t_k)\hat{\mathbf{H}}_{\hat{\mathbf{x}}}(t_k)\right]^T \\ - \hat{\mathbf{K}}(t_k)\hat{\boldsymbol{\Sigma}}_{\boldsymbol{\nu}}\hat{\mathbf{K}}^T(t_k)\end{aligned} \tag{A.3.23}$$

and the Kalman gain, $\hat{\mathbf{K}}(t_k)$, is given by

$$\hat{\mathbf{K}}(t_k) = \hat{\mathbf{P}}(t_k)\hat{\mathbf{H}}_{\hat{\mathbf{x}}}^T(t_k)\left[\hat{\mathbf{H}}_{\hat{\mathbf{x}}}(t_k)\hat{\mathbf{P}}(t_k)\hat{\mathbf{H}}_{\hat{\mathbf{x}}}^T(t_k) + \hat{\boldsymbol{\Sigma}}_{\boldsymbol{\nu}}\right]^{-1} \tag{A.3.24}$$

In Eqs. (A.3.23) and (A.3.24), $\hat{\mathbf{H}}_{\hat{\mathbf{x}}}(t_k)$ represents the measurement sensitivity matrix (*i.e.*, the sensitivity of the measurements with respect to the navigated state).

The instantaneous maneuvers are updated according to the relationship

$$\hat{\mathbf{x}}_j^+ = \hat{\mathbf{x}}_j^- + \hat{\mathbf{d}}\left(\hat{\mathbf{x}}_j^-, \boldsymbol{\Delta}\hat{\mathbf{u}}_j, \boldsymbol{\Delta}\tilde{\mathbf{y}}_j, t_j\right) \tag{A.3.25}$$

The covariance matrix for these instantaneous maneuvers is updated according to the formula

$$\hat{\mathbf{P}}(t_j^+) = \boldsymbol{\beta}\hat{\mathbf{P}}(t_j^-)\boldsymbol{\beta}^T + \hat{\mathbf{D}}_{\boldsymbol{\Delta}\tilde{\mathbf{y}}}(t_j)\hat{\boldsymbol{\Sigma}}_{\boldsymbol{\Delta}\boldsymbol{\eta}}(t_j)\hat{\mathbf{D}}^T_{\boldsymbol{\Delta}\tilde{\mathbf{y}}}(t_j) + \hat{\boldsymbol{\Sigma}}_{\boldsymbol{\Delta}\mathbf{w}}(t_j) \tag{A.3.26}$$

where

$$\hat{\mathbf{D}}_{(\cdot)} = \frac{\partial \hat{\mathbf{d}}}{\partial(\cdot)} \tag{A.3.27}$$

and

$$\boldsymbol{\beta} = \left[[\mathbf{I}]_{\hat{n}\times\hat{n}} + \hat{\mathbf{D}}_{\hat{\mathbf{x}}}(t_j) + \hat{\mathbf{D}}_{\boldsymbol{\Delta}\tilde{\mathbf{y}}}(t_j)\boldsymbol{\Delta}\hat{\mathbf{C}}_{\hat{\mathbf{x}}}(t_j)\right] \tag{A.3.28}$$

The pointing, targeting, and control algorithms are assumed to use the most recent value of the navigation state to compute the continuous and discrete commands, given by Eq. (A.3.29) and (A.3.30), respectively.

$$\hat{\mathbf{u}} = \hat{\mathbf{g}}\left(\hat{\mathbf{x}}, t\right) \tag{A.3.29}$$

$$\boldsymbol{\Delta}\hat{\mathbf{u}} = \boldsymbol{\Delta}\hat{\mathbf{g}}\left(\hat{\mathbf{x}}_j^-, t_j\right) \tag{A.3.30}$$

A.3.4.2 Linear Modeling

The models presented in the preceding section are used to develop the nominal reference trajectory, $\bar{\mathbf{x}}$. These equations are then linearized to produce a set of equations that describe the time evolution of the true state dispersions from the reference, $\boldsymbol{\delta}\mathbf{x}(t) = \mathbf{x}(t) - \bar{\mathbf{x}}$ and the time evolution of the navigation state dispersions from the reference, $\boldsymbol{\delta}\hat{\mathbf{x}}(t) = \hat{\mathbf{x}} - \bar{\mathbf{x}}$. The linearization of the propagation equations presented in A.3.4.1 about the reference results in

$$\boldsymbol{\delta}\dot{\mathbf{x}} = \mathbf{F}_{\mathbf{x}}\boldsymbol{\delta}\mathbf{x} + \mathbf{F}_{\hat{\mathbf{u}}}\hat{\mathbf{G}}_{\hat{\mathbf{x}}}\boldsymbol{\delta}\hat{\mathbf{x}} + \mathbf{w} \tag{A.3.31}$$

$$\boldsymbol{\delta}\dot{\hat{\mathbf{x}}} = \left[\hat{\mathbf{F}}_{\hat{\mathbf{x}}} + \hat{\mathbf{F}}_{\hat{\mathbf{u}}}\hat{\mathbf{G}}_{\hat{\mathbf{x}}}\right]\boldsymbol{\delta}\hat{\mathbf{x}} + \hat{\mathbf{F}}_{\tilde{\mathbf{y}}}\mathbf{C}_{\mathbf{x}}\boldsymbol{\delta}\mathbf{x} + \hat{\mathbf{F}}_{\tilde{\mathbf{y}}}\boldsymbol{\eta} \tag{A.3.32}$$

where the uppercase matrices are the Jacobian matrices of the corresponding lower case function with respect to the subscripted variable evaluated along the reference.

The state updates can also be linearized about the reference, which results in the relationships

$$\boldsymbol{\delta}\mathbf{x}_k^+ = \boldsymbol{\delta}\mathbf{x}_k^- \tag{A.3.33}$$

$$\boldsymbol{\delta}\mathbf{x}_k^+ = \hat{\mathbf{K}}(t_k)\mathbf{H}_{\mathbf{x}}(t_k)\boldsymbol{\delta}\mathbf{x}_k^- + \left[[\mathbf{I}] - \hat{\mathbf{K}}(t_k)\hat{\mathbf{H}}_{\hat{\mathbf{x}}}(t_k)\right]\boldsymbol{\delta}\hat{\mathbf{x}}_k^- + \hat{\mathbf{K}}(t_k)\boldsymbol{\nu}_k \tag{A.3.34}$$

The state corrections for impulsive maneuvers are given by

$$\boldsymbol{\delta}\mathbf{x}_j^+ = \left[[\mathbf{I}] + \mathbf{D}_{\mathbf{x}}(t_j)\right]\boldsymbol{\delta}\mathbf{x}_j^- + \mathbf{D}_{\boldsymbol{\Delta}\hat{\mathbf{u}}}(t_j)\boldsymbol{\Delta}\hat{\mathbf{G}}_{\hat{\mathbf{x}}}(t_j)\boldsymbol{\delta}\hat{\mathbf{x}}_j^- + \boldsymbol{\Delta}\mathbf{w}_j \tag{A.3.35}$$

$$\begin{aligned}\boldsymbol{\delta}\hat{\mathbf{x}}_j^+ = &\left[[\mathbf{I}] + \hat{\mathbf{D}}_{\mathbf{x}}(t_j) + \hat{\mathbf{D}}_{\boldsymbol{\Delta}\hat{\mathbf{u}}}(t_j)\boldsymbol{\Delta}\hat{\mathbf{G}}_{\hat{\mathbf{x}}}(t_j)\right]\boldsymbol{\delta}\hat{\mathbf{x}}_j^- \\ &+ \hat{\mathbf{D}}_{\boldsymbol{\Delta}\tilde{\mathbf{y}}}(t_j)\boldsymbol{\delta}\boldsymbol{\Delta}\mathbf{C}_{\mathbf{x}}(t_j)\hat{\mathbf{x}}_j^- + \hat{\mathbf{D}}_{\boldsymbol{\Delta}\tilde{\mathbf{y}}}(t_j)\boldsymbol{\Delta}\boldsymbol{\eta}_j\end{aligned} \tag{A.3.36}$$

where again the uppercase matrices are the Jacobian matrices of the corresponding lower case function with respect to the subscripted variable evaluated along the reference.

An augmented state vector, $\underline{\mathbf{x}} = (\boldsymbol{\delta}\mathbf{x}\ \boldsymbol{\delta}\hat{\mathbf{x}})^T$, consisting of both the true state dispersions ($\boldsymbol{\delta}\mathbf{x}$) and the navigation state dispersions ($\boldsymbol{\delta}\hat{\mathbf{x}}$) can be created. The linearized equations described in Eqs. (A.3.31)-(A.3.36) reduce to the matrix form

$$\dot{\underline{\mathbf{x}}} = \boldsymbol{\mathcal{F}}\underline{\mathbf{x}} + \boldsymbol{\mathcal{G}}\boldsymbol{\eta} + \boldsymbol{\mathcal{W}}\mathbf{w} \tag{A.3.37}$$

$$\underline{\mathbf{x}}_k^+ = \boldsymbol{\mathcal{A}}(t_k)\underline{\mathbf{x}}_k^- + \boldsymbol{\mathcal{B}}(t_k)\boldsymbol{\nu}_k \tag{A.3.38}$$

$$\underline{\mathbf{x}}_j^+ = \boldsymbol{\mathcal{D}}(t_j)\underline{\mathbf{x}}_k^- + \boldsymbol{\mathcal{M}}(t_j)\boldsymbol{\Delta}\boldsymbol{\eta}_j + \boldsymbol{\mathcal{N}}(t_j)\boldsymbol{\Delta}\mathbf{w}_j \tag{A.3.39}$$

where the matrices are given by

$$\boldsymbol{\mathcal{F}} = \begin{bmatrix} \mathbf{F}_{\mathbf{x}} & \mathbf{F}_{\hat{\mathbf{u}}}\hat{\mathbf{G}}_{\hat{\mathbf{x}}} \\ \hat{\mathbf{F}}_{\tilde{\mathbf{y}}}\mathbf{C}_{\mathbf{x}} & \hat{\mathbf{F}}_{\hat{\mathbf{x}}} + \hat{\mathbf{F}}_{\hat{\mathbf{u}}}\hat{\mathbf{G}}_{\hat{\mathbf{x}}} \end{bmatrix}, \quad \boldsymbol{\mathcal{G}} = \begin{bmatrix} [\mathbf{0}]_{n\times n_y} \\ \hat{\mathbf{F}}_{\tilde{\mathbf{y}}} \end{bmatrix}, \quad \boldsymbol{\mathcal{W}} = \begin{bmatrix} [\mathbf{I}]_{n\times n} \\ [\mathbf{0}]_{\hat{n}\times n} \end{bmatrix} \tag{A.3.40}$$

$$\boldsymbol{\mathcal{A}}(t_k) = \begin{bmatrix} [\mathbf{I}]_{n\times n} & [\mathbf{0}]_{n\times\hat{n}} \\ \hat{\mathbf{K}}(t_k)\mathbf{H}_{\mathbf{x}}(t_k) & [\mathbf{I}]_{\hat{n}\times\hat{n}} - \hat{\mathbf{K}}(t_k)\hat{\mathbf{H}}_{\hat{\mathbf{x}}} \end{bmatrix}, \quad \boldsymbol{\mathcal{B}}(t_k) = \begin{bmatrix} [\mathbf{0}]_{n\times n_y} \\ \hat{\mathbf{K}}(t_k) \end{bmatrix} \tag{A.3.41}$$

$$\boldsymbol{\mathcal{D}}(t_j) = \begin{bmatrix} [\mathbf{I}]_{n\times n} + \mathbf{D}_{\mathbf{x}}(t_j) & \mathbf{D}_{\boldsymbol{\Delta}\hat{\mathbf{u}}}(t_j)\boldsymbol{\Delta}\hat{\mathbf{G}}_{\hat{\mathbf{x}}}(t_j) \\ \hat{\mathbf{D}}_{\boldsymbol{\Delta}\tilde{\mathbf{y}}}(t_j)\boldsymbol{\Delta}\hat{\mathbf{C}}_{\mathbf{x}}(t_j) & [\mathbf{I}]_{\hat{n}\times\hat{n}} + \hat{\mathbf{D}}_{\hat{\mathbf{x}}}(t_j) + \hat{\mathbf{D}}_{\boldsymbol{\Delta}\hat{\mathbf{u}}}(t_j)\boldsymbol{\Delta}\hat{\mathbf{G}}_{\hat{\mathbf{x}}}(t_j) \end{bmatrix} \tag{A.3.42}$$

$$\boldsymbol{\mathcal{M}}(t_j) = \begin{bmatrix} [\mathbf{0}]_{n\times n_{\Delta y}} \\ \hat{\mathbf{D}}_{\boldsymbol{\Delta\tilde{y}}}(t_j) \end{bmatrix}, \quad \boldsymbol{\mathcal{N}}(t_j) = \begin{bmatrix} [\mathbf{I}]_{n\times n} \\ [\mathbf{0}]_{\hat{n}\times n} \end{bmatrix} \tag{A.3.43}$$

A.3.5 Covariance Equations

The equations governing the propagation, update, and maneuver correction for the augmented state vector's, $\underline{\mathbf{x}}$, covariance matrix $\boldsymbol{\Sigma}_{\mathbf{A}} = \mathbb{E}[\underline{\mathbf{x}}\underline{\mathbf{x}}^T]$ are formulated as follows

$$\dot{\boldsymbol{\Sigma}}_{\mathbf{A}} = \boldsymbol{\mathcal{F}}\boldsymbol{\Sigma}_{\mathbf{A}} + \boldsymbol{\Sigma}_{\mathbf{A}}\boldsymbol{\mathcal{F}}^T + \boldsymbol{\mathcal{G}}^T\boldsymbol{\Sigma}_{\boldsymbol{\eta}}\boldsymbol{\mathcal{G}} + \boldsymbol{\mathcal{W}}\boldsymbol{\Sigma}_{\mathbf{w}}\boldsymbol{\mathcal{W}}^T \tag{A.3.44}$$

$$\boldsymbol{\Sigma}_{\mathbf{A}}(t_k^+) = \boldsymbol{\mathcal{A}}(t_k^-)\boldsymbol{\Sigma}_{\mathbf{A}}(t_k^-)\boldsymbol{\mathcal{A}}^T(t_k^-) + \boldsymbol{\mathcal{B}}(t_k^-)\boldsymbol{\Sigma}_{\boldsymbol{\nu}}(t_k^-)\boldsymbol{\mathcal{B}}^T(t_k^-) \tag{A.3.45}$$

$$\begin{aligned} \boldsymbol{\Sigma}_{\mathbf{A}}(t_j^+) = \boldsymbol{\mathcal{D}}(t_j^-)\boldsymbol{\Sigma}_{\mathbf{A}}(t_j^-)\boldsymbol{\mathcal{D}}^T(t_j^-) + \boldsymbol{\mathcal{M}}(t_j^-)\boldsymbol{\Sigma}_{\boldsymbol{\Delta\eta}}(t_j^-)\boldsymbol{\mathcal{M}}^T(t_j^-) \\ + \boldsymbol{\mathcal{N}}(t_j^-)\boldsymbol{\Sigma}_{\boldsymbol{\Delta}\mathbf{w}}(t_j^-)\boldsymbol{\mathcal{N}}^T(t_j^-) \end{aligned} \tag{A.3.46}$$

Where it is noted that since $\mathbb{E}[\mathbf{x}(t)] = \mathbb{E}[\bar{\mathbf{x}}(t)]$ and $\mathbb{E}[\hat{\mathbf{x}}(t)] = \mathbb{E}[\mathbf{x}(t)]$, $\mathbb{E}[\underline{\mathbf{x}}] = 0$. Furthermore, it is assumed that $\mathbf{w}$, $\boldsymbol{\Delta}\mathbf{w}$, $\boldsymbol{\eta}$, $\boldsymbol{\Delta\eta}_j$, and $\boldsymbol{\nu}_k$ are mutually uncorrelated. Along with Eqs. (A.3.19), (A.3.23), (A.3.24), and (A.3.26), Eqs.(A.3.44) - (A.3.46) represents a complete set of linear covariance analysis equations.

A.3.5.1 Dispersion Analysis

The closed-loop GN&C system can be evaluated based upon the true state dispersions, $\bar{\mathbf{D}}$, the navigation state dispersion $\hat{\mathbf{D}}$, and the covariance of the true navigation state errors, $\bar{\mathbf{P}}$. The are given by

$$\bar{\mathbf{D}} = \mathbb{E}[\boldsymbol{\delta}\mathbf{x}(t)\boldsymbol{\delta}\mathbf{x}^T(t)] = [[\mathbf{I}]_{n\times n}\ [\mathbf{0}]_{n\times\hat{n}}]\,\boldsymbol{\Sigma}_{\mathbf{A}}\,[[\mathbf{I}]_{n\times n}\ [\mathbf{0}]_{n\times\hat{n}}]^T \tag{A.3.47}$$

$$\hat{\mathbf{D}} = \mathbb{E}[\boldsymbol{\delta}\hat{\mathbf{x}}(t)\boldsymbol{\delta}\hat{\mathbf{x}}^T(t)] = [[\mathbf{0}]_{\hat{n}\times n}\ [\mathbf{I}]_{\hat{n}\times\hat{n}}]\,\boldsymbol{\Sigma}_{\mathbf{A}}\,[[\mathbf{0}]_{\hat{n}\times n}\ [\mathbf{I}]_{\hat{n}\times\hat{n}}]^T \tag{A.3.48}$$

$$\begin{aligned} \bar{\mathbf{P}} &= \mathbb{E}[(\boldsymbol{\delta}\hat{\mathbf{x}}(t) - \mathbf{M}_{\mathbf{x}}\boldsymbol{\delta}\mathbf{x})(\boldsymbol{\delta}\hat{\mathbf{x}}(t) - \mathbf{M}_{\mathbf{x}}\boldsymbol{\delta}\mathbf{x})^T] \\ &= [-\mathbf{M}_{\mathbf{x}}\ [\mathbf{I}]_{\hat{n}\times\hat{n}}]\,\boldsymbol{\Sigma}_{\mathbf{A}}\,[-\mathbf{M}_{\mathbf{x}}\ [\mathbf{I}]_{\hat{n}\times\hat{n}}]^T \end{aligned} \tag{A.3.49}$$

where it is assumed that the true navigation states are mapped from the states by a function of the form

$$\mathbf{x}_{\mathbf{n}} = \mathbf{m}(\mathbf{x}) \tag{A.3.50}$$

and $\mathbf{M_x} = \partial\mathbf{m}/\partial\mathbf{x}$. With these performance measures in place, $\bar{\mathbf{P}}$ can be compared to $\hat{\mathbf{P}}$ to evaluate the onboard navigation performance, and the ability of the GN&C system to control trajectory errors can be examined by evaluating $\bar{\mathbf{D}}$.

A.4 Proof of Lyapunov's Direct Method

The following proof for Lyapunov's direct method follows that outlined in Refs. [142] and [143].

Proof: Lyapunov's Direct Method for Discrete Dynamical Systems. Choose $r_0 > 0$ such that $\{\mathbf{y}_k : \| \mathbf{y}_k - \mathbf{y}_e \| \leq r_0\} \subset \mathcal{S} \cap \mathcal{D}$. By the continuity of $\mathbf{f}$ there is an $r_1 \leq r_0$ such that $\| \mathbf{f}(\mathbf{y}_k) - \mathbf{y}_e \| \leq r_0$ whenever $\| \mathbf{y}_k - \mathbf{y}_e \| \leq r_1$. Now let $\epsilon > 0$ be given and assume, without loss of generality, that $\epsilon \leq r_1$. Then choose $\delta \in (0, \epsilon)$ so that $\| \mathbf{y}_k - \mathbf{y}_e \| \leq \delta$ implies that

$$V(\mathbf{y}_k) < \phi(\epsilon) \equiv \min\{V(\mathbf{y}_k) : \epsilon \leq \| \mathbf{y}_k - \mathbf{y}_e \| \leq r_0\}$$

This can be achieved using the continuity of V and the fact that $V(\mathbf{y}_k)$ is positive definite. Now suppose there is some $\mathbf{y}_0$ such that $\| \mathbf{y}_0 - \mathbf{y}_e \| \leq \delta$ but $\| \mathbf{y}_{k+1} - \mathbf{y}_e \| > \epsilon$ for some k. Assume that this is the first such k; thus $\| \mathbf{y}_i - \mathbf{y}_e \| \leq \epsilon \leq r_1$, $i = 1, 2, \cdots, k$. Then $\| \mathbf{f}(\mathbf{y}_k) - \mathbf{y}_e \| \leq r_0$ so that $V(\mathbf{f}(\mathbf{y}_k))$ is well-defined and $V(\mathbf{f}(\mathbf{y}_k)) \geq \phi(\epsilon)$. But by the definition of a Lyapunov function

$$V(\mathbf{y}_{k+1}) \leq V(\mathbf{y}_k) \leq \cdots \leq V(\mathbf{y}_0) < \phi(\epsilon)$$

This is a contradiction and stability is proved.

For asymptotic stability, it suffices to consider any sequence $\{\mathbf{y}_k\} \subset \{\mathbf{y}_k : \| \mathbf{y}_k - \mathbf{y}_e \| \leq \epsilon\}$ and show that $\mathbf{y}_k \to \mathbf{y}_e$ as $k \to \infty$, and for this it suffices to show that if $\hat{\mathbf{y}}$ is any limit point of $\{\mathbf{y}_k\}$, then $\hat{\mathbf{y}} = \mathbf{y}_e$. Suppose not, then the mapping

$$r(\mathbf{y}_k) = \frac{V(\mathbf{f}(\mathbf{y}_k))}{V(\mathbf{y}_k)}$$

is well-defined and continuous in some open neighborhood $\mathcal{S}_0$ of $\hat{\mathbf{y}}$ and since $\Delta V < 0$, $r(\hat{\mathbf{y}}) < 1$. Hence, for a given $\alpha \in (r(\hat{\mathbf{y}}), 1)$, there is a $\delta > 0$ such that $r(\mathbf{y}_k) \leq \alpha$ whenever $\| \mathbf{y}_k - \hat{\mathbf{y}} \| \leq \delta$. Therefore, for sufficiently large k_i, the subsequence converging to $\hat{\mathbf{y}}$ satisfies

$$V(\mathbf{y}_{k_i+1}) = V(\mathbf{f}(\mathbf{y}_{k_i+1})) \leq \alpha V(\mathbf{y}_{k_i}) \leq \cdots \leq \alpha V(\mathbf{y}_{k_{i-1}+1}) \leq \cdots \leq \alpha^i V(\mathbf{y}_0)$$

so that $V(\mathbf{y}_{k_i}) \to 0$ as $i \to \infty$. But the continuity of V implies that $V(\hat{\mathbf{y}}) = 0$, and because the Lyapunov function is positive definite, $\hat{\mathbf{y}} = \mathbf{y}_e$ proving asymptotic stability.

For global asymptotic stability, note that for any $\mathbf{y}_0$, the radial unboundedness of the Lyapunov function guarantees that $\{\mathbf{y}_k\}$ is bounded otherwise there would be a subsequence $\{\mathbf{y}_{k_i}\}$ such that $\| \mathbf{y}_{k_i} - \mathbf{y}_e \| \to \infty$ as $i \to \infty$ and hence $V(\mathbf{y}_{k_i}) \to \infty$ as $i \to \infty$. This contradicts the monotone decreasing behavior of $V(\mathbf{y}_k)$ required by $\Delta V < 0$. It now follows precisely as in the case of asymptotic stability that $\mathbf{y}_k \to \mathbf{y}_e$ as $k \to \infty$ proving global asymptotic stability. □

A.5 Proof of Uniform (Exponential) Stability Criterion

The following proofs are adapted from Ref. [150].

A.5.1 Linear Systems

Proof: Uniform (Exponential) Stability for Linear Systems. The positive definite decrescent function $V_k \triangleq \| \mathbf{W}_k \mathbf{y}_k \|$ satisifes

$$\Delta V_k = \| \mathbf{W}_{k+1} \mathbf{A}_k \mathbf{y}_k \| - \| \mathbf{W}_k \mathbf{y}_k \| \leq -(1-\beta) \| \mathbf{W}_k \mathbf{y}_k \| < 0$$

which implies uniform (exponential) asymptotic stability by Lyapunov's direct method proven by Hahn in Ref. [142]. □

A.5.2 Nonlinear Systems

Proof: Uniform (Exponential) Stability for Nonlinear Systems. For any $\mathbf{y} \in \Omega$, the fundamental theorem of calculus gives

$$\mathbf{f}(k,\mathbf{y}) = \mathbf{f}(k,\mathbf{y}) - \mathbf{f}(k,\mathbf{0}) = \left[\int_0^1 \frac{\partial \mathbf{f}}{\partial \mathbf{y}}(k,\lambda\mathbf{y})d\lambda\right]\mathbf{y}$$

Consider the positive definite decrescent function $V(\mathbf{y}) \triangleq \| \mathbf{W}\mathbf{y} \|$. Since Ω is open with $\mathbf{0} \in \Omega$, $d_s \triangleq \sup_d [\{\mathbf{y} \mid V(\mathbf{y} \leq d\} \subset \Omega] > 0$. Define $\mathcal{X}_s \triangleq \{\mathbf{y} \mid V(\mathbf{y}) < d_s\} \subset \Omega$ which is open and $\mathbf{0} \in \mathcal{X}_s$. Then, for any $k \geq 0$, if $\mathbf{y}_k \in \mathcal{X}_s$

$$\begin{aligned}
\Delta V_k &= \| \mathbf{W}\mathbf{y}_{k+1} \| - \| \mathbf{W}\mathbf{y}_k \| \\
&= \| \int_0^1 \mathbf{W}\left[\int_0^1 \frac{\partial \mathbf{f}}{\partial \mathbf{y}}(k,\lambda\mathbf{y})\right]\mathbf{y}_k d\lambda \| - \| \mathbf{W}\mathbf{y}_k \| \\
&\leq -(1-\beta) \| \mathbf{W}\mathbf{y}_k \| < 0
\end{aligned}$$

which implies that $\mathbf{y}_{k+1} \in \mathcal{X}_s$. By induction if $\mathbf{y}_0 \in \mathcal{X}_s$, $\mathbf{y}_k \in \mathcal{X}_s$ and $\Delta V_k < 0 \; \forall k \geq 0$. Given $\mathbf{y}_0 \in \mathcal{X}_s$, choose β_0 such that

$$\sup_k \sup_{\mathbf{v} \in \mathcal{X}_0} \left|\left| \mathbf{W}\left[\frac{\partial \mathbf{f}}{\partial \mathbf{y}}(\mathbf{v})\right]\mathbf{W}^{-1} \right|\right| \leq \beta_0 \leq \beta < 1$$

where $\mathcal{X}_0 \triangleq \{\mathbf{y} \mid V(\mathbf{y}) \leq V(\mathbf{y}_0)\}$. Then $\Delta V_k < -(1-\beta_0)V_k$ and the exponential bounds follows from Lemma 1 with $M = 0$, $\alpha = (1-\beta_0)$, and $c = \| \mathbf{W}^{-1} \|^{-1}$. □

A.6 Proof of Region of Attraction

This proof follows that outlined in Ref. [145]

Proof: Region of Attraction. If $\mathbf{y}_0 \in \mathcal{A}_0$ then the third condition on $w(\mathbf{y})$ shows that $w(\mathbf{y}_1) \leq w(\mathbf{y}_0)$ so that $\mathbf{y}_1 \in \mathcal{A}_0$ and, by induction, $\mathbf{y}_k \in \mathcal{A}_0$ and $w(\mathbf{y}_{k+1}) \leq w(\mathbf{y}_k)$, $k = 2, \cdots$. Hence the sequence $\{w(\mathbf{y}_k)\}$ converges. Also note that the third condition on $w(\mathbf{y})$ implies that

$$\frac{1 - w(\mathbf{f}(\mathbf{y}))}{1 - w(\mathbf{y})} = 1 + \phi(\mathbf{y}), \quad \mathbf{y} \in \mathcal{A}_0$$

so that

$$\frac{1-w(\mathbf{y}_k)}{1-w(\mathbf{y}_0)} = \prod_{i=0}^{k-1} \frac{1-w(\mathbf{y}_{i+1})}{1-w(\mathbf{y}_i)} = \prod_{i=0}^{k-1} 1+\phi(\mathbf{y}_i)$$

Since the left hand side of this equality converges as $k \to \infty$, the right does as well which implies that $\phi(\mathbf{y}_k) \to 0$ as $k \to \infty$. Then the first condition on $w(\mathbf{y})$ and the continuity of ϕ ensures that $\mathbf{y}_k \to \mathbf{y}_e$ as $k \to \infty$. Conversely, suppose that $\mathbf{y}_0 \notin \mathcal{A}_0$ then the third condition on $w(\mathbf{y})$ shows that $w(\mathbf{y}_1) \geq w(\mathbf{y}_0) \geq 1$ so that $\mathbf{y}_1 \notin \mathcal{A}_0$ and, by induction, $w(\mathbf{y}_k) \geq 1,\ k = 2, 3, \cdots$. But if $\lim_{k\to\infty} \mathbf{y}_k = \mathbf{y}_e$, then the continuity of w requires that $\lim_{k\to\infty} w(\mathbf{y}_k) = 0$ which is a contradiction. □

APPENDIX B

PUBLICATIONS

B.1 Journal Articles

B.1.1 Published Journal Articles

- Other articles:

    1. **Steinfeldt, B.A.**, Grant, M.J., Matz, D.A., Braun, R.D., and Barton, G., "Guidance Navigation and Control System Performance Trades for Mars Pinpoint Landing," *Journal of Spacecraft and Rockets*, Vol. 47, No. 1, pp. 188-198, Jan-Feb, 2010.
    2. Grant, M.J., **Steinfeldt, B.A.**, Braun, R.D., and Barton, G.H., "Smart Divert: A New Entry, Descent and Landing Architecture," *Journal of Spacecraft and Rockets*, Vol. 47, No. 3, pp. 385-393, May-June, 2010.

B.1.2 Pending Journal Articles

- Thesis relevant articles:

    1. **Steinfeldt, B.A.** and Braun, R.D., "Use of Dynamical System Theory in Multidisciplinary Design"

       An article describing how to cast the multidisciplinary design problem as a dynamical system theory with an overview of potential application domains based on "Utilizing Dynamical Systems Concepts in Multidisciplinary Design"; submitted to the *AIAA Journal* in November 2012 (in revision; recommended for publication).
    2. **Steinfeldt, B.A.**, Rossman, G.A., Braun, R.D., and Barton, G.H., "Rapid Robust Design of a Deployable for Strategic Systems"

       An article based on "Rapid Robust Design of a Deployable System for Boost-Glide Vehicles" where the complete design of the two mid L/D systems are found using the rapid robust design methodology; submitted to the *Journal of Spacecraft and Rockets* in May 2013.

B.1.3 Planned Journal Articles

- Thesis relevant articles:

    1. **Steinfeldt, B.A.** and Braun, R.D., "Multidisciplinary Design Convergence Criterion Based on Stability Concepts"

       An article describing the convergence criterion derived through stability concepts for various root-finding schemes that is based on "Design Convergence Using Stability Concepts from Dynamical Systems Theory"; targeted for submission to *Engineering Optimization* in Fall 2013.

    2. **Steinfeldt, B.A.** and Braun, R.D., "Using Optimal Control to Incorporate Design Constraints in the Multidisciplinary Design Problem"

       An article describing the use of optimal control techniques to incorporate constraints within the multidisciplinary design problem that is based on "Leveraging Dynamical Systems Theory to Incorporate Design Constraints for Multidisciplinary Design Problems"; targeted for submission to the *ASME Journal of Mechanical Design* in Fall 2013.

    3. **Steinfeldt, B.A.** and Braun, R.D., "Leveraging Estimation Techniques in Multidisciplinary Design"

       An article describing the use of estimation techniques to quantify uncertainty within the multidisciplinary design problem that is based on "Using Estimation Techniques in Multidisciplinary Design"; targeted for submission to *Engineering Optimization* in Fall 2013.

    4. **Steinfeldt, B.A.** and Braun, R.D., "Extensibility of a Linear Rapid Robust Design Methodology"

       An article demonstrating the linear robust design methodology applied to nonlinear designs and the extent to which it is appropriate that is based on "Extensibility of a Linear Rapid Robust Design Methodology"; targeted for submission to the *AIAA Journal* in Fall 2013.

B.2 Conference Papers

B.2.1 Published Conference Papers

- Thesis relevant conference papers:

    1. **Steinfeldt, B.A.**, Theisinger, J.E., Korzun, A.M., Clark, I.G., Grant, M.J., and Braun, R.D., "High Mass Mars Entry, Descent and Landing Architecture Assessment," AIAA-2009-6684, AIAA SPACE 2009 Conference and Exposition, September 2009, Pasadena, California.

2. **Steinfeldt, B.A.**, Braun, R.D., and Paschall, S.C., "Guidance and Control Algorithm Robustness Baseline Indexing," AIAA-2010-8827, AIAA Guidance, Navigation and Control Conference, August 2010, Toronto, Ontario, Canada.
3. **Steinfeldt, B.A.** and Braun, R.D., "Utilizing Dynamical Systems Concepts in Multidisciplinary Design," AIAA-2012-5655, AIAA/ISSMO Multidisciplinary Analysis and Optimization Conference, September 2012, Indianapolis, Indiana.
4. **Steinfeldt, B.A.** and Braun, R.D., "Design Convergence Using Stability Concepts from Dynamical Systems Theory," AIAA-2012-5657, AIAA/ISSMO Multidisciplinary Analysis and Optimization Conference, September 2012, Indianapolis, Indiana.
5. **Steinfeldt, B.A.**, Rossman, G.A., and Braun, R.D., "Rapid Robust Design of a Deployable System for Boost-Glide Vehicles," AIAA-2013-0031, 51st AIAA Aerospace Sciences Meeting including the New Horizons Forum and Aerospace Exposition, January 2013, Grapevine, Texas.
6. **Steinfeldt, B.A.** and Braun, R.D., "Leveraging Dynamical Systems Theory to Incorporate Design Constraints for Multidisciplinary Design Problems," AIAA-2013-1041, 51st AIAA Aerospace Sciences Meeting including the New Horizons Forum and Aerospace Exposition, January 2013, Grapevine, Texas.

- Other conference papers:

1. Thompson, R., Cliatt, L., Gruber, C., **Steinfeldt, B.**, Sebastian, T., and Wilson, J., "Design of an Entry System for Cargo Delivery to Mars," 5th International Planetary Probe Workshop, June 2007, Bordeaux, France.
2. Otero, R.E., Grant, M.J., **Steinfeldt, B.A.**, and Braun, R.D., "Introducing PESST: A Conceptual Design and Analysis Tool for Unguided/Guided EDL Systems," 6th International Planetary Probe Workshop, June 2008, Atlanta, Georgia.
3. **Steinfeldt, B.A.**, Grant, M.J., Matz, D.A., Braun, R.D., and Barton, G.H., "Guidance, Navigation, and Control Technology System Trades for Mars Pinpoint Landing," AIAA-2008-6216, AIAA Atmospheric Flight Mechanics Conference, August 2008, Honolulu, Hawaii.
4. Grant, M.J, **Steinfeldt, B.A.**, Braun, R.D, and Barton, G.H., "Smart Divert: A New Entry, Descent, and Landing Architecture," AIAA 2009-0522, 47th AIAA Aerospace Sciences Meeting Including the New Horizons Forum and Aerospace Exposition, January 2009, Orlando, Florida.
5. **Steinfeldt, B.A.**, and Tsiotras, P., "A State-Dependent Riccati Equation Approach to Atmospheric Entry Guidance," AIAA-2010-8310, AIAA Guidance, Navigation and Control Conference, August 2010, Toronto, Ontario, Canada.

6. Chua, Z. K., **Steinfeldt, B.A.**, Kelly, J. R., and Clark I.G., "System Level Impact of Landing Point Redesignation for High-Mass Mars Missions," AIAA-2011-7296, AIAA SPACE 2011 Conference and Exposition, September 2011, Long Beach, California.
7. Cruz-Ayoroa, J.G., Kazemba, C.D., **Steinfeldt, B.A.**, Kelly, J.R., Clark, I.G., and Braun, R.D., "Mass Model Development for Conceptual Design of a Hypersonic Rigid Deployable Decelerator," 9th International Planetary Probe Workshop, June 2012, Toulouse, France.
8. Miller, M.J., **Steinfeldt, B.A.**, and Braun, R.D., "Mission Architecture Considerations for Recovery of High-Altitude Atmospheric Dust Samples," accepted for presentation at the 2013 AIAA Atmospheric Flight Mechanics Conference, Boston, MA, August 2013.
9. Braun, R.D., Putnam, Z.R., **Steinfeldt, B.A.**, Grant, M.J., and Barton, G.H., "Guidance Development for Aerospace Systems," accepted for presentation at the 2013 AIAA Guidance, Navigation, and Control Conference, Boston, MA, August 2013. (Invited)

B.2.2 Planned Conference Papers

- Thesis relevant conference papers:
  1. **Steinfeldt, B.A.** and Braun, R.D., "Using Estimation Techniques in Multidisciplinary Design"

     Paper describing the use of the Kalman filter in multidisciplinary design to quantify uncertainty; submitted to *SciTech 2014*. (January 13-17, 2014)
  2. **Steinfeldt, B.A.** and Braun, R.D., "Extensibility of a Linear Rapid Robust Design Methodology"

     Paper demonstrating the linear robust design methodology applied to nonlinear designs and the extent to which it is appropriate; submitted to *SciTech 2014*. (January 13-17, 2014)
- Other conference papers:
  1. Miller, M.J, **Steinfeldt, B.A.**, and Braun, R.D., "Supersonic Inflatable Aerodynamic Decelerators for use on Sounding Rocket Payloads," submitted to *SciTech 2014*. (January 13-17, 2014)

REFERENCES

[1] Accreditation Board for Engineering and Technology, Baltimore, Maryland, *Criteria for Accrediting Engineering Programs: Effective for Evaluations During the 2009-2010 Accreditation Cycle*, Dec. 2008.

[2] Ackoff, R. L., *Redesigning the Future: A Systems Approach to Societal Problems*, John Wiley & Sons, Inc., New York, NY, 1974.

[3] Carlock, P. G., Decker, S. C., and Fenton, R. E., "Agency Level Systems Engineering for Systems of Systems," *Systems and Information Technology Review Journal*, 1999.

[4] Carlock, P. G. and Fenton, R. E., "Systems of Systems (SoS) Enterprise Systems Engineering for Information-Intensive Organizations," *Systems Engineering*, Vol. 4, No. 4, 2001.

[5] Kotov, V., Rokicki, T. M., and Cherkasova, L., "CSL: Communicating Structures Library for Systems Modeling and Analysis," Tech. Rep. HPL-98-118, HP Laboratories, 1998.

[6] Pei, R. S., "Systems of Systems Integration (SoSI)-A Smart Way of Acquiring Army C4I2WS Systems," *Proceedings of the Summer Computer Simulation Conference*, San Diego, CA, July 2000.

[7] Lukasik, S. J., "Systems, systems of systems, and the education of engineers," *Artificial Intellience for Engineering Design, Analysis and Manufacturing*, Vol. 12, No. 1, 1998.

[8] William H. J. Manthorpe, J., "The Emerging Joint System of Systems: A Systems Engineering Challenge and Opportunity for APL," *John Hopkins APL Technical Digest*, Vol. 17, No. 3, 1996.

[9] Held, J. M., *Systems of Systems: Principles, Performance, and Modelling*, Ph.D. thesis, The University of Sydney, Sydney, NSW, Feb. 2008.

[10] Jamshidi, M., *Systems of Systems Engineering: Innovations for the 21st Century*, John Wiley & Sons, Inc., Hoboken, NJ, 2008.

[11] Gebala, D. A. and Eppinger, S. D., "Methods for Analyzing Design Procedures," *Design Theory and Methodology*, Vol. 31, 1991, pp. 228–233.

[12] Alexander, C., *Notes on the Synthesis of Form*, Harvard University Press, 1964.

[13] Simon, H. A., *The Sciences of the Artificial*, MIT Press, 1970.

[14] Sobieszczanski-Sobieski, J., "Multidisciplinary Optimization for Engineering Systems: Achievements and Potential," Tech. Rep. TM-101566, NASA, 1989.

[15] Harary, F., *Graph Theory*, Addison-Wesley, 1969.

[16] Wiest, J. D. and Levy, F. K., *A Management Guide to PERT/CPM*, Prentice-Hall, 1977.

[17] Steward, D. V., "The Design Structure System: A Method for Managing the Design of Complex Systems," *IEEE Transactions on Engineering Management*, Vol. 28, 1981, pp. 71–74.

[18] Young, D. A., *An Innovative Method for Allocating Reliability and Cost in a Lunar Exploration Architecture*, Ph.D. thesis, Georgia Institute of Technology, Georgia, May 2007.

[19] McCord, K. R., *Managing the Integration Problem in Concurrent Engineering*, Master's thesis, Massachusetts Institute of Technology, Massachusetts, May 1993.

[20] Berkes, U. L., "Efficient Optimization of Aircraft Structures with a Large Number of Design Variables," *Journal of Aircraft*, Vol. 27, No. 12, 1990.

[21] Martins, J. R. R. A. and Lambe, A. B., "Multidisciplineary Design Optimization: A Survey of Architectures," *AIAA Journal (in press)*.

[22] Sobieszczaanski-Sobieski, J. and Haftka, R. T., "Multidisciplinary Aerospace Design Optimization - Survey of Recent Developments," *34th AIAA Aerospace Sciences Meeting and Exhibit*, Reno, NV, Jan. 1996.

[23] Hajela, P., Bloebaum, C. L., and Sobieszczanski-Sobieski, J., "Application of Global Sensitivity Equations in Multidisciplinary Aircraft Synthesis," *Journal of Aircraft*, Vol. 27, No. 12, 1990.

[24] Sobieszczanski-Sobieski, J., "Sensitivity Analysis and Multidisciplinary Optimization for Aircraft Design: Recent Advances and Results," *Journal of Aircraft*, Vol. 27, No. 12, 1990.

[25] Sobieszczanski-Sobieski, J., "A System Approach to Aircraft Optimization," Tech. Rep. TM-104074, NASA, March 1991.

[26] Sobieszczanski-Sobieski, J., "Sensitivity of Complex, Internally Coupled Systems," *AIAA Journal*, Vol. 28, No. 1, 1990.

[27] Olds, J. R., "System Sensitivity Analysis Applied to the Conceptual Design of a Dual Fuel Rocket SSTO," *5th AIAA/NASA/USAF/ISSMO Symposium on Multidisciplinary Analysis and Optimization*, Panama City Beach, FL, Sept. 1994.

[28] McCormick, D. J., *Distributed Uncertainty Analysis Techniques for Conceptual Launch Vehicle Design*, Ph.D. thesis, Georgia Institute of Technology, Georgia, July 2001.

[29] Rogers, J. L., "A Design Manger's Aid for Intelligent Decomposition–User's Guide," Tech. Rep. TM-101575, NASA, March 1989.

[30] Otero, R. E., *Problem Decomposition by Mutual Information and Force-Based Clustering*, Ph.D. thesis, Georgia Institute of Technology, Georgia, May 2012.

[31] Ledsinger, L., *Solutions to Decomposed Branching Trajectories with Powered Flyback Using Multidisciplinary Design Optimization*, Ph.D. thesis, Georgia Institute of Technology, Georgia, July 2000.

[32] Balling, R. J. and Sobieszczanski-Sobieski, J., "An Algorithm for Solving the System-Level Problem in Multilevel Optimization," Tech. Rep. CR-195015, NASA, Dec. 1994.

[33] Braun, R. D., *Collaborative Optimization: An Architecture for Large-Scale Distributed Design*, Ph.D. thesis, Stanford University, Stanford, CA, May 1995.

[34] Cormier, T. A., Scott, A., Ledsinger, L. A., McCormick, D. J., Way, D., and Olds, J. R., "Comparision of Collaborative Optimization to Conventional Design Techniques for a Conceptual RLV," *AIAA 2000-4885*, Long Beach, CA, Sept. 2000.

[35] Braun, R. D. and Kroo, I. M., "Development and Application of the Collaborative Optimization Architecture in a Multidisciplinary Design Environment," *International Congress on Industrial and Applied Mathematics*, Aug. 1995.

[36] Budianto, I. A., *A Collaborative Optimization Approach to Inprove the Design and Deployment of Satellite Constellations*, Ph.D. thesis, Georgia Institute of Technology, Georgia, Sept. 2000.

[37] Braun, R. D., Gage, P., Kroo, I. M., and Sobieski, I., "Implementation and Performance Issues in Collaborative Optimization," *AIAA 96-4017*, Bellevue, WA, Sept. 1996.

[38] Braun, R. D., Kroo, I. M., and Moore, A., "Use of the Collaborative Optimization Architecture for Launch Vehicle Design," *AIAA 96-4018*, Bellevue, WA, Sept. 1996.

[39] "Merriam-Webster," Nov 2011.

[40] Mavris, D. N., Bandte, O., and Schrage, D. P., "Application of Probabilistic Methods for the Determination of an Economically Robust HSCT Configuration," *AIAA 1996-4090*, Bellevue, WA, Sept. 1996.

[41] DeLaurentis, D. A., *A Probabilistic Approach to Aircraft Design Emphasizing Stability and Control Uncertainties*, Ph.D. thesis, Georgia Institute of Technology, Atlanta, GA, Nov. 1998.

[42] Zhao, K., Glover, K., and Doyle, J. C., *Robust and Optimal Control*, Prentice Hall, Englewood Cliffs, NJ, 1996.

[43] Hazelrigg, G. A., *Systems Engineering: An Approach to Information-Based Design*, Prentice Hall, Upper Saddle Ridge, NJ, 1996.

[44] Siddall, J. N., *Probabilistic Engineering Design*, Marcel Dekker, Inc., 1983.

[45] Mavris, D. N., Bandte, O., and DeLaurentis, D. A., "Robust Design Simulation: A Probabilistic Approach to Multidisciplinary Design," *Journal of Aircraft*, Vol. 36, No. 1, 1999.

[46] Yen, B. and Tung, Y., *Reliability and Uncertainty Analyses in Hydraulic Design*, American Society of Chemical Engineers, New York, NY, 1993.

[47] McCormick, D. J. and Olds, J. R., "System Robustness Comparison of Advanced Space Launch Concepts," *AIAA 98-5209*, Huntsville, AL, Oct. 1998.

[48] DeLaurentis, D. A. and Mavris, D. N., "Uncertainty Modeling and Management in Multidisciplinary Analysis and Synthesis," *AIAA 2000-0422*, Reno, NV, Jan. 2000.

[49] DeLaurentis, D. A., Mavris, D. N., Calise, A. C., and Schrage, D. P., "Generating Dynamic Models Including Uncertainty for Use in Aircraft Conceptual Design," *AIAA 97-3590*, New Orleans, LA, Aug. 1997.

[50] Mavris, D. N., DeLaurentis, D. A., and Soban, D. S., "Probabilistic Assessment of Handling Qualities Constraints in Aircraft Preliminary Design," *AIAA 98-0492*, Reno, NV, Jan. 1998.

[51] Mavris, D. N., DeLaurentis, D. A., Bandte, O., and Hale, M. A., "A Stochastic Approach to Multi-disciplinary Aircraft Analysis and Design," *AIAA 98-0912*, Reno, NV, Jan. 1998.

[52] Mavris, D. N., Bandte, O., and Schrage, D. P., "Effect of Mission Requirements on the Economic Robustness of an HSCT Concept," *Proceedings of the 18th Annual Conference of the International Society of Parametric Analysts*, Cannes, France, June 1996.

[53] Mavris, D. N., Bandte, O., and DeLaurentis, D. A., "Determination of System Feasibility and Viability Employing a Joint Probabilistic Formulation," *AIAA 99-0183*, Reno, NV, Jan. 1999.

[54] Mavris, D. N. and Bandte, O., "A Probabilistic Approach to UCAV Engine Sizing," *AIAA 98-3264*, Anaheim, CA, July 1998.

[55] Roth, B. A., Mavris, D. N., and Elliott, D., "A Probabilistic Approach to Multivariate Constrained Robust Design Simulation," *AIAA 98-3264*, Cleveland, OH, July 1998.

[56] Mavris, D. N. and Bandte, O., "Comparison of Two Probabilistic Techniques for the Assessment of Economic Uncertainty," *Proceedings of the 19th Annual Conference of the International Society of Parametric Analysts*, New Orleans, LA, May 1997.

[57] Lafleur, J. M., "Trading Robustness Requirements in Mars Entry Trajectory Design," *AIAA 2009-561*, Chicago, IL, Aug. 2009.

[58] Vysocanskii, D. and Petunin, J., "Justification of the 3σ Rule for Unimodal Distributions," *Theory of Probability and Mathematical Statistics*, Vol. 21, 1980, pp. 25–36.

[59] Hogg, R. V. and Tanis, E. A., *Probability and Statistical Inference*, Pearson Prentice Hall, Upper Saddle River, NJ, 2006.

[60] Roos, O. V., "A Formal Solution of Liouville's Equation," Tech. Rep. 32-10, Jet Propulsion Laboratory, March 1960.

[61] Fuller, A. T., "Analysis of Nonlinear Stochastic Systems by Means of the Fokker-Planck Equation," *International Journal of Control*, Vol. 9, No. 6, 1969.

[62] Risken, H., *The Fokker-Planck Equation: Methods of Solution and Applications*, Springer, New York, NY, 1996.

[63] Kalos, M. H. and Whitlock, P. A., *Monte Carlo Methods*, Wiley-VCH, 2008.

[64] Chen, W., Allen, J. K., Schrage, D. P., and Mistree, F., "Statistical Experimentation Methods for Achieving Affordable Concurrent Systems Design," *AIAA Journal*, Vol. 35, No. 5, 1997.

[65] Unal, R., Stanley, D., Engelund, W., and Lepsch, R., "Design for Quality Using Response Surface Methods: An Alternative to Taguchi's Parameter Design Approach," *Engineering Management Journal*, Vol. 6, No. 3, 1994.

[66] Klenijen, J. P., *Statistical Tools for Simulation Practitioners*, Marcel Dekker, New York, NY, 1987.

[67] Chen, W., Tsui, K.-L., Allen, J. K., and Mistree, F., "Integration of Response Surface Method with the Compromise Decision Support Problem in Developing a General Robust Design Procedure," *Advances in Design Automation*, Vol. 82, No. 2, 1995.

[68] Mavris, D. N. and Bandte, O., "Economic Uncertainty Assessment Using a Combined Design of Experiments/Monte Carlo Simulation Approach with Application to an HSCT," *17th Annual Conference of the International Society of Parametric Analysts*, San Diego, CA, May 1995.

[69] Madsen, H. O., Krenk, S., and Lind, N. C., *Methods of Structural Safety*, Prentice Hall, Englewood Cliffs, NJ, 1986.

[70] Wu, Y. T., "Structural Reliability Analysis Methods for Implicit Performance Functions," *Proceedings of the ASCE Special Conference in Probabilistic Mechanics and Structural and Geotechnical Reliability*, New York, NY, 1992.

[71] Khalessi, M. R., Wu, Y. T., and Torng, T. Y., "Most-Probable-Point-Locus Reliability Method in Standard Normal Space," *ASME Design Engineering*, Vol. 30, 1991.

[72] Wirshing, P. H. and Martin, W. S., "Fracture Mechanics Fatigue Reliability Assessment Employing the Most Probable Point Locus Method," *Proceedings of the the 5th ASCE Special Conference in Probabilistic Methods in Civil Engineering*, New York, NY, 1988.

[73] Wu, Y. T., Millwater, H. R., and Cruse, T. A., "An Advanced Probabilistic Structural Analysis Method for Implicit Performance Functions," *AIAA Journal*, Vol. 28, No. 9, 1990.

[74] Liu, W. K. and Belytschko, T., *Computational Mechanics of Reliability Analysis*, Elmepress International, Lauseanne, WA, 1989.

[75] Wu, Y. T. and Wirsching, P. H., "Demonstration of a Fast, New Probability Integration Method for Reliability Analysis," *ASME Journal of Engineering for Industry*, Vol. 109, 1987.

[76] Wu, Y. T. and Wirsching, P. H., "Advanced Reliability Methods for Probabilistic Structural Analysis," *ASCE Structural Safety and Reliability*, Vol. 3, 1989.

[77] Wu, Y. T. and Wirsching, P. H., "New Algorithm for Structural Reliability Estimation," *ASCE Journal of Engineering Mechanics*, Vol. 113, No. 9, 1987.

[78] Southwest Reserach Institute, San Antonio, TX, *FPI User's Manual and Theoretical Manual*, 1995.

[79] Du, X. and Chen, W., "A Most Probable Point Based Method for Uncertainty Analysis," *Journal of Design and Manufacturing Automation*, Vol. 4, 2001.

[80] Mahadevan, S. and Cruse, T. A., "Advanced First-Order Method for System Reliability," *Proceedings of the the ASCE Special Conference in Probabilistic Mechanics and Geotechnical Reliability*, New York, NY, 1992.

[81] Lin, H. Z. and Khalessi, M. R., "Calculation of Failure Probability by Using X-Space Most-Probable-Point," *AIAA 93-1624*, La Jolla, CA, 1993.

[82] Geller, D. K., "Linear Covariance Techniques for Orbial Rendezvous Analysis and Autonomous Onboard Mission Planning," *Journal of Guidance, Control, and Dynamics*, Vol. 29, No. 6, 2006, pp. 1404–1414.

[83] Christensen, D. and Geller, D., "Terrain-Relative and Beacon-Relative Navigation for Lunar Powered Descent and Landing," *AAS 009-057*, Breckenridge, CO, Jan. 2009.

[84] Geller, D. K. and Christensen, D. P., "Linear Covariance Analysis for Powered Lunar Descent and Landing," *Journal of Spacecraft and Rockets*, Vol. 46, No. 6, 2009.

[85] Du, X. and Chen, W., "Methodolgoy for Managing the Effect of Uncertainty in Simulation-Based Design," *AIAA Journal*, Vol. 38, No. 8, 2000.

[86] Kawata, T., "Fourier Analysis in Probability Theory," *Probability and Mathematical Statistics, A Series of Monographs and Textbooks*, Vol. 55, No. 3, 1975.

[87] Hoybye, J. A., "Model Error Propagation and Data Collection Design: An Application in Water Quality Modeling," *Water, Air, and Soil Pollution*, Vol. 103, No. 1, 1998.

[88] Isukapalli, S. S. and Georgopoulos, P. G., "Stochastic Response Surface Methods (SRSMs) for Uncertainty Propagation: Application to Environmental and Biological Systems," *Risk Analysis*, Vol. 18, No. 3, 1998.

[89] Cheng, W., *Parametric Uncertainty Analysis for Complex Engineering Systems*, Ph.D. thesis, Massachusetts Institute of Technology, Massachussetts, June 1999.

[90] Kumar, M., Singla, P., Chakravorty, S., and Junkins, J. L., "A Multi-Resolution Approacch for Steady State Uncertainty Determination in Nonlinear Dynamic Systems," *Proceedings of the 38th Southeastern Symposium on System Theory*, Cookeville, TN, March 2006.

[91] Kumar, M., Singla, P., Chakravorty, S., and Junkins, J. L., "The Partition of Unity Finite Element Approach to the Stationary Fokker-Planck Equation," *AIAA 2006-6285*, Keystone, CO, Aug. 2006.

[92] Muscolino, G., Ricciardi, G., and Vasta, M., "Stationary and Nonstationary Probability Density Function for Nonlinear Oscillators," *International Journal of Non-Linear Mechanics*, Vol. 32, No. 6, 1997.

[93] Paola, M. D. and Sofi, A., "Approximate Solution of the Fokker-Planck-Kolmogorov Equation," *Probabilistic Engineering Mechanics*, Vol. 17, No. 4, 2002.

[94] Iyengar, R. N. and Dash, P. K., "Study of the Rangom Vibration of Nonlinear Systems by the Gaussian Closure Technique," *Journal of Applied Mechanics*, Vol. 45, No. 1, 1978.

[95] Roberts, J. B. and Spanos, P. D., *Random Vibration and Statistical Linearization*, Wiley, New York, NY, 1990.

[96] Lefebvre, T., Bruyninckx, H., and Schutter, J. D., "Kalman Filters of Non-Linear Systems: A Comparison of Performance," *International Journal of Control*, Vol. 77, No. 7, 2004.

[97] Lefebvre, T., Bruyninckx, H., and Schutter, J. D., "Comment on a New Method for the Nonlinear Transformations of Means and Covariances," *IEEE Transactions on Automatic Control*, Vol. 47, No. 8, 2002.

[98] Terejanu, G., Singla, P., Singh, T., and Scott, P. D., "Uncertainty Propagation for Nonlinear Dynamic Systems Using Gaussian Mixture Models," *Journal of Guidance, Control, and Dynamics*, Vol. 31, No. 6, 2008.

[99] Acton, D. E. and Olds, J. R., "Computational Frameworks for Collaborative Multidisciplinary Design of Complex Systems," *AIAA 98-4972*, St. Louis, MO, Sept. 1998.

[100] Braun, R. D., Powell, R. W., Lepsch, R. A., Stanley, D. O., and Kroo, I. M., "Comparison of Two Multidisciplinary Optimization Strategies for Launch-Vehicle Design," *AIAA 98-4972*, St. Louis, MO, Sept. 1998.

[101] Brown, N. F. and Olds, J. R., "Evaluation of Multidisciplinary Optimization Techniques Applied to a Reusable Launch Vehicle," *Journal of Spacecraft and Rockets*, Vol. 43, No. 6, 2006.

[102] Olds, J. R., "The Suitability of Selected Multidisciplinary Design and Optimization Techniques to Conceptual Aerospace Vehicle Design," *AIAA 92-4791*, Cleveland, OH, Sept. 1992.

[103] Perez, R., Liu, H., and Behdinan, K., "Evaluation of Multidisciplinary Optimization Approaches for Aircraft Conceptual Design," *AIAA 2004-4537*, Albany, NY, Aug. 2004.

[104] Park, G., Lee, T., Lee, K., and Hwang, K., "Robust Design: An Overview," *AIAA Journal*, Vol. 44, No. 1, 2006.

[105] Sundaresan, S., Ishii, K., and Houser, D. R., "A Robust Optimization Procedure with Variatons on Design Variables and Constraints," *Advances in Design Automation*, Vol. 69, No. 1, 1993.

[106] Chen, W., Allen, J. K., Tsui, K.-L., and Mistree, F., "A Procedure for Robust Design," *Journal of Mechanical Design*, Vol. 118, No. 4, 1996.

[107] Bras, B. A. and Mistree, F., "A Compromise Decision Support Problem for Robust and Axiomatic Design," *Journal of Mechanical Design*, Vol. 117, No. 1, 1995.

[108] Iyer, H. V. and Krishnamurty, S., "A Preference-Based Robust Design Metric," *ASME DAC5625*, Atlanta, GA, Sept. 1998.

[109] Chen, W., Wiecek, M. M., and Zhang, J., "Quality Utility: A Compromise Programming Approach to Robust Design," *Journal of Mechanical Design*, Vol. 121, No. 2, 1999.

[110] Taguchi, G., Chowdhury, S., and Wu, Y., *Taguchi's Quality Engineering Handbook*, Wiley, 2004.

[111] Vuchkov, I. N. and Boyadjieva, L. N., *Quality Improvement with Design of Experiments: A Response Surface Approach*, Kluwer Academic Publishers, Norwell, MA, 2001.

[112] Taguchi, G., *System of Experimental Design: Engineering Methods to Optimize Quality and Minimize Costs*, Kraus International Publicaitons, White Plains, NY, 1987.

[113] Way, D. W., *Uncertainty Optimization Applied to the Monte Carlo Analysis of Planeary Entry Trajectories*, Ph.D. thesis, Georgia Institute of Technology, Atlanta, GA, July 1998.

[114] Steinfeldt, B. A., Braun, R. D., and Stephen C. Paschall, I., "Guidance and Control Algorithm Robustness Baseline Indexing," *AIAA 2010-8287*, Toronto, Ontario, Aug. 2010.

[115] Du, X. and Chen, W., "Towards a Better Understanding of Modeling Feasibility Robustness in Engineering Design," *Journal of Mechanical Design*, Vol. 122, No. 4, 2000.

[116] Mavris, D. N., DeLaurentis, D. A., Bandte, O., and Hale, M. A., "A Stochastic Approach to Multi-disciplinary Aircraft Analysis and Design," *AIAA 98-8287*, Reno, NV, Jan. 1998.

[117] Sues, R. H., Oakley, D. R., and Rhodes, G. S., "Multidisciplinary Stochastic Optimization," *Proceedings of the 10th Conference on Engineering Mechanics*, Boulder, CO, May 1995.

[118] Koch, P. N., Simpson, T. W., Allen, J. K., and Mistree, F., "Statistical Approximations for Multidisciplinary Design Optimization: The Problem of Size," *Journal of Aircraft*, Vol. 36, No. 1, 1999.

[119] Batill, S. M., Renaud, J. E., and Gu, X., "Modeling and Simulation Uncertainty in Multidisciplinary Design Optimization," *AIAA 2000-4803*, Long Beach, CA, Sept. 2000.

[120] Parkinson, A., Sorensen, C., and Pourhassan, N., "A General Approach for Robust Optimal Design," *Journal of Mechanical Design*, Vol. 115, No. 1, 1993.

[121] Yu, J.-C. and Ishii, K., "Design for Robustness Based on Manufacturing Variation Patterns," *Journal of Mechanical Design*, Vol. 120, No. 1, 1998.

[122] Gu, X., Renaud, J. E., and Batill, S. M., "An Investigation of Multidisciplinary Design Subject to Uncertainity," *AIAA 98-4747*, St. Louis, MO, Sept. 1998.

[123] Gu, X., Renaud, J. E., Batill, S. M., Branch, R. M., and Budhiraja, A. S., "Worst Case Propagated Uncertainty of Multidisciplinary Systems in Robust Design Optimization," *Structural and Multidisciplinary Design Optimization*, Vol. 20, No. 3, 2000.

[124] Du, X. and Chen, W., "Efficient Uncertainty Analysis Methods For Multidisciplinary Robust Design," *AIAA JOURNAL*, Vol. 40, 2001, pp. 545–552.

[125] Du, X. and Chen, W., "Collaborative Reliability Analysis for Multidisciplinary Systems Design," *AIAA 2002-5474*, Atlanta, GA, Sept. 2002.

[126] Scheinverman, E. R., *Invitation to Dynamical Systems*, Prentice Hall, Upper Saddle River, NJ, 1995.

[127] Appa, K. and Argyris, J., "Non-linear multidisciplinary design optimization using system identification and optimal control theory," *Computer Methods in Applied Mechanics and Engineering*, Vol. 128, 1995.

[128] Smith, R. P., Eppinger, S. D., and Gopal, A., "Testing an Engineering Design Iteration Model in an Experimental Setting," Tech. Rep. WP 3386-92-MS, Massachusetts Institute of Technology, Cambridge, Massachusetts, Feb. 1992.

[129] Lewis, K. and Mistree, F., "Modeling Interactions in Multisciplinary Design: A Game Theoretic Approach," *AIAA Journal*, Vol. 35, No. 8, 1998.

[130] Grant, M. J., Clark, I. G., and Braun, R. D., "Rapid Entry Corridor Trajectory Optimization for Conceptual Design," *AIAA 2010-7810*, Toronto, Ontario, Canada, Aug. 2010.

[131] Grant, M. J., *Rapid Simultaneous Hypersonic Aerodynamic and Trajectory Optimization for Conceptual Design*, Ph.D. thesis, Georgia Institute of Technology, Georgia, May 2012.

[132] Brogan, W. L., *Modern Control Theory*, Prentice Hall, Upper Saddle River, NJ, 1991.

[133] Burden, R. L. and Faires, J. D., *Numerical Analysis*, Brooks/Cole, Boston, MA, 2011.

[134] Julier, S. J. and Uhlmann, J. K., "A General Method for Approximating Nonlinear Transformations of Proability Distributions," Tech. rep., University of Oxford, Nov. 1996.

[135] Simon, D., *Optimal State Estimation*, John Wiley & Sons, Hoboken, NJ, 2006.

[136] Zill, D. G. and Cullen, M. R., *Advanced Engineering Mathematics, 3rd Ed.*, Jones and Bartlett, 2006.

[137] Khalil, H. K., *Nonlinear Systems, 3rd Ed.*, Prentice Hall, 2002.

[138] Kalman, R. E. and Bertram, J. E., "Control System Analysis and Design Via the "Second Method" of Lyapunov: I—Continuous-Time Systems," *Journal of Basic Engineering*, Vol. 82, No. 2, 1960.

[139] Kalman, R. E. and Bertram, J. E., "Control System Analysis and Design Via the "Second Method" of Lyapunov: II—Discrete-Time Systems," *Journal of Basic Engineering*, Vol. 82, No. 2, 1960.

[140] Boltyanskii, V. G., *Optimal Control of Discrete Systems*, John Wiley & Sons, Inc., New York, NY, 1978.

[141] Ogata, K., *Discrete-Time Control Systems*, Prentice Hall, Upper Saddle River, NJ, 1995.

[142] Hahn, W., "Uber die Anwendung der Methode von Lyapunov auf Differenzengleichen," *Mathematische Annalen*, Vol. 136, 1958, pp. 430–441.

[143] Ortega, J. M., "Stability of Difference Equations and Convergence of Iterative Processes," *SIAM Journal on Numerical Analysis*, Vol. 10, No. 2, April 1973, pp. 268–282.

[144] Haddad, W. M. and Chellaboina, V., *Nonlinear Dynamical Systems and Control*, Princetoon University press, Princeton, NJ, 2008.

[145] O'Shea, R., "The Extension of Zubov's Method to Sample-Data Control Systems Described by Autoonomous Difference Equations," *IEEE Transactions on Automatic Contric*, Vol. 9, 1964, pp. 62–69.

[146] Prajna, S., Papachristodoulou, A., and Wu, F., "Nonlinear Control Synthesis by Sum of Squares Optimization: A Lyapunov-based Approach," *Proceedings of the American Control Conference*, 2004.

[147] Prajna, S., Papachristodoulou, A., and Parrilo, P., "Introducing SOSTOOLS: A General Purpose Sum of Squares Programming Solver," *Proceedings of the IEEE Conference on Decision and Control*, 2002.

[148] Sturm, J., "Using SeDuMi 1.02, A Matlab Toolbox for Optimization Over Symmetric Cones," *Optimization Methods and Software*, Vol. 11–12, 1999, pp. 625–653.

[149] Tarn, T. J. and Rasis, Y., "Observers for Nonlinear Stochastic Systems," *IEEE Transactions on Automatic Control*, Vol. 21, No. 4, August 1976, pp. 441–448.

[150] Aitken, V. C. and Schwartz, H. M., "On the Exponential Stability of Discrete-Time Systems with Applications in Observer Design," *Proceedings of the American Control Conference*, Baltimore, MD, June 1994.

[151] Bryson, A. E. and Ho, Y.-C., *Applied Optimal Control*, Taylor & Francis, New York, NY, 1975.

[152] Hull, D. G., *Optimal Control Theory for Applications*, Springer-Verlag, New York, NY, 2003.

[153] Vanderplaats, G. N., *Numerical Optimization Techniques for Engineering Design*, Vanderplaats Research & Development, Inc., 2005.

[154] Nocedal, J. and Wright, S., *Numerical Optimization*, Springer, New York, NY, 1999.

[155] Meyers, R. A., *Mathematics of Complexity and Dynamical Systems*, Springer, New York, NY, 2012.

[156] Hsu, H. P., *Schaum's Outlines: Signals and Systems*, McGraw-Hill, 2010.

[157] Ng, K.-M., *A Continuous Approach for Solving Nonlinear Optimization Problems with Discrete Variables*, Ph.D. thesis, Stanford University, California, June 2002.

[158] Kalman, R. E., "A New Approach to Linear Filtering and Prediction Problems," *Journal of Basic Engineering*, Vol. 82, 1961.

[159] Kalman, R. E. and Bucy, R. S., "New Results in Linear Filtering and Prediction Theory," *Journal of Basic Engineering*, Vol. 83, 1961.

[160] Brammer, K. and Siffling, G., *Kalman-Bucy Filters*, Artesch House, Norwood, MA, 1989.

[161] Chui, C. K. and Chen, G., *Kalman Filtering with Real-Time Applications*, Springer-Verlag, New York, NY, 1991.

[162] Gelb, A., *Applied Optimal Estimation*, The MIT Press, Cambridge, MA, 1971.

[163] Otero, R. E. and Braun, R. D., "The Planetary Entry Systems Synthesis Tool: A Conceptual Design and Analysis Tool for EDL Systems," *IEEEAC 1331*, Big Sky, MT, March 2010.

[164] Martins, J. R. R. A., Sturdza, P., and Alonso, J. J., "The Complex-Step Derivative Approximation," *ACM Transactions on Mathematical Software*, Vol. 29, No. 3, Sept. 2003, pp. 245–262.

[165] Lantoine, G., *A Methodology for Robust Optimization of Low-Thrust Trajectories in Multi-Body Environments*, Ph.D. thesis, Georiga Institute of Technology, Georgia, Dec. 2010.

[166] Gill, P. E., Murray, W., and Saunders, M. A., "User's Guide for SNOPT Version 7: Software for Large-Scale Nonlinear Programming," Tech. rep., Department of Mathematics, University of California, San Diego, La Jolla, California, June 2008.

[167] Gavin, H. P., "Introductory Optimization Example: Design of a Two-Bar Truss," Tech. rep., Duke University, 2012.

[168] Gates, K. L., McRonald, A. D., Nock, K. T., and Aaron, K. M., "Trading Robustness Requirements in Mars Entry Trajectory Design," *AIAA 2010-7974*, Toronto, Ontario, Canada, Aug. 2010.

[169] Lu, F. K., Hyungwon, K., and McNay, L. N., "A Simplified Trajectory Analysis Model for Small Satellite Payload Recovery from Low Earth Orbit," *Aerospace Science and Technology*, Vol. 7, No. 3, 2003.

[170] Bloetscher, F. and Pinnell, W. R., "Correlation of Analytical and Empirical Techniques for Designing Supersonic and Hypersonic Decelerators," *AIAA 1966-1517*, 1966.

[171] Dwyer-Cianciolo, A. M., Davis, J. L., Komar, D. R., Munk, M. M., Samareh, J. A., Powell, R. W., Shidner, J. D., Stanley, D. O., Wilhite, A. W., Kinney, D. J., McGuire, M. K., Arnold, J. O., Howard, A. R., Sostaric, R. R., Studak, J. W., Zumwalt, C. H., Llama, E. G., Casoliva, J., Ivanov, M. C., Clark, I., and Sengupta, A., "Entry, Descent and Landing Systems Analysis Study: Phase 1 Report," Tech. Rep. TM-2010-216720, NASA, July 2010.

[172] Brown, G. J., Lingard, J. S., Darley, M. G., and Underwood, J. C., "Aerocapture Decelerators for Mars Orbiters," *AIAA 2007-2543*, Williamsburg, VA, May 2007.

[173] Jaremenko, I., "BALLUTE Characteristics in the 0.1 to 10 Mach Number Speed Regime," *Journal of Spacecraft and Rockets*, Vol. 4, No. 8, 1967.

[174] Pepper, W. B., "Development of a Composite Structure Hypersonic Parachute," *Journal of Spacecraft and Rockets*, Vol. 6, No. 4, 1969.

[175] Kyser, A. C., "The Rotornet: A High-Performance Hypersonic Decelerator for Planetary Entry," Tech. Rep. CR-247, NASA, June 1965.

[176] Trabandt, U., Koeler, H., and Schmid, M., "Deployable CMC Hot Structure Decelerator for Aerobrake," *AIAA 2003-2169*, Monterey, CA, May 2003.

[177] Green, M. J., Swenson, B. L., and Balakrishnan, A., "Aerothermodynamic Environment for a Titan Probe with Deployable Decelerator," *AIAA 1985-1063*, Williamsburg, VA, June 1985.

[178] Venkatapathy, E., Arnold, J., Fernandez, I., Kenneth R. Hamm, J., Kinney, D., Laub, B., Makino, A., McGuire, M. K., Peterson, K., Prabhu, D., Empey, D., Dupzyk, I., Huynh, L., Hajela, P., Gage, P., Howard, A., and Andrews, D., "Adaptive Deployable Entry and Placement Technology (ADEPT): A Feasibility Study for Human Missions to Mars," *AIAA 2011-2608*, Dublin, Ireland, May 2011.

[179] Horvath, T. J., ., T. F. O., Cheatwood, F. M., Prabhu, R. K., and Alter, S. J., "Experimental Hypersonic Aerodynamic Characteristics of the 2001 Mars Surveyor Precision Lander with Flap," *AIAA 2002-4408*, Monterey, CA, Aug. 2002.

[180] Lockwood, M. K., Powell, R. W., Sutton, K., Prabhu, R. K., Graves, C. A., Epp, C. D., and Carman, G. L., "Entry Configurations and Performance Comparisons for the Mars SMART Lander," *Journal of Spacecraft and Rockets*, Vol. 43, No. 2, 2006.

[181] Wilhite, A. W., Bush, L. B., Cruz, C. I., Lepsch, R. A., Morris, W. D., Stanley, D. O., and Wurster, K. E., "Advanced Technologies for Rocket Single State to Orbit Vehicles," *Journal of Spacecraft and Rockets*, Vol. 28, No. 6, 1991.

[182] Capricci, M., "European Crew and Logistics Vehicles for ISS and Exploration Missions," *AIAA 2005-3252*, Capua, Italy, May 2005.

[183] Allen, H. J. and A. J. Eggers, J., "A Study of the Motion and Aerodynamic Heating of Ballistic Missiles Entering the Earth's Atmosphere at High Supersonic Speeds," Tech. Rep. 1381, NACA, 1957.

[184] Walberg, G. D., "A Survery of Aeroassisted Orbit Transfer," *Journal of Spacecraft*, Vol. 22, No. 1, 1985, pp. 3–18.

[185] Wilhite, A., Arrington, J., and McCandless, R., "Performance Aerodynamics of Aero-Assisted Orbital Transfer Vehicles," *AIAA-84-0406*, Reno, NV, Jan. 1984.

[186] Talay, T., White, N., and Naftel, J., "Impact of Atmospheric Uncertainties and Viscous Interation Effects on the Performance of the Aero-Assisted Orbital Transfer Vehicles," *AIAA-84-0408*, Reno, NV, Jan. 1984.

[187] "OTV Propulsion Issues," Tech. Rep. CP-2347, NASA, Cleveland, OH, April 1984.

[188] Kinney, D. J., "Aero-Thermodynamics for Conceptual Design," *AIAA 2004-13382, 2004 AIAA Aerospace Sciences Meeting and Exhibit*, Reno, NV, Jan. 2004.

[189] "The Apollo Entry Guidance: A Review of the Mathematical Development and Its Operational Characteristics," Tech. Rep. T75-14618, NASA, 1969.

[190] Mendeck, G. F. and Craig, L. E., "Entry Guidance for the 2011 Mars Science Laboratory mission," *AIAA 2011-6639*, Portland, OR, Aug. 2011.

[191] Rao, A. V., Benson, D. A., Darby, C. L., Patterson, M. A., Francolin., C., Sanders, I., and Huntington, G. T., "Algorithm 902: GPOPS, A MATLAB Software for Solving Multiple-Phase Optimal Control Problems Using the Gauss Psuedospectral Method," *ACM Transactions on Mathematical Software*, Vol. 37, No. 2, 2010.

[192] Benson, D. A., Huntington, G. T., Thorvaldsen, T. P., and Rao, A. V., "Direct Trajectory Optimization and Costate Estimation via an Orthogonal Collocation Method," *Journal of Guidance, Control, and Dynamics*, Vol. 29, No. 6, 2006.

[193] Garg, D., Patterson, M. A., Darby, C. L., Francolin, C., Huntington, G. T., Hager, W. W., and Rao, A. V., "Direct Trajectory Optimization and Costate Estimation of Finite-Horizon and Infinite-Horizon Optimal Control Problems Using a Radau Pseudospectral Method," *Computational Optimization and Applications*, Vol. 49, No. 2, 2011.

[194] Garg, D., Patterson, M. A., Hager, W. W., Rao, A. V., Benson, D. A., and Huntington, G. T., "A Unified Framework for the Numerical Solution of Optimal Control Problems Using Pseudospectral Methods," *Automatica*, Vol. 46, No. 11, 2010.

[195] Garg, D., Hager, W. W., and Rao, A. V., "Pseudospectral Methods for Solving Infinite-Horizon Optimal Control Problems," *Automatica*, Vol. 47, No. 4, 2011.

[196] Sutton, K. and Graves, R. A., "A General Stagnation-Point Convective-Heating Equation for Arbitrary Gas Mixtures," Tech. Rep. TR-R-376, NASA, 1971.

[197] Krivoshapko, S. N., "Research on General and Axisymmetric Ellipsoidal Shells Used as Domes, Pressure Vessels, and Tanks," *Journal of Applied Mechanics*, Vol. 60, No. 6, 2008.

[198] Laub, B. and Venkatapathy, E., "Thermal Protection System Technology and Facility Needs for Demanding Future Planetary Missions," *International Workshop on Planetary Probe Atmospheric Entry and Descent Trajectory Analysis and Science Proceedings*, Lisbon, Portugal, Oct. 2003.

[199] Maimon, O. and Braha, D., "On The Complexity of the Design Synthesis Problem," *IEEE Transactions on Systems, Man, and Cybernetrics—Part A: Systems and Humans*, Vol. 26, Jan. 1996, pp. 142–151.

[200] Braha, D. and Maimon, O., "The Design Process: Properties, Paradigms, and Structure," *IEEE Transactions on Systems, Man, and Cybernetrics—Part A: Systems and Humans*, Vol. 27, March 1997, pp. 146–166.

[201] Braha, D. and Maimon, O., "The Measurement of a Design Structure and Functional Complexity," *IEEE Transactions on Systems, Man, and Cybernetrics—Part A: Systems and Humans*, Vol. 28, No. 4, July 1998, pp. 527–535.

[202] Braha, D. and Maimon, O., *A Mathematical Theory of Design: Foundations, Algorithms and Applications*, Kluewer Academic Publishers, New York, NY, 1998.

[203] Vallado, D. A., *Fundamentals of Astrodynamics and Applications*, Microcosm Press, El Segundo, CA, 2001.

[204] Augustine, N. R., Austin, W. M., Chyba, C., Kennel, C. F., Bejmuk, B. I., Crawley, E. F., Lyles, L. L., Chiao, L., Greason, J., and Ride, S. K., "Review of U.S. Human Spaceflight Plans Committee: Seeking a Human Spaceflight Program Worthy of a Great Nation," Tech. rep., Office of Science and Technology Policy, Oct. 2009.

[205] Auvinen, H., Bardsley, J. M., Haario, H., and Kauranne, T., "Large-scale Kalman filtering using the limited memory BFGS method," *Electronic Transactions on Numerical Analysis*, Vol. 35, 2009, pp. 217–233.

[206] Lafleur, J. M., *A Markovian State-Space Framework for Integrating Flexibility into Space System Design Decisions*, Ph.D. thesis, Georgia Institute of Technology, Georgia, Dec. 2011.

[207] Stuart, A. M. and Humphries, A. R., *Dynamical Systems and Numerical Analysis*, Cambridge University Press, Cambridge, CB2 IRP, 1996.

[208] Koon, W. S., Lo, M. W., Marsden, J. E., and Ross, S. D., *Dynamical Systems, the Three-Body Problem and Space Mission Design*, 2011.

[209] Anderson, J. D., *Computational Fluid Dynamics: The Basics with Applications*, McGraw-Hill, New York, NY, 1995.

[210] Dorf, R. C. and Bishop, R. H., *Modern Control Systems*, Pearson Prentice Hall, Upper Saddle River, NJ, 2005.

[211] Acikmese, B. and Ploen, S., "Convex Programming Approach to Powered Descent Guidance for Mars Landing," *Journal of Guidance, Control, and Dynamics*, Vol. 30, No. 5, Sept. 2007, pp. 1353–1366.

[212] Lobo, M., Vandenberghe, L., Boyd, S., and Lebret, H., "Applications of Second-Order Cone Programming," *Linear Algebra and its Applications*, Vol. 284, Nov. 1998, pp. 193–228.

[213] Julier, S. J., Uhlmann, J. K., and Durrant-Whyte, H. F., "A New Approach For Filterning Nonlinear Systems," *Proceedings of the American Control Conference*, Seattle, WA, June 1995.

[214] Chen, G., *Approximate Kalman Filtering*, World Scientific Publishing, River Edge, NJ, 1993.

[215] Bhattacharyya, S. P., Chapellat, H., and Keel, L. H., *Robust Control – The Parametric Approach*, 2013.

[216] Astrom, K. J., *Introlduction to Stochastic Control Theory*, Dover, Mineola, NY, 1970.

[217] PHX, "Model Center 8.0," Tech. rep., Phoenix Intgration, Inc., Blacksburg, VA, 2008.

[218] Van der Velden, A., Koch, P., and Wujek, B., "iSIGHT-FD, a Tool for Multi-Objective Data Analysis," *AIAA 2008-5988*, Victoria, British Columbia, Canada, Sept. 2008.

[219] Billingsley, P., *Probability and Measure*, John Wiley & Sons, Inc., 1979.

[220] Fristedt, B. and Gray, L., *A Modern Approach to Probability Theory*, Birkhaeuser, 1996.

VITA

Bradley Alexander Steinfeldt was born March 8, 1983 in Bridgeton, Missouri. He graduated from James Martin High School in Arlington, Texas in June 2001 and subsequently enrolled at the University of Texas at Austin where he obtained a Bachelor of Science degree in Aerospace Engineering with Highest Honors in August 2006.

During his undergraduate career, Bradley participated in the cooperative education program at the Jet Propulsion Laboratory (JPL) in the Advanced Mechanical Systems and the Structures and Configuration groups. While at JPL he was exposed to advanced concept design for future missions to Venus and Mars and developed testing protocol and hardware for the entry, descent, and landing of the Mars Science Laboratory. In addition, he developed flight hardware for the European Space Agency's Herschel Space Observatory which was launched into orbit on May 14, 2009.

While at the University of Texas, he was actively involved as an officer in the student branch of the American Institute of Aeronautics and Astronautics (AIAA). He also participated in NASA's Reduced Gravity Student Flight Opportunities Program where he helped advance fluidic momentum controller development for small satellites. Bradley was also the guidance, navigation, and control lead for the Platform for Autonomous Rendezvous and Docking with Innovative GN&C Methods (PARADIGM) picosatellite project, part of NASA's LONESTAR program.

Following graduation with his undergraduate degree, Bradley came to the Georgia Institute of Technology where he began work under Dr. Robert D. Braun in the Space Systems Design Lab focusing on guidance, navigation, and control techniques for planetary entry, descent, and landing. His current research focuses on blending system design with dynamical systems concepts. In May 2008, he received his Master

of Science degree in Aerospace Engineering. His Master's project title was "Guidance, Navigation, and Control Technology System Trades for Mars Pinpoint Landing".

During his graduate career, Bradley was a Draper Visiting Fellow at the Charles Stark Draper Laboratory at both the Cambridge, MA and Houston, TX locations. While at Draper, he has worked various aspects of guidance and control flight algorithm development for the Orion Crew Exploration Vehicle and the Autonomous Lunar Hazard and Avoidance Technology (ALHAT) program.

He is a member of various professional organizations including the American Institute of Aeronautics and Astronautics, American Astronautical Society, Sigma Gamma Tau, Tau Beta Pi, and the Planetary Society. Bradley currently serves as the Chair for AIAA's Society and Aerospace Technology Technical Committee and was a founding officer of The Planetary Society at Georgia Tech.

Bradley is an author or co-author of fifteen technical papers.